

The University of Nottingham

UNITED KINGDOM · CHINA · MALAYSIA

CHEMICALLY DIVERSE POLYACRYLATE AND POLYACRYLAMIDE SURFACES FOR HUMAN CARDIOMYOCYTE CULTURE AND THEIR EFFECT ON PHENOTYPE

ASHA KUMARI PATEL, MPharm.

Thesis submitted to the University of Nottingham
for the degree of Doctor of Philosophy

School of Medicine

JANUARY 2014

ABSTRACT

Human pluripotent stem cell (hPSC) derived cardiomyocytes can provide robust *in vitro* models for pharmaceutical drug screening and modelling cardiac disease. To fully realise these potentials, hPSC-cardiomyocytes must be reproducibly cultured to a more mature state than has thus far been achieved. Defined and well controlled culture conditions underpin the ability to derive hPSC-cardiomyocytes of consistent quality. These include cell source, culture medium and substrate. This thesis is concerned with the latter; culture substrates are currently biological in nature creating inherent variability in culture conditions.

There is limited knowledge on the interaction between cardiomyocytes and synthetic, non-biological substrates making rational design of materials impractical. To aid discovery of novel culture substrates, 115 polyacrylate and polyacrylamide substrates were microarrayed and investigated using a parallel screening approach. The use of polyacrylates and polyacrylamides as biomaterials has been demonstrated previously, including contact lenses, bone cements and hydrogels to support cells. The diverse chemistry exhibited across the range of polymers enables modelling of structure-activity relationships between substrate chemistry and cardiomyocyte behaviour.

Cardiomyocytes derived from human embryonic stem cells (hESC) were cultured on the microarrays in the presence and absence of serum . Attachment density (nuclei count *via* DAPI staining) and cardiomyocyte spread (surface area using sarcomeric α-actinin immunostaining) on each substrate was acquired by automated fluorescence microscopy and image analysis software.

From this primary screen, 70 % of polymers were found to support cardiomyocytes adhesion in serum conditioned arrays, BM34 (fufuryl methacrylate) supported the highest relative cell density (0.59 ±0.28) and also the largest cell size (1364 ±937 μm^2), which was comparable to gelatin control. In serum free conditions, only 10 % of polymers supported cardiomyocyte attachment. The highest relative cell density was on AM38 (Dimethylamino-propyl acrylate) and largest cell size on BM49 (Tert-butylamino-ethyl

methacrylate), 274 ±75 μm^2, which was significantly lower than cell density and cell area (2019 ±596 μm^2) on gelatin control.

To investigate if synergy exists between polymers that enable adhesion in serum free conditions and those that support larger cell areas in serum conditioned arrays, 24 polymers were mixed pair-wise to form second generation microarrays comprising of 576 co-polymers. This diverse library enabled unique combinations of chemical moieties to be explored and co-polymers were found to have a greater proportion (74 %) that supported cardiomyocyte attachment in serum free conditions, largest average cell size was now 1089 ±260 μm^2 on BM80/AM64 (Methacryloyloxy)ethyl acetoacetate/ Hexadecafluoro-9-(trifluoromethyl)decyl acrylate). Five co-polymers were chosen to perform more detailed characterisation of cardiomyocytes cultured on them for 5 and 25 days. Electrophysiological profiling and quantification of myofibril organisation identified co-polymers AD17/BM54 (Hexanediol ethoxylate diacrylate/ Ethoxyethyl methacrylate) and BM80/AD17 to be comparable to control gelatin.

Partial least squares multivariate regression analysis correlated chemical species from the polymeric substrate, identified using time of flight secondary ion mass spectrometry, with cardiomyocyte response and identified moieties beneficial or detrimental for cardiomyocyte adhesion and cell area. This may aid rational design of tailor-made non-biological substrates for cell culture.

In summary, the parallel screening of co-polymers of acrylates and acrylamides has been the first step in a discovery process of lead materials capable of progressing the culture of cardiomyocytes in more reproducible, economical and defined conditions. Only five substrates were analysed in detail, leaving a large library of co-polymers worthy of further investigation, including the physical properties of the polymers that need to be considered for practical use of the polymers in culture.

ACKNOWLEDGEMENTS

I would like to thank my supervisors Professors, Chris Denning, Morgan Alexander and Martyn Davies for their guidance and support over the last 3 years.

I am grateful to Emily Smith (school of chemistry) for acquisition of XPS data and Nigel Smith (dept. of genetics) for performing karyotyping and to CellProfiler for allowing open access to their software.

For their patient training in microarray printing and ToF-SIMS, I'd like to thank Andrew Hook, Adam Celiz and David Scurr from the laboratory of biophysics and surface analysis. For guidance with cell culture, I'd like to thank members of the Wolfson centre of stem cells, tissue engineering and modelling, in particular Vinoj George and Emily Dick. I am also appreciative of the constant support from technical and administrative staff; Maria Muñoz, Jayson Bispham, Caroline Reffin and Elizabeth Attenborough.

Finally, I extend my gratitude to a loving family and supportive friends who remind me there is life beyond the lab.

ABBREVIATIONS

Abbreviation	Description
AP	Action potential
APA	Action potential amplitude
APD	Action potential duration
APD50	Action potential duration at 50% of the repolarisation curve
APD90	Action potential duration at 90% of the repolarisation curve
BMP	Bone morphogenic protein
Brachyury T	Brachyury protein T
BSC	Biological safety cabinet
CHO	Chinese Hamster Ovary
cTnI	Cardiac Troponin I
CY3	Cyanine dye 3
DAPI	Di-amino phenyl-indole
EB	Embryoid body
ECM	Extracellular matrix
FBS	Foetal bovine serum
FGF	Fibroblast growth factor
FITC	Fluorescein iso-thiocyanate
GATA 4	Gene binging to 'GATA' DNA sequence
hESC	Human Embryonic Stem Cell
hiPSC	Human induced pluripotent stem cell
hPSC	Human pluripotent stem cell including hESC and hiPSC
HUES7	Harvard University embryonic stem cell line 7
Isl1	Islet 1
KDR	Cardiac progenitor marker also known as Flk1
MDP	Maximal diastolic potential/ resting membrane potential
Mef 1	Myeloid Elf-*1*-like Factor
Mesp 1	Mesoderm Posterior 1 transcription factor
MLC 2a/v	Myosin Light Chain 2 atrial/ventricular
MYH	Myosin Heavy Chain
Nanog	Homeobox transcription factor
Nkx2-5	NK 2 Homeobox 5
Oct 3/4	Octamer binding transcription factor 3/4
pHEMA	Poly(2-hydroxyethyl methacrylate)
PLS	Partial least squares
S-Act	Sarcomeric α actinin
S.D	Standard deviation
S.E.M	Standard error of the mean
Sox 2	SRY (Sex Determining Region)- box 2
Tbx 5/20	T-box transcription factor
ToF-SIMS	Time of Flight Secondary Ion Mass Spectrometry
VECAM	Vascular Endothelial Cell Adhesion Molecule
WCA	Water Contact Angle
XPS	X-Ray Photoelectron Spectroscopy

CONTENTS

ABSTRACT ..... **I**

ACKNOWLEDGEMENTS ..... **III**

ABBREVIATIONS ..... **IV**

CONTENTS ..... **V**

LIST OF FIGURES..... **VIII**

LIST OF TABLES..... **X**

1. CHAPTER 1. INTRODUCTION **1**

1.1. UTILITY OF HUMAN STEM CELL DERIVED CARDIOMYOCYTES 2

1.2. CARDIOMYOGENESIS 6

1.2.1. Cardiac Development: In Vivo 6

1.2.2. Cardiac Differentiation: In Vitro Methods 7

1.3. CHARACTERISTICS OF HUMAN CARDIOMYOCYTES 13

1.3.1. Ultrastructure 13

1.3.2. Electrophysiology 16

1.3.3. Cardiomyocyte Maturation 18

1.4. SUBSTRATES FOR *IN VITRO* CELL CULTURE 21

1.4.1. Physicochemical Properties of Culture Substrates 23

1.5. SYNTHETIC MATERIALS DISCOVERY 26

1.5.1. Parallel Screening Platforms 28

1.6. THESIS RATIONALE 29

2. CHAPTER 2. EXPERIMENTAL METHODS **30**

2.1. CELL CULTURE 31

2.1.1. Culture Media 31

2.1.2. Human Embryonic Stem Cell (hESC) Culture 31

2.1.3. hESC Differentiation 35

2.2. CELL SEEDING ON MICROARRAYS 37

2.3. CELL ANALYSIS 37

2.3.1. Karyotyping 37

2.3.2. Flow Cytometry 38
2.3.3. Immunostaining 39
2.3.4. Whole Cell Patch Clamp Electrophysiology 40
2.4. MICROARRAY FABRICATION 41
2.4.1. Substrate formation 41
2.4.2. Piezo Printing 41
2.4.3. Contact Printing 42
2.5. SURFACE ANALYSIS 43
2.5.1. Time of Flight Secondary Ion Mass Spectrometry 43
2.5.2. Water Contact Angle Measurement 43
2.5.3. X-Ray Photoelectron Spectroscopy 43
2.6. IMAGE ACQUISITION AND ANALYSIS 43
2.7. MULTIVARIATELINEAR REGRESSION : PLS 44
3. CHAPTER 3. SCREENING POLYMER MICROARRAYS 46
3.1. INTRODUCTION 47
3.1.1. Cardiomyocyte Derivation 47
3.1.2. Polymer Microarrays 48
3.2. RESULTS 53
3.2.1. Human Cardiomyocyte and Fibroblast Derivation from HUES7. 53
3.2.2. Microarray fabrication 61
3.2.3. Automated Image Analysis 66
3.3. SCREENING CARDIOMYOCYTE ATTACHMENT AND MORPHOLOGY ON FIRST GENERATION HOMOPOLYMER MICROARRAYS. 71
3.3.2. Monomers chosen to take forward for fabrication of second generation co-polymer arrays. 78
3.4. SECOND GENERATION CO-POLYMER MICROARRAYS. 80
3.5. DISCUSSION 89
3.6. LIMITATIONS AND FUTURE WORK 91
4. CHAPTER 4. DETAILED CARDIOMYOCYTE CHARACTERISATION 93
4.1. INTRODUCTION 94
4.1.1. Myofibril Organisation 94
4.1.2. Electrophysiology 95
4.2. RESULTS 101

4.2.1. Substrate Format for Further Characterisation 101
4.2.2. Z line Measurement 103
4.2.3. Patch Clamp Electrophysiology 107
4.2.4. Ion Channel Distribution in HUES7-cardiomyocytes 110
4.3. DISCUSSION 115
4.4. LIMITATIONS AND FUTURE WORK 118

5. CHAPTER 5. INFLUENCE OF SURFACE CHEMISTRY ON CARDIOMYOCYTE BEHAVIOUR 119

5.1. INTRODUCTION 120
5.1.1. Time of Flight Secondary Ion Mass Spectrometry 120
5.1.2. X ray Photoelectron Spectroscopy 122
5.1.3. Wettability 123
5.1.4. Partial Least Squares for the Prediction of Cell Response using Surface Chemistry. 124
5.2. RESULTS 126
5.2.1. Modelling Surface Chemistry and Cell Response 126
5.2.2. X-ray Photoelectron Spectroscopy 136
5.2.3. Water Contact Angle 139
5.3. DISCUSSION 142
5.3.1. Multivariate Linear Regression of ToF-SIMS data using PLS 142
5.3.2. Water Contact Angle and XPS Elemental Composition 145
5.3.3. Limitations and Future Work 146

6. CHAPTER 6.GENERAL DISCUSSION 148

BIBLIOGRAPHY 153

APPENDICES 170

Appendix 1. Monomer Identity **172**

Appendix 2. a) Cardiomyocyte density and area on first generation serum pre-conditioned array **176**

b) Cardiomyocyte density and area on second generation in serum free conditions **179**

Appendix 3. Water contact Angle and XPS data **193**

List of Figures

Figure 1.1 Cardiac Differentiation Methods of Human Pluripotent Stem Cells..... 12

Figure 1.2 Ultrastucture of Myofibril Contractile Proteins 15

Figure 1.3. Model Subtype Action Potentials and Major Contributing Ionic Currents..... 17

Figure 3.1 Substrate Preparation for Piezo and Contact Printing..... 49

Figure 3.2. Photoinitiated polymerisation of acrylates 50

Figure 3.3. Library of commercially available acrylate and acrylamide monomers. 51

Figure 3.4. Characterisation of the human embryonic stem cell line HUES7. 53

Figure 3.5 HUES7 derived fibroblast characterisation. 54

Figure 3.6. Derivation of i) Cardiomyocytes and ii) fibroblasts from HUES7 human embryonic cells. 55

Figure 3.7 Characterisation of dissagregated HUES7-cardiomyocytes on 0.1% Gelatin. 58

Figure 3.8. Cardiomyocyte population within beating clusters determined using A) Immunostained cell counts and B) Fluorescence Activated Cell Sorting (FACS). 60

Figure 3.9 Structure of pHEMA. 61

Figure 3.10. Piezo Printed microarray. A) Polymer Array Layout. B) Brightfield image of printed array. C) Distribution of background pHEMA ion $C_2H_5O_2$-. D) Seeded with HUES7 fibroblasts and stained with nuclear marker DAPI. 62

Figure 3.11 Contact printed microarray A) Seeded with HUES7 fibroblasts and stained with nuclear marker DAPI. B) Distribution of background pHEMA ion $C_2H_5O_2$-. 63

Figure 3.12 Contact printed array using amended blotting protocol. 64

Figure 3.13. HUES7-fibroblast nuclei count using CellProfiler 67

Figure 3.14 CellProfiler count of DAPI stained nuclei of fibroblasts seeded onto a polymer spot. 68

Figure 3.15 Example of CellProfiler protocol to count number of cells attached and..... 69

Figure 3.16 (A) Segregation of touching cardiomyocytes by CellProfiler and Volocity (B) Incorrect cell identification due to background fluorescence of polymer. 70

Figure 3.17. HUES7-cardiomyocyte attachment on 115 different poly acrylate and polyacrylamide substrates at 24 hours on serum conditioned arrays..... 73

Figure 3.18. HUES7-cardiomyocyte attachment on 115 different polyacrylate and polyacrylamide substrates cultured for 7 days on serum pre-conditioned arrays. 74

Figure 3.19. Comparison of cardiomyocyte density and area on first generation homopolymer array on serum free and FBS pre-conditioned polymers and 0.1% gelatin cultured for 7 days. 75

Figure 3.20 Cardiomyocyte morphology observed on polymers that supported highest attachment at 24 hours and 7 days. 76

Figure 3.21 Change in Cardiomyocyte Density on Polymers from 24 hours to 7 days Culture on Polymers. 77

Figure 3.22 Layout of Secondary generation Co-polymer Array. 81

Figure 3.23 Time of Flight Secondary Ion Mass Spectrometry of Second Generation Co-polymer Array. 82

Figure 3.24 Cardiomyocytes Cultured on Serum Pre-conditioned Co-polymer Array..... 84

Figure 3.25 Cardiomyocytes Cultured on Co-polymer Array in Serum free Conditions... 85

Figure 3.26 Synergy Observed in Co-Polymer AM38/BM39. 86

Figure 3.27 Five Selected Co-Polymers that Support Cardiomyocyte Attachment in Serum Free Conditions to be forwarded for Detailed Cardiomyocyte Characterisation... 88

Figure 4.1 Primary Human Ventricular Cardiomyocytes; (A) Fetal and (B) Adult, immunostained for sarcomeric alpha actinin. 94

Figure 4.2 Sarcomere Length and Cross-Bridge Formation..... 95

Figure 4.3 Patch Clamp Electrophysiology..... 96

Figure 4.4 Array Format for Electrophysiological Measurement. 102

Figure 4.5 Delamination of co-polymer BM34/AD24. 103

Figure 4.6 Quantification of Z lines of Cardiomyocytes. 105

Figure 4.7 Comparison of Myofibril Alignment of Cardiomyocytes Cultured on Different Substrates..... 106

Figure 4.8. Action Potential Profiles of HUES7 derived Cardiomyocytes..... 107

Figure 4.9 Comparison of Ventricular Action Potential Phenotype of Cardiomyocytes on Polymer Substrates Compared to Gelatin Control..... 109

Figure 4.10 Dual Staining of Sodium ($Na_V1.5$) or Potassium (Kir2.1) Ion Channels with respective cardiac markers, Cardiac Troponin I (cTnI) and Sarcomeric Alpha Actinin (s/actinin) of Cardiomyocytes Cultured on 0.1% Gelatin. 112

Figure 4.11 Potassium (Kir2.1) channel and Sarcomeric Alpha Actinin staining of Cardiomyocytes Cultured on Co-polymers. 113

Figure 4.12 Sodium ($Na_V1.5$) channel and Cardiac Troponin I staining of Cardiomyocytes Cultured on Co-polymers. 114

Figure 5.1 (A) Schematic of secondary ion generation in ToF-SIMS. (B) Negative ion mass spectrum of pHEMA. 121

Figure 5.2 (A) Schematic of the photoelectric effect. (B) XPS survey of pHEMA. 122

Figure 5.3 Schematic of water contact angles of relatively hydrophobic and hydrophilic surfaces..... 123

Figure 5.4 Oxygen plasma treatment of polystyrene..... 124

Figure 5.5 Partial Least Squares modelling..... 125

Figure 5.6 PLS model of cardiomyocyte attachment and area on polymers in first generation serum pre-conditioned arrays. 128

Figure 5.7 A) Cardiomyocyte attachment and B) area plotted against ion intensity of m/z 59 and 41 identified by PLS as being positive and negative for cell attachment and spread. 130

Figure 5.8 (A) Intensity of ions m/z 44 and 81 in all homopolymers (B) Fluorescent images of cardiomyocyte attachment on BM49 and BM34. 131

Figure 5.9 PLS measured verses predicted values for cardiomyocyte attachment and area on co-polymers in (A,C) Serum preconditioned (B,D) Serum free conditions. 134

Figure 5.10 XPS wide survey scan of a fluorinated polymer, AM58 (A), a nitrogen containing polymer, AM36 (B) and a high sensitivity scan for the nitrogen peak of AM36 (C). 136

Figure 5.11Fluorine XPS analysis of array 137

Figure 5.12 Elemental composition as determined by XPS and influence on cardiomyocyte adhesion and area on serum pre-conditioned first generation homopolymer arrays. 138

Figure 5.13 PLS model using elemental composition to predict cardiomyocyte attachment and area on serum preconditioned homopolymers. 138

Figure 5.14 WCA measurements on homopolymers (A) and general trend of WCA with fluorine and oxygen elemental composition (B). 139

Figure 5.15 (A) Cardiomyocyte density and (B) area plotted against WCA of homopolymers in first generation array pre-conditioned with serum. 140

Figure 5.16 Cardiomyocyte density and area plotted against WCA of second generation co-polymers on (A) serum pre-conditioned arrays and (B) serum free conditions. Colour coded by major monomer. 141

Figure 5.17 hESC-cardiomyocyte adhesion on amino acrylates in serum free conditions. 143

List of Tables

Table 1.1 Characteristics of Mature Vs Immature Human Cardiomyocytes..... 20

Table 2.1 Composition of culture media 32

Table 3.1. Chosen 24 monomers to take forward for second generation array. 79

Table 3.2 Top ten co-polymers that support cardiomyocyte attachment in serum free conditions. 87

Table 4.1 Reported Action Potential Measurement from Human Ventricular Cardiomyocytes. 98

Table 4.2 Identity of Monomers in Co-polymers chosen from array 6.2..... 101

Table 5.1 Ions identified by PLS as influential for Cardiomyocyte Attachment and Area on first generation serum preconditioned homopolymer array. 129

Table 5.2 Chemical Moieties identified by PLS to be influential for cardiomyocyte adhesion and cell area on serum pre-conditioned co-polymer arrays..... 135

Table 5.3 Chemical Moieties identified by PLS to be influential for cardiomyocyte adhesion on co-polymer arrays in serum free conditions. 135

CHAPTER 1

Introduction

1.1. UTILITY OF HUMAN STEM CELL DERIVED CARDIOMYOCYTES

Failure of drugs to progress after heavy investment during phase II and III trials is a major contributor to crippling costs (now over $1bn) involved in drug development (Khanna, 2012). Approximately 30% of these failures are due to safety concerns not picked up during *in vitro* and *in vivo* animal model screening (Kola and Landis, 2004). This economic impact is met with serious patient safety issues when 28 % of drugs that reach the market are withdrawn due to cardiotoxicity (Gwathmey et al., 2009). Consider, the weight loss drug, sibutramine. This compound was released for clinical use in 2001 and withdrawn from the UK market in 2010 following the outcome of a post-market surveillance study (SCOUT) which was conducted over six years and concluded in 2009 (James et al., 2010). The potential for sibutramine to prolong QT interval was only identified when a patient suffered cardiac arrest after taking the drug. (Kim et al., 2009).

This case is representative of many that have resulted in economic attrition and severe adverse reactions in patients (Wysowski and Swartz, 2005). There has therefore been an interest in developing better screening models. Cardiomyocytes derived from human pluripotent stem cells (hPSC), include those derived from human embryonic stem cells (hESC) and human induced pluripotency stem cells (hiPSC) and have shown to display appropriate physiology and expected response to known pharmacological agents (Dick et al., 2010, Braam et al., 2010, Harris et al., 2013). For these reasons, they show promise as pre-clinical predictors for pharmacological toxicity and efficacy and for *in vitro* study of cardiac development and disease modelling (Itzhaki et al., 2011a, Matsa et al., 2011). Development of hPSC-cardiomyocyte assay platforms also assists the adoption of the '3Rs' principle outlined by the House of Lords in 2002 to reduce, refine and replace animal use within research (www.nc3rs.org.uk).

Current Screening Models

The bulk of early toxicity data comes from *in vitro* ion channel assays carried out in transformed cell lines, such as HEK (Human Embryonic Kidney) or

CHO (Chinese Hamster Ovary) cells, cellular models such as the H9c2 line derived from embryonic rat ventricle (Ertracht et al., 2011) and *ex vivo* organ assays such as the rabbit isolated Langendorff heart model (Lawrence et al., 2006). This is later followed by *in vivo* rodent/non-rodent models.

Forced expression of the HERG encoded potassium channel involved in the regulation of the cardiac action potential creates a specific model for screening arrhythmogenic potential of drugs *via* hERG blockade and although provides an interim assay, is not representative of the multiple ion channels expressed in the human heart and does not identify arrhythmia caused by non-hERG mechanisms (Anson et al., 2011, Ma et al., 2011a). This is exemplified by the testing of verapamil in CHO cells transformed to express the hERG potassium channel. According to this assay, verapamil blocks the potassium channel indicating prolongation of the QT interval and will lead to arrhythmia. In practise verapamil is used routinely for safe treatment of cardiovascular conditions. Long QT is not seen in patients receiving verapamil because the drug also blocks inward L-type calcium channels which negates the effect of potassium channel blockade (Meyer et al., 2004). Animal derived cardiomyocytes can capture a more intricate electrophysiological profile. However, there are significant inter-species differences that make translation difficult. For example, the ventricular cardiomyocyte from mice has an action potential that is shorter, 50ms compared to human, 400ms, and has an indistinct plateau phase (Nerbonne, 2004). In the human action potential, alteration of this plateau phase is particularly indicative of QT prolongation because the hERG potassium channel contributes to the I_{Kr} current that is responsible for repolarisation (see section 1.3). However, the I_{Kr} current in mice is absent, replaced by I_{to} and $I_{K,slow}$ currents (Sanguinetti and Tristani-Firouzi, 2006, Davis et al., 2011). In conventional rabbit models, the I_{Ks} current is insensitive to blockade (Peng et al., 2010). There is therefore a need for more representative cardiac models which could be met by hPSC-cardiomyocytes.

Validation of hPSC-Cardiomyocyte *In Vitro* Utility

In order for hPSC-cardiomyocytes to be accepted as a screening tool their response to pharmaceuticals requires validation against current models. A study

by GlaxoSmithKline, tested ten compounds with a mixture of hERG, Na^+ and Ca^{2+} channel blocking properties and compared multi electrode array (MEA) acquired parameters such as QT and QRS intervals from *ex vivo* rabbit ventricular tissue and *in vivo* rodent/non-rodent electrocardiograms and compared them to pharmacological effects on hPSC-cardiomyocytes at a given concentration to determine translational ability of the cells. The authors reported a good correlation with existing pre-clinical assays, thereby justifying the use of hPSC-cardiomyocytes for electrophysiological cardiac safety screening (Harris et al., 2013).

hPSC-cardiomyocytes have been proposed to be more sensitive than other in vitro assays (Anson et al. 2011; Kamp and Lyons 2009; Ma et al. 2011). For example, comparison of hESC-cardiomyocytes with primary human ventricular cardiomyocytes, shows a strong quantitative similarity in terms of β1- and β2 adrenoreceptor response, unlike other animal models tested (Brito-Martins et al., 2008). Superior sensitivity of hPSC-cardiomyocytes for toxicity detection at lower drug concentrations that are more physiologically relevant has also been demonstrated. Peng *et al*, reported a response to 0.03 μM nifedipine, an L-type calcium channel blocker which shortens action potential duration (APD), compared to a canine model which required more than 10 μM to elicit APD shortening. Similarly, potassium current (I_{kr}) blockade and subsequent plateau lengthening by risperidone can be detected at 0.1μM in hPSC-cardiomyocytes, whereas guinea-pig myocytes require a ten-fold higher dose to exert this effect (Bussek et al., 2009, Drolet et al., 2003).

In vivo Potential

Regeneration of the human heart *in vivo* has been shown to be poor, with a rate of cardiomyocyte renewal estimated to be around 1 % per year as calculated by post-mortem C^{14} dating made possible by the nuclear pulse generated during Cold War weapons testing (Bergmann et al., 2009). The lack of regenerative capacity of this vital organ makes it a priority candidate for cell therapy.

Consequently, cardiomyocytes have been trialled for *in vivo* clinical use to regenerate myocardium that is damaged during, for example, the more than

100,000 hearts attacks that occur each year in the U.K. Of which 70% go on to develop progressive heart failure due to detrimental re-modelling around the damaged tissue (Keil, 1999). The CADUSEUS and ALLSTAR trials involve intra-coronary infusions of autologous and allogeneic cardiac stem cells (CSCs), respectively. The former phase 1 trial has shown, in addition to safety, significant benefit to scar tissue shrinkage and increased viability in human patients (Makkar et al., 2012). The ALLSTAR trial aims to address the poor retention rate of CSCs identified during CADUSEUS by developing hydrogel materials, emphasizing the need for better delivery materials (Smith et al., 2013).

Barriers to Overcome for Adoption of hPSC-Cardiomyocytes

The full potential of hPSC-cardiomyocytes will be met by addressing the following issues:

Scalability; Cardiac differentiation efficiency from hPSCs can be low depending on method used (see section 1.2.2). Beating clusters of cardiomyocytes tend to contain multiple cell types and require enrichment for pure populations of cardiomyocytes. Substitution of expensive growth factors required to improve differentiation efficiency with synthetic small molecules can enable cost-effective production of cardiomyocytes. A universal method for scalable production is not currently used.

Immaturity; hPSC-cardiomyocytes are immature in terms of ultra-structure and electrophysiology (see table1.1). Myofibril organisation, important for contractility, is relatively disorganised and current density of sodium (I_{Na}), calcium and potassium (I_{Kr}) is lower than adult cardiomyocytes which can increase pro-arrhythmic risk leading to false positives during toxicity testing (Ehrlich, 2008, Satin et al., 2004). Development of cell culture platforms that produce functionally mature cardiomyocytes are a high priority for pharmaceutical companies. For example, GlaxoSmithKline in conjunction with NC3Rs have recently provided funding to improve cardiomyocyte culture (http://www.crackit.org.uk/crack/2013/2013_challenges/Challenge13-Inpulse).

Variability; Cardiomyocytes vary in sub-type produced during differentiation which may be atrial, ventricular or nodal. The relative maturity of

cardiomyocytes within the same population can also vary as well as purity of the cardiomyocyte population.

1.2. CARDIOMYOGENESIS

1.2.1. Cardiac Development: *In Vivo*

Improvement of *in vitro* cardiomyocyte culture ultimately relies on an understanding of the molecular mechanisms involved during *in vivo* cardiogenesis. Mechanisms of cardiac development are based largely on rodent, avian and amphibian studies (Dyer et al., 2001, Garcia-Martinez and Schoenwolf, 1993, Lohr and Yost, 2000), fewer human embryonic cases (Sathananthan et al., 2011) and more recently, *in vitro* hESC differentiation studies (Paige et al., 2010, Sinclair and Singh, 2007). The heart is the first functioning organ to form by 3 weeks of human embryonic development (Sylva et al., 2013). The key milestones in development are **i)** mesoderm induction, **ii)** mesoderm patterning and **iii)** cell specification (Willems and Mercola, 2011).

As the embryo develops, gastrulation occurs *via* an epithelial to mesenchymal transition (EMT) to form intermediate mesendoderm characterised by the expression of BrachyuryT (Rodaway and Patient, 2001) followed by spatial organisation into three germ layers; the ectoderm, endoderm and mesoderm (Rangel et al., 2012). Each germ layer is now committed to a particular set of lineages. It is the mesoderm that will give rise to the cells within the cardiovascular system, as well as bone, fat and cartilage depending on the signalling environment (Evseenko et al., 2010).

Post-gastrulation, cardiogenesis proceeds with a shift from primitive mesoderm to cardiac mesoderm triggered by paracrine signalling, including fibroblast growth factor (FGF) and Bone Morphogenetic Protein (BMP2 and 4), from adjacent ectoderm and endoderm (Dyer et al., 2001, Lough and Sugi, 2000). Brachyury induction of mesoderm posterior 1 (MESP1) transcription factor further drives expression of cardiac mesodermal markers such as NKX2.5, TBX5, HAND1/2, GATA4, ISL1 and GATA4 (Verma et al., 2013).

Within the cardiac mesoderm, progression to cardiac progenitor cells (CPCs) occurs. CPCs will be of the first or second heart field (FHF/SHF). Specialisation of CPCs in the FHF occurs before the SHF and will give rise to cells within the left ventricle, atria and conductive system, modulated by BMP4 (Dierickx et al., 2012). Those in the SHF continue to proliferate until down regulation of the canonical Wnt pathway, through temporal secretion of Wnt antagonists such as Dickkopf-1 (Dkk-1), halts proliferation and a switch to non-canonical Wnt signalling (Olson and Schneider, 2003, Marvin et al., 2001) initiates differentiation to cells in the outflow tract and right ventricle (Buckingham et al., 2005, Yang et al., 2013).

To enable terminal differentiation of cardiac progenitors to functional cardiomyocytes, Serum response factor (SRP) is thought to regulate expression of contractile proteins (Dierickx et al., 2012). Factors involved in further maturation of cardiomyocytes are not well understood and would be pivotal for development of improved *in vitro* differentiation strategies.

Although there is much to be deciphered in the development of the heart, it is apparent that four primary signalling pathways are implicated in cardiogenesis and applied to *in vitro* culture methods; Nodal, Wnt, BMP and FGF (Arnold and Robertson, 2009) which must be effected in a stage specific manner due to their dual inductive and inhibitory roles (Burridge et al., Kattman et al., 2011).

1.2.2. Cardiac Differentiation: In Vitro Methods

Prior to gastrulation, pluripotent cells within the inner cell mass (ICM) of the blastocyst are harvested for production of *in vitro* embryonic stem cell lines The first stable human embryonic stem cell (hESC) line was generated in 1998 (Thomson et al., 1998). In 2007, pioneering work established the production of human induced pluripotent stem cells (hiPSC) from somatic cells (Takahashi et al., 2007). Induction of pluripotency in somatic cells using virus-free methods (Mehta et al., 2011) improves clinical prospects but low efficiency of conversion

may currently limit scalability. However, they offer an alternative to the ethically controversial embryonic source, with the advantage of being able to carry the genetics of the patient from which they were derived to enable specific study of a disease (Carvajal-Vergara et al., 2010, Liang et al., 2013), which may not be available in the current registry of disease specific hESC lines (*www.iscr-admin.com*). Pluripotent stem cells hold the potential of producing any cell type in the body as well as self-renewal (Odorico et al., 2001) making them a suitable source for production of cells of interest.

Generation of cardiomyocytes from human pluripotent stem cells (hPSC), including hESCs and hiPSCs, has been achieved using a variety of methods which aim to mimic *in vivo* cardiac development. The three most widely reported are embryoid body, monolayer and co-culture methods described next.

1.2.2.1. Embryoid Body Differentiation

The differentiation of pluripotent stem cells into all three germ layers can be encouraged by agglomeration of cells into 'embryoid bodies'. This three-dimensional culture emulates early embryogenesis and allows complex cell to cell signalling within the construct to spontaneously generate cells of the three germ layers as was first observed in mouse embryonic cell culture (Evans and Kaufman, 1981). This principal was applied to derive the first cardiomyocytes from hESCs in 2001 (Kehat et al., 2001) and hiPSCs in 2009 (Zhang et al., 2009). Variations of the EB method differ in technique used to form the embryoid body and factors used to promote cardiac lineage commitment that can improve differentiation efficiency from under 10 % (Kehat et al., 2001) to over 90 % (Burridge et al., 2011).

Unaided EB formation relies on random agglomeration in low adherence dishes, of hPSCs in suspension (Kattman et al., 2011). Improvements in probability of EB formation and uniformity of cell density per EB have been made by use of facilitated agglomeration techniques. Addition of polyvinyl alcohol (PVA) can initiate aggregation of hPSCs and consistency of EB size can be controlled by use of V microwell plates. Each well contains a defined number of cells which aggregate at the bottom to form an EB via gravitational or centrifugal

force (Burridge et al., 2007). Generation of one EB per well also overcomes aggregation of individual EBs which has been shown to inhibit cell growth and differentiation (Dang et al., 2004). Adaptations of the microwell plate for facilitated EB formation are Matrigel™ coated wells which serve the purpose of being a suitable substrate for hPSC proliferation followed by *in situ* differentiation. A cardiomyocyte population of 3% was reported for this method (Mohr et al., 2010).

Factors to promote cardiac differentiation are applied in a staggered fashion to mimic *in vivo* development. To initiate mesoderm induction, a combination of BMP4, FGF and/or Activin A are required and applied during early EB formation. Following mesoderm induction, cardiac specification is encouraged by addition of fetal bovine serum (FBS) to produce beating EBs containing 64–89 % cardiomyocytes, the highest proportion reported thus far (Burridge et al., 2011). However, different batches of serum contain various undefined factors that can either hinder or encourage cardiac differentiation impacting the reproducibility of the method. Rigorous batch testing is therefore required to find the most cardio-inductive serum. A more defined approach is to inhibit the Wnt pathway at this stage using for example, Dkk1 or small molecules including IWR-1, XAV939 or the BMP antagonists, dorsomorphin and noggin (Ren et al., 2011, Willems et al., 2011, Yuasa et al., 2005). Additional variation arises from hPSC source and propagation in culture. For example, Willems *et al*, report hESC culture directly on a mouse embryonic fibroblast layer followed by removal of hESC colonies to initiate differentiation risking contamination of EBs with MEFs which may lead to reduced differentiation efficiency (Willems et al., 2011, Weitzer, 2006).

1.2.2.2. Co-culture Differentiation

Co-culture is based on the knowledge gained from avian and amphibian developmental studies, which uncovered a fundamental role of the definitive endoderm layer for cardiac specification of the mesoderm (Lough and Sugi, 2000).

The visceral endoderm-like cell line (END-2) is derived from mouse embryonal carcinoma P19 cells (van der Heyden and Defize, 2003). Co-culture of hESC lines with END-2 cells was first described in 2003 by Mummery and colleagues. END-2 cells formed a feeder layer upon which hESCs were cultured. By 10 days, beating regions could be observed. The type of hESCs used in this study are not normally capable of undergoing spontaneous cardiogenesis, therefore the authors attributed the differentiation exclusively to the influence of the END-2 cells. Sporadic regions of beating could be observed in 35% of the wells which was a total efficiency of approximately 3% (Mummery et al., 2003, Mummery et al., 2012). Improvements in efficiency by over 24-fold were achieved by removal of FBS and addition of ascorbic acid to the culture medium (Passier et al., 2005).

The co-culture system provides a good model for further elucidation of endoderm directed cardiac specification. However, for clinical use, contamination of the cardiomyocyte clusters with END-2 derivatives must be considered.

Attempts to overcome direct contact with the mouse cell line involve use of END-2 conditioned medium which resulted in more than 10 % cardiomyocyte population. This was doubled by addition of compound SB203580, found to promote early mesoderm formation (Graichen et al., 2008).

Culture conditions of hPSCs have been shown to influence END-2 co-culture differentiation efficiency. A study by Ojala *et al*, compared hESCs and hiPSCs propagated in three different culture conditions prior to differentiation; **1**. MEF feeder layer, in DMEM medium supplemented with KSR (Knockout Serum Replacement, **2**. SNL feeder layer (SNL is a transformed mouse embryonic fibroblast line) in the same medium and **3**. Matrigel™ in mTeSR1™ medium. The only hESC line tested was H7 and displayed significantly higher differentiation efficiency when cultured on MEF or SNL feeder layers in DMEM compared to on Matrigel™ in mTeSR™. Four hiPSC lines were tested; two of which also displayed higher differentiation when propagated on the feeder layers. However, one showed no difference between the three and another was significantly higher on Matrigel™ compared to MEF layer (Ojala et al., 2012). This highlights the

difficulty in comparing differentiation methods due to cell line variability and culture conditions.

1.2.2.3. Monolayer Cardiac Differentiation

Monolayer culture is potentially more reproducible, scalable and amenable to automation as it circumvents diffusional barriers or gradients that may be created within an EB and challenging downstream disaggregation of beating clusters. Monolayer differentiation of the H7 hESC line on Matrigel™ in MEF conditioned media (CM) was reported by Laflamme *et al.* At day 7, cardiac differentiation is induced by replacing MEF-CM with RPMI-B27 medium supplemented with Activin A. After 24 hours the medium is replaced BMP4 supplementation. After 4 days, this media is replaced with non-supplemented RPMI-B27. Spontaneous beating of cell cultures was normally observed after 12 days of induction. The authors reported a cardiomyocyte yield of >30% using this method (Laflamme et al., 2007). Differentiation efficiency of the same cell line was increased to 65% using sequential induction and inhibition of pathways. BMP4, Activin A and FGF initiates mesoderm induction, followed by Noggin then Dkk1 and a retinoic acid receptor antagonist to promote cardiac specification. As well as an increase in efficiency, authors reported an increased cardiomyocyte population of the ventricular sub-type thought to be influenced by retinoid signalling (Zhang et al., 2011).

Currently, there is single method that has proved to be superior. Efficiency of differentiation, proportion of cardiomyocytes within beating clusters, cardiomyocyte functionality and scalability of the method are parameters that would all ideally be met in one protocol. Cell line variability and culture conditions of hPSC prior to differentiation make direct comparison of differentiation methods difficult. A summary of differentiation methods can be found in figure 1.1.

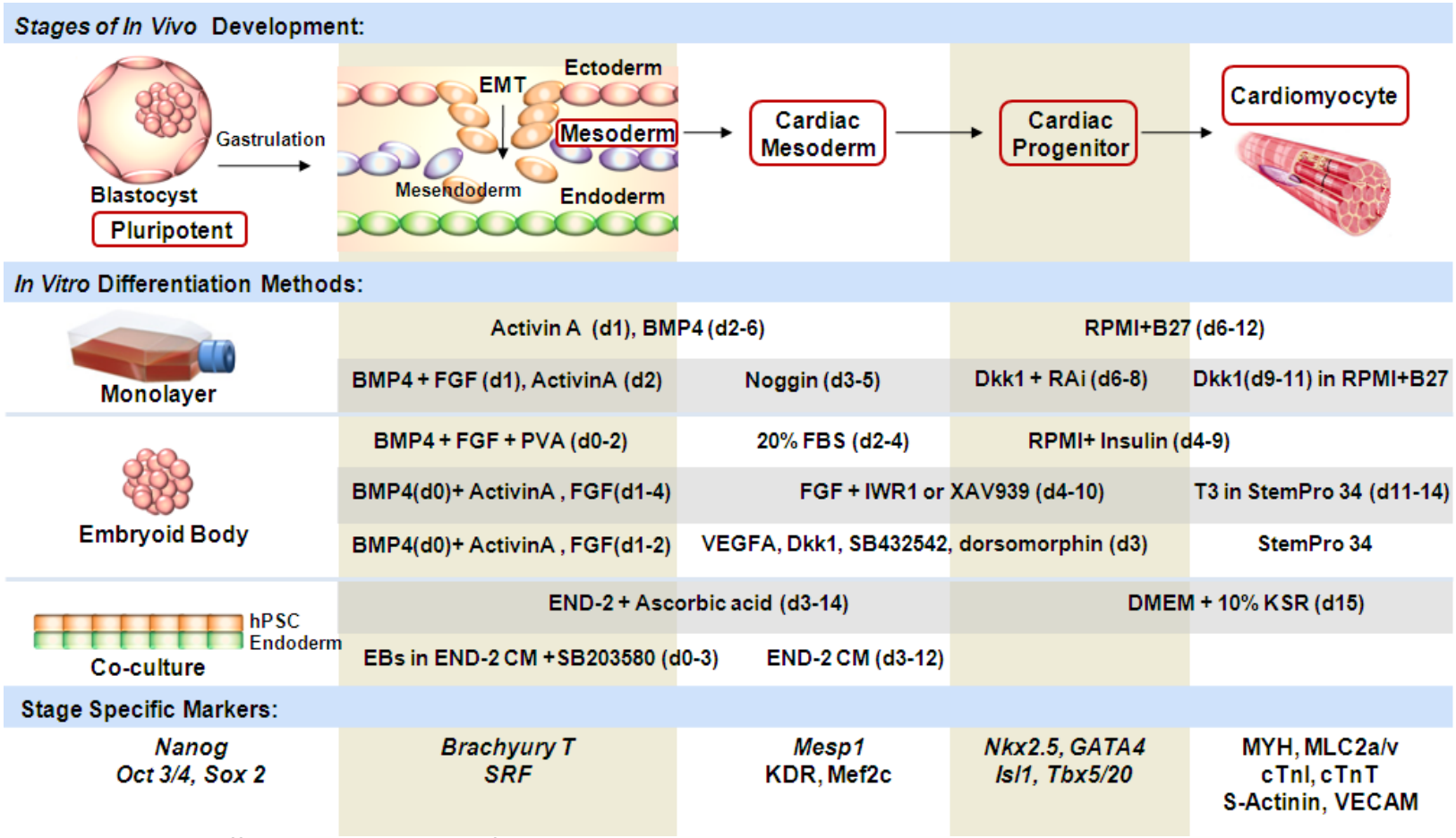


Figure 1.1 Cardiac Differentiation Methods of Human Pluripotent Stem Cells

Developmental knowledge on stages of *in vivo* cardiomyogenesis has aided design of *in vitro* differentiation strategies using various signal inducer/inhibitors. Bone morphogenic protein4 (BMP4), fibroblast growth factor (FGF), dickkopf homolog 1 (Dkk1). Activin/Nodal inhibitor: SB432542. BMP signal inhibitor: dorsomorphin. WNT signal inhibitors IWR-1 and XAV939. Vascular endothelial growth factor A (VEGFA). Thyroid hormone: Tri-iodothyronine, T3. Stages of differentiation can be confirmed by the presence of markers shown at the bottom of the figure, full names can be found in the glossary.

1.3. CHARACTERISTICS OF HUMAN CARDIOMYOCYTES

Macroscopically, the heart can be divided into three regions; the outer epicardium, the inner endocardium which lines the chambers and the middle myocardium which makes up the bulk of the heart and is where the contractile force of the heart is generated. The myocardium is composed of cardiomyocytes, cardiac fibroblasts, nerve cells, smooth muscle and endothelial cells. Similar to other muscle cells, cardiomyocytes contain bundles of myofibrils which are an arrangement of contractile proteins that actuate the pumping mechanism of the heart (Cooper 2000). Fibroblasts are integral for synthesis and turnover of extracellular matrix (ECM). The structural integrity of the heart is increased by smooth muscle and endothelial cells (Banerjee et al., 2006).

1.3.1. Ultrastructure

Contractile Proteins

Myofibrils are made up of contractile units termed sarcomeres and make up approximately 50% of the cell volume, the remainder consists of mitochondria, nucleus, sarcoplasmic reticulum (SR), and the cytosol. Contractile proteins make up about 80% of the myofibril, with the remainder being regulatory and structural proteins (Opie, 2004). Immunostaining of contractile proteins including myosin light chain (MLC-2), sarcomeric α actinin (s-Act) and cardiac troponin I (cTnI) enable visualisation of myofibril alignment by highlighting the A bands and Z lines of the sarcomeres (fig.1.2) (Zhang et al., 2009). Cardiomyocytes from adult human biopsy show that the cells have a rod shaped morphology with myofibrils that are well aligned throughout the length of the cardiomyocyte highlighted in figure 1.2 (Drouin et al., 1995, Mummery et al., 2003, Bird et al., 2003). In contrast fetal human cardiomyocytes are multi-angular and display discrete regions of myofibril alignment but is not uniform throughout the cell (Mummery et al., 2003). Immunostaining of hPSC-cardiomyocytes show morphology and myofibril organisation akin to that of the fetal cardiomyocyte (Gherghiceanu et al., 2011). Over prolonged *in vitro* culture (>60 days) myofibril alignment has been shown to improve when in clusters of cells (Snir et al., 2003,

Lundy et al., 2013). However, single isolated cardiomyocytes lose myofibril organisation over time (Bird et al., 2003).

T tubule System

T-tubules are invaginations of the membrane occurring regularly near Z-lines (Driesen et al., 2007, Kostin et al., 1998, Nelson and Benson, 1963). The system is undeveloped in hPSC-cardiomyocytes which is of significance because ion channels such as L type Ca^{2+} channels, the Na^{+}/Ca^{2+} exchanger and adrenergic receptors reside in the T-tubules, its absence may contribute to lack of ion current density and pharmacological response (Guo et al., 2013).

The ryanodine (RyR) receptors are closely associated with the T-tubules. Punctate immunostaining of RYR2 can be seen in the cytosol and in the peri-nuclear region of hPSC-cardiomyocytes (Itzhaki et al., 2011b). Unlike the highly localised staining observed at Z-lines in adult mouse ventricular cardiomyocytes (Escobar et al., 2011).

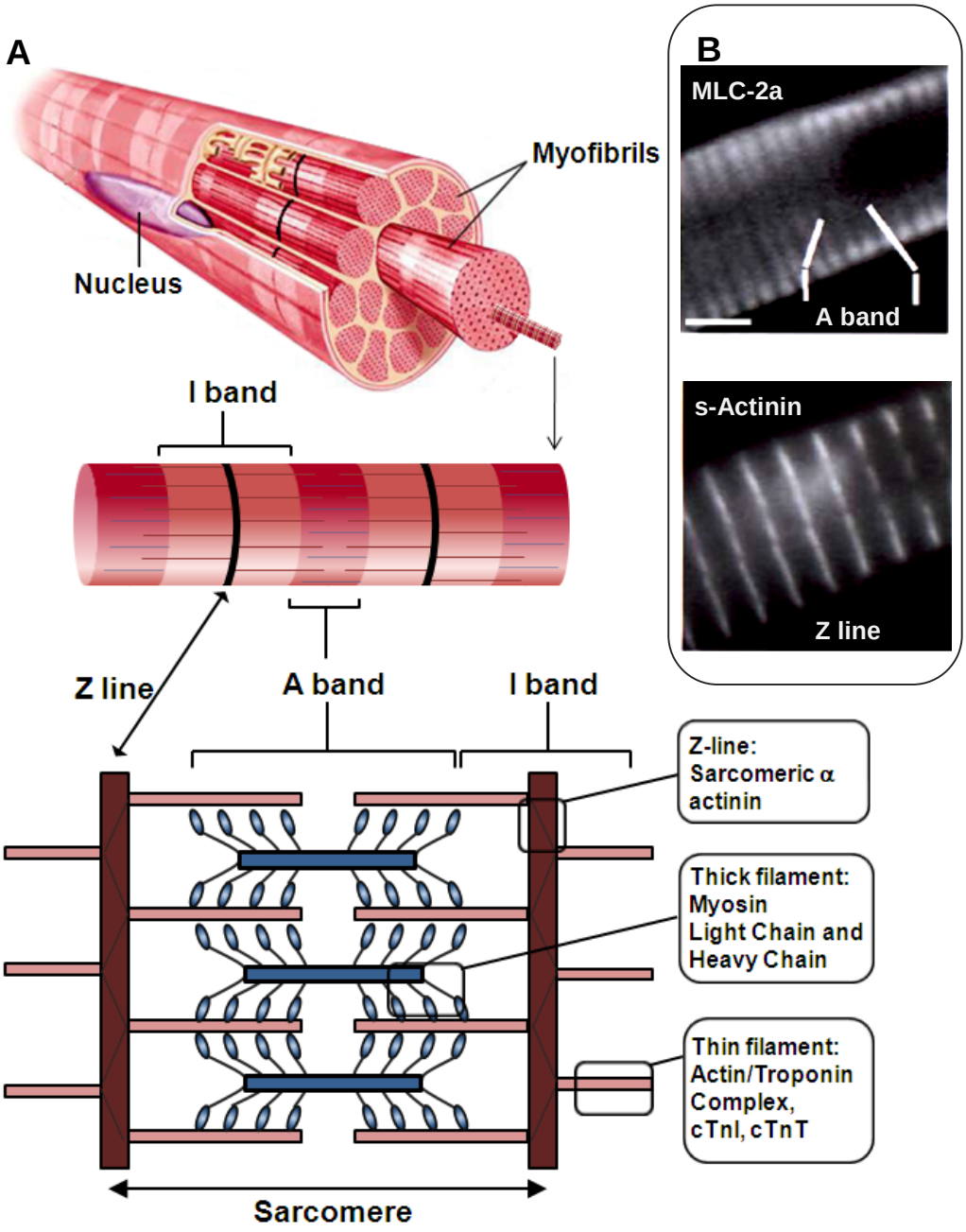


Figure 1.2 Ultrastucture of Myofibril Contractile Proteins
(A) The contractile unit of the myofibril is the sarcomere which consists of actin and myosin cross-bridging. *Adapted from Iaizzo 2009.*(B) Immunostaining of Myosin Light Chain – 2 atrial and sarcomeric alpha actinin in human adult cardiomyocyte*, taken from Bird et al, 2003.*

1.3.2. Electrophysiology

The regulation of contraction in the cardiomyocyte is a membrane depolarisation from a negative resting membrane potential to a more positive potential initiated by the movement of ions. Once the threshold potential is reached a full action potential is triggered, the change in membrane polarity opens voltage gated calcium channels leading to an influx of Ca^{2+} ions which bind to troponin C to initiate a conformational change in the troponin complex and generate physical contraction (Barnett, 2005).

Action Potential Profile

Cardiomyocytes derived from hPSCs consist of a heterogeneous population of ventricular, atrial or nodal sub-types (Braam et al., 2009). They can be distinguished by their action potential profile. Each sub-type has a distinct profile due to the varying presence varying ionic currents (fig.1.3).

The plateau of the ventricular action potential (phase 2) is prolonged due to a sustained inward calcium current (I_{Ca}) through L-type Ca^{2+} channels and maintenance of potassium via a slow outward K^+ current (I_{KS}), an inward rectifier current (I_{K1}) and rapid delayed rectifier current, I_{Kr}, (conducted by hERG channels) (Sanguinetti and Tristani-Firouzi, 2006, Schram et al., 2002). This delayed repolarisation means that, *in vivo*, the ventricle is refractory to premature excitation thereby preventing fatal ventricular arrhythmias (Sanguinetti and Keating, 1997). A shortening or lengthening of this plateau phase by external agents indicates interference of this mechanism. Ventricular cardiomyocytes are therefore useful early indicators of pro-arrhythmogenic compounds. The nodal sub-type has a highly active I_f current necessary for its pacemaker function that enables action potential to be triggered at a lower threshold (Verkerk et al., 2007).

Action potential profiles from ventricular hPSC-cardiomyocytes are immature and comparable to fetal cardiomyocytes as determined by the following parameters; **1.** Upstroke velocity at phase 0 is slow, **2**. Resting membrane potential is at phase 4 is more positive, **3**. Amplitude is smaller (see chapter 4). Similar to myofibril organisation, hESC-cardiomyocytes display a degree of electrophysiological maturation with increasing time in *in vitro* culture

indicated by hyperpolarized resting potentials, increased action potential amplitudes, and faster upstroke velocities (Lundy et al., 2013).

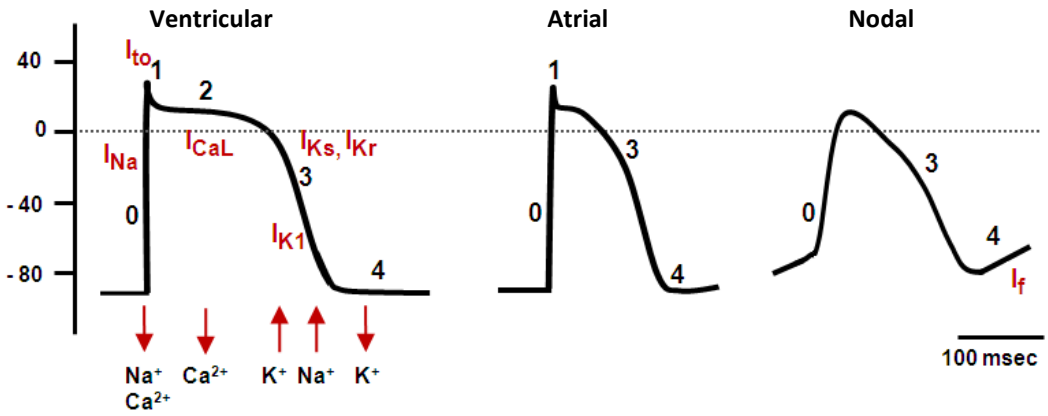


Figure 1.3. Model Subtype Action Potentials and Major Contributing Ionic Currents. The sodium current I_{Na} is a major contributor to the upstroke velocity during depolarisation (phase 0). Sustained calcium current through L type Ca channels (I_{CaL}) maintains the plateau phase (2). Repolarisation (3)outward K current. A hyper-polarised resting membrane potential at phase (4) is maintained by action of I_{K1} in ventricular and atrial cardiomyocytes. However, the I_f current is prominent at phase 4 in nodal cells. Downward arrow represents inward movement of ions. *Adapted from Lieu et al 2012 and Schram et al 2002.*

Excitability

Atrial and ventricular cardiomyocytes are autonomically innervated allowing for chronotropic and inotropic regulation; spontaneous excitability of these cells is not normally exhibited *in vivo* (Iaizzo, 2009, Satin et al., 2004). However, *in vitro* hPSC-cardiomyocytes of all sub-types have displayed spontaneous contraction. The mechanism of this excitability was investigated by Satin and colleagues who found that a lack of inward rectifier potassium (Kir) channel contribution to the I_{K1} current creates a more positive resting membrane potential (RMP) that allows an action potential to be triggered (Satin et al., 2004). Consistent with these findings, spontaneous excitability was abolished in hESCs that were forced to express of Kir2.1 (Lieu et al., 2013). The authors also acknowledged high activity of the I_f current, contributes to spontaneous excitability, although to a lesser extent. The ventricular myocardium of the

developing fetal heart undergoes a concomitant increase in I_{K1} and reduction in I_f current density (Nass et al., 2008). Sartiani *et al*, found that prolonged culture of hESC-cardiomyocytes over 90 days, mimicked this pattern (Sartiani et al., 2007).

Conflicting reports for electrophysiological properties of cardiomyocytes derived from either human embryonic or induced pluripotent cells exist. One study found comparable beat rate and expected pharmacological response to positive and negative chronotropic compounds (Mandel et al., 2012). In another study, calcium transients were found to be significantly smaller in hiPSC-cardiomyocytes compared to hESC-cardiomyocytes due to under-developed sarcoplasmic reticulum (Lee et al., 2011). Whereas, Sheng and colleagues found no such difference but reported a significantly higher sodium current in hiPSC-CMs during prolonged culture which did not occur in hESC-CMs and subsequently had a markedly different response to lidocaine (Sheng et al., 2012). This highlights the need for validation of cardiomyocytes regardless of source, before they can be used as investigational tools.

1.3.3. Cardiomyocyte Maturation

Cardiomyocytes derived *in vitro* from hPSCs are functionally immature (see table 1.1) but capable of maturing as shown by prolonged time in culture (Lundy et al., 2013). More controlled strategies to mature include addition of soluble factors to the culture medium (Lee et al., 2010), genetic engineering (Lieu et al., 2013), manipulation of the culture substrate, mechanical loading (Tulloch et al., 2011) and electrical stimulation.

Serum is often added to culture medium and contains a milieu of growth promoting factors. Some individual components have been identified to play an important role in cardiogenesis and scattered reports have cited various compounds including insulin-like growth factor, vitamin D3 and thyroid hormone as being important regulators of maturation (Engelmann et al., 1989, Pantos et al., 2004, Nibbelink et al., 2007). Mixtures of mesodermal cells

including fibroblasts, smooth muscle and endothelial cells may be co-cultured to achieve optimal results which may be due to lay down of ECM by fibroblasts, paracrine factors or cell to cell contact (Dimarakis et al., 2006).

Nunes *et al*, engineered a 'biowire' device. This consisted of surgical sutures that were capable of being electrically stimulated using platinum wires. The cardiomyocytes, along with other supportive cells such as fibroblasts and smooth muscle cells, were seeded onto the suture using a mixture of collagen I and Matrigel. Stimulated cardiomyocytes displayed more organised Z-line banding and electrophysiological measurements found a greater density of IK1 in stimulated cells (Nunes et al., 2013).

Taylor *et al* (2000) found that substrates can alter cellular response to its environment. The authors provoked maturation of neonatal rat ventricular cardiomyocytes using phenylephrine. This maturation was indicated by increased volume and myofibrillar protein content. The response to phenylephrine-induced maturation was absent when the cardiomyocytes were cultured on gelatin but present when they were cultured on fibronectin or laminin (Taylor et al., 2000), suggesting that cell signalling responses to soluble factors can be disrupted by the culture substrate.

A study by Young *et al* 2011, aimed to improve cardiomyocyte maturation by altering substrate stiffness in a time dependent manner to mimic *in vivo* developmental changes in stiffness observed in chicken myocardium, which undergoes a 9-fold increase in stiffness during ontogeny. Collagen I coated hyaluronic acid (HA) gels which were cross linked with poly(ethylene glycol), stiffened from 1.9 to 8.2 kPa over 70 hours Chicken embryonic heart cells were reported to display a higher degree of myofibril alignment compared to polyacrylamide hydrogels that did not stiffen over time (Young and Engler, 2011).

Table 1.1 Characteristics of Mature Vs Immature Human Cardiomyocytes
Below are characteristics that can be measured to quantify maturity of hPSC-cardiomyocytes. Those derived in vitro resemble values in the immature column.

Characteristic	Mature	Immature	References
Upstroke velocity (Vmax)	150-350V/s	5-50V/s	Braam *et al*. 2009 Satin 2004 Mummery2012
Amplitude	110-120mV	70-90mV	Mummery *et al*. 2012
T- tubule system for calcium handling.	Present, indicated by expression of ryanodine receptors	Undeveloped/ Low incidence.	Liu *et al*. 2007 Dick *et al*. 2010 Snir *et al*. 2003 Iaizzo 2009
Inward rectifier potassium (Kir) channels	Present. Indicated by Ik1 current in action potential	Reduced– may be driver for spontaneous action potential.	Satin *et al*. 2004 Ehrlich *et al*. 2008 Liang *et al*. 1999
Sarcomeric structure.	Parallel bundles of sarcomeres.	Disorganised myofibrils	Vidarsson *et al*. 2010 Sanger *et al*. 2005
Sarcomere Length (µm)	1.8 – 2.5	< 1.7	Rhee *et al* 1994 Gordon *et al* 2000.
Approx. Cell Size (µm)	120 x 20 (7:1, length: width)	25 x 10	Snir *et al*. 2003 Del Monte *et al*. 2002 Harding *et al*. 2007
Shape	Rod	Multiangular	Kuo *et al*. 2012
Maximal diastolic (resting) potential	-85mV	-40mV	Braam *et al*. 2009
Structural Proteins	MLC2v high MLC2a Low	MLC2v low MLC2a High	Mummery *et al*. 2012
Dose response to adrenergic stimulation.	Present	Less sensitive. Similar to adult failing heart.	Brito-Martin *et al*. 2008 Harding *et al*. 2007
Metabolism type	Low Glucose High Fatty Acid	High Glucose Low Fatty Acid	Mummery *et al*. 2002

1.4. SUBSTRATES FOR *IN VITRO* CELL CULTURE

In an *in vitro* system, the culture substrate is important due the role it plays in cell adhesion, survival, morphology and functional maturity of cardiomyocytes.

Tissue culture polystyrene (TCP) has become one of the most commonly used substrates for cell culture. It first became popular in the 1970's providing a substantial improvement for cell attachment compared to the glass surfaces that were used previously (Ryan, 2008). However, to allow adhesion of more fastidious cells types including hESCs, cardiomyocytes and hepatocytes, TCP requires additional surface modification using biological coatings (Woodcock and Matkovich, 2005). To facilitate adhesion, cells may lay down their own extracellular matrix (ECM), a milieu of proteins that the cells adhere to *via* integrin mediated binding (Frisch and Ruoslahti, 1997). Based on the supportive role fibroblasts play in the heart, ECM was obtained from mouse cardiac fibroblast cells (cardiogel). The substrate appeared to support more mature differentiation of mESC derived cardiomyocytes compared to Matrigel indicated by greater hypertrophy and myofibrillar organisation. The authors cited the increased stiffness of cardiogel compared to Matrigel™ as being one of the promoters for this maturation (Baharvand et al., 2005, VanWinkle et al., 1996).

Matrigel™ is ECM that is extracted from murine Engelbreth-Holm-Swarm sarcoma cells (Kleinman et al., 1982). This matrix consists of macromolecules such as laminin-111, collagen IV, enactin and heparin sulphate and various other uncharacterized soluble factors including the growth factors TGF β1 and FGF (Xu et al., 2001, Rodin et al., 2010). Any xeno-derived biological substrate is subject to batch to batch variation and vulnerable to contamination, as seen in 2007 when several lots of BD Matrigel™ were infected with the lactate dehydrogenase elevating virus (Nagaoka et al., 2010). This highlights the need for elimination of xenogeneic products both in substrate and culture media.

Isolated proteins found in the ECM, including laminin, fibronectin, collagen or gelatin (hydrolysed collagen) are also used as more defined alternatives to whole ECM (Rodin et al., 2010) and commonly used for

cardiomyocyte culture. During cardiac development, undifferentiated human cardiomyocyte progenitor cells (CPCs) were found to express collagen I, III, IV and fibronectin which increased during differentiation. In addition, elastin is produced which was not detected in undifferentiated cells (Bax et al., 2012). Elastin has therefore gained interest as a potential culture substrate for cardiomyocytes. Annabi *et al*, cross-linked synthetic human tropoelastin (a major component of elastin), with methacrylate to improve mechanical properties and stability which then enabled surface topography to be manipulated. Neonatal rat cardiomyocytes aligned to a greater extent than methacrylate only gels. However, the gels required pre-conditioning with media, which contains 10% FBS, for 16 hours prior to cell seeding (Annabi et al., 2013b, Annabi et al., 2013a) so although the underlying substrate is a defined, human protein, xenogenic serum components were still required to facilitate adhesion.

Defined biological substrates, although an improvement to undefined mixtures, remain vulnerable to batch to batch variation and contamination issues. In addition, biological coatings can exert an uncontrolled exogenous influence on cardiomyocyte function that may hinder consistency of data derived from screening assays.

Increasing knowledge of cell adhesion mechanisms is guiding the design of synthetic surfaces modified with specific binding motifs occurring on ECM proteins (Rahmany and Van Dyke, 2012, Derda et al., 2007). For example, Synthemax is the first commercial product to conjugate bioactive components, bone sialo protein and fibronectin, to methacrylate surfaces for hESC culture. The proteins are modified to terminate with an amino acid containing a free amine group in its side chain (e,g Lysine, Ornithine) to allow for conjugation to occur with a free carboxyl group in the methacrylate (Melkoumian et al., 2010).

A fully defined, serum free, system that supported embryonic rat cardiomyocytes was reported by Das *et al* in 2004. Cells were plated on a glass slide coated with N-1 (3-(trimethoxysilyl) propyl) diethylenetriamine (DETA) in serum-free medium survived for more than 8 weeks *in vitro* and maintained their contractile and electrophysiological properties. However, no comparison studies

were performed to assess the suitability of the surface in terms of numbers of cells adhered or functional maturity against control cells (Das et al., 2004).

Synthetic non-biological substrates are necessary for reproducible cell culture because they not associated with the inherent variability of biologically derived substrates. They are more amenable to controlled modifications (Abraham et al., 2009). Such modifications may be tailored to the cell type. Some of the physicochemical properties that can be manipulated for improved cell culture are discussed ahead. In addition, synthetic surfaces are more economical for scalable culture as their shelf life and cost is not as limiting as biological substrates.

1.4.1. Physicochemical Properties of Culture Substrates

Stiffness

Substrate stiffness has reported to be important for the culture of cardiomyocytes. Human myocardium stiffness ranges from 10 kPa at the beginning of diastole to 500 kPa at the end (Venugopal et al., 2012) which is substantially more compliant than tissue culture polystyrene, which is 1-2 GPa (Kolahi et al., 2012). Many studies have therefore investigated manipulating the stiffness of the culture substrate in order to improve *in vitro* propagation of cardiomyocytes. Manipulation of substrate stiffness is usually achieved by modifying the cross-linking density of a polymer (Ross et al.).

Jacot *et al*, found that optimal sarcomere alignment of neonatal rat ventricular cardiomyocytes occurred on collagen coated polyacrylamide (PA) gels with a stiffness of 10 kPa compared to softer (1 kPa) or stiffer (50 kPa) gels after 7 days of culture. Greater force generation and development of calcium stores was also noted (Jacot et al., 2008). Similar to Engler et al, who found optimum myofibril alignment of quail cardiomyocytes on 11kPa collagen I coated PA gels compared to 1 or 34 kPa gels. On a softer substrate, the cardiomyocyte does less work to shorten during contraction thereby exerting less force on its neighbouring cells and reducing mechanical loading (Engler et al., 2008). Stiffer

substrates, similar to fibrotic cardiac tissue post-infarct, will cause myocytes to hyper-strain resulting in loss of function due to a reduction in striated myofibrils (Young and Engler, 2011). Increased contractility, higher intracellular calcium and longer sarcomere length was exhibited in neonatal rat cardiomyocytes cultured for 5 days on fibronectin coated polydimethylsiloxane (PDMS) substrates that had a stiffness of 15 kPa compared to 3, 8 or 10 kPa (Rodriguez et al., 2011).

A stiffer range of laminin coated PDMS gels (7, 27, 117 and 255 kPa) was investigated by Galie *et al*. Adult rat ventricular cardiomyocytes maintained well organised sarcomeres only on the stiffest (255 kPa) and most complaint (7 kPa) gels after 48 hours of culture (Galie et al., 2013).

Topography and Patterning

A more mature phenotype of cardiomyocytes cultured *in vit*ro can be encouraged by micro or nanoscale engineering of topography (Wang et al., 2011). Microgrooved PDMS, coated in fibronectin, was found to align hiPSC-cardiomyocytes and resulted in greater myofibril organisation compared to non-patterned PDMS. Faster calcium transients was also observed in cardiomyocytes which was determined to be due to improved Ca^{2+} release from sarcoplasmic reticulum shown by enhanced released in response to caffeine. However, there was no difference observed in electrophysiology determined by action potential morphology (Rao et al., 2012).

Micropatterning of ECM proteins has also shown to encourage rod shaped morphology and myofibril alignment(Feinberg et al., 2012). Kuo *et al*, micropatterned fibronectin on PDMS in varying length to width aspect ratios which all occupied 2500 μm^2 to limit adhesion to one cardiomyocyte per patterned area. Neonatal rat cardiomyocytes displayed contractile function which correlated with shape; faster calcium transients and optimal sarcomere organisation were observed on fibronectin that had aspect ratios between 5:1 to 7:1 compared to higher (>9:1) or lower (<3:1) ratios (Kuo et al., 2012). This is not surprising as adult cardiomyocytes have been shown to have a length to width ratio of 7:1 (see table 1.1).

Surface Chemistry

The investigation of the effect of surface chemistry on cardiomyocyte culture is limited. The studies that have attempted to uncover the influence of chemical modification have done so with a small number of surfaces. For example, glass coverslips were functionalised with mercaptoundecanoic acid and mercaptoundecanol to provide comparison of carboxyl and hydroxyl presenting surface chemistry, respectively. It was found that the number of attached embryonic rat cardiomyocytes and beating cells was significantly lower on hydroxyl surfaces than carboxyl surfaces. The authors also noted an increased action potential duration of beating cardiomyocytes on hydroxy surfaces which requires further investigation that was not carried out (Natarajan et al., 2008).

Ikonen *et al*, evaluated six nanofiber hydrogels that were modified to present multiple different chemistries to study attachment of hESC-and neonatal rat cardiomyocytes (NRCs) compared to 0.1% gelatin control substrate. Four substrates supported attachment of NRCs whereas only two of the six surfaces supported attachment of hESC-cardiomyocytes comparable to control. The chemistries were not reported to be chosen based on prior knowledge of cardiomyocyte behaviour. Ultrastructural or functional comparisons were not reported (Ikonen et al., 2012).

Cell adhesion to different surfaces is mediated by cell adhesion to proteins that are adsorbed onto the surface. A study by Keselowsky et al, functionalised gold coated glass slides with alkanethiols presenting different chemical moieties; CH_3, OH, COOH and NH_2. The surfaces were conditioned with fibronectin (Fn) prior to seeding with MC3T3 cells, an osteoblast cell line. Using integrin specific antibodies they found that surface chemistry modulated the integrins displayed by the adsorbed fibronectin. Cell adhesion was greatest on OH > COOH = NH_2 > CH_3 which correlated to integrin $\alpha_5\beta_1$ display which also followed this order, suggesting that the conformation of fibronectin is altered by surface chemistry (Keselowsky et al., 2003). As well as cell density, fibronectin adsorption has also been reported to influence cell area (Seo et al., 2013).

Relying on the adsorption of culture medium proteins onto synthetic surfaces for cell adhesion is limited by poor reproducibility due to uncontrolled deposition that may create a non-uniform substrate and desorption during culture (Dawson et al., 2008).

As well as cell adhesion, surface chemistry has been reported to alter signalling pathways within cells to guide stem cell differentiation. Human mesenchymal stem cells (MSC) were cultured on glass slips functionalised with CH3, NH2, SH, OH and COOH groups. It was found that control and –CH3 surfaces maintained the MSC phenotype. The NH2 and SH modified surfaces promoted and maintained osteogenesis both in the presence and absence of biological stimuli; And the OH and COOH modified surfaces promoted and maintained chondrogenesis again both in the presence and absence of biological stimuli (Curran et al., 2006).

Surface chemistry therefore plays an important role in cell adhesion, morphology, promotion and maintenance of phenotype. However, the number of chemistries available to study is vast and little is known about which chemistries should be favoured over another and for what purpose. For these reasons discovery of new materials has been slow. The next section describes methods to expedite this discovery process.

1.5. SYNTHETIC MATERIALS DISCOVERY

The transition of high through put assays from a traditional drug discovery setting to that of polymeric microarrays for interrogating cell substrate behaviour has gained steady interest (Anderson et al. 2004, Flaim et al. 2005, Ayala et al. 2011, Zhang Bradley2013) and can be applied to both hypothesis driven screening and more importantly, to identify novel interactions in research areas where progress is restricted by limited knowledge of the relationship between the material and biological processes (Kell and Oliver, 2004).

To improve the reproducibility and reliability of cell culture, a move towards developing non-biological synthetic substrates is being pursued for many valuable cell types using parallel screening strategies. The suitability of high throughput investigation of materials for cell behaviour was demonstrated in 1998 by Brocchini *et al.* The authors screened fibroblast proliferation on 115 different polyarylates co-polymers, based on a combination of 14 diphenols and 8 diacids, and found a range of responses that was comparable to TCP to complete absence of proliferation (Brocchini et al., 1998).

Nano-litre scale synthesis of arrayed biomaterials and its application to human embryonic stem cell culture was first described by Anderson *et al* in 2004. Combinatorial chemistry allowed a library of 576 diverse polymers to be generated from 24 acrylate monomers (Anderson et al., 2004). This study demonstrated the use of a high throughput platform for the study of substrate interaction with clinically relevant cell types.

Polymer microarrays have subsequently led to the use of polyacrylates for the propagation of hESCs in defined conditions. N-(3-Aminopropyl) methacrylamide hydrochlorid was scaled up to coat the bottom of a 12 well plate and was able to support culture of hESCs in defined medium, mTeSR1, over 20 passages. Pre-conditioning of the surface was not required however, the medium contained bovine serum albumin (BSA) which the authors believed was crucial for attachment (Irwin et al., 2011).

Hepatocytes have the potential to provide more relevant metabolic models for *in vitro* drug screening assays. However, hESC derived hepatocytes can be phenotypically unstable. Hay *et al*, used microarrays consisting of 380 polyurethanes and polyacrylates to screen for substrates that would maintain hepatic function. Six polymers were selected based on cell adhesion. Hepatic function was then assessed by gene expression and drug metabolism studies.

1.5.1. Parallel Screening Platforms

To assist parallel screening of materials, suitable platforms need to be fabricated. Earlier methods consisted of masking a substrate so that only particular regions were exposed to enable coating of that region with materials of interest (Lowe, 1995). This masking may be done multiple times to protect and uncover regions to be modified with a new type of material. However, the additional masking procedure means that this method of producing arrayed materials is relatively inefficient. The printing of materials allows microarrays to be fabricated using small volumes of material (nano to microlites) to be deposited onto suitable substrates, such as glass slides (Hook et al., 2009). A Several factors need to be taken into account when materials are arrayed onto a substrate. The polymerisation reaction must be relatively facile, differing rheological properties of material solutions may influence their ability to be arrayed and bonding of the polymeric materials to the surface needs to be robust enough to withstand biological interrogation.

Polymerisation Techniques

Free radical polymerisation is an attractive method due to compatibility with many different monomers and versatility of reaction conditions. However, there is little control over molecular weight of the polymer produced or building well defined co-polymers e.g, block co-polymers (Odian, 2004). Controlled radical polymerisation methods include atom transfer radical polymerisation, (ATRP), nitroxide mediated polymerisation (NMP) and reversible addition-fragmentation chain-transfer polymerisation (RAFT) which all require restrictive conditions including specialised catalysts and/or initiators, purification of final polymer and exhibit slower reaction kinetics limiting their use for rapid microarray fabrication (Chiefari et al., 1998, Georges et al., 1993, Wang and Matyjaszewski, 1995).

1.6. THESIS RATIONALE

In order for *in vitro* hESC-cardiomyocytes for pharmaceutical screens and models to be reliably predictive, the culture system requires standardisation. This applies to the culture surface, which currently consists of plastics coated with biological substrates that inherently suffer from batch variation. Non-biological synthetic surfaces are lacking for cardiomyocyte culture and cell-surface interaction is poorly understood to make rational design of surfaces difficult

Chemical properties of the substrate can modify biological responsiveness and in order to investigate the effects of varying surface chemistry on the behaviour of hESC-cardiomyocytes, an *in situ* polymerised microarray platform will be employed. This will allow parallel screening of polyacrylates and polyacrylamides to find materials that support cardiomyocyte culture. In addition, cardiomyocyte response to surface chemistry will be modelling using a mutivariate regression technique to investigate if surface chemistry can predict cardiomyocyte behaviour so that chemistries can potentially be used for rational design of future materials.

CHAPTER 2

Experimental Methods

2.1.1. CELL CULTURE

Cell culture was performed in a type II biological safety cabinet. Medium and enzymes were warmed to 37ºC in a water bath prior to use. Incubation was carried out at 37ºC and 5% CO_2 [Heraeus HERAcell 150].

2.1.1.1. Culture Media

Culture media were sterilised (prior to addition of growth factors) by passing through a 0.2µm filter (VWR: 89004-822). They were stored at 2-4ºC for up to 3 weeks. Table 2.1 lists the composition of media used for cell culture.

2.1.1.2. Human Embryonic Stem Cell (hESC) Culture

Growth and Passage of hESC

Routine culture of the human embryonic stem cell line, HUES7, involved daily medium changes with 5 mL of medium conditioned with mouse embryonic fibroblast cells (hESC-MEF medium) supplemented with 8ng/ml bFGF. The cells were grown on T25, tissue culture polystyrene flasks [NUNC, 163371], coated with Matrigel™ [BD Biosciences: 354234].

Cells were harvested by enzymatic passage; **1**- A T25 flask of cells was washed with 4 mL of PBS [Invitrogen: 14190] and incubated with 0.5 mL of 0.05% Trypsin-EDTA for 1 minute. **2**- The enzyme was quenched with 4.5 mL of hESC-medium and 10 µL taken for a cell count using a haemocytometer. **3-** The cell suspension was centrifuged for 4 minutes at 160 G [SIGMA 3-16 Mid-bench centrifuge; 10270] and the pellet re-suspended in a volume of hESC-MEF medium equivalent to 1 mL per 1 million cells. **4-** A Matrigel™ coated T25 flask was seeded with 1.5 x 10^6 cells (i.e 1.5 mL of cell suspension) and made up to a total volume of 5 mL with hESC-MEF medium. Passage of cells was performed every 48 hours when cells appeared confluent with very few gaps in the monolayer of cells, cell counts were approximately 4 x 10^6 cells at 48 hours.

Table 2.1 Composition of culture media

MEDIUM and USE	COMPONENT	CONC.
MEF-medium: Mouse Embryonic Fibroblast culture.	DMEM (Base)	88 %
	FBS	10 %
	NEAA	1 %
	GlutaMAX	1 %
hESC-medium: Human Embryonic Stem Cell culture. **hESC-MEF medium:** This is hESC medium that has conditioned for 24 hours by MEF cells.	DMEM:F12 (Base)	83 %
	KSR	15 %
	NEAA	1 %
	GlutaMAX	1 %
	β-mercaptoethanol	100 µM
	bFGF	8 ng/ml
DIFF-medium hESC-fibroblast derivation and maintenance.	DMEM (Base)	78 %
	FBS	20 %
	NEAA	1 %
	GlutaMAX	1 %
	β-mercaptoethanol	100 µM
RPMI-PVA medium For initiation of cardiac differentiation.	0.4% PVA in RPMI (Base)	98 %
	ITS	1 %
	Chemically defined lipid	1 %
	1-Thioglycerol	400 µM
	bFGF	6 ng/ml
	BMP 4	20 ng/ml
RPMI-FBS medium For day 2 of cardiac differentiation	RPMI (Base)	80 %
	FBS	20 %
	1-Thioglycerol	400 µM
CM-medium Cardiomyocyte maintenance culture.	RPMI	98 %
	ITS	1 %
	Chemically defined lipid	1 %
	1-Thioglycerol	400 µM

COMPONENT	MANUFACTURER
bFGF: Basic Fibroblast Growth Factor	R&D
β-mercaptoethanol	SIGMA
BMP -4: Bone Morphogenetic Protein (recombinant human)	Peprotech
Chemically Defined Lipids	Invitrogen/Life
DMEM/ F12: Dulbeccos Modified Eagles Medium	Invitrogen/Life
FBS: Fetal Bovine Serum	PAA/Gibco
Glutamax	Invitrogen/Life
ITS: Insulin Transferrin Selenium	Invitrogen/Life
KSR: Knockout Serum Replacement	Invitrogen/Life
NEAA: Non-Essential Amino Acids	Invitrogen/Life
RPMI: Roswell Park Memorial Institute Medium, 1640	Invitrogen/Life
1 – thioglycerol	SIGMA

Matrigel™ coating was performed as follows, using chilled pipettes and vessels throughout; Matrigel was thawed overnight on ice at 2-4ºC, it was then diluted in cold DMEM at 1:100. The diluted Matrigel™ was immediately dispensed into the required culture vessels at a volume of 0.8ml/cm^2. The coated vessels were left either at room temperature for 1 hour or at 2-4ºC overnight to allow the Matrigel™ to polymerise onto the surface. Before use, flasks were washed once with sterile PBS to remove unpolymerised Matrigel™ and warmed to 37ºC.

Mouse Embryonic Fibroblasts (MEF)

MEFs were required to condition hESC medium which was then used to feed hESCs daily. MEFs excrete factors that propagate hESC proliferation and maintain pluripotency. hESC medium was conditioned by adding 25 mL to a 75 cm^2 flask (T75) [NUNC 153732] containing a monolayer of MEFs and incubating for 24 hours. The T75 flask of MEFs could be used to condition medium every 24 hours for 7 days after which they were discarded. The following describes isolation of MEFs from mice to generate a MEF bank and growth of MEFs for hESC-MEF medium supply.

MEF isolation:

MEFs were obtained from the embryos of pregnant type CD1 mice, 13.5 days post-coitus. Pregnant mice were sacrificed by cervical dislocation, the embryo's decapitated and red visceral tissue removed and discarded in a type I BSC. The remainder of the embryo was placed in a 50 ml Universal tube containing PBS and transferred to a type II BSC in the stem cell culture suite. Embryos were then placed in a 90 mm Petri dish containing 5 ml of 0.25% trypsin-EDTA [Invitrogen: 25200-072] and were finely diced using a scalpel. The embryo-enzyme milieu was transferred to a 250 ml container, where the volume of trypsin was topped up to 2 ml per embryo. This was vortexed and incubated in a 37ºC water bath for 5 minutes repeatedly until a uniform cell suspension with minimal tissue clumps was achieved. To quench the enzyme, 4 ml of MEF medium, supplemented with 1 % penicillin and streptomycin (Invitrogen: 15870-

063), was added per embryo. The suspension was vortexed and allowed to stand at room temperature for 1 minute to allow any large tissue clumps to sediment and adipose cells to float to the top. The supernatent in the middle region was transferred to a fresh container and seeded into 175 cm2 tissue culture (T175) flasks [NUNC: 156502] at a density equivalent to 2 embryos per flask which was topped up to 30 ml using MEF medium +1 % pen/strep. The flasks were incubated for 24 hours after which the medium was replaced with fresh MEF medium without antibiotic. Cells were allowed to grow to confluency and then passaged using 3 mL of 0.05% trypsin. After 2 minutes of incubation, enzyme was quenched with 12 mL of MEF medium and centrifuged at 200G for 5 minutes. The pellet was re-suspended in 10 % Dimethyl Sulfoxide [SIGMA: D2650] in FBS using a volume equivalent to 3 mL per T175 and a sample was taken for mycoplasma testing. The cell suspension was portioned into CryoTube vials [Nunc 343958], 1mL per vial. The vials were cryopreserved at -80ºC for 24 hours in an isopropanol cryorack [Thermo Scientific, Nalgene™ 5100-0001] after which they were transferred to liquid nitrogen. A vial was thawed once a week to maintain a regular supply of MEFs.

MEF Growth and Passage for Conditioning Media

A cryovial of MEFs was placed in a 37ºC water bath for 1 minute and then promptly transferred into a tube containing 9 mL of MEF medium. The cell suspension was centrifuged at 200G for 5 minutes and the cell pellet re-suspended in 15mL of MEF medium which was seeded into a T75 flask. The flask was incubated for 48 hours after which the flask was passaged with 1.5 mL of 0.05% trypsin for 2 minutes. The enzyme was quenched with 10 mL of MEF medium and centrifuged as above. The pellet was re-suspended in 45 mL of MEF medium which was seeded into three T75 flasks, 15 mL per flask. The flasks were incubated for a further 72 hours after which they were passaged as above, cells from each T75 flask was seeded into four new flasks totalling a final number of 12 flasks. These flasks were incubated to confluency and then mitotically inactivated using Mitomycin-C (MMC) [SIGMA, M4287] to prevent further proliferation. Briefly, medium was replaced with 5 mL of MEF medium containing 10 µg/mL of MMC and flasks incubated for 2.5 hours. MEF flasks were

washed twice with PBS and then passaged. A sample was taken for a cell count. Cells were centrifuged and re-suspended in a volume equivalent to 10 mL MEF medium per 4.8 x 10^6 cells. The cell suspension was seeded into T75 flasks that had been treated with 0.1% Gelatin for 1 hour to prevent curling up of confluent MEFs. Cells were seeded at a volume of 10 mL per T75. After 24 hours of incubation the MEF flasks are ready to be used for conditioning hESC medium. The flasks are washed twice with PBS and medium replaced with 25 mL of hESC medium that should be harvested and replaced every 24 hours for up to 7 days.

2.1.1.3. hESC Differentiation

Cardiomyocyte Derivation

A sub-confluent (~60% confluency) flask of HUES7 cells was trypsin passaged and the cell pellet re-suspended in RPMI-PVA medium (see table 2.1). To initiate embryoid body formation, an untreated polystyrene 96V-well plate [NUNC, 249662] was seeded with 4,000 cells in 100 µL of medium per well and incubated for 48 hours. Medium was then changed to RPMI-FBS medium and incubated for a further 48 hours. At day 4 of differnetiation, embryoid bodies were transferred to a tissue culture polystyrene 96U-well plate [NUNC, 168136] in 150L of CM-medium per well. The plate was incubated for 4 days and on day 8 of differentiation, 120 µL of medium was exchanged with fresh CM medium. Screening for beating clusters in wells was performed on days 9 and 10.

Cardiomyocyte cluster disaggregation

Beating clusters of cells within differentiated HUSE7 cultures were manually dissected, leaving behind any non-beating regions, and transferred to an eppendorf containing PBS. Clusters were left to settle and then transferred to an eppendorf containing a mixture of 0.05% trypsin and AccuMax [Innovative CellTech, AM105] in a 3:1 ratio and incubated for 8 minutes (with vortexing at 4 minute intervals for 30 seconds). A volume of 250 µL of enzyme was sufficient for 10 beating clusters. The beating clusters may not be completely dissociated after 8 minutes, this was confirmed with gentle pipetting. Large clusters were

allowed to settle and then transferred to fresh enzyme mix to repeat the incubation and vortex process. Meanwhile, the remaining enzyme-cell suspension was quenched with an equal volume of RPMI supplemented with 20% FBS and centrifuged in a microcentrifuge for 2.5 minutes at 295G. A small pellet was visible, the supernatant was gently aspirated off and the pellet re-suspended in a small volume of CM-medium until all clusters were disaggregated and then pooled together and made up to the required volume.

Fibroblast Derivation

The method involves embryoid body (EB) formation by forced aggregation. On day 0 of differentiation, EB formation was initiated by seeding V-96 plates with 4,000 cells/well in MEF conditioned medium and centrifuging at 950g for 5 minutes. EBs were maintained in V-96 plates for 4 days in conditioned medium, and on day 4,were transferred to untreated 90mm petri dishes in 10 mL of cardiac differentiation media (DIFF media, see appendix I). EBs were maintained in suspension for 6 days to allow germ layer formation. On day 10, EBs were transferred to untreated U-96 well plates at a density of one EB/well, in DIFF medium. EBs were cultured in the U-bottom plates for 10 days (this is day 20 of differentiation). EBs were transferred to a 20ml Universal tube and centrifuged at 200g for 5 minutes. Following centrifugation, the supernatant was aspirated and the EBs were incubated with 2 ml of 0.05% trypsin for 3 minutes. The EBs were vortexed, trypsin inactivated with 18ml of DIFF medium and centrifuged once again and supernatant aspirated. EBs were re-suspended in 10ml of DIFF medium, and were transferred to a 90 mm tissue culture polystyrene dish [NUNC: 150350] which was incubated for 4 days to allow EB attachment to the plates. DIFF medium was exchanged every 2 days. After 4 days, the EBs were washed with 10 ml PBS and visible cell clumps were removed by aspiration. Remaining cells were incubated with 1.5 ml 0.05% trypsin for 3 minutes. The trypsin was inactivated with 8.5ml of DIFF medium, and the cells were transferred to a 20ml Universal tube to be centrifuged for 5 minutes, at 200g. The pellet was re-suspended in 5 ml DIFF medium and the cells were seeded into a T25 flask. Once the cells were

confluent, they were passaged and split 1:3. This was repeated to expand cells and then cryopreserved in 10% DMSO for future use.

2.1.2. Cell Seeding on Microarray

Array Preparation

Polymer microarrays were UV sterilised in a type II biological safety cabinet for 15 mins on each side. The array was balanced between two petri dishes to avoid the slide touching the surface of the cabinet. Using sterile forceps the array was placed inside a four well rectangular plate. The array was submerged in 4 mL of PBS for 1 minute and then aspirated off. This was repeated 3 times. To condition the arrays, 4 mL of CM medium (serum free conditions) or 4 mL of CM medium + 20 % FBS was dispensed onto the array and incubated for 1 hour. Prior to cell seeding, the medium was aspirated and 2 mL of CM medium was dispensed onto the array and immediately aspirated off.

Array Seeding

Cardiomyocyte cluster that were approximately 15 days old post-differentiation, were disaggregated as stated above. To seed first generation arrays (115 x 6 polymer spots), approximately 20 beaters were disaggregated and re-suspended in 4 mL of CM medium. To seed second generation arrays (consisting of 576 x 3 polymer spots), 40 beaters were used per slide. Accurate cell counts could not be made using trypan blue because the nuclei could not be seen under the microscope.

2.1.3. CELL ANALYSIS

2.1.3.1. Karyotyping

To capture the maximum number of cells in metaphase, T-flask cultures of HUES7 cells close to doubling time (approx. 24hours post-seeding) were

incubated with 5 mL of 0.1µg/ml of KaryoMAX® Colcemid™ [Invitrogen: 15212012] in hESC-MEF medium for 1h. The KaryoMAX containing medium was then collected in a 30ml universal tube. Remaining cells attached to the T-flask were harvested using 0.05% trypsin-EDTA, and pooled with the KaryoMAX medium. The cells were centrifuged at 300g for 5 minutes and the cell pellet was re-suspendeded drop-wise on a vortex, in 10 mL of 0.6% sodium citrate [Fisher Scientific: S/3320] and incubated at room temp. for 20 min. The cells were then centrifuged at 300g for 5 min, and re-suspended drop-wise in a fixative consisting of 16.7% glacial acetic acid in methanol. The cells were centrifuged and re-suspended in the fixative twice more and finally re-suspended in 1 mL of fixative and stored at -20^{0}C until ready for G-banding analysis. 30 metaphase spreads were analysed for each sample by Mr Nigel Smith (Nottingham City Hospital, UK) in accordance with the International System for Human Cytogenetic Nomenclature International Guidelines (ISCN, 2005).

2.1.3.2. Flow Cytometry

50 beating clusters at day 15 post-differentiation were dissaggregated into a single cell suspension as described in section 2.1.3.2. The final cell suspension was centrifuged at 295G for 2 min [SIGMA 3-16 Mid-bench centrifug] and re-suspended in PBS to wash the cells. Centrifuging was repeated and the pellet re-suspended in 100 µL of 4% paraformaldehyde (PFA) and incubated at room temperature for 15 min after which the suspension was centrifuged at 295G for 2 min. The pellet was washed in PBS and then resuspended in 100 µL of triton X in PBS for 15 min. Centrifuge and re-suspend in 0.1% Tween 20 to wash the cells and centrfuge. Re-suspend in 500 µL of blocking solution; 10% fetal bovine serum (FBS) in PBS for 30 min. Portion half into another eppendorf, to use for controls. Centrifuge both eppendorfs and re-suspend each pellet in 500 µL 0.1% Tween20. Spin at 4000rpm for 2min in the microcentrifuge. Incubate one eppendorf with 1mL of 10 antibody (1:1000, cardiac troponin I raised in rabbit, Spectral Diagnostics; PA-1010) in 10% FBS in PBS overnight at 40ºC and the control with 1mL of 10%FBS only. Repeat spin. Wash the pellet in 0.1% Tween-20 in PBS (500ul). From the control tube portion 250uL for the 20 only control.

Incubate the sample and 20 only control cells with 500ul of 20 antibody (1:1000, anti-rabbit Alexafluor488, Invitrogen) in 10% FBS for 45min at room temperature covered in aluminium foil. Incubate negative control with 10% FBS only. Spin all 3 eppendorfs at 4000rpm for 2min. Wash the pellets 2x in 0.1% Tween-20 in PBS (100ul) and resuspend final pellet in 150ul PBS.

2.1.3.3. Immunostaining

Fix cells in 4 % Paraformaldehyde for 15min at room temp. (RT), wash with PBS x 3. Permeabilise cells for 15min RT with 0.1% Triton X. (10uL in 10mL PBS) followed by3 x 1min wash in PBS. Incubate cells with 4% normal goal serum [Dako] in PBS at RT for 1hr (200uL in 5mL PBS).

Incubate cells with primary antibody in 4% NGS in PBS overnight in fridge (listed below for each cell type). After 24hr: 3 x 10mins washes in 0.1%Tween20 in PBS (10uL in 10mL). Incubate with secondary antibody (and phalloidin in 4% NGS for 1hour at RT if cardiomyocyte). Followed by 3 x 5min washes with 0.1% Tween20 in PBS. Finally, incubate cells with DAPI (Sigma D9542) in PBS (1:1000) for 10mins at RT. Wash cells 1x PBS and mount in plain vectasheild. Seal around coverslip with varnish.

For ion channel staining, the 24 hour incubation was omitted; The first primary staining was for 1 hour at RT, followed by tween wash and then corresponding secondary for 1 hour at RT. After a further tween wash, the next primary body was incubated for 1 hour at RT, followed by final incubation secondary for 1 hour at RT and then DAPI staining as above.

hESC

Primary: Monoclonal anti-Oct3/4, raised in mouse (Santa Cruz; SC-5279). 1:200. *Secondary:* Cy3 conjugated goat anti-mouse (Jackson Imm 115-165-068) 1:250.

Cardiomyocytes

Primary: Monoclonal anti sarcomeric α-actinin, raised in mouse (Sigma A7811). 1:800. *Secondary* is Cy3 conjugated goat anti-mouse (Jackson Imm 115-165-068) 1:250.

Alexa488 conjugated Phalloidin. This is an F-actin marker and is not an antibody, will stain most eukaryotic cells and was used to identify all cells including non-cardiomyocytes. (Fisher VXA12379). 3.3U/mL (Yildirim et al., 2007).

Ion channels

Kir2.1. *Primary:* Kir2.1 raised in rabbit anti-human (Sigma HPA029109), 1:150. *Secondary:* Alexa-fluor488 Goat anti-rabbit.

Actinin: *Primary:* Monoclonal anti sarcomeric α-actinin anti-human, raised in mouse (Sigma A7811). 1:800. *Secondary:* Cy3 conjugated goat anti-mouse (Jackson Imm 115-165-068) 1:250

$Na_v1.5$. *Primary:* (SCN5A) raised in mouse, anti-human (Abcam Ab62388), 1:100. *Secondary:* Cy3 (Jackson Imm 115-165-068) 1:250.

cTnI: *Primary:* Polyclonal Cardiac Troponin I raised in rabbit (spectral diagnostics PA1010), 1:1000. *Secondary:* Alexa488 Goat, anti-rabbit

Fibroblasts

Primary: P4HB (5B5) raised in mouse (Abcam, ab4497971).

Secondary: Alexafluor488, Goat anti-mouse.

2.1.4. Whole Cell Patch Clamp Electrophysiology

Cardiomyocyte clusters were disaggregated as described in 2.1.3.2. and seeded onto 35mm dishes printed with the polymer of interest or 35 mm glass bottomed dishes [MatTek corp, P35G-1.5-14-C] coated with 0.1% gelatin [Sigma, G9391]. Prior to patch clamp analysis, medium was changed to Normal Tyrodes buffer (NaCl, Glucose, HEPES, KCL, $MgCl_2$, $CaCl_2$, adjusted to pH 7.4 with KOH). Glass capillary pipettes of 10cm length and 0.84 mm internal diameter [World Precision Instruments, 1B150F-4] were pulled on a Sutter P-97 micropipette puller to achieve resistances between 2 and 5M Ω when filled with ionic solution

(145 mM KCl, 5 mM NaCl, 2 mM $CaCl_2$, 2 mM $MgCl_2$, 4 mM ethylene glycol tetra-acetic acid, 10 mM HEPES, adjusted to pH 7.3 with KOH). Whole cell recordings were obtained at 37ºC, in normal atmospheric conditions, in current clamp mode using an ECP-10 HEKA amplifier. Data was recorded using the Pulse software (HEKA) and analysed using Clampfit v9.0 (Molecular Devices).

2.1.5. Microarray Fabrication

2.1.5.1. Substrate formation

Glass slides

Epoxy coated glass slides [Genetix] were dip-coated in a 4 % (w/v) pHEMA [Sigma, P3932] in 95 % (v/v) ethanol/water. The pHEMA solution was left in a sonicator for 24 hours to dissolve. For dip-coating, in a laminar flow hood slides were dipped into the pHEMA solution, and withdrawn at a rate of 3 mm/sec, such that the withdrawal rate is ≤ the rate of capillary drainage. Slides were then maintained in a vertical position with each end of the slide resting on a holder for at least 10 min to allow for drainage before being placed into a slide rack and placed in a vacuum oven for 1 hour.

35mm Dishes

A 4 % pHEMA solution was prepared as above, 500 µL was pipetted into a 35 mm tissue culture polystyrene dishes [NUNC, 150318] and left to evaporate in a fume hood for 24 hours.

2.1.5.2. Piezo Printing

First Generation Homopolymer Microarray and 35 mm dishes

Polymer microarrays were formed using an ink-jet printer (*i*) (SciflexarrayerS5, Scienion) with the help of Dr. Andrew Hook. The printer was prepared for printing by flushing with 10 ml wash solution (DMF) at 60 µl/s. Nozzle was then connected to the system and flushed with a further 5 mls of DMF at 10 µl/s. The nozzle used was a 90 µm hydrophobic nozzle. Printing conditions were O_2 1300±300 ppm, 23ºC, 50% humidity, 10 drops per spot, spot

size approximately 200 pL, 500 Hz frequency, 180 V pulse and 47 µs pulse width. The array layout of monomers on this array is shown in fig.3.10. The spacing between spots was 0.9mm in the *x* and *y* axis. This pattern was repeated 6 times on each slide.

Polymerisation solution was composed of 50 % (v/v) monomer in DMF with 1% (w/v) photoinitiator 2,2-dimethoxy-2-phenylacetophenone. An oxygen free atmosphere is important to prevent quenching of free radicals, this was achieved by purging the system with argon at a flow rate of 30 L/min for 1 hr, whereupon the flow rate could then be reduced to 18 L/min. Once formed arrays were dried at <50 mTorr for 7 days. For all arrays the region on the glass slide with no pHEMA coating was kept to the right.

2.1.5.3. Contact Printing

First and Second Generation Homopolymer Array

Polymer microarrays 6.1c were formed using a contact printer (*c*) (Biodot). Printing conditions were O_2<1300 ppm, 25ºC, 40% humidity. Slotted metal pins (946MP8B, Arrayit) with a diameter of 295 µm were used to transfer approximately 4 nL of monomer solution onto 10 substrates before slides were irradiated with a long wave UV source for 10 s. The spacing between spots was 1.125 mm in the *x* and *y* axis. The pattern was replicated 6 times per slide.

Polymerisation solution was composed of 75% (v/v) monomer in DMF with 1% (w/v) photoinitiator 2,2-dimethoxy-2-phenylacetophenone. The argon atmosphere was achieved by purging the system with argon at a flow rate of 35 L/min. Once formed arrays were dried at <50 mTorr for 7 days. For all arrays the region on the glass slide with no pHEMA coating was kept to the right.

2.1.6. Surface Analysis

2.1.6.1. Time of Flight Secondary Ion Mass Spectrometry

ToF-SIMS analysis was carried out using a ToF-SIMS IV instrument (ION-TOF GmbH, Münster, Germany) using a Bi_3^+ primary ion source operated at 25 kV. A 1 pA pulsed primary ion beam was rastered and secondary ions were collected from a 10 × 10 mm area at a resolution of 100 × 100 pixels per mm^2, with 8 ion pulses per pixel. To compensate for a surface build up of positive primary ions, low energy electrons (20eV) were delivered via a flood gun. Data analysis was carried out using Surfacelab6 software.

2.1.6.2. Water Contact Angle Measurement

To measure the wettability of the polymer surfaces a Kruss DSA 100 piezo dropper dispensed a drop of ultrapure water at a volume of approximately 400 pL. Videos were captured for each drop and the contact angle determined retrospectively using the first frame of water contact. DSA3 software determined the contact angle using a circle fitting function.

2.1.6.3. X-Ray Photoelectron Spectroscopy

Emily Smith from the School of Chemistry, University of Nottingham performed XPS analysis on the first generation microarrays using a Kratos Axis Ultra spectrometer using a mono-chromated Aluminium X-ray gun, with a charge-compensating electron flood.

Elemental quantification was achieved using CASA software loaded with the Kratos elemental library. A Tougaard background correction was applied to scans.

2.1.7. Image Acquisition and Analysis

2.1.7.1. Microscopy

Imstar automated platform with an Olympus IX51 microscope was programmed with microarray co-ordinates. ‘Landmarks’ were placed across the

array which are manually set focus points. An auto-offset function was performed so that all fluorescent channels focussed at the same time using one landmark. A x10 objective was used to capture one polymer region per image.

Higher resolution images for myofibril analysis were taken on a Nikon 90i microscope.

2.1.7.2. CellProfiler

CellProfiler v10997 cell image analysis software was downloaded from www.cellprofiler.org.

Primary objects identified were cardiomyocyte nuclei, and given an object size guide of 10 – 38 pixels. A manual thresholding method was chosen and typically set at 0.0075, although this was varied depending on background fluorescence. Object shape was used to distinguish clumped objects and intensity was chosen to draw dividing lines between clumped objects.

Secondary objects were identified using sarcomeric actinin staining. A propagation method was chosen to identify secondary objects based on nuclei input and then draws a dividing line between merged actinin staining which is brighter at the edge of the cell. If this change in intensity is not detected, then the adjacent input primary objects will have a diving line drawn at an equal distance between the two. Thresholding was again manual and was typically 0.003.

A conversion of 0.647 µm per pixel was used to convert pixels to microns for images taken at x10 objective.

2.1.8. Multivariate LINEAR Regression Analysis – Partial Least Squares

To correlate surface analytical data with cell response PLS was carried out using the Eigenvector PLS toolbox 5.2.2 for Matlab using the SIMPLS algorithm (de Jong, 1993). A peak list was generated for the homopolymer array which consisted of 1397 ions and the co-polymer array which consisted of 2023 ions.

Mean centred data pre-processing was applied and a leave one out cross validation was carried out to obtain errors for latent variables.

CHAPTER 3

Screening Of Polyacrylate And Polyacrylamide Surfaces For Cardiomyocyte Culture.

3.1. INTRODUCTION

This chapter sets out to screen polymers of commercially available acrylate and acrylamide monomers for their ability to support hESC derived cardiomyocyte attachment. To enable high throughput screening (HTS) of over a hundred different monomers a microarray format was adopted. This chapter aims to optimise the three key resources required for parallel screening of cardiomyocyte behaviour on the polymers. These are to; **i)** generate cardiomyocytes from hESCs, **ii)** investigate microarray fabrication techniques and **iii)** develop protocols for automated image analysis of cardiomyocyte attachment and morphology.

Finally, monomers that support cardiomyocyte adhesion and spreading, determined by cell density and surface area, will be forwarded for fabrication of a second generation co-polymer array for the purpose of; **i)** increasing the diversity of potential materials available for cardiomyocyte culture, **ii)** investigate if co-polymers of monomers behave in synergy, **iii)** downstream analysis of the relationship, if any, of cardiomyocyte behaviour and surface chemistry. For this purpose, monomers that displayed poor adhesions and/or spreading were also included to enable modelling of positive and negative cell response.

3.1.1. Cardiomyocyte Derivation

As detailed in chapter 1, there are three main methods available for derivation of cardiomyocytes from human stem cells. These include embryoid body (EB) formation, monolayer and co-culture system. The co-culture system was ruled out as a method to use in our HTS format due to a potential risk of contamination of cell cultures with mouse endoderm (END-2) cells and relatively low differentiation efficiencies of 3-20 % that have been reported (Mummery et al., 2003, Graichen et al., 2008). The monolayer method is amenable to scale up for high volume use and avoids laborious dissection of beating clusters that is involved in the embryoid body method but unfortunately the efficiency of cardiomyocyte differentiation in our hands was highly variable making the use of this method impractical at this stage.

Modification of the EB method has increased differentiation efficiency from 10 % (Kehat et al., 2001) to approximately 25% by improving uniformity of embryoid body size (Burridge et al., 2007) to more recently over 90% efficiency by application of stage specific growth factors which direct differentiation towards the cardiac lineage (Burridge et al., 2011). This latest method was adopted for HUES7 differentiation in this substrate screening study.

Cell culture on microarrays requires initial assessment of several parameters; **1.** Cytotoxicity of the arrays. **2.** Sterility of the microarray following UV treatment **3**. Quality of microarray in terms of surface chemistry and robustness during culture. **4.** Seeding with an appropriate number and volume of cells to get distribution on polymers at a density that can be analysed using automated software. To optimise these parameters, fibroblasts derived from hESCs using a modified embryoid body differentiation method were used. Once fibroblasts were derived they could be expanded and cryopreserved so that they could be readily accessed. Cardiomyocytes however, show limited proliferative capacity, and need to be repeatedly derived from hESCs hindering their use for initial optimisation experiments.

The human embryonic stem cell line HUES7 (Cowan et al., 2004) was chosen to derive cardiomyocytes and fibroblasts. This hESC line has been widely reported to generate functional cardiomyocytes (Pal et al., 2009, Matsa et al., 2011). There is also expertise in the culture of this cell line within the lab (Denning et al., 2006).

3.1.2. Polymer Microarrays

3.1.2.1. Array Fabrication

Polymer microarrays provide a high-throughput format for investigation of cell-surface interaction (Anderson et al., 2005, Tourniaire et al., 2006). Nano-litre volumes of monomer can be arrayed into spatially discrete regions on a substrate by techniques including piezo (ink-jet) and contact printing. The former technique ejects a known volume of material through a nozzle and the

latter, dips a solid pin into the material to be deposited (fig. 3.1). Monomers are subsequently polymerised *in situ*.

Piezo printing allows for rapid 'drop in drop' mixing of different monomers enabling rapid fabrication of second generation co-polymer arrays by circumventing preparation of pre-mixed source plates. The wetting behaviour of the monomer solution and nozzle material highly influence droplet formation (de Gans et al., 2004), therefore for monomers with wide ranging hydrophilicities, fabrication of uniformly sized polymer spots across the array may require an adjusted amount of voltage to be applied to the piezo crystals for each material being printed.

Contact printing affords greater control over spot size because it is predominantly the geometry of the pin that determines the size of polymer spot. Viscous solutions are also easier to print (Davies et al., 2010). Both techniques require optimisation to enable reproducible array fabrication of large numbers of polymers printed in discrete and identifiable regions.

To prevent background cell and biomolecule adhesion between polymer spots that may lead to cross-talk, a bio-resistant polymer is used to coat the substrate that is to be printed upon (Hook et al., 2010). Poly(2-hydroxyethyl methacrylate) (pHEMA) is used to make soft contact lenses because of its optical, biocompatible and protein resistant properties (Chen et al., 2010, Holly and Refojo, 1975). This makes pHEMA suitable as a low fouling substrate to coat epoxy glass slides to provide a cell adhesion resistant background (fig.3.1).

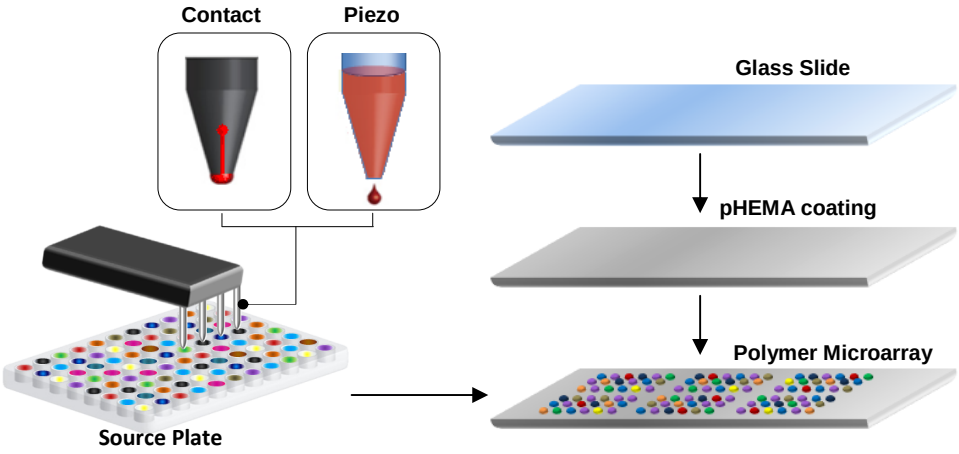


Figure 3.1 Substrate Preparation for Piezo and Contact Printing.
Glass slides (75mmx25mm) are coated with pHEMA to prevent background adhesion of biomolecules and cells. This is subsequently printed upon using contact or piezo printing.

Use of micro-arrayed materials to rapidly identify those permissive for stem cell culture was first described by Anderson *et al* in 2004 and forms the basis of experimental printing conditions employed in this study. Acrylate and acrylamide monomers were mixed with a free radical initiator, 2,2-dimethoxy-2-phenylacetophenone, which induces polymerisation upon exposure to UV light to allow *in situ* microarray fabrication (fig. 3.2).

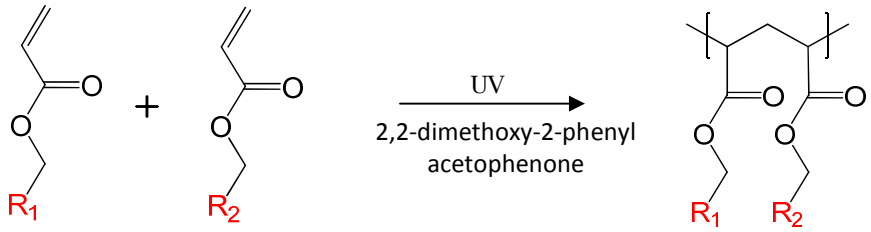


Figure 3.2. Photoinitiated polymerisation of acrylates
Polymerisation of acrylates occurs upon UV exposure *via* free radical photo-initiation. *Adapted from (Fouassier and Rabek, 1993).*

3.1.2.2. Acrylate Library

The utility of acrylate polymers such as polymethyl methacrylate as biomaterials has been demonstrated ranging from contact lenses to bone cements. Therefore, their use as potential cell culture substrates is warranted. As well as ease of polymerisation, they are commercially available with a diverse range of chemistries along the acrylate backbone which may be modified with, for example, fluorine, aromatic groups, glycols, nitrogen, amines, methyl groups (methacrylates) and amides (acrylamides) (fig 3.3) making the materials especially suitable for high throughput investigation of the effects of varying surface chemistry. A full list of monomers can be found in appendix 1.

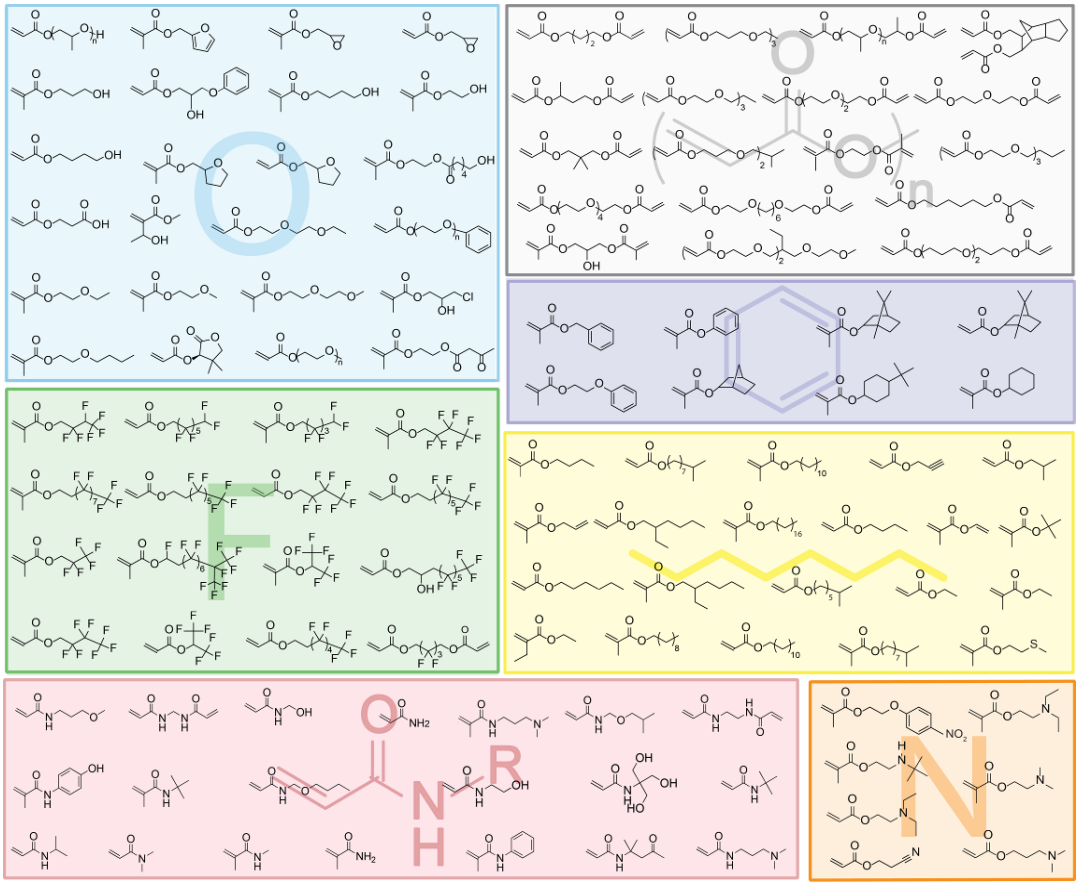


Figure 3.3. Library of commercially available acrylate and acrylamide monomers.
Available monomers in our library consist of (clockwise from top left); oxygen/ glycol monomers (blue region), multiacrylates (grey), aromatics (purple), hydrocarbons (yellow), nitrogen containing monomers (orange), acrylamides (pink) and finally fluorine containing monomers (green region). These are not exclusive groups with overlap in some cases but demonstrates the range of chemistries available. *Adapted from (Celiz et al., 2013).*

3.1.2.3. Chapter aims

1. Differentiate the human embryonic stem cell line HUES7 into cardiomyocytes and fibroblasts and characterise the two cell types to confirm phenotype.

2. Optimise disaggregation protocol of cardiomyocyte clusters and determine morphology of the disaggregated cells on control 0.1% gelatin surfaces.

3. Determine the proportion of cardiomyocytes to other cell types within the population of cells from beating clusters to establish whether cell enrichment is required.

4. Fabricate first generation homopolymer microarrays and characterise surface chemistry using time of flight mass spectrometry (ToF-SIMS) to confirm chemical identity and diversity.

5. Optimise cell seeding and automated analysis protocols for microarrays using fibroblasts initially and then cardiomyocytes.

6. Screen cardiomyocyte attachment and morphology on polymer substrates.

7. Identify monomers to take forward for second generation co-polymer arrays and repeat screening study on second generation array.

3.2. RESULTS

3.2.1. Human Cardiomyocyte and Fibroblast Derivation from HUES7 Embryonic Stem Cells.

3.2.1.1. HUES7 characterisation

Before attempting cardiomyocyte derivation, the pluripotency of the hESCs was assessed by OCT 4 immunostaining which is a transcription factor whose activity confirms potential to differentiate into a variety of cell types (Nichols et al., 1998). An average of 97±4 %,(s.d, n=3) of HUES7 cells expressed OCT 4 (fig 3.4). Chromosomal abnormalities that may affect cellular function was ruled out by a normal 46 XY karyotype (≥ 95% confidence). 30 metaphase spreads were analysed at passage 22, by Mr Nigel Smith. The normal 46 XY karyotype was present in 26 spreads, 4 spreads displayed single deletions of chromosome X, 6, 13, or 17. This low frequency is considered to originate from spontaneous mutations rather than an abnormal cell population.

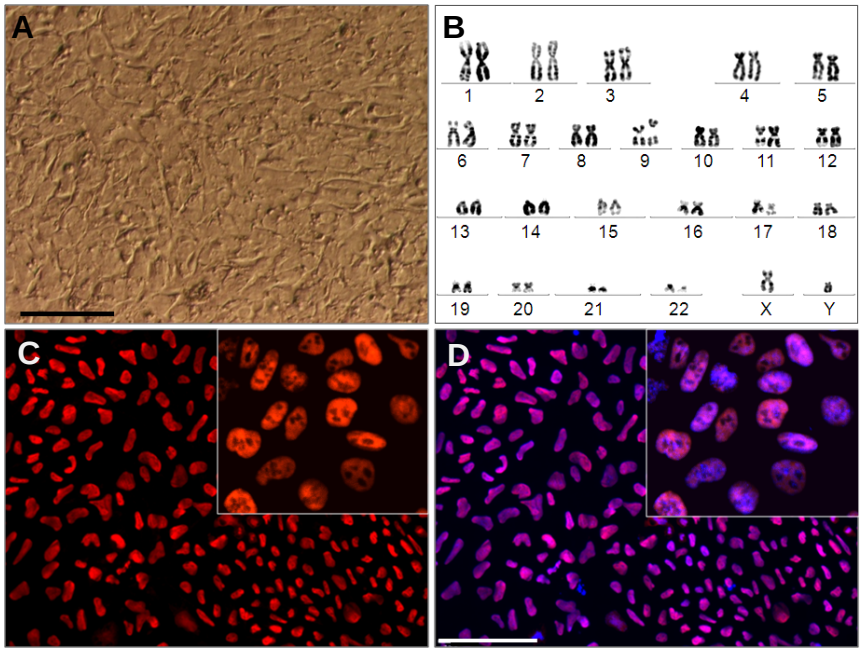


Figure 3.4. Characterisation of the human embryonic stem cell line HUES7.
A) Bright field image of a confluent monolayer of HUES7 cells cultured on Matrigel exhibiting typical morphology. **B)** Representative karyogram shows a normal 46, XY, set of chromosomes. **C)** Presence of pluripotency marker, Oct 4 (red), is confirmed to be present in the nucleus of cells **D)** as shown by overlay with the nuclear marker DAPI (blue). Scale = 100 µm.

3.2.1.2. Fibroblast Characterisation

The characterised HUES7 cell line was then differentiated into fibroblasts. Embryoid body formation began in 96 V well plates. Four days after seeding hESCs into V well plates, uniform spheres termed embryoid bodies (EBs) with typical diameters of 500 µm formed as shown in figure. 3.6. To derive fibroblasts an established 'in house' protocol was followed (see section 2.1) as shown in figure 3.6.ii.

A characteristic elongated cell morphology was observed for the derived fibroblasts (fig 3.5). Immunostaining for the fibroblast specific antigen, P4HB, was used to confirm identity and homogeneity of the population of cells. An average of 76±9 % (s.d, n = 3) of cells expressed P4HB.

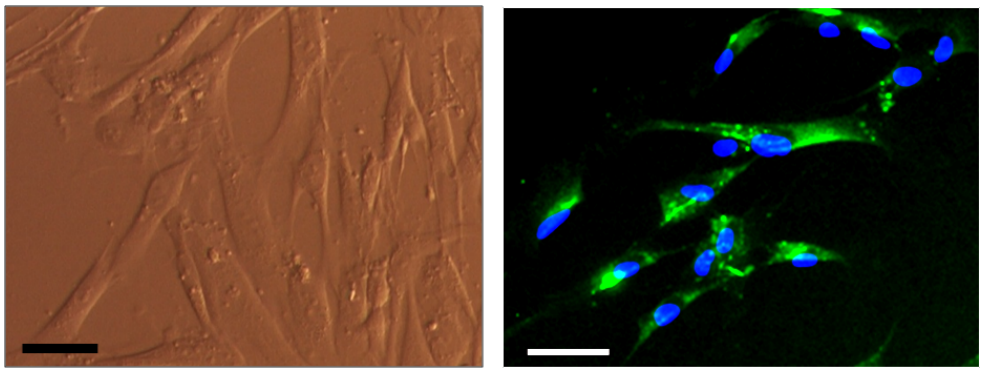
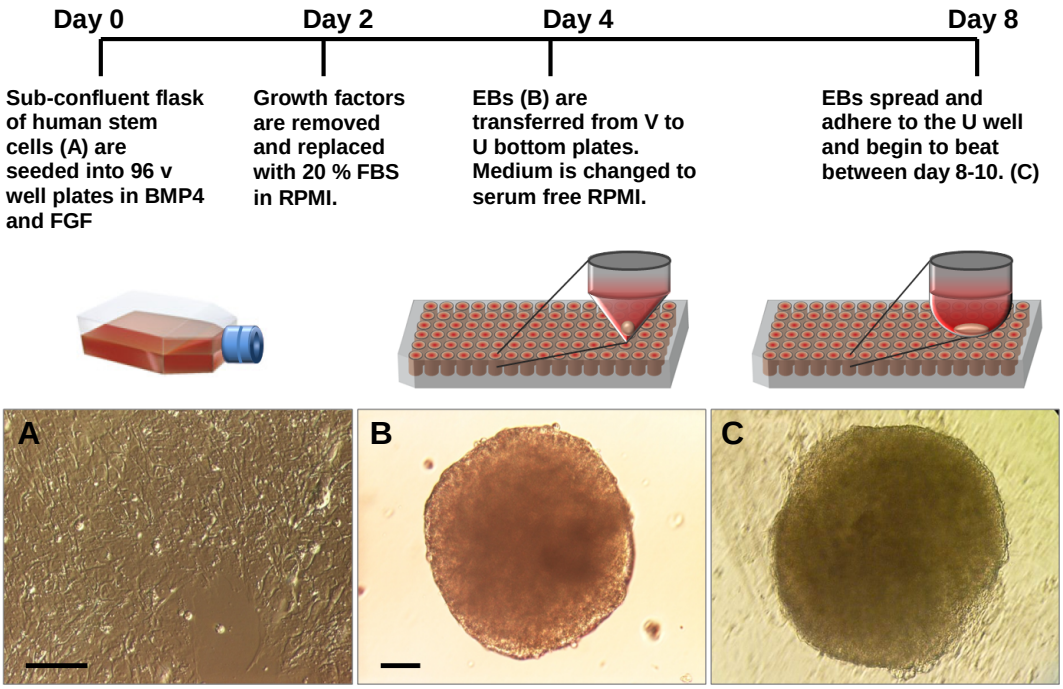


Figure 3.5 HUES7 derived fibroblast characterisation.
The bright field image shows typical elongated morphology and the fluorescent image confirms the presence of the fibroblast specific P4HB antigen (green) against a nuclear stain, DAPI overlay (blue). Scale = 50µm

3.2.1.3. Cardiomyocyte Derivation

Cardiomyocyte derivation was achieved following a protocol published by Burridge *et al* 2011. The main adaptations to this method for optimal HUES7 differentiation was the number of cells seeded for EB formation (4,000 cells per EB compared to 5,000 Burridge used in paper) and the concentration of factors to promote mesoderm induction during day 2, BMP4 (20 ng/mL) and FGF (4 ng/mL) compared to 25 and 5 ng/mL, respectively that was used in the Burridge paper. This optimisation was necessary due to stem cell line variability (Sheng et al., 2012).

i. Cardiomyocyte derivation:



ii. Fibroblast derivation:

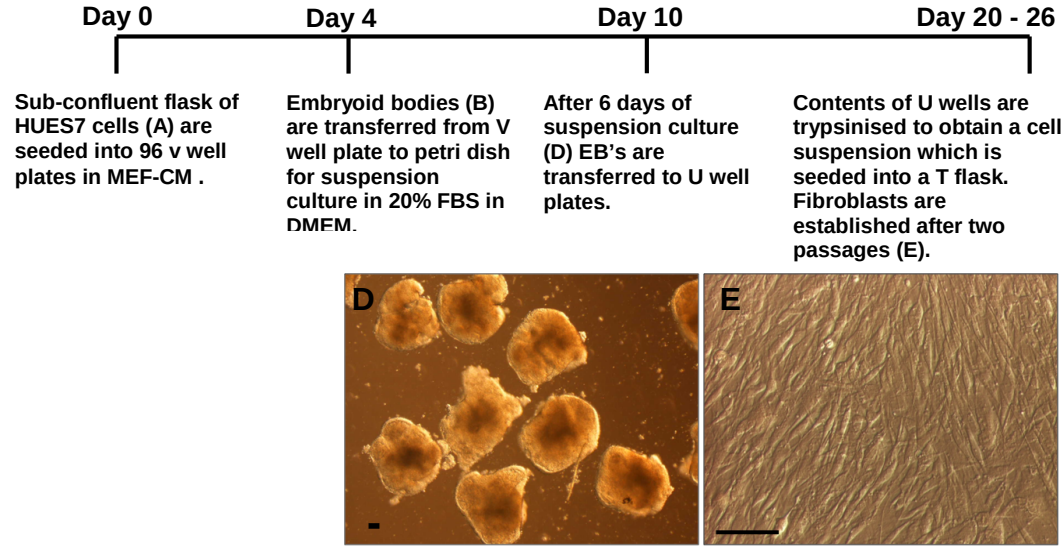


Figure 3.6. Derivation of i) Cardiomyocytes and ii) fibroblasts from HUES7 human embryonic cells.

(A) A sub-confluent layer of HUES7 cells is trypsinised to form **(B)** embryoid bodies approximately 500 µm in diameter. Following the cardiac differentiation protocol 70- 90% of EBs began to beat between day 8 to 10**. (C)** Beating EBs adhere to the well through a layer of non cardiomyocytes which are discarded during dissection of the beater.

(D) Embryoid bodies for fibroblast derivation are left in suspension culture to form outgrowths. These EBs are left to proliferate in U well plates for 10 days after which they are disaggregated using trypsin and seeded into a T flask. The rapid proliferation of fibroblasts means they outgrow any other cell types that may be present and a uniform layer of elongated fibroblasts can be observed by the second passage **(E)**. Scale = 100 µm.

Disaggregation of Beating Cluster

At day 8 of differentiation the EB adheres to the U well *via* a layer of non-cardiomyocytes such as fibroblasts which facilitates adhesion and the central body of cells will beat as shown in figure 3.6.C. The beating cluster first needs to be dissected from the U wells and then enzymatically disaggregated to generate a single cell suspension. Previous methods used within the lab employed collagenase B to disaggregate beaters but problems in batch variation of the enzymatic action of the collagenase necessitated use of an alternative method. Cardiomyocytes have been shown to mature over time in culture (Sartiani et al., 2007) and so age of beater selected for experiments was standardised to 15 days post-beating, which is around 25 days from initial set up of differentiation.

Enzyme combinations were explored and a mixture of Trypsin and AccuMax in a 3:1 ratio was found to achieve the best results. For example, AccuMax alone seemed to be too gentle and required extra manual pipetting which physically sheared and damaged the cells. Similarly, Trypsin alone was enzymatically damaging to cells and caused blebbing; bulging of the damaged cell membrane, as shown by the black arrows in figure 3.7.A.

3.2.1.4. Cardiomyocyte Characterisation

Phenotype of disaggregated cardiomyocytes was confirmed using anti-human sarcomeric alpha actinin (s-act) immunostaining (fig 3.7). Following disaggregation, cardiomyocytes were seeded onto MatTek dishes coated with gelatin 0.1% or gelatin 0.1% plus 20% FBS in RPMI (CM medium, see section 2.1) (G-FBS) as controls for cardiomyocytes seeded on serum free and serum pre-conditioned arrays. Staining was performed after 24 hours and 7 days post-seeding onto gelatin. At 24 hours, surface area of attached cardiomyocytes averaged 351±119 μm^2 on gelatin and 807±305 μm^2 on G-FBS which, are not significantly different as determined by unpaired t-test, $p>0.05$ (± standard deviation, n=3). (fig. 3.7.B). At 7 days cells have significantly spread on both gelatin and G-FBS substrates ($p<0.05$) and display alignment of myofibrils as indicated by parallel Z lines that can be seen in the corresponding immunostain (inset Fig 3.7.C). Average surface area of cardiomyocytes on gelatin was

2019±596 μm^2 and G-FBS was 3024±997 μm$^{2.}$ (±s.d, n =3) which again were not significantly different to each other.

At 20 days culture, 17±4 % of cardiomyocytes cultured on G-FBS lost myofibril architecture and cells enlarged to an average of 5746±4803 μm^2. Actinin staining appeared punctate as can be seen in figure 3.7.D. This occurred less in cardiomyocytes cultured on gelatin alone; 9±3 %, 3986±1053 μm^2 (s.d, n=3).

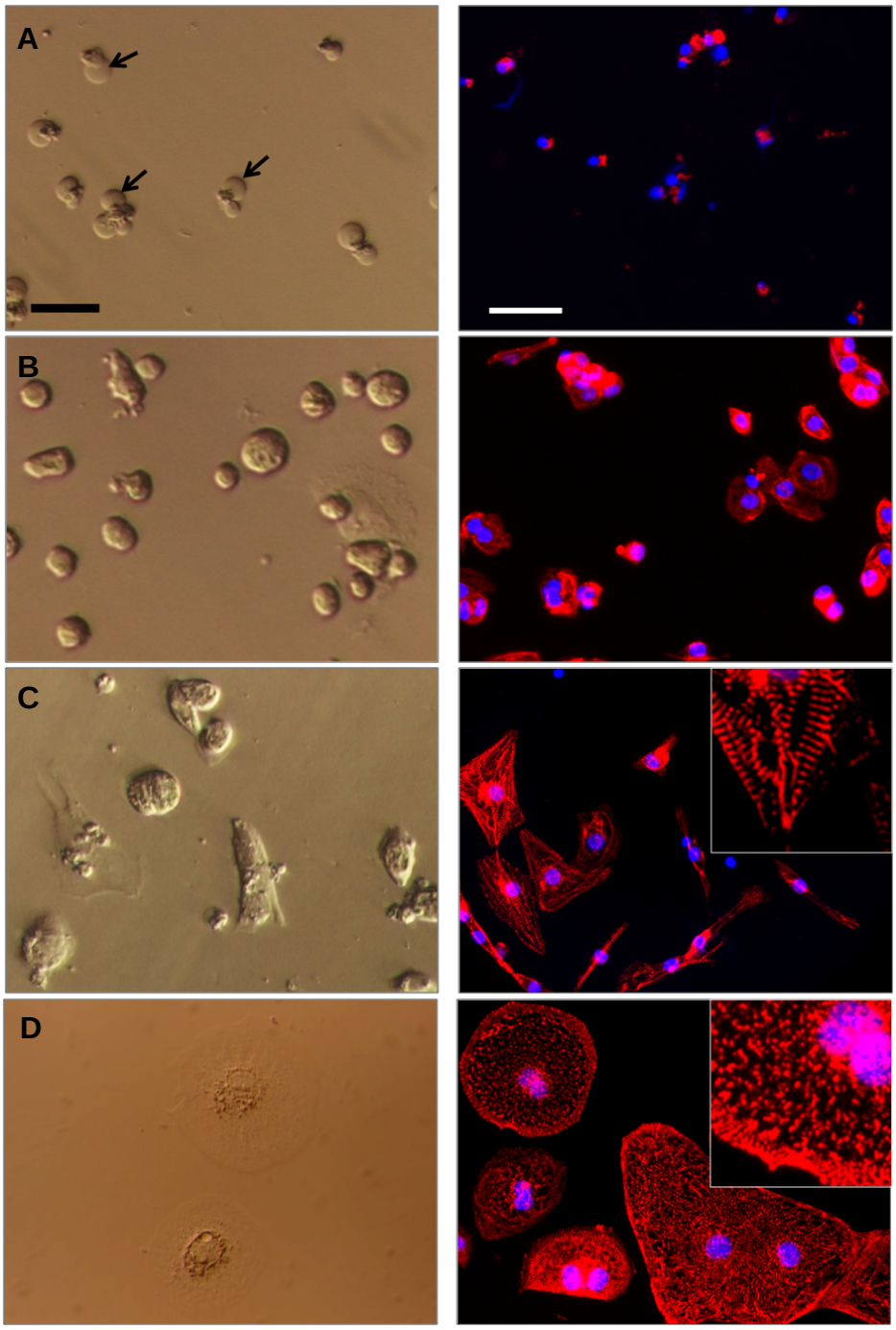


Figure 3.7 Characterisation of dissagregated HUES7-cardiomyocytes on 0.1% Gelatin.
A) Brightfield image shows poorly disaggregated cardiomyocytes using trypsin. The arrows point to bulges in the cell membrane caused by enzyme damage. The immunostain shows a lack of sarcomeric alpha actinin staining. **B)** A healthier morphology can be seen at 24 hours when disaggregated using a mixture of 3:1 AccuMax and Trypsin. Cells have an average area of 351 μm^2. **C)** Cardiomyocytes 7 days after disaggregation, a variety of morphologies can be observed, ranging from rounded to elongated. Average area is larger, 2019 μm^2 and banding of Z lines can be seen in the immunostain indicating a degree of organisation.
D) Cardiomyocytes can lose myofibril integrity after 20 days culture on gelatin as indicated by punctate actinin staining and hypertrophy, with average area of 5746 μm^2. Sarcomeric alpha actinin (Red), DAPI (Blue). Scale = 50µm.

Purity of Cardiomyocyte Population in Beating Cluster

The efficiency of cardiomyocyte differentiation was determined by the number of EBs that began to beat from the total number of EBs set up. 80±11% (s.d, n = 10) of EBs that would start to beat between day 8 and 10 of differentiation. However, the beating clusters were not pure cardiomyocytes. As mentioned earlier, the EB adhered to the well through a layer of adherent cells. Although, these cells are discarded during dissection of the beater, there may still be a population of non-cardiomyocytes within the beater.

To determine the proportion of cardiomyocytes to non-cardiomyocytes, cell counting of immuno-stained cells and fluorescence activated cell sorting (FACS) was carried out. Cardiomyocytes from three samples of disaggregated beaters were identified using immunostaining of sarcomeric alpha actinin. The proportion of cells expressing this marker in the sample was 83±2 % (n=3). FACS was performed on the same samples using a different cardiomyocyte maker, cardiac troponin I (cTnI), which from previous experience within the lab is a more accurate marker to use for FACS, and was found to be expressed in 91±5 % of cells(n=2) (fig.3.8).

This section of work has established methods to derive validated fibroblast and cardiomyocyte cells from the HUES7 hESC line. There is a high proportion of cardiomyocytes within beating clusters which will not require enrichment. The next steps were to fabricate polymer microarrays to begin cell seeding experiments.

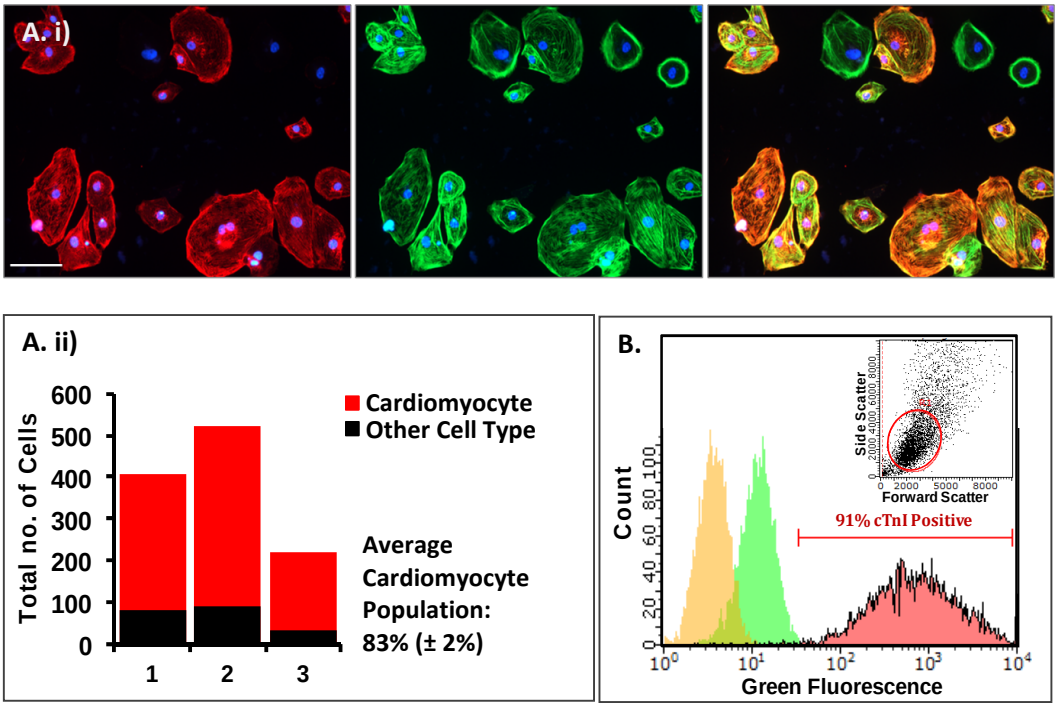


Figure 3.8. Cardiomyocyte population within beating clusters determined using A) Immunostained cell counts and B) Fluorescence Activated Cell Sorting (FACS).
A.i. Phalloidin (green) is an F-actin marker and highlights all cell types, while sarcomeric alpha actinin (red) stains cardiomyocytes only. Merged fluorescent images, identify 3 non-cardiomyocytes within the sample. **A.ii**. Using Cell Profiler over 1000 cells from 3 samples of disaggregated beaters were counted and the average cardiomyocyte population was found to be 83±2 %. **B**. FACS analysis found the cardiomyocyte population to be 91±5 % as determined by cardiac troponin I positive staining (n=2).

3.2.2. Microarray fabrication

3.2.2.1. Piezo Printing

Microarrays were initially fabricated by piezo printing using the monomers listed in figure 3.10.A. 86 monomers were printed in 6 replicates on a 25x75mm pHEMA coated glass slide. The identity of the monomers can be found in appendix 1. To validate if the polymers were printed in discrete identifiable regions, the surface chemistry of the arrays was analysed using time of flight secondary ion mass spectrometry (ToF-SIMS), more on the principles of method can be found in chapter 5. The relative intensities of the chemical species that are detected on the surface by ToF-SIMS can be used to retrospectively build an image of the chemical species of interest. To determine if polymer spots were in discrete regions, the ion at m/z 61 ($C_2H_5O_2$-), specific to the background pHEMA coating (fig. 3.9), was reconstructed. Figure 3.10.C displays the distribution of this ion which should be prominent around each polymer island, the lower the intensity of the ion (counts per pixel) the darker the colour and so polymer spots should appear as dark islands on a bright background. However, this is not the case as a high degree of spreading of the printed polymer spots can be observed, it is important to note that this spreading is not visible using brightfield microscopy.

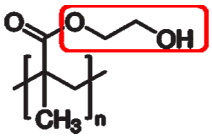


Figure 3.9 Structure of pHEMA.
The characteristic ion of pHEMA is circled in red ($C_2H_5O_2^+$, m/z 61)and is rebuilt in the ToF-SIMS image to distinguish printed polymer spots which should not contain any pHEMA.

HUES7-fibroblasts were seeded onto the arrays to firstly see if 7 days of vacuum extraction post-printing was sufficient to remove toxic unpolymerised monomers from the array and if the sterilisation procedure was sufficient to prevent contamination in our antibiotic free culture environment. It was confirmed that the extraction and sterilisation procedure were sufficient to enable cell attachment in a sterile environment. DAPI staining of the seeded fibroblasts (fig3.10.D) highlighted regions of cell attachment in between polymer spots corresponding to the regions of polymer spread identified using ToF-SIMS. Therefore, the main process to optimise going forward was printing of the array.

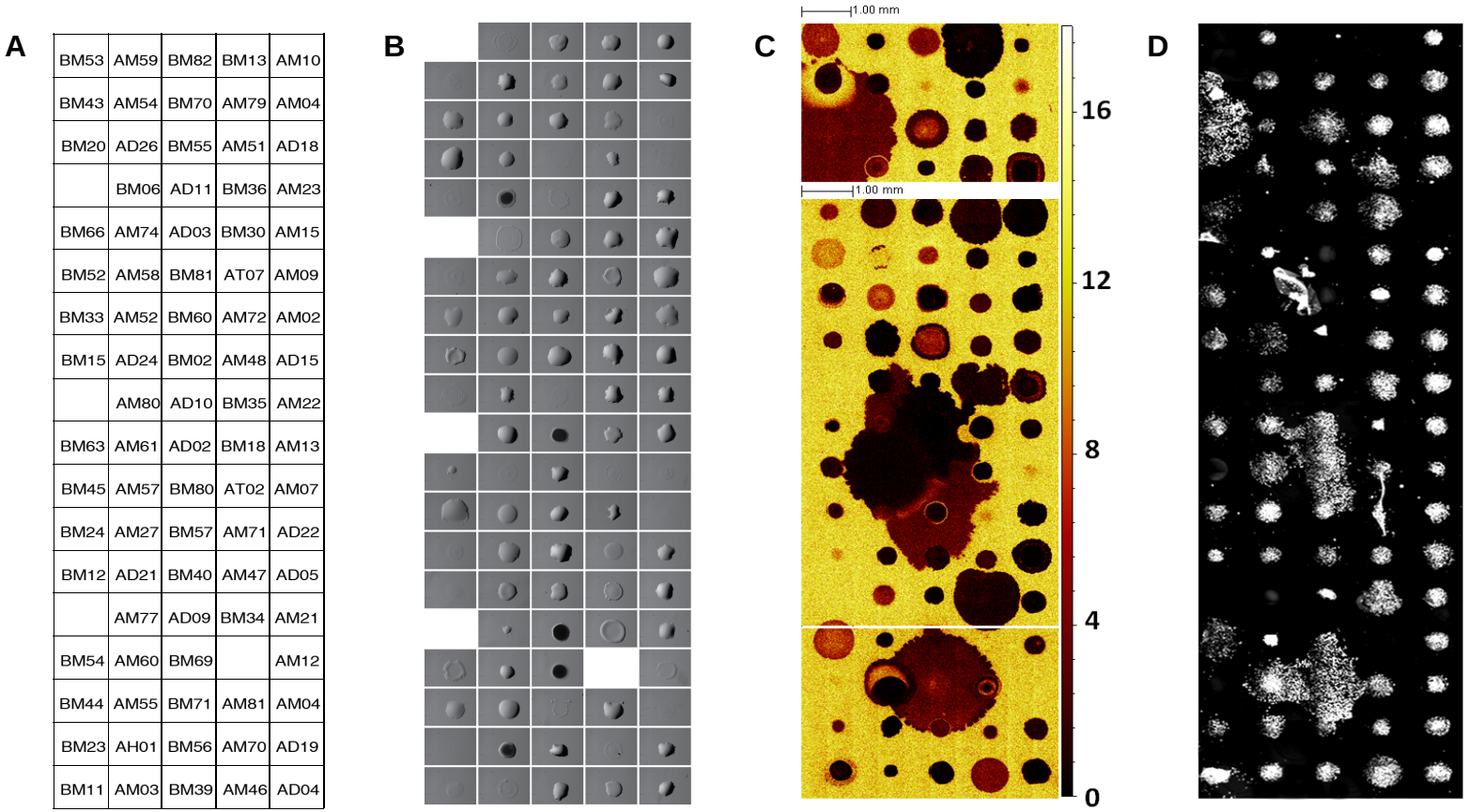


Figure 3.10. Piezo Printed microarray. A) Polymer Array Layout. B) Brightfield image of printed array. C) Distribution of background pHEMA ion $C_2H_5O_2$-. D) Seeded with HUES7 fibroblasts and stained with nuclear marker DAPI.

Darker regions in ToF-SIMS image (B) are the printed polymer which masks background the pHEMA ion (scale is counts per pixel). It can be seen that there is extensive chemical spreading in some regions and this corresponds to fibroblast adhesion in between polymer regions, seen in image D. Scale bar of 1mm in C also applies to B and D.

3.2.2.2. Contact Printing

The array was re-printed using contact printing which reduced spreading as seen in figure 3.11.B. The monomers BM13 (ethylhexyl methacrylate), BM71 (octafluoropentyl methacrylate) and AM57 (dodecafluroheptyl acrylate) were amongst the highest spreading monomers whose printing was improved using the contact method.

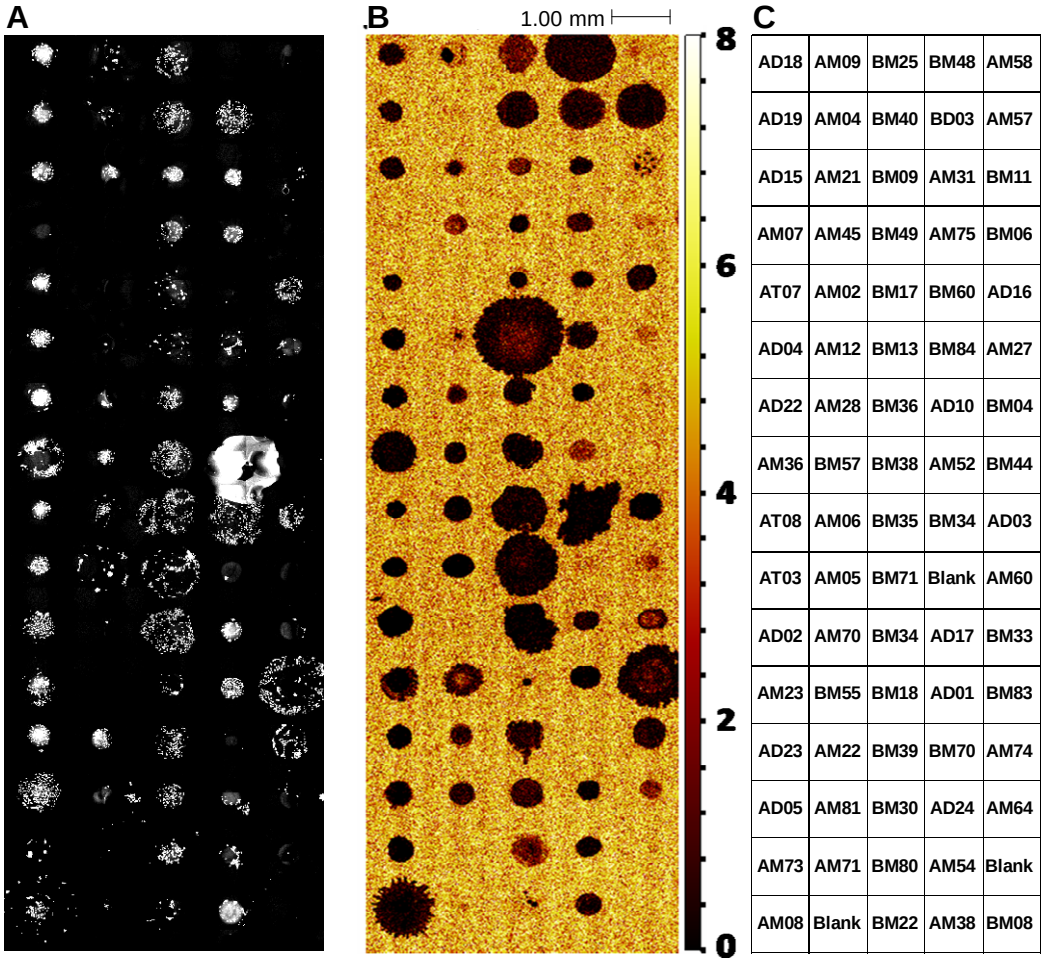


Figure 3.11 Contact printed microarray A) Seeded with HUES7 fibroblasts and stained with nuclear marker DAPI. B) Distribution of background pHEMA ion $C_2H_5O_2$-.
C) Monomer layout of array.
The fluorescence image (A) indicates discrete regions of cell attachment. There is no overlap of monomers as indicated by the ToF-SIMS image (B) but there remains some spreading during printing which may require further refinement. Scale bar of 1mm in B also applies to C.

To further improve some of the spreading that could be seen in the contact printed array, the blotting protocol was adjusted. Blotting the pins on a slide before printing onto the microarray removes excess monomer solution. The number of blots that the robot performs before printing was increased and further improved the printing of discrete polymer regions (fig. 3.12.A).

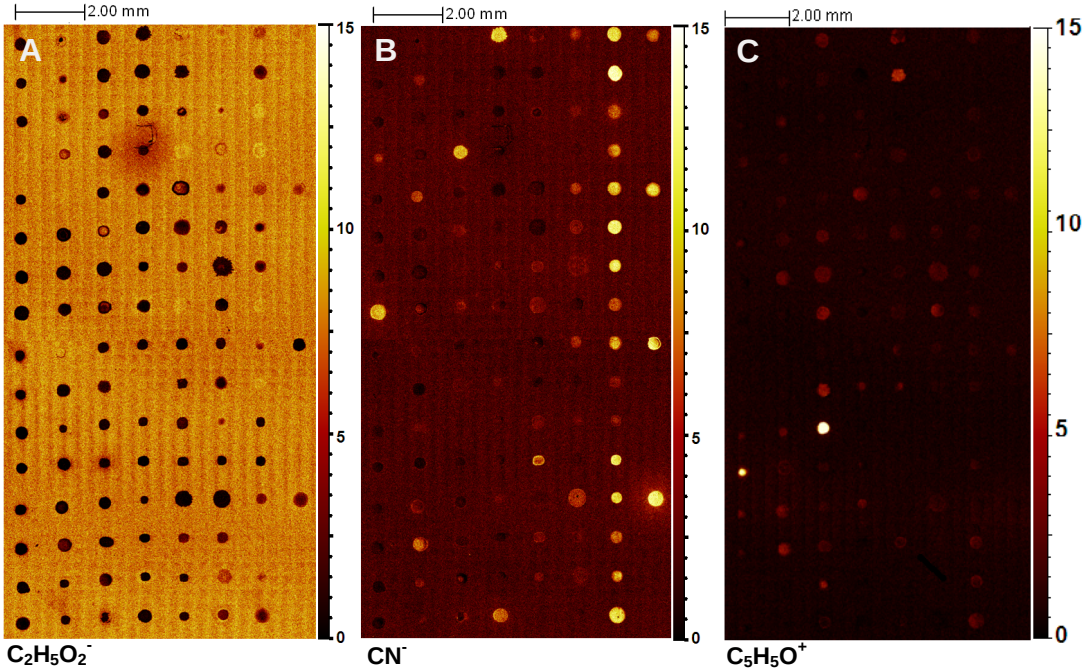


Figure 3.12 Contact printed array using amended blotting protocol.
A) ToF-SIMS showing distribution of the pHEMA specific ion $C_2H_5O_2$-. **B)** Distribution of the CN- ion confirms locations of nitrogen containing monomers, which overlap with red and orange coded regions in the array layout in **D**). The monomer specific ion $C_5H_5O_5$+ can be seen in **C)** highlighted in regions correctly corresponding to BM34 (fufuryl methacrylate) and AM22 (tetrahydrofurfuryl acrylate).

3.2.2.3. Surface Characterisation

The final layout of the array contained 115 polymers printed as 6 replicates on a 25x75mm glass slide (fig.3.12D). To confirm chemical layout of the array, various ions of interest can be rebuilt. For example, the CN- ion will highlight all nitrogen containing polymers. Figure 3.12.B confirms the location of nitrogen containing monomers including the acrylamides down the right hand side of the array (fig. 3.12.B/D). Monomer specific ions can also be re-built, for example the $C_5H_5O^+$ ion is a 5 membered cyclic ion present in furfuryl methacrylate (BM34) and tetrahydrofurfuryl acrylate (AM22).

This section has validated contact printing as a suitable method to array over one hundred different materials on pHEMA coated glass slides. The UV sterilisation procedure outlined in the methods section has been confirmed to achieve sterility in an antibiotic free environment and the vacuum extraction removes toxic monomers which enabled fibroblasts to be cultured on the arrays. To analyse the microarrays a high content screening platform must be optimised which will be discussed next.

3.2.3. Automated Image Analysis

3.2.3.1. Software

Automation of image acquisition was required due to the large numbers of arrayed material. Microarrays consisted of 115 polymers printed in 6 replicates (fig 3.12.D). This requires image acquisition for 690 polymers per slide. Automated image capture was achieved using the Imstar fluorescent microscope. Automated analysis of such large sets is important for high throughput screening to reach its potential. Three software packages, Image J, Volocity and CellProfiler were assessed for their ability to count nuclei and measure cardiomyocyte size based on actinin staining. Image J enables a wide range of measurements to be made but construction of multi-step protocols for batch analysis was not possible and so was not suitable for high content analysis. Volocity allows easy construction of analytical protocols but did not enable a satisfactory level of cell identification based on dual staining and therefore cell debris could not be satisfactorily discounted. In contrast, CellProfiler was able to identify cells based on nuclei first and then identify the secondary stain based on its associated nuclei. Therefore, secondary stains that had no nuclei, such as can happen with cell debris, were not counted. (fig.3.16.A). Therefore, CellProfiler was chosen to develop further for image analysis due to ease of construction of multi-stage analysis protocols ability to apply the protocol to multiple images and good user control over cell identification parameters.

3.2.3.2. Automated Nuclei Count

Due to the ease of maintaining HUES7-fibroblasts, they were used to automate nuclei count of adhered cells to the polymers using CellProfiler. It became apparent that the software had a limit for the number of cells it could separate and count. Therefore, to obtain accurate counts for statistically meaningful data, seeding density had to be optimised to avoid very high numbers of cells that CellProfiler could not accurately count. Fibroblasts were seeded in low, medium and high densities of 0.7, 1.4 and 7 x 10^5 cells in 4 mL onto each array. The coefficient of variation (s.d/mean x 100) between cell counts on the same polymer was 39 %, 43 % and 79 % respectively (n=4). A

seeding density of 1.4 x 10^5 cells per array was found to be optimal for automated cell counting, although the co-efficient of variation is slightly higher than 0.7 x 10^5 cells per array, the higher density maintains important cell to cell contact. At 7 x 10^5 cells per array, the software could not adequately separate nuclei in highly dense regions of cell attachment (fig.3.13).

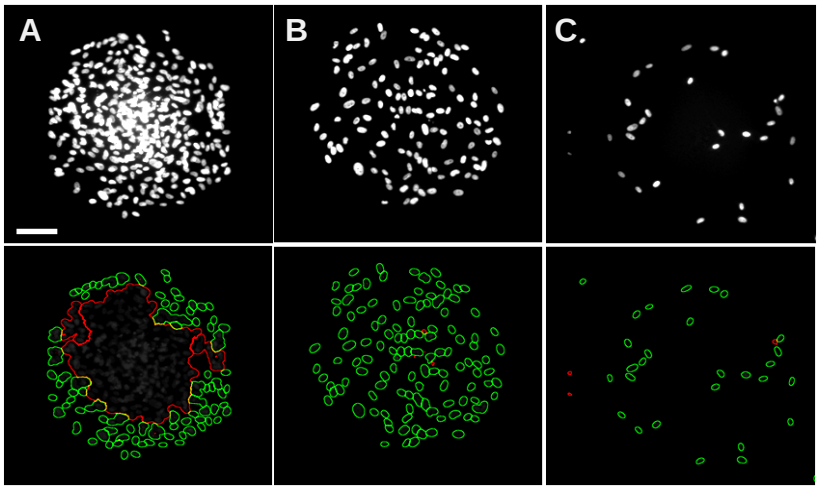


Figure 3.13. HUES7-fibroblast nuclei count using CellProfiler
Fluorescent images in top row are DAPI nuclear stains of HUES7-fibroblasts on the same polymer at three different seeding densities; 7 x10^5 (A) 1.4 x 10^5 (B) and 0.7 x 10^5(C) cells per array. The Software is unable to separate high density regions of cells (A), the red outline showing the central region that was counted as large objects outside of the size guide and so discarded. The red outlines in B and C have correctly been discarded due to the objects being below the size guide. Scale = 100µm.

However, even at this seeding density, improvements were still required for segregating touching nuclei. The software offers various options to separate objects based on shape or intensity and typical size of object. Those that don't display a significant difference towards the edge of the object in terms of shape or fluorescent intensity will be difficult to separate and the software will then rely on the typical size of object to estimate segregation. Figure 3.14.B is an example of the software merging touching nuclei because the minimum radius of an object has been set too high. Similarly, setting the minimum radius too low will over-segment objects (fig 3.14.C). Figure 3.14.D shows the results of the final nuclei counting protocol which primarily used shape to separate touching objects and a minimum radius value of 10 pixels which was found by measuring nuclei and finding an average. This will be different based on the cell type, for

example the average area of fibroblast nuclei was bigger, 321±78 μm^2, than those for cardiomyocytes, 112±32 μm^2 (s.d, n=3), fig3.14E. This was simple to adjust due to the manual control offered by CellProfiler.

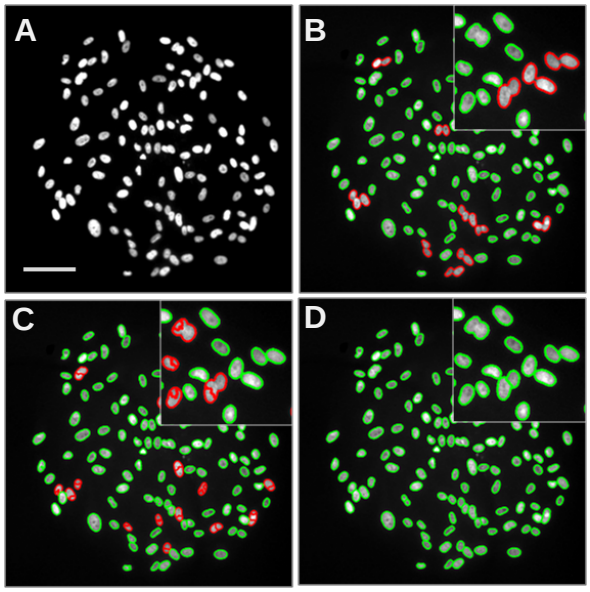
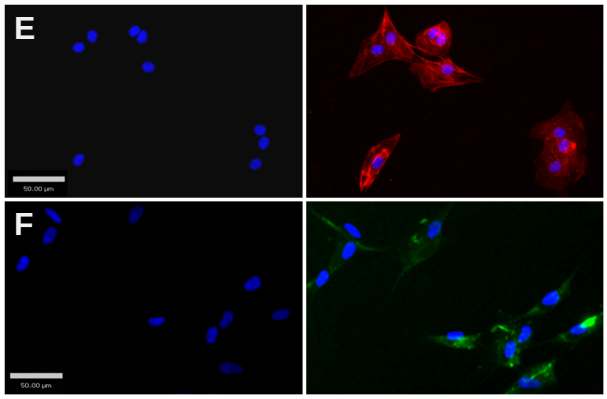


Figure 3.14 CellProfiler count of DAPI stained nuclei of fibroblasts seeded onto a polymer spot.
(A) Original input DAPI file acquired using automated Imstar microscope. (B) Output file from CellProfiler using a minimum radius that is too high, outlines in green what has been counted by the software. Nuclei that should have been segregated but the software merged has been highlighted in red. (C) Output file using a minimum radius that is too low has over segmented nuclei (red). (D) Final protocol used shape to segregate and a minimum radius value of 10 pixels.



The minimum radius will depend on cell type. It was found that nuclei of cardiomyocytes were smaller (112 μm^2) than fibroblasts (321 μm^2) and therefore protocol needed minor adjustment. (E) Cardiomyocytes stained against sarcomeric actinin (red) and (F) fibroblasts stained against P4HB (green) both with DAPI nuclear staining (blue). Scale = 100 μm^2.

3.2.3.3. Automated Cardiomyocyte Analysis

Once the array cell seeding and automated analysis platform had been established with fibroblasts, it was possible to apply similar parameters to the more challenging HUES7 derived cardiomyocytes. For the identification of cardiomyocytes, the immunostaining of human sarcomeric alpha actinin (s-act) needs to be measured during analysis. This confirms that what is being counted is a cardiomyocyte and as well as cell attachment, can measure other parameters such as shape and area of the cardiomyocyte. Figure 3.15 demonstrates how CellProfiler uses the DAPI image to identify 'primary' objects (nuclei). These

primary objects are used to help identify 'secondary' objects which are the s-act stain. The software can then merge the primary and secondary images and place outlines around the nucleus and s-act stain. These outlines are important so that a visual inspection of how the software has identified objects can be carried out.

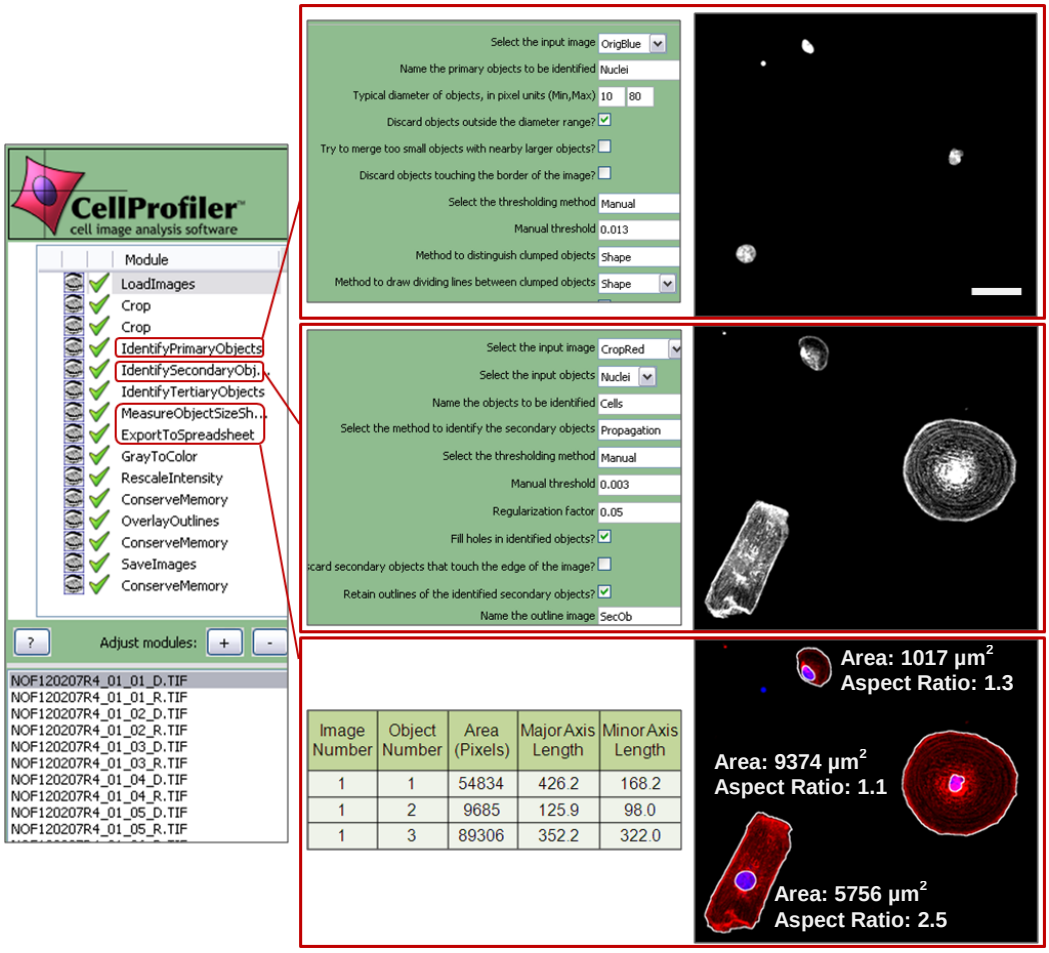


Figure 3.15 Example of CellProfiler protocol to count number of cells attached and measure cardiomyocyte shape (aspect ratio) and spread (area).
Images are processed as separate grey scale images (A) nuclei (DAPI) are identified first as primary objects and then used to find (B) the corresponding secondary object which is the sarcomeric α actinin stain. (C) A merged colour image of nuclei and s-actinin stain with outlines is constructed by the software. A file containing all measurement data is generated and includes cell count, area and shape. Scale = 50µm.

The propagation method was chosen to separate touching cells which takes into account the change in intensity which tends to get brighter towards the edge of the cell and also considers the distance of the primary objects (nuclei)

to then draw a dividing line between the two objects (fig 3.16.A). One disadvantage is that cardiomyocytes can be bi-nucleated, in which case it is counted as two cells by the software. This constant systematic error would occur across all samples so should not cause bias when comparing cell counts between different polymers.

Visual inspections are important as background fluorescence of the polymer can occur and will interfere with cell counting. In these cases a manual count was performed. On average, 7±2 % of images required manual counting (fig 3.16).

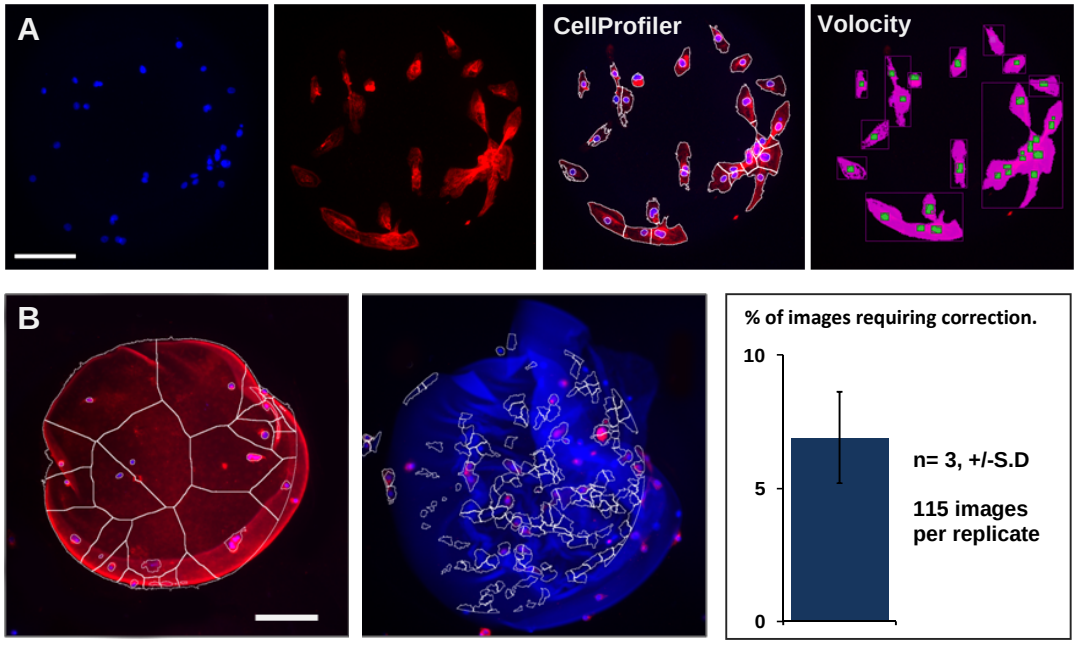


Figure 3.16 (A) Segregation of touching cardiomyocytes by CellProfiler and Volocity (B) Incorrect cell identification due to background fluorescence of polymer.
(A) Two input images of DAPI stained nuclei and s-act stained cardiomyocytes are analysed by CellProfiler and Volocity. The cellprofiler output image shows white outlines of counted cardiomyocytes that have been segregated depending on actinin fluorescence and position of nuclei. Volocity identifies nuclei (green) and actinin (pink) but does not segregate the cells because the two stains are measured independently. B) Background fluorescence can occur in either one of the fluorescent channels or both and will lead to mis-counting by the software which has to be manually adjusted, as occurs in approximately 7% of images. Scale = 100µm.

3.3. SCREENING CARDIOMYOCYTE ATTACHMENT AND MORPHOLOGY ON FIRST GENERATION HOMOPOLYMER MICROARRAYS.

This section aims to screen 115 potential substrates for cardiomyocyte culture using the resources that have been established thus far. Screening was based on density of attachment and cell size of adhered cardiomyocytes. This was done in a high throughput manner using automated image acquisition and analysis. Each image contained one polymer substrate which was then constructed into a mosaic of the whole array. A heat map displays the attachment density of the cardiomyocytes on each substrate. The cell count has been normalised by dividing the density on each polymer by the density on the polymer which supported the highest number of cells/mm^2 so that substrates could be ranked from 0 – 1. This also accounts for variation in seeding density between different arrayed slides that would appear as large differences if actual cell number was used.

Disaggregated beating clusters (dissected day 15 post-differentiation) were seeded onto microarrays that were preconditioned for 1 hour with either serum free medium or medium containing 20% fetal bovine serum (FBS) and incubated for either 24 hours or 7 days. This gave an indication of which substrates allowed for relatively rapid attachment and which allowed for stable attachment over the 7 days. The influence of serum proteins on cell attachment could also be investigated.

3.3.1.1. Serum Pre-conditioned Arrays

Serum pre-conditioned microarrays seeded with cardiomyocytes for 24 hours displayed attachment on 67 % of the polymers. The highest cell count from each replicate averaged 234±26 cells/mm^2 (n=3). Relative cell densities displayed in the heat map in figure 3.17 were normalised to this average. The greatest cell density was 0.72 on polymers AM71, Heptafluorobutyl acrylate (±0.25) and AM70, Hexafluoroisopropyl acrylate (±0.40) (±s.d, n=4). Cardiomyocyte size, as determined by surface area of s-act staining, was largest on BM08 (514±277 µm^2, n=4), which was smaller than control Gelatin-FBS but not significantly (807±305 µm^2), ($p>0.05$, ± s.d, n=3, unpaired t-test).

At 7 days, 70 % of polymers supported cardiomyocyte attachment and highest average cell count was 264±45 cells/mm^2. The highest cell density was observed on BM34 (furfuryl methacrylate), 0.59±0.28 (s.d, n=4, fig.3.18). Cardiomyocyte size was also largest on BM34, 1364±937 μm^2 and again is smaller than Gelatin-FBS control which averaged 3024±997 μm^2 but was not statistically, as determined by unpaired t-test ($p>0.05$, ± s.d, n=3).

When the difference in attachment was compared from 24 hours to 7 days, it could be seen that some substrates had high attachment initially which then reduced drastically at 7 days (fig 3.21). For example AM64 (Hexadecafluoro-9-(trifluoromethyl)decyl acrylate) had a relatively high cell density of 0.59±0.24 at 24 hours which dropped to 0.02±0.02 at 7 days. Whereas, BD03 (ethylene glycol dimethacrylate) had poor attachment at 24 hours, 0.08±0.03 which increased at 7 days to 0.56±0.2 (fig.3.19). These two monomers were selected to take forward to see if a co-polymer of the two would have any synergy to improve overall attachment.

3.3.1.2. Serum Free Arrays

Homopolymer arrays that were cultured in serum free conditions for 7 days displayed poor cardiomyocyte attachment (fig.3.18). Attachment was observed on only 10 % of polymers, the highest on AM38 Dimethylamino-propyl acrylate (72±25 cells/mm^2) which was significantly lower than serum preconditioned arrays ($p<0.01$, ± s.d, n=3). Relative cell density on AM38 (was significantly lower than gelatin control. The 12 substrates that did allow attachment displayed average cell sizes that were relatively small (fig.3.19). The largest average cardiomyocyte size was 274±75 μm^2 (n=4, ±s.d) on BM49 (fig. 3.20.D) and is significantly smaller compared to control gelatin (2019±596 μm^2, n=3) ($p<0.05$, unpaired t-test).

Regardless of the comparatively small cell size, due to the limited number of polymers that supported cardiomyocyte attachment in serum free conditions, all 12 substrates that did not require pre-incubation with serum containing medium were chosen to take forward to second generation arrays to

investigate if co-polymers containing these monomers would exhibit improved cardiomyocyte attachment and size in serum free conditions.

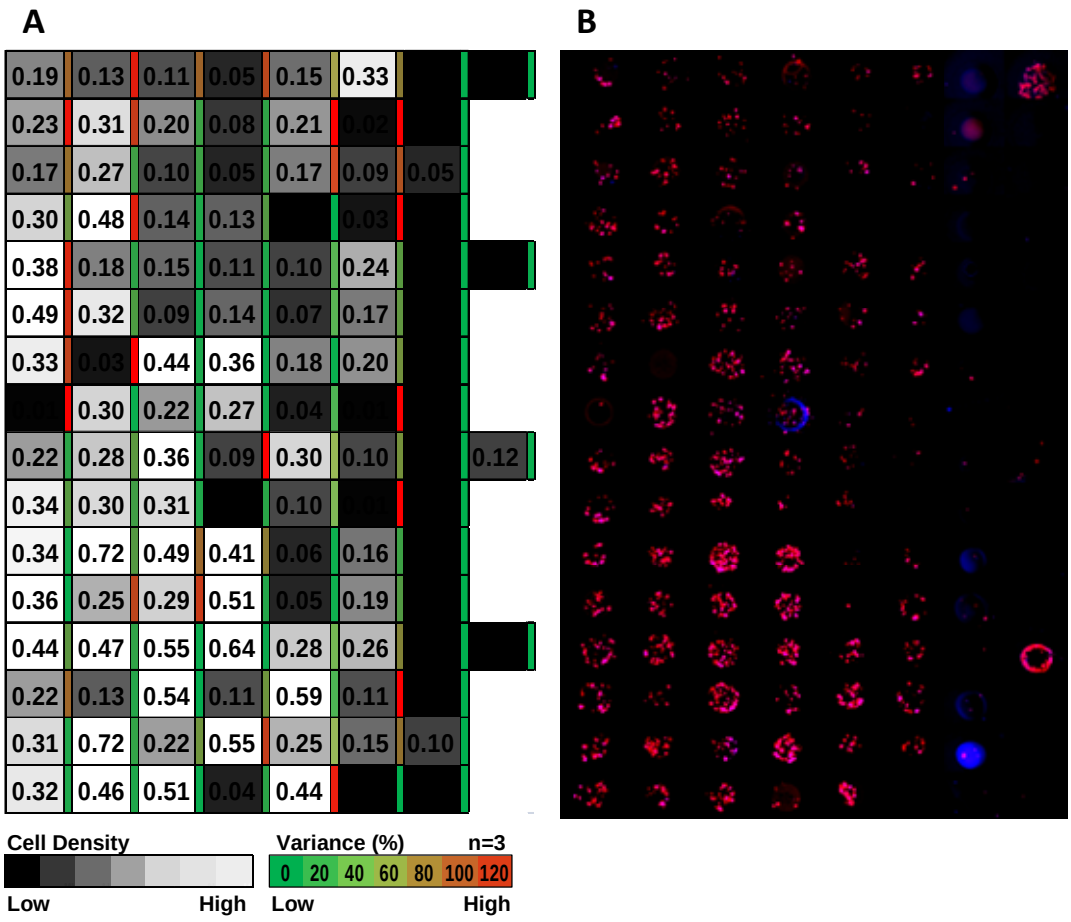


Figure 3.17. HUES7-cardiomyocyte attachment on 115 different poly acrylate and polyacrylamide substrates at 24 hours on serum conditioned arrays.

(A) Cell density at 24 hours on microarray pre-incubated with 20% serum containing medium. Variance (s.d/mean x 100) is displayed to allow comparison across array. Highest density is 0.72 displayed on AM71 and AM70.

(B) Fluorescent mosaic of attached cardiomyocytes immunostained with anti-human sarcomeric alpha actinin (red) and DAPI (blue).

(C) Array Layout, see figure3.11 for colour codes.

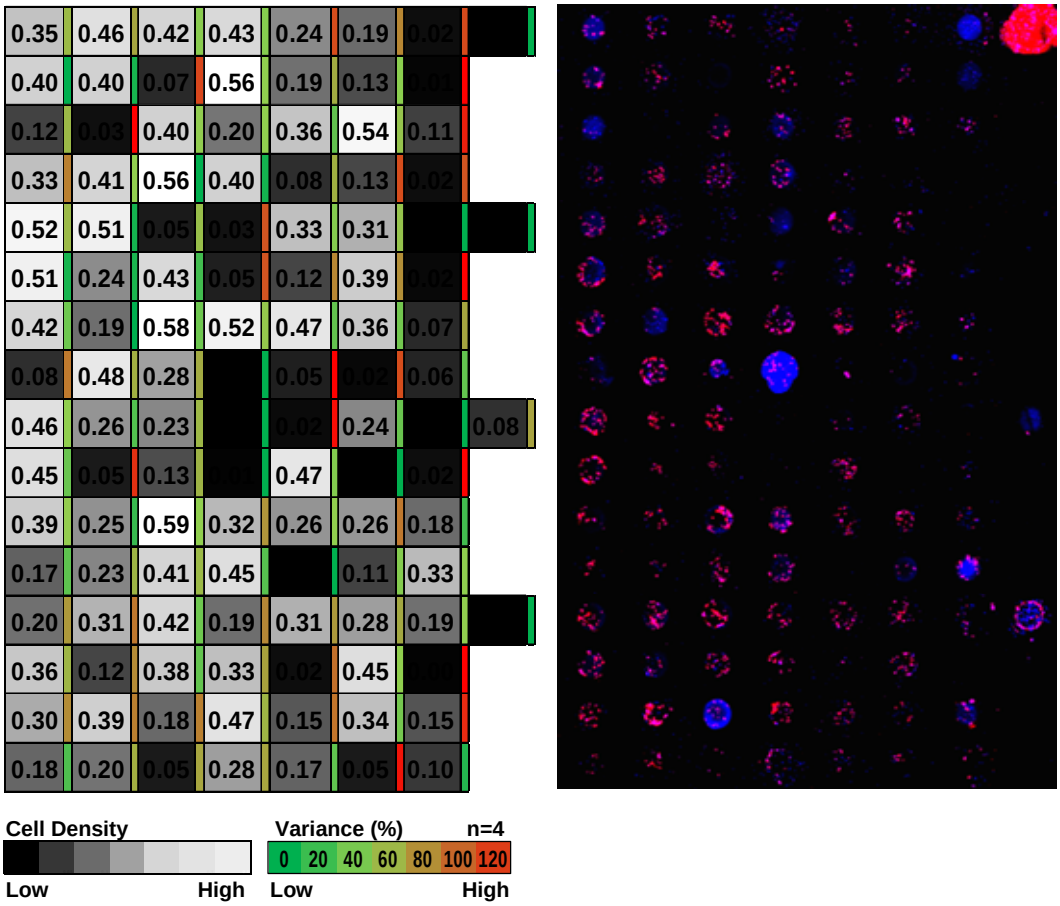


Figure 3.18. HUES7-cardiomyocyte attachment on 115 different polyacrylate and polyacrylamide substrates cultured for 7 days on serum pre-conditioned arrays.
Highest cell density after 7 days of culture is 0.59 on BM34. Corresponding fluorescent mosaic of attached cardiomyocytes immunostained with anti-human sarcomeric alpha actinin (red) and DAPI (blue). Intense blue staining is background staining and CM13 in top right corner exhibits intense background fluorescence emitting red fluorescence.

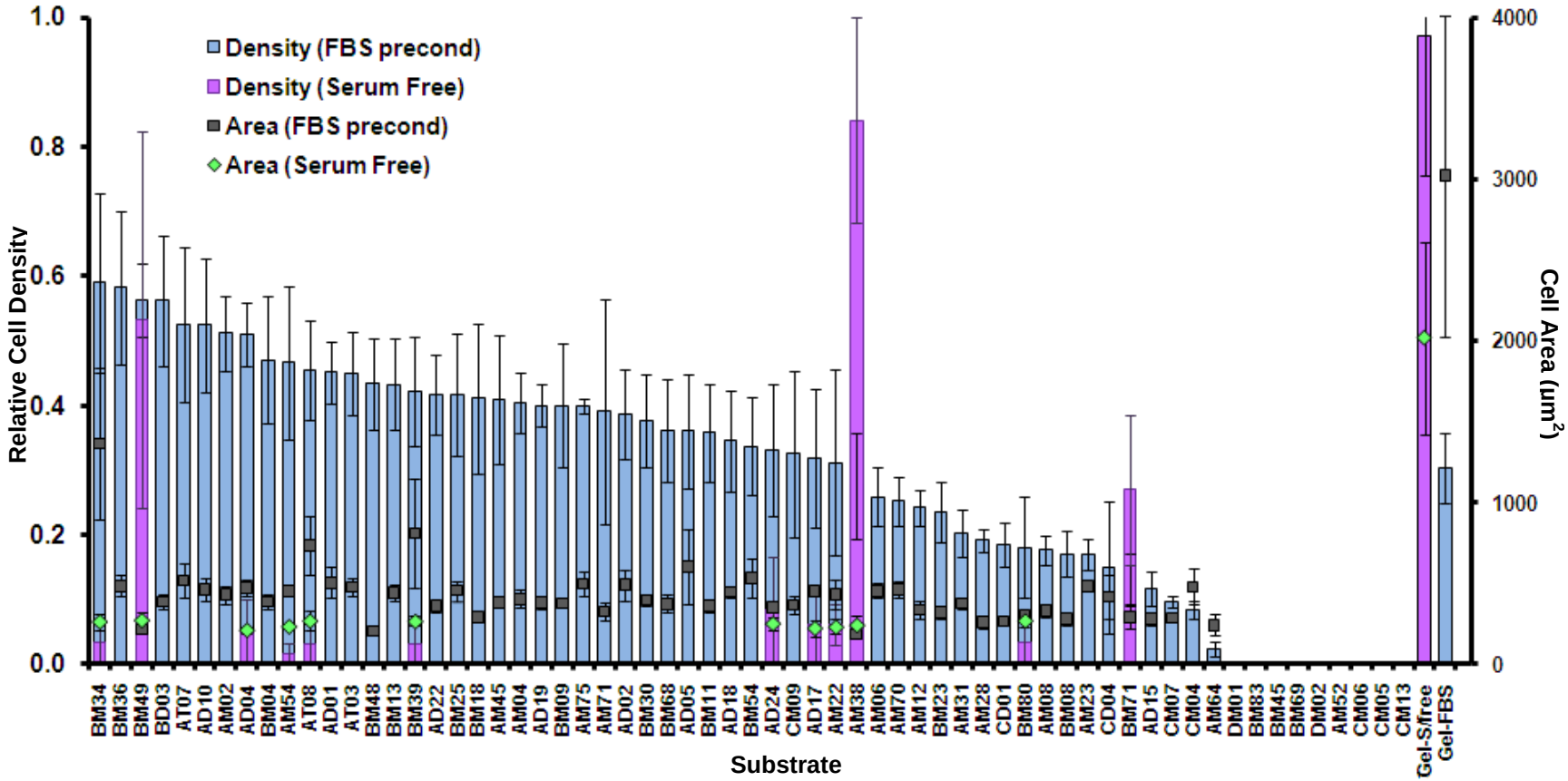


Figure 3.19. Comparison of cardiomyocyte density and area on first generation homopolymer array on serum free and FBS pre-conditioned polymers and 0.1% gelatin cultured for 7 days.

Cell density and area of cardiomyocytes cultured on 63 serum pre-conditioned polymers (blues bars and black squares) is displayed. These were selected based on a relatively low variance, those with very high variance, >60%, were excluded. Polymers that supported cardiomyocyte attachment in serum free conditions (purple bars and green triangles) were selected regardless of variance due to the limited number and potential improvement that may occur when co-polymerised. (± s.e.m, n=4)

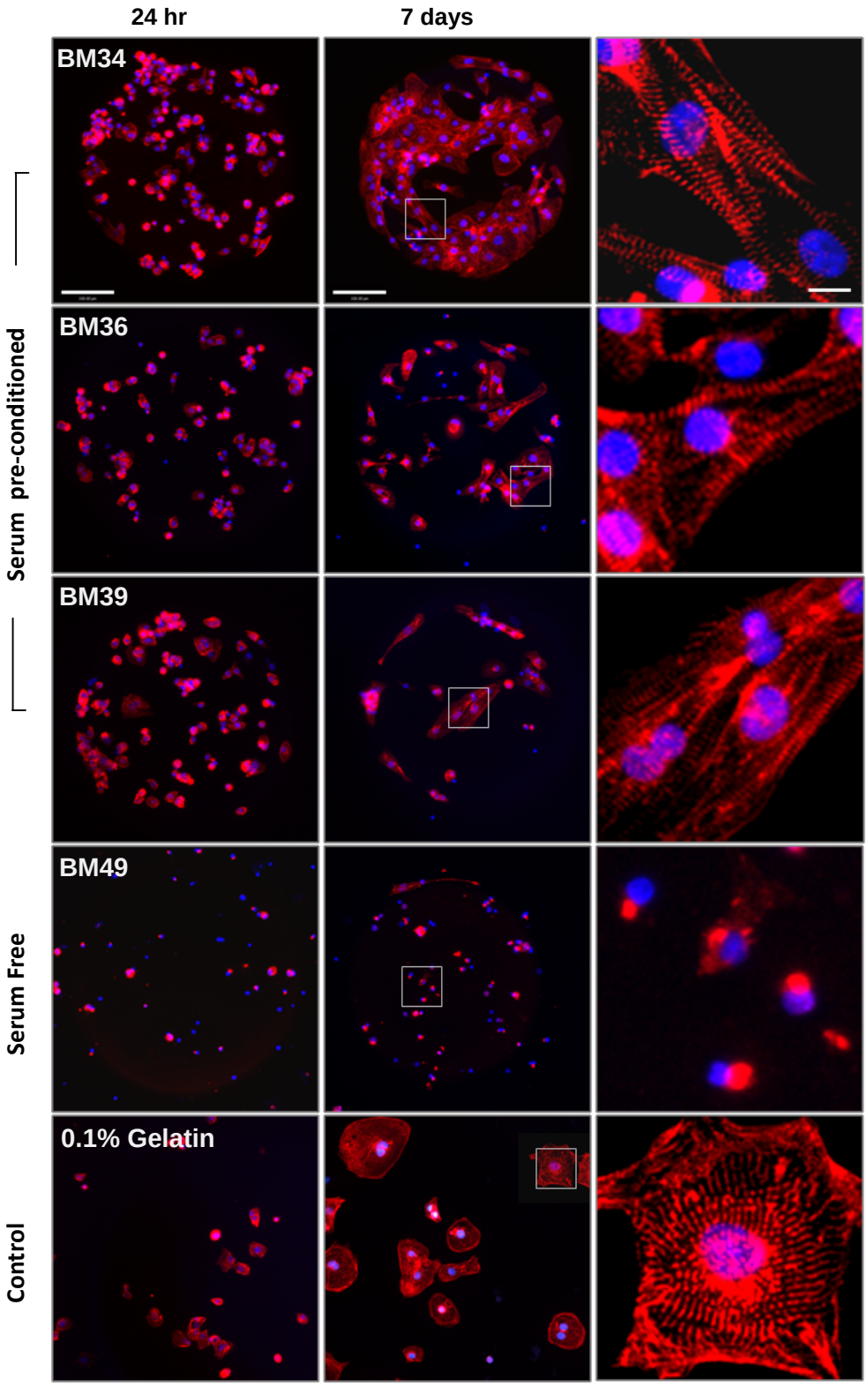


Figure 3.20 Cardiomyocyte morphology observed on polymers that supported highest attachment at 24 hours and 7 days.

With serum preconditioning. (BM34 fufuryl methacrylate, BM36 Isobornyl methacrylate and BM39 Benzyl methacrylate) myofibril architecture was visible at 7 days with parallel banding of Z-lines visualised by sarcomeric α actinin staining (red) that is comparable to gelatin control. In serum free conditions, BM49 Tert-butylamino-ethyl methacrylate, compared to control gelatin surface no myofibril organisation was not observed.

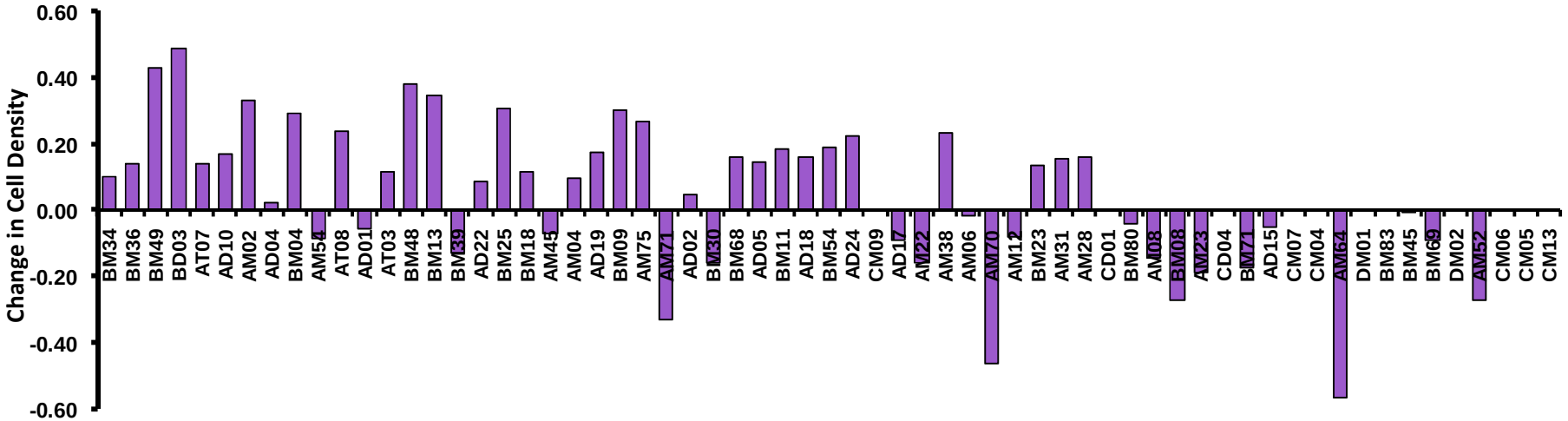


Figure 3.21 Change in Cardiomyocyte Density on Polymers from 24 hours to 7 days Culture on Polymers.

The 63 polymers displayed in figure 3.19 are compared here for their ability to support cardiomyocyte attachment over 24 hours and 7 days. Some polymers display high attachment at 24 hours which drops at 7 days, indicated by a negative change e.g AM70 (Hexafluoroisopropyl acrylate) and AM64 (Hexadecafluoro-9-(trifluoromethyl)decyl acrylate) . Some are slower at supporting attachment which increases over time e.g BM49 (Tert-butylamino-ethyl methacrylate) and BD03 (Ethylene glycol dimethacrylate). Others support stable attachment indicated by a small or zero change in density.

3.3.2. Monomers chosen to take forward for fabrication of second generation co-polymer arrays.

The final substrates chosen comprised of 24 monomers (table 3.2). This is so that they can be mixed pair wise at a ratio of 70/30 (v/v) to generate a second generation array comprising of 576 co-polymers. Previous studies have optimised this number of arrayed materials to generate a well spaced microarray of 3 replicates of 576 materials on one slide (Urquhart et al., 2008). The number of possible monomers could be bigger than the list of 24 but due to limited resources and time this was not exceeded.

Ultimately, it is stable attachment that is required so data from the 7 day screens were used to further select monomers of interest, apart from those already identified including the 12 that enabled attachment in serum free conditions (fig.3.19). To enable direct comparison of standard deviation, the coefficient of variation was used. To increase the probability of the chosen polymers performing as they did in the microarray, those with variation over 60 % were excluded.

The monomers chosen display a range of cell density and area to provide positive and negative responses to enable downstream investigation of the relationship of these parameters with surface chemistry can be attempted.

In summary, this section has identified a relatively large list of serum pre-conditioned polymers that support cardiomyocyte attachment but only a limited number that will support attachment in serum free conditions.

Table 3.1. Chosen 24 monomers to take forward for second generation array.
Of the 24 monomers chosen, half supported cardiomyocyte attachment in serum free conditions. The values shown below are from serum pre-conditioned arrays cultured for 7 days. Those marked with an asterisk also supported attachment in serum free conditions.

ID	Name	Cell Density at 7 days	Cell Area at 7 days (μm^2)	Change in density 24h vs 7d
BM34*	Furfuryl methacrylate	0.59	1364	0.10
BM36	Isobornyl methacrylate	0.58	483	0.14
BM49*	Tert-butylamino-ethyl methacrylate	0.56	215	0.43
BD03	Ethylene glycol dimethacrylate	0.56	387	0.49
AD04*	Hexamethylene diacrylate	0.51	473	0.02
AM54*	Poly(propylene glycol) acrylate	0.47	456	-0.09
AT08*	Glycerol propoxylate triacrylate	0.46	736	0.24
AT03	Trimethylolpropane triacrylate	0.45	477	0.11
AD01	Butanediol diacrylate	0.45	506	-0.06
BM39*	Benzyl methacrylate	0.42	810	-0.13
BM18	Lauryl methacrylate	0.41	291	0.12
AM71	Heptafluorobutyl acrylate	0.39	327	-0.33
BM54	Ethoxyethyl methacrylate	0.34	533	0.19
AD24*	Poly(propylene glycol) diacrylate	0.33	354	0.22
CM09	N-(Isobutoxymethyl)acrylamide	0.33	368	0.10
AD17*	Hexanediol ethoxylate diacrylate	0.32	451	-0.09
AM22*	Tetrahydrofurfuryl acrylate	0.31	435	-0.16
AM38*	Dimethylamino-propyl acrylate	0.28	186	0.23
BM80*	Methacryloyloxy)ethyl acetoacetate	0.18	300	-0.04
CD04	N,N'-Methylenebisacrylamide	0.15	416	0.01
BM71*	Octafluoropentyl methacrylate	0.13	217	-0.17
CM04	N-(Butoxymethyl)acrylamide	0.08	479	0.01
AM64	Hexadecafluoro-9-(trifluoromethyl)decyl acrylate	0.02	121	-0.56
CM13	N-(3-Aminopropyl) methacrylamide hydrochloride	0.00	N/A	0.00

3.4. SECOND GENERATION CO-POLYMER MICROARRAYS.

Second generation arrays were fabricated by mixing, pair wise, 24 monomers chosen from the first generation homopolymer array in a 70/30 % v/v mix to create 552 novel co-polymers, plus the 24 constituent homopolymers, totalling 576 substrates for investigation (fig.3.22). These proportions were chosen to maximise investigational space and reduce the redundancy that a 50/50 mix would create. A source plate was prepared which contained the major/minor monomer mixtures with photoinitiator and was contact printed in triplicate on a 25 x 75mm pHEMA coated glass slide and UV polymerised *in situ*.

3.4.1.1. Surface Analysis

ToF-SIMS analysis of the co-polymer array shows that some spots have spread. The most extensive spreading had occurred in the bottom right corner of the array, in co-polymers which contain BM71 (Octafluoropentyl methacrylate). Ideally, the array should be re-printed with highly spreading monomer omitted. However, the spreading and possible mixing of adjacent monomers will be captured by ToF-SIMS and downstream analysis of cell-surface interaction will include all chemistry that may be present in any given polymer region.

Monomer specific ions such as the amine C_2H_6N+ and aromatic C_7H_7+ present in AM38 (dimethylamino-propyl acrylate) and BM39 (benzyl methacrylate) respectively were re-built for a section of the array (fig.3.26) and it can be seen that the amine ion is present in co-polymers of AM38 and the aromatic ion present in co-polymers of BM39. This enables the chemical layout of the array to be confirmed. Note that the C_7H_7+ ion is unexpectedly present in BM18/AM64 (lauryl methacrylate/ Hexadecafluoro-9-(trifluoromethyl)decyl acrylate) indicating chemical contamination in this co-polymer.

	1	2	3	4	5	6	7	8	9	10	11	12	13	14	15	16	17	18	19	20	21	22	23	24
24	AM22	AD17/ BM34	AM22/ BM80	AD17/ BM39	AM22/ AD24	AD17/ AM54	AM22/ AT08	AD17/ BM54	AM22/ AD01	AD17/ BM49	AM22/ BM18	AD17/ BM71	AM22/ BM36	AD17/ CD04	AM22/ DM07	AD17/ AD04	CM04	CM04/ BD03	CM04/ CM09	CM04/ AM71	CM04/ AM38	CM04/ AD17	CM04/ AT03	CM04/ AM64
23	BM39/ AM22	AD01/ BM34	BM39/ BM80	AD01/ BM39	BM39/ AD24	AD01/ AM54	BM39/ AT08	AD01/ BM54	BM39/ AD01	AD01/ BM49	BM39/ BM18	AD01/ BM71	BM39/ BM36	AD01/ CD04	BM39/ DM07	AD01/ AD04	CD04/ CM04	CD04/ BD03	CD04/ CM09	CD04/ AM71	CD04/ AM38	CD04/ AD17	CD04/ AT03	CD04/ AM64
22	AD17/ AM22	AM22/ AM64	AD17/ BM80	AM22/ AT03	AD17/ AD24	AM22/ AD17	AD17/ AT08	AM22/ AM38	AD17/ AD01	AM22/ AM71	AD17/ BM18	AM22/ CM09	AD17/ BM36	AM22/ BD03	AD17/ DM07	AM22/ CM04	CM04/ AD04	CM04/ CD04	CM04/ BM71	CM04/ BM49	CM04/ BM54	CM04/ AM54	CM04/ BM39	CM04/ BM34
21	AD01/ AM22	BM39/ AM64	AD01/ BM80	BM39/ AT03	AD01/ AD24	BM39/ AD17	AD01/ AT08	BM39/ AM38	AD01	BM39/ AM71	AD01/ BM18	BM39/ CM09	AD01/ BM36	BM39/ BD03	AD01/ DM07	BM39/ CM04	CD04/ AD04	CD04	CD04/ BM71	CD04/ BM49	CD04/ BM54	CD04/ AM54	CD04/ BM39	CD04/ BM34
20	AM22/ BM34	AD17/ AM64	AM22/ BM39	AD17/ AT03	AM22/ AM54	AD17	AM22/ BM54	AD17/ AM38	AM22/ BM49	AD17/ AM71	AM22/ BM71	AD17/ CM09	AM22/ CD04	AD17/ BD03	AM22/ AD04	AD17/ CM04	CM04/ DM07	CM04/ BM36	CM04/ BM18	CM04/ AD01	CM04/ AT08	CM04/ AD24	CM04/ BM80	CM04/ AM22
19	BM39/ BM34	AD01/ AM64	BM39	AD01/ AT03	BM39/ AM54	AD01/ AD17	BM39/ BM54	AD01/ AM38	BM39/ BM49	AD01/ AM71	BM39/ BM71	AD01/ CM09	BM39/ CD04	AD01/ BD03	BM39/ AD04	AD01/ CM04	CD04/ DM07	CD04/ BM36	CD04/ BM18	CD04/ AD01	CD04/ AT08	CD04/ AD24	CD04/ BM80	CD04/ AM22
18	BM34/ AM22	AT08/ BM34	BM34/ BM80	AT08/ BM39	BM34/ AD24	AT08/ AM54	BM34/ AT08	AT08/ BM54	BM34/ AD01	AT08/ BM49	BM34/ BM18	AT08/ BM71	BM34/ BM36	AT08/ CD04	BM34/ DM07	AT08/ AD04	AD04/ CM04	AD04/ BD03	AD04/ CM09	AD04/ AM71	AD04/ AM38	AD04/ AD17	AD04/ AT03	AD04/ AM64
17	AT03/ AM22	BM49/ BM34	AT03/ BM80	BM49/ BM39	AT03/ AD24	BM49/ AM54	AT03/ AT08	BM49/ BM54	AT03/ AD01	BM49	AT03/ BM18	BM49/ BM71	AT03/ BM36	BM49/ CD04	AT03/ DM07	BM49/ AD04	BM36/ CM04	BM36/ BD03	BM36/ CM09	BM36/ AM71	BM36/ AM38	BM36/ AD17	BM36/ AT03	BM36/ AM64
16	AT08/ AM22	BM34/ AM64	AT08/ BM80	BM34/ AT03	AT08/ AD24	BM34/ AD17	AT08	BM34/ AM38	AT08/ AD01	BM34/ AM71	AT08/ BM18	BM34/ CM09	AT08/ BM36	BM34/ BD03	AT08/ DM07	BM34/ CM04	AD04	AD04/ CD04	AD04/ BM71/	AD04/ BM49	AD04/ BM54	AD04/ AM54	AD04/ BM39	AD04/ BM34
15	BM49/ AM22	AT03/ AM64	BM49/ BM80	AT03	BM49/ AD24	AT03/ AD17	BM49/ AT08	AT03/ AM38	BM49/ AD01	AT03/ AM71	BM49/ BM18	AT03/ CM09	BM49/ BM36	AT03/ BD03	BM49/ DM07	AT03/ CM04	BM36/ AD04	BM36/ CD04	BM36/ BM71/	BM36/ BM49	BM36/ BM54	BM36/ AM54	BM36/ BM39	BM36/ BM34
14	BM34	AT08/ AM64	BM34/ BM39	AT08/ AT03	BM34/ AM54	AT08/ AD17	BM34/ BM54	AT08/ AM38	BM34/ BM49	AT08/ AM71	BM34/ BM71	AT08/ CM09	BM34/ CD04	AT08/ BD03	BM34/ AD04	AT08/ CM04	AD04/ DM07	AD04/ BM36	AD04/ BM18	AD04/ AD01	AD04/ AT08	AD04/ AD24	AD04/ BM80	AD04/ AM22
13	AT03/ BM34	BM49/ AM64	AT03/ BM39	BM49/ AT03	AT03/ AM54	BM49/ AD17	AT03/ BM54	BM49/ AM38	AT03/ BM49	BM49/ AM71	AT03/ BM71	BM49/ CM09	AT03/ CD04	BM49/ BD03	AT03/ AD04	BM49/ CM04	BM36/ DM07	BM36	BM36/ BM18	BM36/ AD01	BM36/ AT08	BM36/ AD24	BM36/ BM80	BM36/ AM22
12	AM64/ AM22	BM54/ BM34	AM64/ BM80	BM54/ BM39	AM64/ AD24	BM54/ AM54	AM64/ AT08	BM54	AM64/ AD01	BM54/ BM49	AM64/ BM18	BM54/ BM71	AM64/ BM36	BM54/ CD04	AM64/ DM07	BM54/ AD04	DM07/ CM04	DM07/ BD03	DM07/ CM09	DM07/ AM71	DM07/ AM38	DM07/ AD17	DM07/ AT03	DM07/ AM64
11	AD24/ AM22	AM71/ BM34	AD24/ BM80	AM71/ BM39	AD24	AM71/ AM54	AD24/ AT08	AM71/ BM54	AD24/ AD01	AM71/ BM49	AD24/ BM18	AM71/ BM71	AD24/ BM36	AM71/ CD04	AD24/ DM07	AM71/ AD04	CM09/ CM04	CM09/ BD03	CM09	CM09/ AM71	CM09/ AM38	CM09/ AD17	CM09/ AT03	CM09/ AM64
10	BM54/ AM22	AM64	BM54/ BM80	AM64/ AT03	BM54/ AD24	AM64/ AD17	BM54/ AT08	AM64/ AM38	BM54/ AD01	AM64/ AM71	BM54/ BM18	AM64/ CM09	BM54/ BM36	AM64/ BD03	BM54/ DM07	AM64/ CM04	DM07/ AD04	DM07/ CD04	DM07/ BM71	DM07/ BM49	DM07/ BM54	DM07/ AM54	DM07/ BM39	DM07/ BM34
9	AM71/ AM22	AD24/ AM64	AM71/ BM80	AD24/ AT03	AM71/ AD24	AD24/ AD17	AM71/ AT08	AD24/ AM38	AM71/ AD01	AD24/ AM71	AM71/ BM18	AD24/ CM09	AM71/ BM36	AD24/ BD03	AM71/ DM07	AD24/ CM04	CM09/ AD04	CM09/ CD04	CM09/ BM71	CM09/ BM49	CM09/ BM54	CM09/ AM54	CM09/ BM39	CM09/ BM34
8	AM64/ BM34	BM54/ AM64	AM64/ BM39	BM54/ AT03	AM64/ AM54	BM54/ AD17	AM64/ BM54	BM54/ AM38	AM64/ BM49	BM54/ AM71	AM64/ BM71	BM54/ CM09	AM64/ CD04	BM54/ BD03	AM64/ AD04	BM54/ CM04	DM07	DM07/ BM36	DM07/ BM18	DM07/ AD01	DM07/ AT08	DM07/ AD24	DM07/ BM80	DM07/ AM22
7	AD24/ BM34	AM71/ AM64	AD24/ BM39	AM71/ AT03	AD24/ AM54	AM71/ AD17	AD24/ BM54	AM71/ AM38	AD24/ BM49	AM71	AD24/ BM71	AM71/ CM09	AD24/ CD04	AM71/ BD03	AD24/ AD04	AM71/ CM04	CM09/ DM07	CM09/ BM36	CM09/ BM18	CM09/ AD01	CM09/ AT08	CM09/ AD24	CM09/ BM80	CM09/ AM22
6	BM80/ AM22	AM38/ BM34	BM80	AM38/ BM39	BM80/ AD24	AM38/ AM54	BM80/ AT08	AM38/ BM54	BM80/ AD01	AM38/ BM49	BM80/ BM18	AM38/ BM71	BM80/ BM36	AM38/ CD04	BM80/ DM07	AM38/ AD04	BD03/ CM04	BD03	BD03/ CM09	BD03/ AM71	BD03/ AM38	BD03/ AD17	BD03/ AT03	BD03/ AM64
5	AM54/ AM22	BM18/ BM34	AM54/ BM80	BM18/ BM39	AM54/ AD24	BM18/ AM54	AM54/ AT08	BM18/ BM54	AM54/ AD01	BM18/ BM49	AM54/ BM18	BM18/ BM71	AM54/ BM36	BM18/ CD04	AM54/ DM07	BM18/ AD04	BM71/ CM04	BM71/ BD03	BM71/ CM09	BM71/ AM71	BM71/ AM38	BM71/ AD17	BM71/ AT03	BM71/ AM64
4	AM38/ AM22	BM80/ AM64	AM38/ BM80	BM80/ AT03	AM38/ AD24	BM80/ AD17	AM38/ AT08	BM80/ AM38	AM38/ AD01	BM80/ AM71	AM38/ BM18	BM80/ CM09	AM38/ BM36	BM80/ BD03	AM38/ DM07	BM80/ CM04	BD03/ AD04	BD03/ CD04	BD03/ BM71/	BD03/ BM49	BD03/ BM54	BD03/ AM54	BD03/ BM39	BD03/ BM34
3	BM18/ AM22	AM54/ AM64	BM18/ BM80	AM54/ AT03	BM18/ AD24	AM54/ AD17	BM18/ AT08	AM54/ AM38	BM18/ AD01	AM54/ AM71	BM18	AM54/ CM09	BM18/ BM36	AM54/ BD03	BM18/ DM07	AM54/ CM04	BM71/ AD04	BM71/ CD04	BM71	BM71/ BM49	BM71/ BM54	BM71/ AM54	BM71/ BM39	BM71/ BM34
2	BM80/ BM34	AM38/ AM64	BM80/ BM39	AM38/ AT03	BM80/ AM54	AM38/ AD17	BM80/ BM54	AM38	BM80/ BM49	AM38/ AM71	BM80/ BM71	AM38/ CM09	BM80/ CD04	AM38/ BD03	BM80/ AD04	AM38/ CM04	BD03/ DM07	BD03/ BM36	BD03/ BM18	BD03/ AD01	BD03/ AT08	BD03/ AD24	BD03/ BM80	BD03/ AM22
1	AM54/ BM34	BM18/ AM64	AM54/ BM39	BM18/ AT03	AM54	BM18/ AD17	AM54/ BM54	BM18/ AM38	AM54/ BM49	BM18/ AM71	AM54/ BM71	BM18/ CM09	AM54/ CD04	BM18/ BD03	AM54/ AD04	BM18/ CM04	BM71/ DM07	BM71/ BM36	BM71/ BM18	BM71/ AD01	BM71/ AT08	BM71/ AD24	BM71/ BM80	BM71/ AM22

Figure 3.22 Layout of Secondary generation Co-polymer Array.
24 monomers were mixed in 70/30 ratios and mixed pair-wise to generate the 552 co-polymers and 24 homopolymers (total 576 polymers).

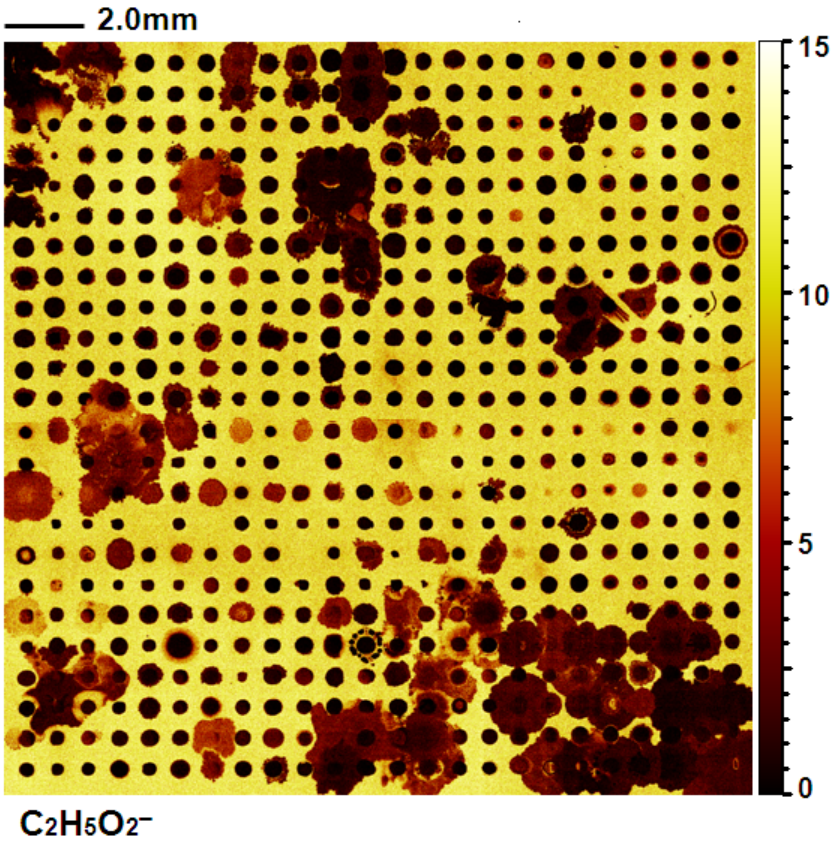


Figure 3.23 Time of Flight Secondary Ion Mass Spectrometry of Second Generation Co-polymer Array.
This image is an ion intensity map of the background pHEMA specific ion $C_2H_5O_2$-. Brightest regions indicate high intensity of the ion (scale is counts per pixel). Regions of polymer spreading can be seen, especially in the bottom right, which are predominantly co-polymers of BM71 – see figure 3.21.

3.4.1.2. Screening of Cardiomyocyte Attachment

The aim of screening at this stage was to choose five polymers that supported the greatest cardiomyocyte attachment and relatively large cell size which indicates that the cardiomyocyte is capable of spreading on the polymer and therefore more likely to display myofibril organisation. Cardiomyocytes cultured on these five polymers will undergo more detailed characterisation for morphology and electrophysiology. A limited number of co-polymers were chosen due to the low throughput nature of focussed characterisation. Arrays were seeded for 7 days on both serum free (pre-conditioned for 1 hour CM medium) and serum conditioned arrays (pre-conditioned in CM medium plus 20% FBS, see methods section).

Arrays supported cardiomyocyte attachment on 82 % and 74 % of polymers on serum preconditioned and serum free arrays, respectively (fig.3.24 and 25). However, as seen in homopolymer arrays, serum preconditioning modulates cell adhesion and the actual number of cardiomyocytes attached to polymers on serum pre-conditioned arrays was higher than on serum free arrays. The highest average attachment on serum conditioned arrays was on co-polymer AD01/BM54 with 516±132 cells/mm^2 (±s.d, n=2). Whereas, the highest average cell count on serum free arrays was significantly lower at 143±44 cells/mm^2 (n=2) on BD03/AT08 (unpaired t-test, $p<0.05$). Cardiomyocytes displayed largest average size of 661±36 µm^2 on co-polymer AD01/BM80 when serum pre-conditioned and 1089±260 µm^2 on BM80/AM64 in serum free culture.

3.4.1.3. Synergy

Another purpose of co-polymerising monomers was to see if the overall density or cardiomyocyte area could be improved for substrates that displayed good density or size but not both. This is important for increasing the choice of materials available for potential cardiomyocyte culture, not only for the purpose of improving attachment and morphology of cardiomyocytes but also to diversify the nature of the polymers which may need particular properties for successful scale up. These may include brittleness, opacity and stiffness of the polymer which may all be widely different in co-polymers.

An example of improvement in a co-polymer compared to its constituent homopolymers is AM38/BM39, (Dimethylamino-propyl acrylate/ Benzyl methacrylate), (fig.3.26). In the first generation screen, AM38 supported relatively high attachment in serum free conditions but cell size was small with no myofibril organisation, this was also observed in the second generation array (fig.3.26). However, when co-polymerised with BM39, cell area was improved (612± 170 µm^2) compared to AM38 alone (126 ±6 µm^2).

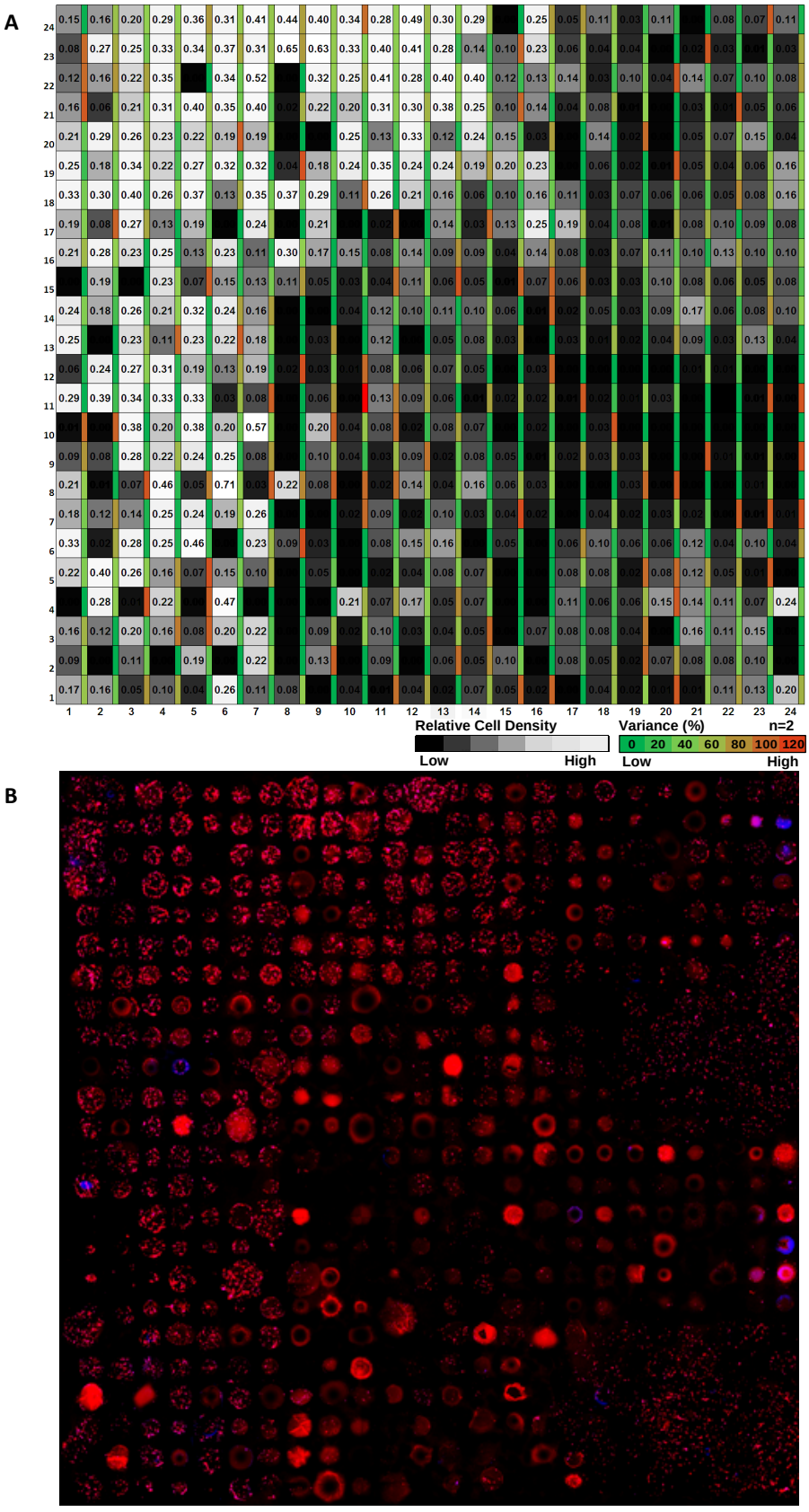


Figure 3.24 Cardiomyocytes Cultured on Serum Pre-conditioned Co-polymer Array
A) Relative cell density on polymer is higher in whiter regions. Coefficient of variation is lower when green (n=2). **B)** Mosaic of immunostained microarray with sarcomeric alpha actinini (red) and DAPI (blue). Individual images of each polymer were taken at x10 magnification.

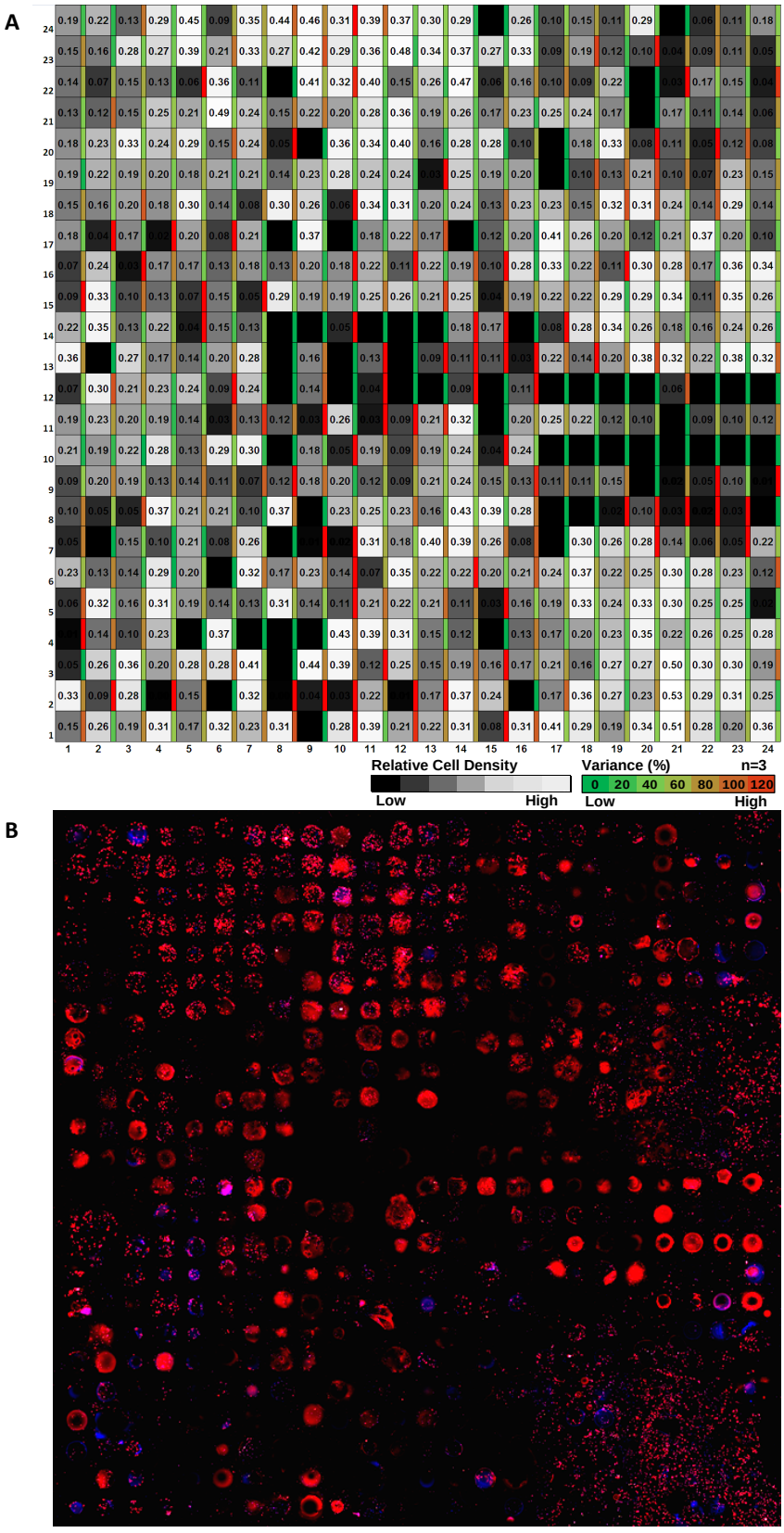


Figure 3.25 Cardiomyocytes Cultured on Co-polymer Array in Serum free Conditions.

A) Relative cell density on polymer is higher in whiter regions. Coefficient of variation is lower when green (n=3). **B)** Mosaic of immunostained microarray with sarcomeric alpha actinin (red) and DAPI (blue). Individual images of each polymer were taken at x10 magnification.

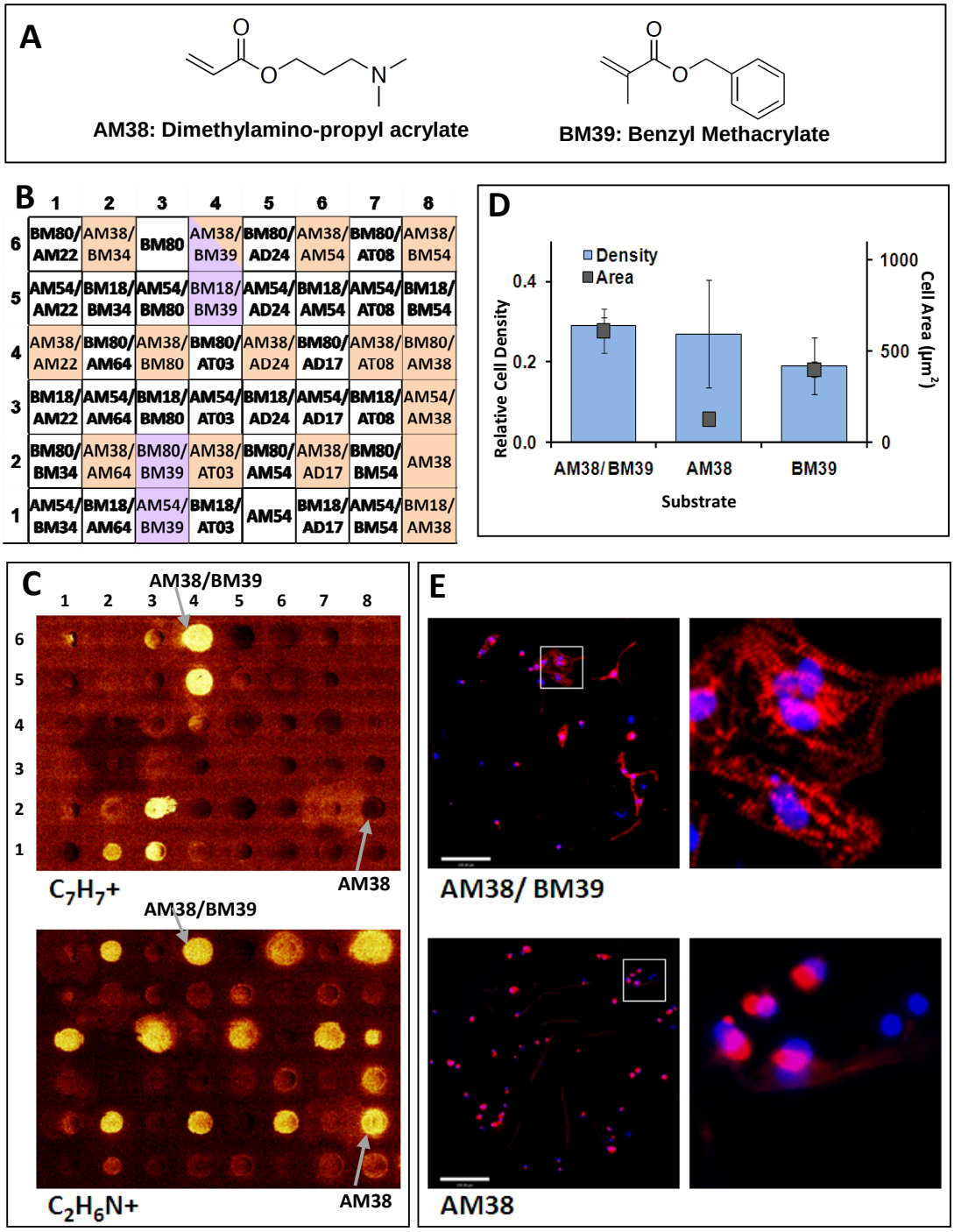


Figure 3.26 Synergy Observed in Co-Polymer AM38/BM39.
The bottom left section of the layout shown in figure 3.21 is shown in **B)** and highlights co-polymers containing either BM39 (purple) or AM38 (orange) or both (structures in panel **A**). Chemical distribution of the BM39 specific ion C_7H_7+ and AM38 specific ion C_2H_6N+ can be seen in corresponding ToF-SIMS images **C)** which shows high intensity (bright regions) that overlap with the purple and orange regions respectively. Both ions are present in the co-polymer. The chart **D)** compares cardiomyocyte attachment and size on AM38/BM49, which displays improved cell area on the co-polymer compared to AM38 alone (± s.e.m, n=3). The improved cell area on co-polymer AM38/BM39 corresponds to more organised myofibril alignment seen in immunolabelled sarcomeric α actinin (red) in the images in panel **E**.

3.4.1.4. Polymer Selection for Detailed Cardiomyocyte Characterisation

Due to the high proportion of successful attachment on second generation co-polymer arrays in serum free conditions, the five substrates chosen to take forward for more detailed characterisation of cardiomyocytes cultured on them were all chosen from this array. Although, actual cell numbers attached to the polymers was lower than serum-conditioned arrays, it is serum free, defined conditions that are a preferred culture option.

The top ten polymers which had the highest cell density and top ten which had the largest cell size are listed in table 3.2. The selected polymers can be seen in figure 3.26 and were chosen based on cardiomyocytes having both high cell density and cell size on the substrates.

Table 3.2 Top ten co-polymers that support cardiomyocyte attachment in serum free conditions.
Listed are the top ten substrates which exhibited the highest cardiomyocyte density alongside those which had the highest cell density in serum free conditions. There is little overlap between the two except AD17/BM54 (9) which is in the top ten for both density and area. (±s.e.m, n=3).

	Co-polymer	Cell Density	Co-Polymer	Cell Area (μm^2)
1	**BD03/ AT08**	0.53 ±0.14	**BM80/ AM64**	1089 ±150
2	**BM71/ AT08**	0.51 ± 0.20	**BM39/ AT08**	1043 ±257
3	**BM71/ BM54**	0.50 ± 0.09	**AD17/ AD24**	1039 ±510
4	**BM39/ AD17**	0.49 ± 0.13	**AM71/ AM22**	1035 ±469
5	**AD01/ BM71**	0.48 ± 0.05	**AM71/ AD24**	1022 ±275
6	**AM22/ BD03**	0.47 ± 0.10	**AD24/ BM39**	999 ±334
7	**AM22/ AD01**	0.46 ± 0.18	**BM39/ AM22**	975 ±72
8	**AM22/ AD24**	0.45 ± 0.08	**AM38/ BM49**	914 ±67
9	**AD17/ BM54**	0.44 ± 0.22	**AD17/ BM54**	899 ±100
10	**BM18/ AD01**	0.44 ± 0.18	**AD24/ AM22**	883 ±318

The final five substrates chosen to take forward are listed below. Whilst cell density is comparable to gelatin control, surface area of adhered cardiomyocytes is smaller. Cardiomyocytes will be characterised further to see if culture on different substrates has any effect on electrophysiology, myofibril organisation and ion channel distribution which are all important for cardiomyocyte functionality.

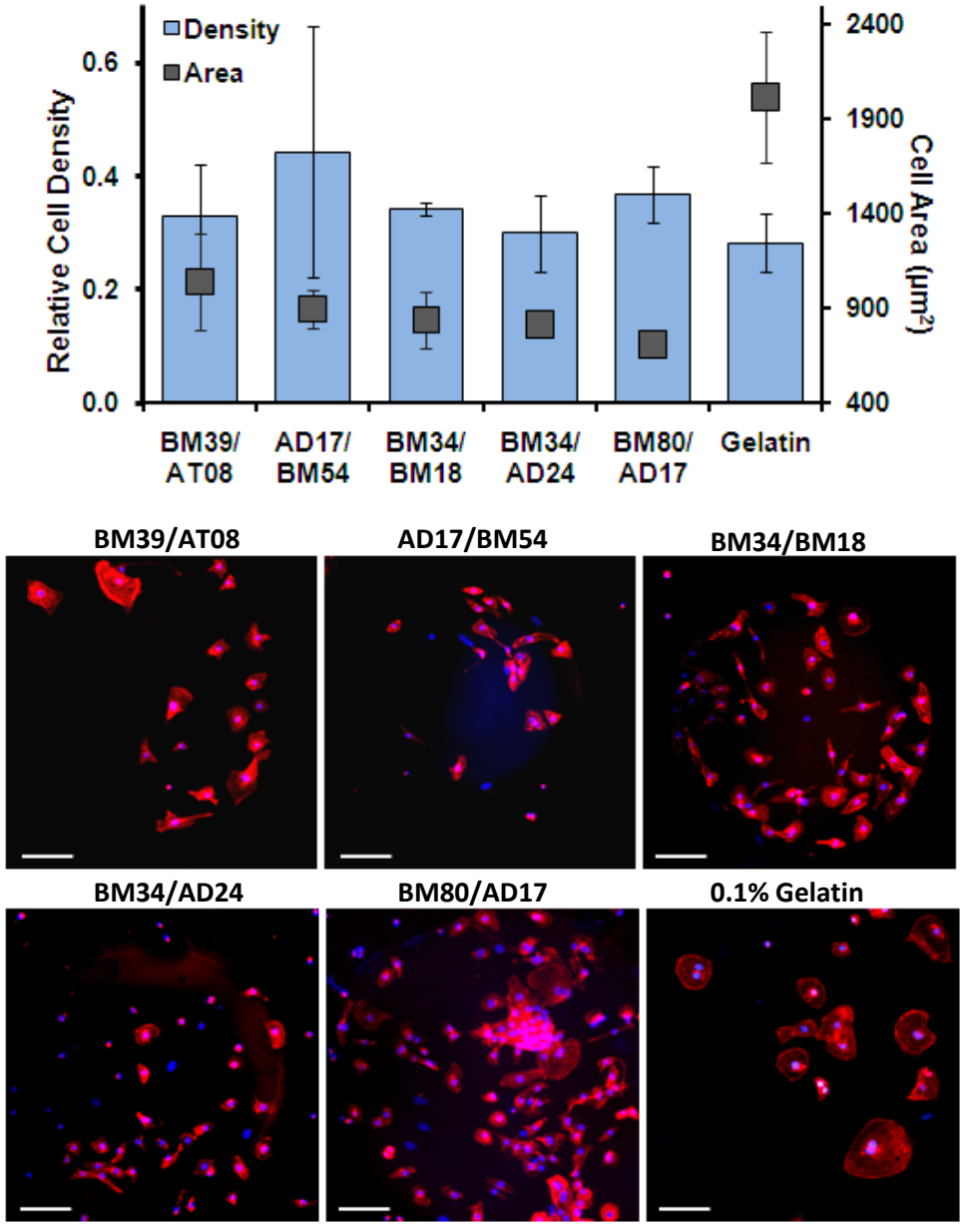


Figure 3.27 Five Selected Co-Polymers that Support Cardiomyocyte Attachment in Serum Free Conditions to be forwarded for Detailed Cardiomyocyte Characterisation.
The five co-polymers chosen supported relatively high attachment and cell spread (±s.e.m, n=2). Corresponding immunostained images are shown below the chart. Cardiomyocytes were stained with anti-human sarcomeric alpha actinin (red) and a nuclear marker, DAPI (blue). Scale bar = 100µm.

3.5. DISCUSSION

Generation of relatively high purity populations of human cardiomyocytes has been achieved using an embryoid body method optimised for the HUES7 cell line that did not require enrichment or cell sorting prior to use. This enabled adequate cell numbers to be produced for screening attachment on replicates of 115 polymers contained in a first generation homopolymer array followed by 576 co-polymers in a second generation co-polymer array.

A higher proportion of substrates in the co-polymer array were able to support attachment in serum free conditions (74 %) compared to the first generation homopolymer array (10 %). This is to be expected as the chemical diversity was reduced from 115 randomly chosen monomers to 24 that were selected based on performance, to generate a co-polymer array. 12 of the 24 were found to support cardiomyocyte attachment and/or larger cell area in serum free conditions. Monomers that supported relatively poor or no attachment were also selected to generate co-polymers so that cell-surface relationships could be studied downstream. Finally 5 co-polymers have been selected to perform more detailed analysis of cardiomyocytes cultured on them.

3.5.1.1. Morphology of HUES7-cardiomyocytes.

The culture of hESC derived cardiomyocytes on control 0.1% gelatin highlights the variability in morphology of the cardiomyocytes with regards to their size, shape and myofibril alignment. As well as cell attachment density, these parameters are important for selecting substrates from microarrays to investigate if synthetic surfaces are capable of supporting cardiomyocyte behaviour that is at least comparable to control and at best improves the maturity and consistency of cardiomyocytes.

The typical size of control HUES7-cardiomyocytes on gelatin at 24 hours post-disaggregation was found to be 351 μm^2 , which is similar to literature values of hESC-cardiomyocytes reported to be 25 x 10 μm^2 (Snir et al., 2003). At 7 days post-disaggregation, the cardiomyocytes spread on the gelatin and their

surface area increased to an average of 2019 μm^2 which is similar to that reported for adult human cardiomyocytes from biopsy 20 x 120 μm^2 (del Monte et al., 1995) (fig.3.7) but has a markedly different morphology. Adult cardiomyocytes being rod shaped with an aspect ratio around 6. However, HUES7-cardiomyocytes at 7 days display more rounded morphologies.

HUES7-cardiomyocytes cultured on polymer microarrays displayed surface areas between 250 μm^2 to 1400 μm^2 which is within the range of those seen on gelatin. The morphology of cells did not appear to be related to surface chemistry and so was not used as a parameter to select surfaces and has been reported to be dependent on surface patterning and stiffness which was not controlled in this study (Rao et al., 2012, Boudou et al., 2011).

No enrichment of cardiomyocytes was required due to the high proportion of cardiomyocytes within the beaters as determined by immunostaining and FACS.

3.5.1.2. Serum Pre-conditioning

The main purpose of discovery of synthetic materials is to enable cardiomyocyte culture in more defined conditions. Therefore, attachment in serum free conditions was the favoured option. Both FBS conditioning and serum free culture conditions were included during screening so that downstream investigation of surface chemistry and serum modulated adhesion could be investigated.

The diverse range of adhesion and spread on the serum treated polymers supports the well reported phenomena that surface chemistry can alter protein adsorption and/or conformation that can subsequently influence cell adhesion (Shen and Horbett, 2001, Keselowsky et al., 2003). For example, with the aid of serum proteins BM34, furfuryl methacrylate is capable of supporting a significantly greater cell density compared to BM80, Methacryloyloxy)ethyl acetoacetate ($p<0.05$, ANOVA, n=4). However, in serum free conditions both polymers support similarly low densities of cardiomyocytes. The higher proportion of attachment on serum coated arrays demonstrates that the lack of

adhesion in serum free conditions is due to the absence of adhesive proteins and not the underlying substrate. The diverse behaviour of cardiomyocytes on these arrays confirms that a range of chemistries with differing effects on serum proteins have been included in a microarray format to enable parallel investigation.

3.5.1.3. Combinatorial Development of Novel Substrates

Serum free culture on first generation homopolymer arrays only identified 12 polymers that supported cardiomyocyte attachment. The cells that did attach displayed a small surface area and no myofibril banding compared to 0.1 % gelatin and serum pre-conditioned arrays (fig3.20). The importance of combinatorial chemistry is demonstrated here with co-polymerisation yielding 429 substrates that supported cardiomyocyte attachment, larger cell area and myofibril banding in serum free conditions (fig.3.26). Cell attachment now approaches densities comparable to gelatin control, however cell area remains relatively small on the co-polymers. Further investigation is required to determine whether this is detrimental to cardiomyocyte functionality.

3.5.1.4. High throughput Screening

Little is known about cardiomyocyte behaviour and surface chemistry. Small sets of materials have been analysed (Natarajan et al., 2008, Curran et al., 2006). To enable parallel investigation, a system has been optimised to allow screening of human cardiomyocytes and microarray format has shown to be a platform to expedite the discovery of potential substrates for cardiomyocyte culture. Due to the large diversity of chemistries surveyed there is opportunity to discern cell surface chemistry relationships will be discussed in chapter 5.

3.6. LIMITATIONS AND FUTURE WORK

This thesis will next focus on cardiomyocyte interaction with chosen co-polymers only and then attempt to model cell – surface chemistry relationship.

However, with the aid of greater resources, there is potential to investigate 1. Synergy, 2. Difference in immediate and prolonged attachment, 3. Surface elasticity and topography.

The uncontrolled free radical polymerisation may be a limitation for scaling up hit polymers. Crosslinking can occur at differing degrees, this shouldn't effect surface chemistry but mechanical properties i.e stiffness can be altered with each polymerisation and this is known to effect cardiomyocyte behaviour.

High content screening could be optimised at this stage so that quantified myofibril alignment could be used as a parameter to select potential polymers for culture.

CHAPTER 4

Characterisation of Cardiomyocytes on Selected Substrates in Serum Free Conditions.

4.1. INTRODUCTION

In chapter 3, parallel screening of various polyacrylates and polyacrylamides has identified co-polymers that allowed hESC derived cardiomyocyte attachment and spread in serum free conditions. As discussed in chapter 1, the maturity of hPSC-cardiomyocytes is currently a predominant issue in the pharmaceutical industry who are looking to complement toxicological and efficacy drug testing with more relevant *in vitro* models (Harris et al., 2013). In order to assess the structural and functional maturity of cardiomyocytes on the synthetic polymers compared to those cultured on gelatin, the cells were characterised for myofibril organisation, electrophysiological profile and ion channel distribution of the $Na_v1.5$ sodium channel and Kir2.1 potassium channel, all of which enable objective measurement of maturity.

4.1.1. Myofibril Organisation

The organisation of the bundles of myofibrils that make up the cardiomyocyte underlie the contractile properties of the cell (Blazeski et al., 2012) . They may be visualised using immunostaining of proteins such as sarcomeric alpha actinin and cardiac troponin I which reside in the Z lines and A bands of the myofibrils respectively (fig. 1.2). The alignment of myofibrils are parallel and highly organised throughout rod shaped primary adult human cardiomyocytes, whereas fetal human cardiomyocytes display multi-angular regions of locally organised myofibrils but are generally disorganised throughout the cell as can be seen in figure 4.1 (Mummery et al., 2003, Bird et al., 2003). Cardiomyocytes derived *in vitro* from hESCs tend to display myofibril organisation similar to the fetal phenotype (Vidarsson et al., 2010).

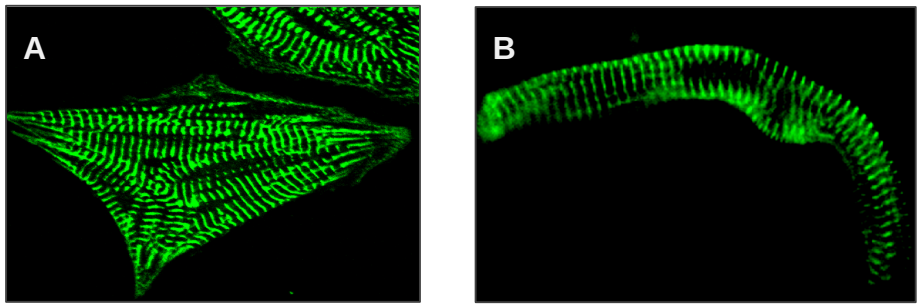


Figure 4.1 Primary Human Ventricular Cardiomyocytes; (A) Fetal and (B) Adult, immunostained for sarcomeric alpha actinin.
The fetal cardiomyocyte displays a multi-angular morphology with generally disorganised myofibrils (z-lines). The adult cardiomyocyte has rod shaped morphology with highly organised parallel myofibrils throughout the cell. From Mummery et al 2003.

The spacing between the Z lines correlates to sarcomere length and may also hold information about cardiac maturity. Rhee *et al*, found that chick cardiomyocytes display spacing between Z lines of less than 1.4 µm in immature myofibrils, whereas fully formed fibrils had a spacing greater than 1.8 µm (Rhee et al., 1994). In humans, an increase of sarcomere length from 1.7 to 2.3 µm results in increased contractile force (van der Velden et al., 2000). This mechanism of increased contractility with sarcomere length forms the basis of the Frank-Starling law where increased ventricular volume increases output (Katz, 2002). The two main explanations for this relationship are **i)** an increased degree of thick and thin filament overlap, increasing probably of actin-myosin cross bridge formation (Rodriguez et al., 2011) (fig.4.2) and **ii).** increased calcium sensitivity upon an increase in sarcomere length generating greater force at a lower calcium concentration (de Tombe et al., 2010).

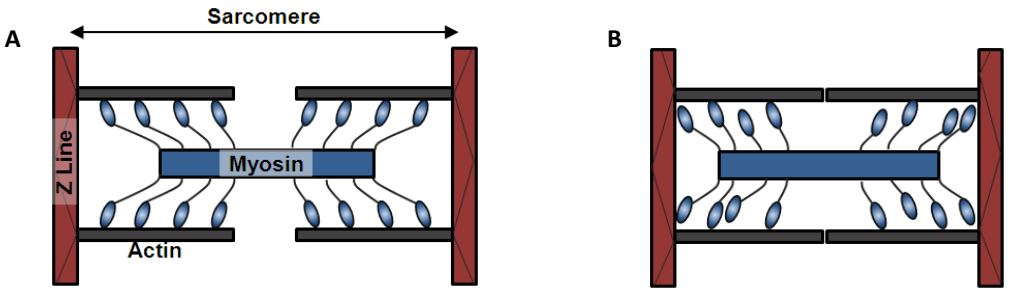


Figure 4.2 Sarcomere Length and Cross-Bridge Formation
Distance between Z lines correlates to sarcomere length. At longer lengths actin and myosin cross-bridging is optimal **(A)**. At shorter lengths, there are less actin-myosin cross-bridges formed which impedes generation of contractile force **(B)** and also reduces sensitivity to calcium.
(Adapted from de Tombe et al 2010 and (Iaizzo, 2009))

4.1.2. Electrophysiology

In 'current clamp' mode, whole cell patch clamp electrophysiology records the current moving across a contracting cardiomyocyte when a gigaseal is created between the patch pipette and cell membrane and a pulse of suction is applied to remove a small patch of the membrane to gain access to the cell interior (fig.4.3). A circuit is created between the reference electrode that sits in

the NT buffer and the recording electrode that is in the patch pipette. Ionic currents in the picoampere range are converted to voltage by an amplifier (Penner, 1995, Neher and Sakmann, 1976). An action potential (AP) is generated during each contraction and its profile depends on the combined contribution of the ionic currents.

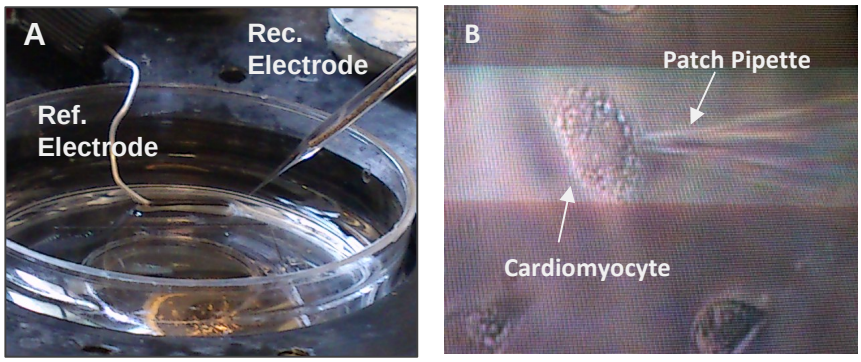


Figure 4.3 Patch Clamp Electrophysiology
(A) Patch Clamp electrophysiology detects the ionic currents moving across the cell membrane using a recording electrode that is within the patch pipette (B) which remove a patch of cell membrane get an intracellular recording and is calibrated to the reference electrode.

In contrast, the multielectrode array (MEA) uses fixed electrodes on a chip which is seeded with whole beating clusters and records the electrical activity extracellularly (Meyer et al., 2004). The MEA technique can obtain data relatively quickly because it does not involve highly skilled and time intensive membrane patching and can perform longer time frame measurements because the cell membrane integrity is not compromised but limits the data that it garners to field potential recordings. These recordings are less information rich, ionic currents cannot be measured for example. However, MEA can measure conduction velocities between adjacent cells which is not available from single cell action potential recordings (Natarajan et al., 2011) but the MEA chip requires coating with ECM proteins such as fibronectin or Matrigel™ upon which the beating cluster is seeded and so does not enable direct analysis of cardiomyocytes on the polymer substrates. Also, fibroblasts could retard electrical recordings especially if cultured for longer than 2 days because

fibroblasts can proliferate rapidly (Wang et al., 2013). For these reasons patch clamp analysis was employed.

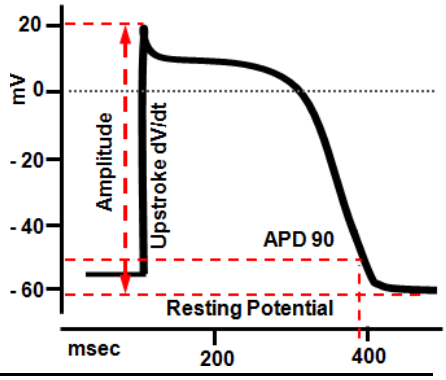
Measurement of AP parameters can give a detailed description of phenotype. Upstroke velocities of 5 – 50 V/s and resting potentials (also called maximal diastolic potential, MDP) of approximately -40 to -50 mV have been observed in hPSC derived ventricular-like cardiomyocytes (He et al., 2003, Xu et al., 2002, Mummery et al., 2012). These values suggest functional immaturity of the cells compared to values reported for human adult ventricular cardiomyocytes which have upstroke velocities and resting potentials between 150 – 300 V/s and -85mV respectively (Mummery et al., 2003, Drouin et al., 1995) (see table 4.1).

One study reported more negative membrane resting potentials and faster upstroke velocities from hESC derived cardiomyocytes and attributed the more mature values to the fact that their hESC lines are cultured on human feeder cells which may secrete factors that enhance cardiac maturity compared to the animal feeder cells used in other studies (Pekkanen-Mattila et al., 2010).

Patch clamp measurements are typically performed on cardiomyocytes that have been seeded onto gelatin, fibronectin or Matrigel™ coated dishes. There is limited characterisation data of cardiomyocytes on synthetic surfaces. Electrophysiological comparison of rat cardiomyocytes on two synthetic surfaces in serum free conditions has been reported by Natarajan *et al* 2008. Glass coverslips were modified to present either hydroxy or carboxy groups. It was found that a significantly lower number of cardiomyocytes attached to the hydroxy surface and those that did attach had an ‘unusually’ large action potential duration compared to the carboxy surface. However, the study did not attempt to distinguish between the cardiomyocyte sub-types and could have been comparing different populations of sub-type with each other which would inherently have significant differences as highlighted in fig.1.3.

Table 4.1 Reported Action Potential Measurement from Human Ventricular Cardiomyocytes.

Action potential duration (APD), amplitude (APA), resting/maximal diastolic potential (MDP) and upstroke velocity (±s.e.m) reported for human cardiomyocytes. Direct comparison is difficult due to differences in cell source, maintenance, differentiation method and age (shown in brackets where available). There is a general trend for hESC derived cardiomyocytes to display MDP and Upstroke velocities closer to the human fetal phenotype. The figure on the right displays where these measurements are made on the ventricular-like action potential.



Cell Source	Diff method	n =	APD 90 (ms)	APA (mV)	MDP (mV)	dV/dt (V/s)	Reference
Primary							
Human Fetal (16wks)	-	6	370.0 ±45.8	69.0 ±9.1	- 38.5 ±1.6	8.9 ±4.3	(Mummery et al., 2003)
Human Adult (14-46 yrs)	-	14	330 ±16	105 ±2	- 87 ±1	234 ±28	(Drouin et al., 1995)
hESC derived							
HES-2	Co-culture (20 d) (60 d)	10 39	629±58 474±35	Data missing	-61±2 -61±1	14.9±2 24.9±1	(Sheng et al., 2012)
H9	EB (35 d)	39	475 ±35	79 ±22	Data missing	16 ±3	(Wei et al., 2012b)
H7	Monolayer (60-90 d)	42	286 ±53	86.8 ±12.4	- 62.3 ±8.6	11.4 ±2.8	(Zhang et al., 2011)
Regea 06/015 HS346	EB	34	232 ±90	120.3 ±10.0	- 74.8 ±3.9	154.6 ±55.7	(Pekkanen-Mattila et al., 2010)
Regea 06/015 HS346	Co-culture	28	265 ±56	113.3 ±10.7	- 67.3 ±4.5	129.4 ±105.0	(Pekkanen-Mattila et al. 2010)
H1	EB (20-40 d) (56-84 d)	12 11	228 ±11 395 ±51	62.5 ±4.7 67.9 ±3.3	- 47 ±7 - 53 ±4	4.2±0.6 6.0±0.4	(Sartiani et al., 2007) Supp info.
H9.2	EB	6	425 ±150	100	- 60	12 ±2	(Satin et al., 2004)
HES-2	Co-culture	28	436 ±55	80.0 ±3.5)	- 48.0 ±1.7	7.0 ±0.8	(Mummery et al. 2003)
H1, H7, H9,H14	EB(95d)	60	247 ±67	85.3 ±9.3	-53.9 ±8.6	13.2 ±6.2	(He et al., 2003)

Ion Channel Distribution

The action potential is regulated by movement of potassium, sodium and calcium ions through various inward and outward channels as described in chapter 1. As seen in table 4.1, the resting potential and upstroke velocity are markedly immature in hESC derived cardiomyocytes.

The influx of potassium ions through the KCNJ2 encoded Kir2.1 channel generates the I_{K1} (inward rectifier current) which aids hyper-polarisation and maintenance of a negative maximal diastolic potential (MDP) (Doss et al., 2012). The I_{K1} current has been shown to be functionally absent in cardiomyocytes derived from hiPSC and hESC (collectively termed hPSC) (Satin et al., 2004, Jonsson et al., 2012). I_{K1} deficiency has been reported to be one of the biggest contributors to the immature phenotype of hPSC-cardiomyocytes (Lieu et al., 2013). Expression of Kir2.1 has been shown to correlate to MDP, with forced expression of Kir2.1 leading to a significantly more negative MDP in mouse ESC-cardiomyocytes (Liao et al., 2013) and hESC-cardiomyocytes (Lieu et al., 2013).

The efflux of sodium ions through the SCN5A encoded $Na_V1.5$ channel functions to depolarise the membrane and once above threshold, generate an action potential (Jonsson et al., 2012, Berecki et al., 2010). The upstroke velocity in mature cardiomyocytes is relatively fast and a reduction in sodium current (I_{NA}) density correlated to a decrease in upstroke velocity in mouse ESC-cardiomyocytes (Davis et al., 2012).

In order for these channels to execute their function, they need to be expressed at the membrane. The $Na_V1.5$ channel has been shown to localise at the sarcolemma and at T-tubules of ventricular cardiomyocytes from adult mice (Mohler et al., 2003). In human and other mammalian ventricular myocardium, the T-tubules have been shown to be invaginations of the membrane occurring regularly near Z-lines (Driesen et al., 2007, Kostin et al., 1998, Nelson and Benson, 1963). Consequently, $Na_V1.5$ channel staining appears most intense at the plasma membrane and at Z-lines (Petitprez et al., 2011). Similarly, Kir2.1 has been shown

to be expressed at the sarcolemma and T-tubules of ventricular cardiomyoyctes from adult mice (Clark et al., 2001, Ma et al., 2011a).

Reports for cellular localisation of $Na_V1.5$ and Kir2.1 in hPSC-cardiomyocytes are limited. Doss *et al*, presented immunostaining of Kir2.1 in hiPSC-cardiomyocytes at 160 days post-differentiation which exhibited diffuse staining throughout the cell, without any prominent localisation at the membrane (Doss et al., 2012).

4.1.2.1. Chapter Objectives:

1. Print an array consisting of one type of 'hit' polymer to facilitate further characterisation.

2. Quantify structural integrity of cardiomyocytes cultured on different substrates by performing detailed characterisation of myofibril alignment.

3. Quantify functional maturity by measurement of electrophysiological activity of spontaneously beating cardiomyocytes cultured on different substrates

4. Visualise ion channel distribution of the $Na_V1.5$ sodium and Kir2.1 potassium channels.

5. Perform the above characterisation at two time points, 5 days and 25 days post-differentiation to capture any time dependent differences and compare to gelatin control.

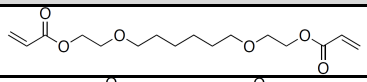
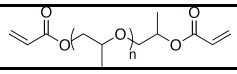
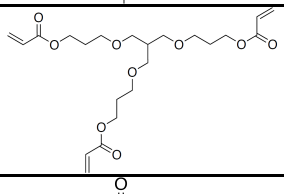
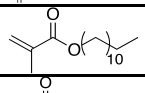
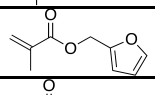
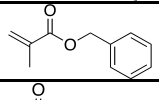
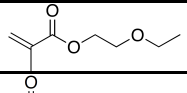
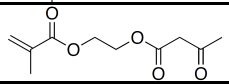
4.2. RESULTS

4.2.1. Substrate Format for Further Characterisation

Five co-polymers identified in chapter 3 that supported relatively high cardiomyocyte attachment and area in serum free conditions (fig.3.25) were chosen to perform further characterisation of the cardiomyocytes cultured on them. These were; **1.** AD17/BM54, **2.** BM80/AD17, **3**. BM34/AD24, **4.** BM39/AT08, **5.** BM34/BM18. The identities of the monomers that make up these co-polymers are listed below in table 4.2.

A suitable substrate format was required to carry out electrophysiological recordings in the 35 mm dish that the patch clamp rig supports (fig.4.4.A). The 25 x 75 mm glass was cut into 25 mm^2 pieces which fit into the 35mm dishes. They were pHEMA coated as previously had been done for the microarrays and 100 spots of the same co-polymer was printed per slide. However, after 10 days the pHEMA coating became unstable and began to delaminate from the glass slide (fig 4.5.A) which was not seen during microarray screening because cardiomyocytes were only cultured for 24 hours and 7 days.

Table 4.2 Identity of Monomers in Co-polymers chosen from array 6.2

ID	Name	Structure
AD17	Hexanediol ethoxylate diacrylate	
AD24	Poly(propylene glycol) diacrylate	
AT08	Glycerol propoxylate triacrylate	
BM18	Lauryl methacrylate	
BM34	Furfuryl methacrylate	
BM39	Benzyl methacrylate	
BM54	Ethoxyethyl methacrylate	
BM80	Methacryloyloxy)ethyl acetoacetate	

Printing directly into a pHEMA coated 35 mm^2 TCP dish was attempted according to a protocol published by *Kou et al*, which describes coating a large surface with an even layer of polymer (Kou et al., 2012). Briefly, 2 mL of 4 % pHEMA solution was dispensed into the dish and left to evaporate in a 40 ºC vacuum oven which was increased 10 ºC/hour up to 80 ºC at which point vacuum was generated. However, this formed a relatively thick layer of pHEMA on the well plate. The polymer swells in an aqueous environment and bubbles could be seen throughout the layer during culture (fig.4.4.C) which weren't apparent when coated epoxy glass slides were used. This made observation of the cells on the polymer difficult. Reduced volumes of pHEMA were tested; 1.5 mL, 1 mL, 500 µL and 250 µL. It was found that 500 µL was sufficient to evenly coat the whole surface of the 35 mm dish which prevented background cell adhesion and provide an optically clear surface (fig.4.4.D). Piezo printing was employed due to flexibility that the platform offers for printing into various culture vessels (fig.4.4.E). The contact printer currently only holds 25x75mm slides for printing. Only one type of co-polymer was printed per dish to avoid any cross-contamination.

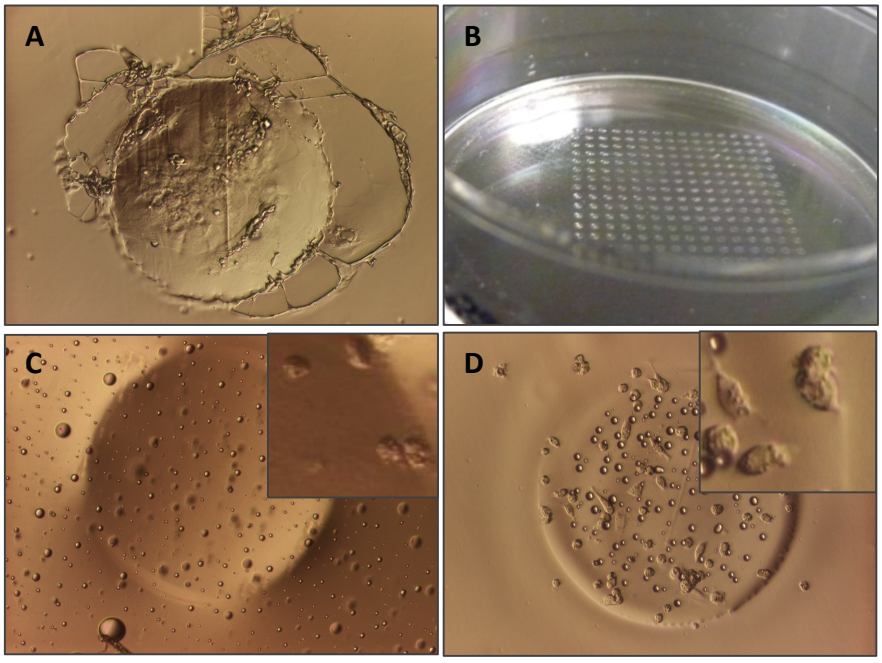


Figure 4.4 Array Format for Electrophysiological Measurement.
(A) Delamination of pHEMA around printed polymer from epoxy glass. **(B)** Inkjet printed polymer into 35mm pHEMA coated dish. **(C, D)**. Coating of 35mm dish with 2 mL and 500 µL of pHEMA respectively, cardiomyocytes can be seen inset.

4.2.2. Z line Measurement

In order to quantify myofibril organisation, Z-line measurements were performed on cardiomyocytes stained with anti-human sarcomeric alpha actinin which is a contractile protein that resides in the Z-lines of sarcomeres (fig.1.2).

4.2.2.1. Z line Uniformity

The length of the Z-line in relation to cardiomyocyte width is associated with uniformity of myofibril alignment. When the Z-line length is similar to that of the minor axis (width) of the cardiomyocyte, this indicates well aligned myofibrils throughout the cell. Z-line lengths that are much smaller than the cell width indicates regions of disorganised myofibril alignment throughout the cell that is similar to the fetal phenotype in figure 4.1. Hence, the ratio of Z-line length to cell width represents uniform organisation of myofibrils when approaching a value of 1. CellProfiler was used to apply background correction and enhancement of features to enable measurement of the Z-lines (fig 4.7).

The uniformity of myofibril alignment could only be measured on four of the co-polymers due to the delamination of BM34/AD24 from the pHEMA coated dish (fig. 4.5). Delamination occurs because polymers are not covalently bound to the substrate. Printing onto pHEMA coated glass slides at high humidity (35 %), causes the pHEMA to swell and when the printed monomer is polymerised in situ it remains adhered to the pHEMA through physisorption. However, in this case, the polymer is not physically adsorbed to the pHEMA to a high enough degree.

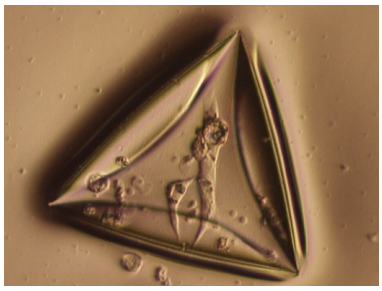


Figure 4.5 Delamination of co-polymer BM34/AD24.

Z line measurements were made in five regions of four images from two biological replicates (fig.4.6.B). In control cultures on 0.1 % gelatin, there was a reduction in uniformity of myofibril alignment at 25 days, 0.25 ±0.12, compared to 5 days culture, 0.59 ±0.19 (±standard deviation, n=2, p>0.05, two way ANOVA). This difference was not statistically significant due to the large standard deviations and highlights the variability in the population (fig 4.7.A).

At 5 days culture, there was no significant difference in myofibril organisation between the synthetic polymers and 0.1% gelatin control; Z-line length/cell width ratios were 0.79 ±0.10 on AD17/BM54, 0.72 ±0.09 on BM80/AD17, 0.62 ±0.12 on BM39/AT08 and 0.70 ±0.12 on BM34/BM18.

At 25 days culture, cardiomyocytes on AD17/BM54 and BM80/AD17 displayed significantly more organised myofibril alignment (0.69 ±0.18, and 0.62 ±0.12 respectively, both $p<0.05$, n=2) compared to control. Myofibril organisation on BM39/AT08 (0.32 ±0.10) was similar to control but relatively poor compared to the other three co-polymers. Therefore, this polymer was not taken forward for electrophysiological measurements.

4.2.2.2. Z line spacing

The spacing between Z lines correlates to sarcomere length. On control gelatin substrates, cardiomyocytes displayed an average sarcomere length of 1.8 ± 0.1 µm at 5 days. This did not change at 25 days (0.18 ±0.2 µm).

There was no significant difference of sarcomere length between cardiomyocytes cultured on the synthetic co-polymers and control at 5 days; AD17/BM54 1.8 ±0.2 µm, BM80/AD17 1.9 ±0.2 µm, BM39/AT08 1.6 ±0.1 µm, BM34/BM18 1.9 ±0.2 µm or at 25 days; 2.1 ±0.3 µm, 1.9 ±0.2 µm, 1.8 ±0.2 µm, 2.0 ±0.2 µm, respectively.

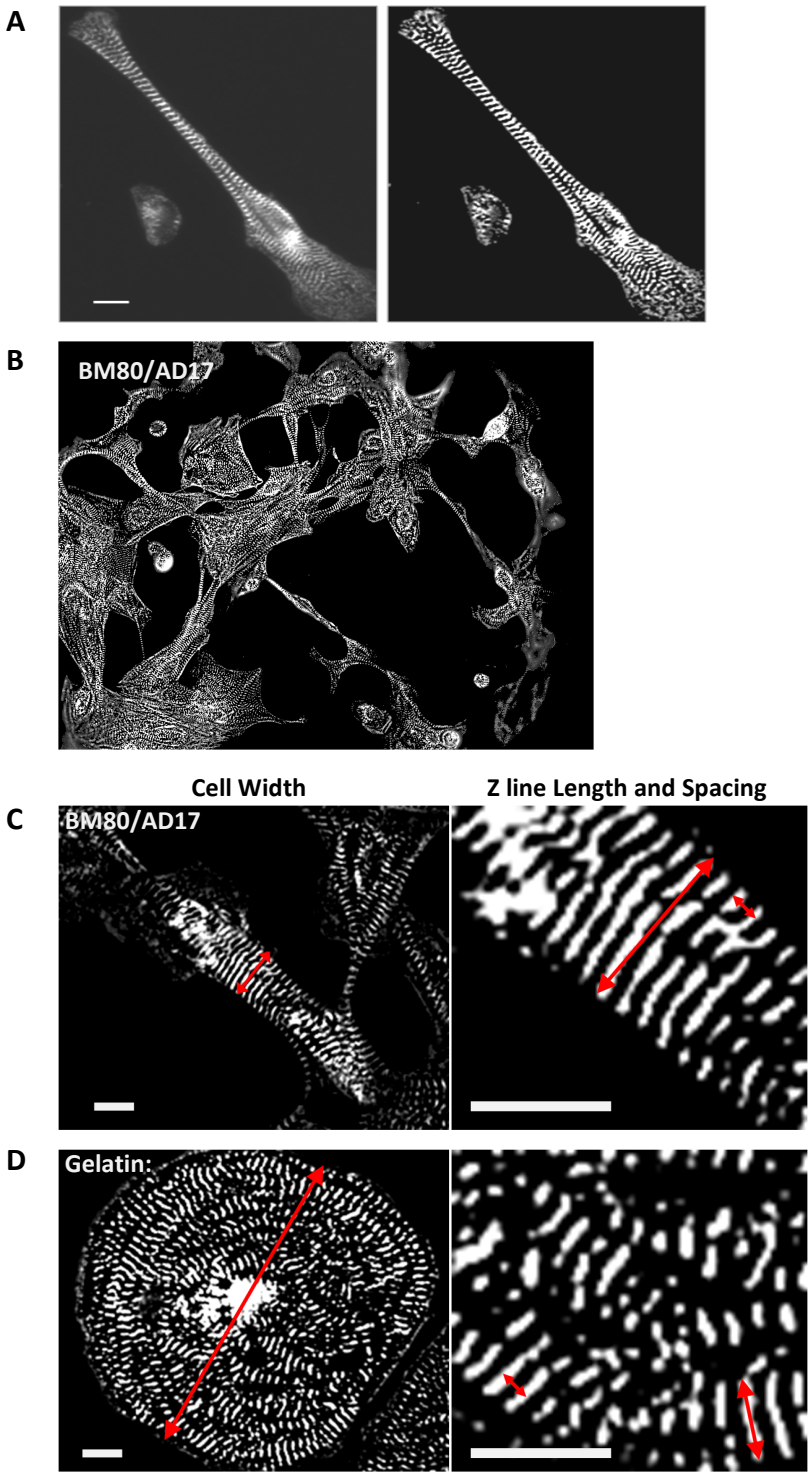


Figure 4.6 Quantification of Z lines of Cardiomyocytes.
Cardiomyocytes were stained with anti-human sarcomeric alpha actinin. To quantify alignment, images were first background corrected and features enhanced using CellProfiler software (A). Five regions were randomly selected from one image such as (B). This enabled measurement of the distance between the z-lines (sarcomere length) and length of the Z-line, as shown in cardiomyocytes cultured on polymer (C) and gelatin (D) for 5 days. The length of the Z-line can be divided by the width of the cell. Image (C) would have a z-line length to cell width ratio close to 1 which describes well aligned myofibrils throughout the cardiomyocyte. However, (D) would have a ratio much less than 1 due to the smaller regions of alignment within but not throughout the cell. Scale = 10 µm.

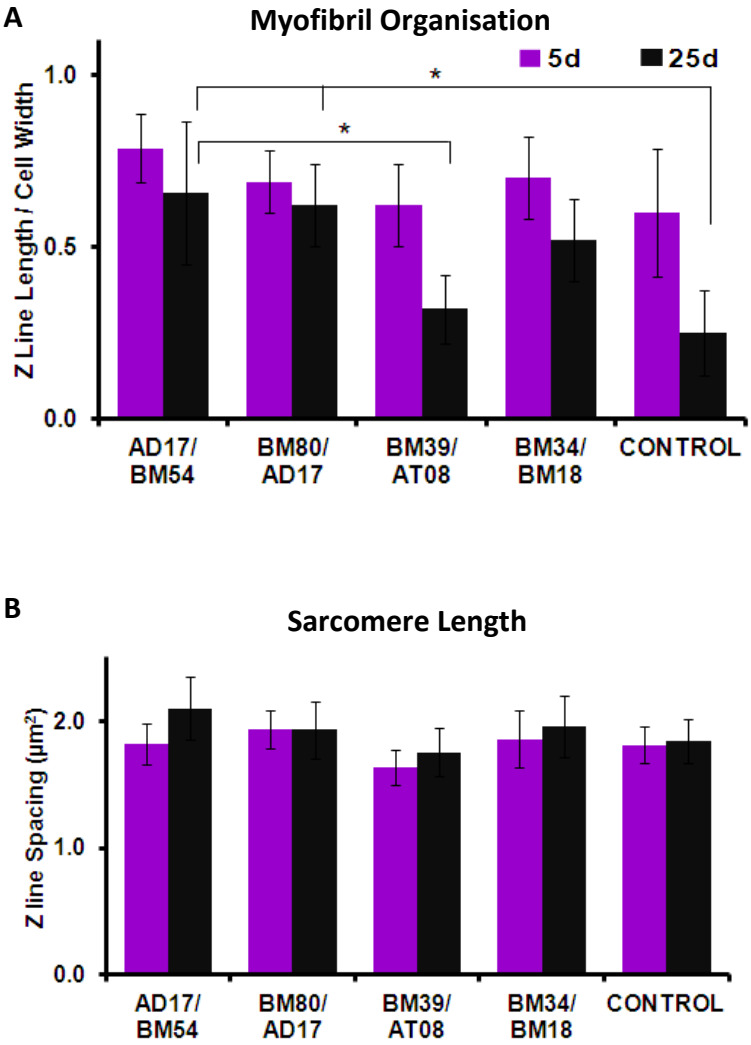


Figure 4.7 Comparison of Myofibril Alignment of Cardiomyocytes Cultured on Different Substrates

No significant difference in myofibril organisation on any of the substrates was observed at 5 days. At 25 days, cardiomyocytes cultured on co-polymers AD17/BM54 and BM80/AD17 retained significantly more organised myofibrils than control gelatin.

Sarcomere length was not significantly different between any of the cardiomyocytes that displayed Z-lines on different substrates. (Two way ANOVA, n=2, *$p<0.05$).

4.2.3. Patch Clamp Electrophysiology

The electrophysiology of a cardiomyocyte gives an insight into functional maturity paramount for use of these cells. The difference in action potential (AP) phenotype can also indicate the sub-type of cardiomyocyte. In the HUES7-derived cardiomyocytes, the majority sub-type was ventricular (59%) identified by the distinctive plateau phase (fig 4.8), which is similar to proportions reported in the literature (Braam et al., 2010, Ma et al., 2011b, Wei et al., 2012a). Atrial and nodal cardiomyocytes made up a smaller proportion; 25 % and 16 % respectively.

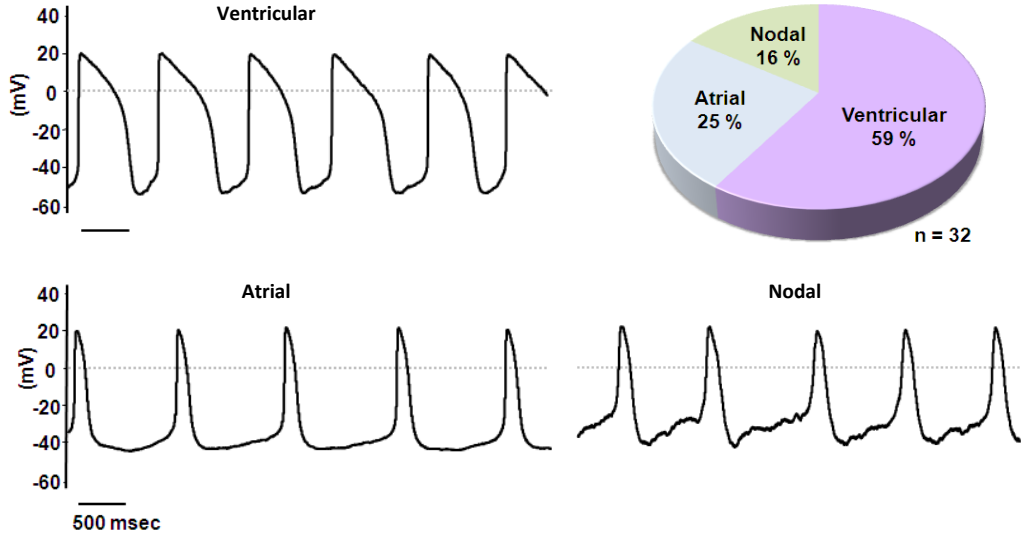


Figure 4.8. Action Potential Profiles of HUES7 derived Cardiomyocytes.
HUES7-cardiomyocytes displayed APs similar to those of the three main sub-types. Ventricular like cardiomyocytes displayed a distinctive plateau phase. The atrial and nodal like sub-types lack this plateau but can be difficult to distinguish from each other. The nodal sub-type can be clearly separated when an 'If' current is present which prevents the resting potential returning to baseline. The ventricular sub-type made up the majority of the population at 59%.

The ventricular cardiomyocyte can be considered as the most important sub-type for predicting cardiotoxicity of fatal ventricular arrhythmias and QT prolongation. Thus, the ventricular sub-type was focussed on for profiling of measurements such as action potential duration at 90% repolarisation (APD90), upstroke velocity (dV/dt), amplitude (APA) and resting potential (also called maximal diastolic potential (MDP) which can give an indication of functional maturity.

Atrial and nodal cardiomyocytes tend to have a less negative resting membrane potential and slower upstroke velocities (Schram et al., 2002) so it is important to elucidate the subtype before comparison of these parameters, which would be different when using different subtypes regardless of maturity. This was done by obtaining the ratio of action potential duration at 90 % repolarisation over the duration at 50 % repolarisation as described in the literature (Matsa et al., 2011, Sheng et al., 2012). Those with ratios less than 1.4 were classified as ventricular, this effectively describes a steeper drop towards membrane resting potential after the plateau phase. Those with an APD90 more than 1.4 times longer than at APD50, were designated non-ventricular and describes a steadier return to the resting potential. Visual inspections were also made to try to distinguish between atrial and nodal cells. Nodal cells will display the I_f or 'pace-maker' current which may be missing in immature cells, in which case atrial and nodal are difficult to distinguish and can remain grouped as 'non-ventricular' cells (Peng et al., 2010).

Two way ANOVA reveals that ventricular cardiomyocytes cultured on the synthetic polymer surfaces in serum free conditions for 5 days have significantly immature phenotypes compared to 0.1% gelatin control (see fig.4.9 for p values) as indicated by smaller amplitudes (BM80/AD17: 78±10 mV, BM34/BM18: 53±3 mV, AD17/BM54: 53±3 mV, gelatin: 89±12 mV) and less negative resting potentials (-15±1 mV, -31±3 mV,-29±2 mV, -48±2 mV respectively). Measurements were made on averaged action potential traces as indicated in table 4.1.

The APD90 was also shorter on the polymers compared to controls (167±57 ms, 128±15 ms, 165±12 ms, 362±121 ms respectively). However, these differences are abolished after 25 days culture, with no significant differences in action potential profile of cardiomyocytes cultured on polymers compared to control for 25 days, with the exception of resting potential, which remained less negative on co-polymer AD17/BM54 (-8±5 mV) compared to gelatin control (-26±6 mV).

Upstroke velocity was faster than control on all three polymers at both time points. Although this was not statistically significant and would require more replicates to determine the importance of this.

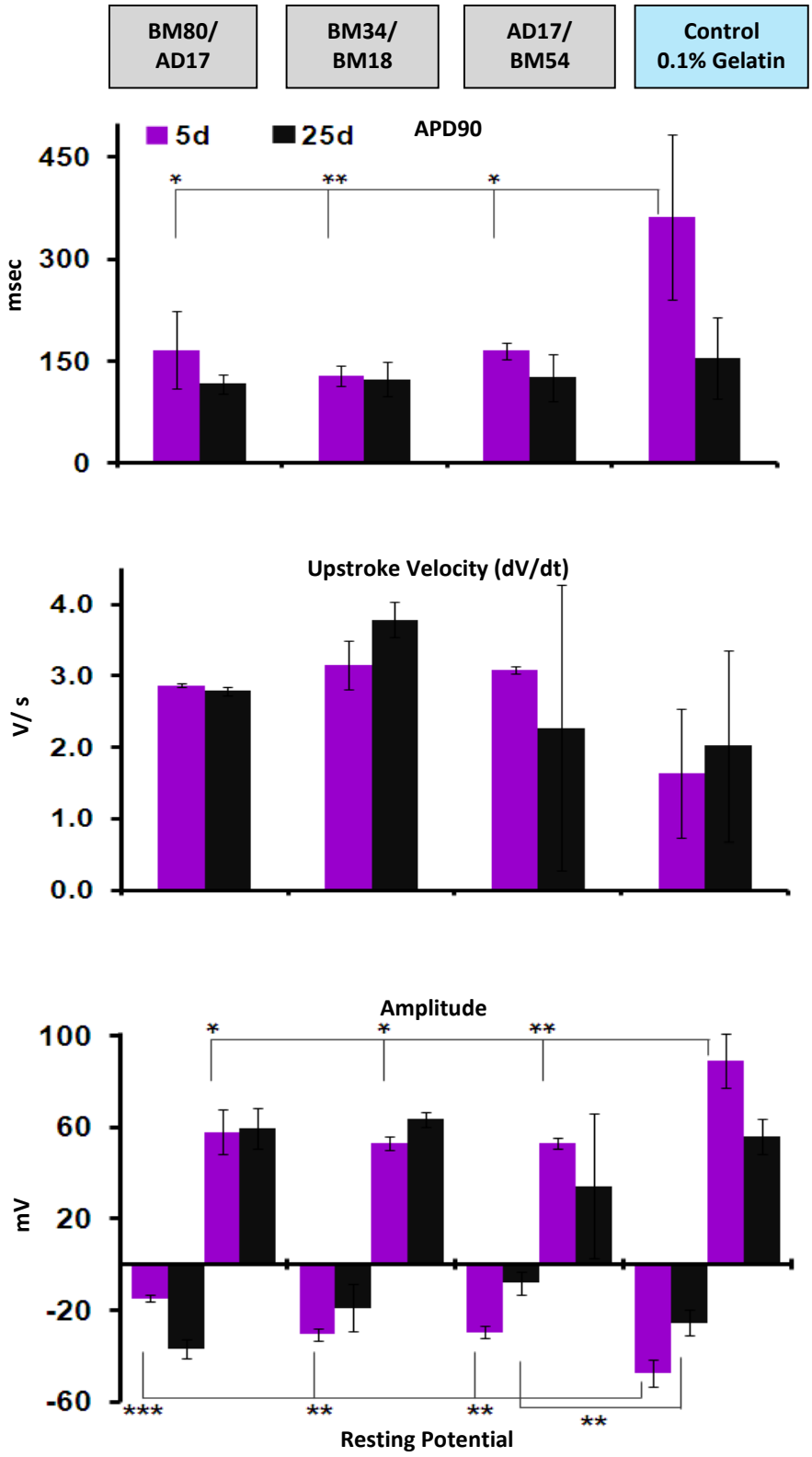


Figure 4.9 Comparison of Ventricular Action Potential Phenotype of Cardiomyocytes on Polymer Substrates Compared to Gelatin Control.

Action potential duration was significantly better on gelatin than polymers at 5 days. This was abolished at 25 days. Upstroke velocity was faster on polymers than control. This was not found to be significant. Amplitude and resting potential was larger and more negative on control than polymers at 5 days but not at 25 days. Except resting potential of cardiomyocytes on AD17/BM54 which remained more positive than control.

± Standard deviation. n = 2 on polymers, n = 5 and 3 for 5 and 25 day controls

4.2.4. Ion Channel Distribution in HUES7-cardiomyocytes

Immunostaining of the $Na_V1.5$ and Kir2.1 ion channels was performed on HUES7-cardiomyocytes cultured on 0.1% gelatin and on co-polymers AD17/BM54, BM80/AD17 and BM34/BM18.

4.2.4.1. Kir2.1 Potassium Channel

Dual staining of Kir2.1 (green) with the cardiomyocyte marker sarcomeric alpha actinin (red) was performed using a simultaneous staining method. However, although primary antibodies were raised in different species, cross-reactivity was observed with both stains being identical (fig. 4.10.A).

The immunostaining was repeated using a sequential method which clearly visualised Z-line banding and punctate ion channel staining that localised in or around the nucleus (fig.4.10.B), confocal microscopy would be required to determine this. In 8% of cardiomyocytes cultured on gelatin for 5 days, Kir2.1 could be seen localised at the Z–lines (fig.4.10.C) similar to that reported in adult ventricular mammalian cardiomyocytes. Cardiomyocytes cultured on the co-polymers for 5 days showed similar ion channel distribution to those cultured on gelatin; 10% and 8% of cardiomyocytes on AD17/BM54 and BM80/AD17 respectively displayed Kir2.1 ion channel localisation at Z-lines, with the remainder of the population exhibiting punctate staining throughout the cytosol and high intensity in/around the nucleus (n=2) (fig.4.11). BM34/BM18 displayed high background fluorescence when excited at a wavelength of 495 nm so Kir2.1-Alexaflour488 staining could not be distinguished from background on this polymer (fig 4.11).

At 25 days culture on 0.1% gelatin, 7% of cardiomyocytes displayed Kir2.1 localisation at Z-line. On co-polymers AD17/BM54 and BM80/AD17 this occurred in 4 and 5 % of cardiomyocytes, respectively (fig.4.11.C).

4.2.4.2. $Na_V1.5$ Sodium Channel

$Na_V1.5$ ion channel distribution in cardiomyocytes at both 5 and 25 days culture on 0.1% gelatin displayed punctate staining throughout the cytosol (fig

4.10.D,E). The intense localisation observed for Kir2.1 at the nucleus was not apparent for Nav1.5. Nor was any localisation at the Z-lines. However, in contrast to control, cardiomyocytes cultured on AD17/BM54 and BM80/AD17 had prominent intensity in the nuclear/ peri-nuclear region at both time points (fig.4.12).

Neither ion channel was highly expressed at the membrane of the cardiomyocyte indicating that they could be a trafficking issue which would ultimately alter the action potential phenotype and may be one of the reasons why hESC-cardiomyocytes have an electrically immature phenotype.

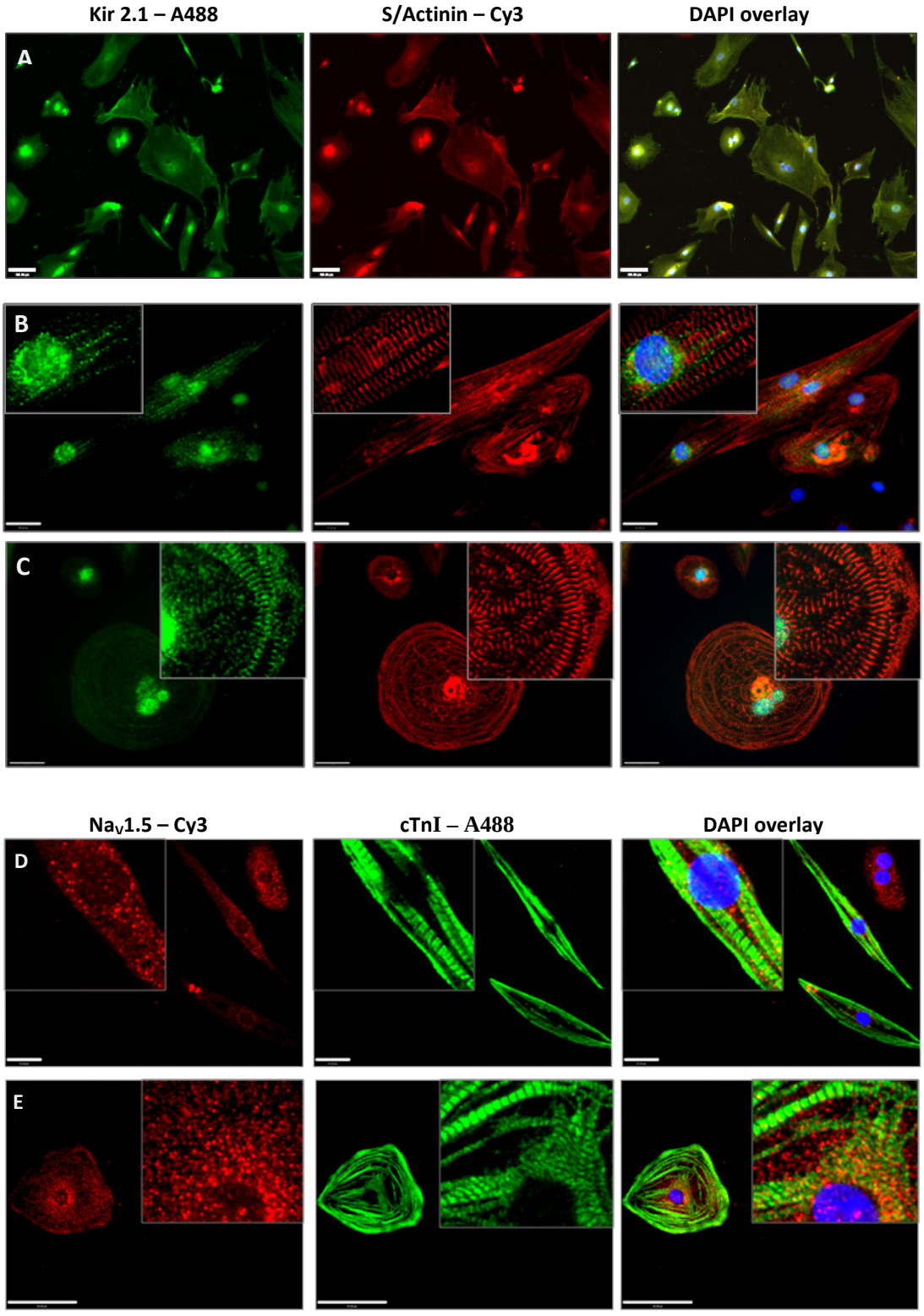


Figure 4.10 Dual Staining of Sodium ($Na_V1.5$) or Potassium (Kir2.1) Ion Channels with respective cardiac markers, Cardiac Troponin I and Sarcomeric Alpha Actinin of Cardiomyocytes Cultured on 0.1% Gelatin.

A) A simultaneous dual staining procedure lead to cross reactivity of the antibodies for kir2.1 (Green) and s/actinin (red). **B)** A sequential staining procedure was taken forward which shows punctate staining of Kir2.1, with higher distribution at the nucleus of control cardiomyocytes. **C)** Localisation of kir2.1 at Z-lines could be seen in 8% of cardiomyocytes at 5 days. **D)** $Na_V1.5$ staining appears punctate throughout the cardiomyocyte at 5 days and 25 days **E).**

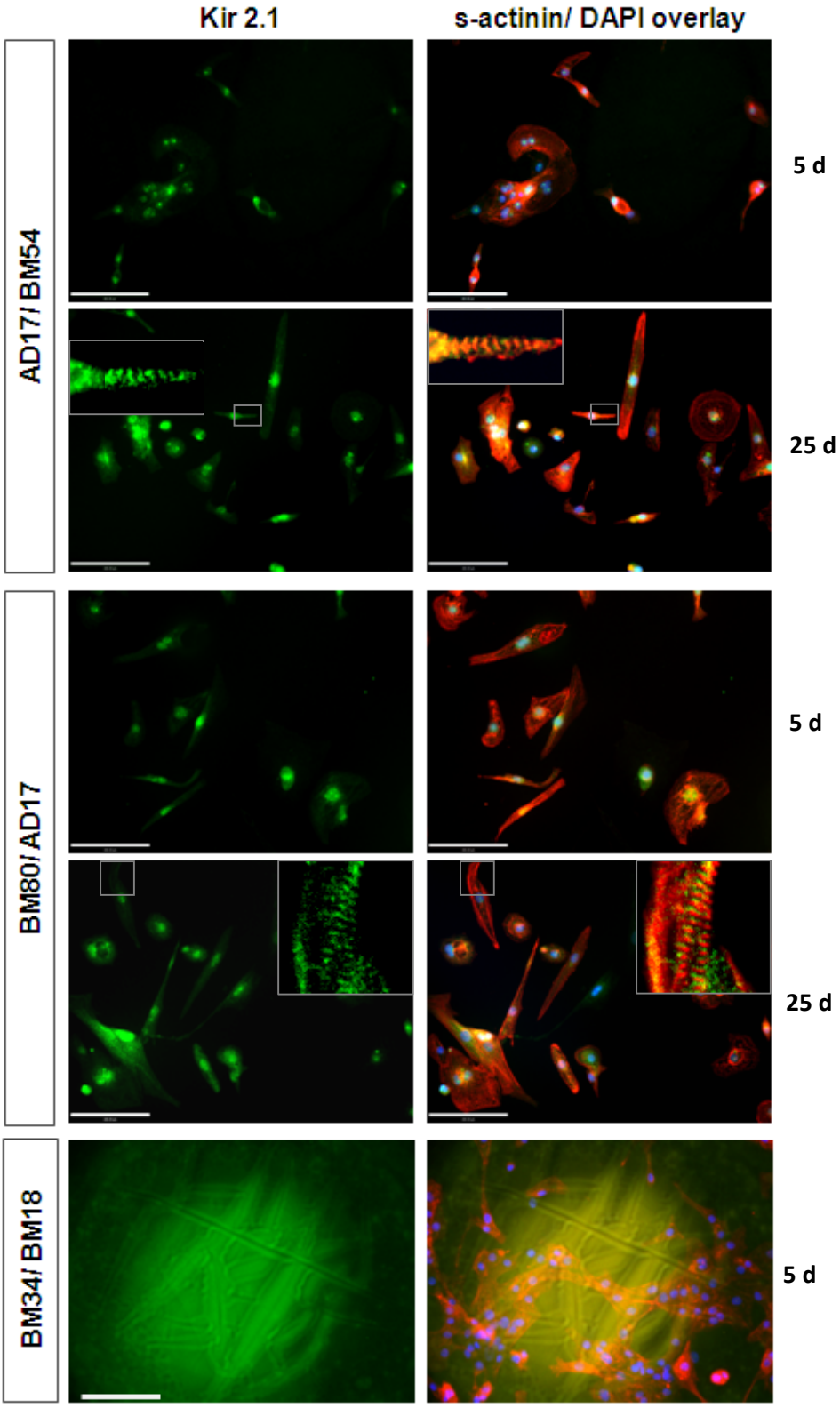


Figure 4.11 Potassium (Kir2.1) channel and Sarcomeric Alpha Actinin staining of Cardiomyocytes Cultured on Co-polymers.
Kir2.1 was localised at Z-lines in 10 and 8 % of cardiomyocytes cultured on AD17/BM54 and BM80/AD17 respectively. This fell to 4 and 5 % at 25 days (n=2). High background fluorescence was observed on BM34/BM18 and kir2.1 staining could not be distinguished from background.

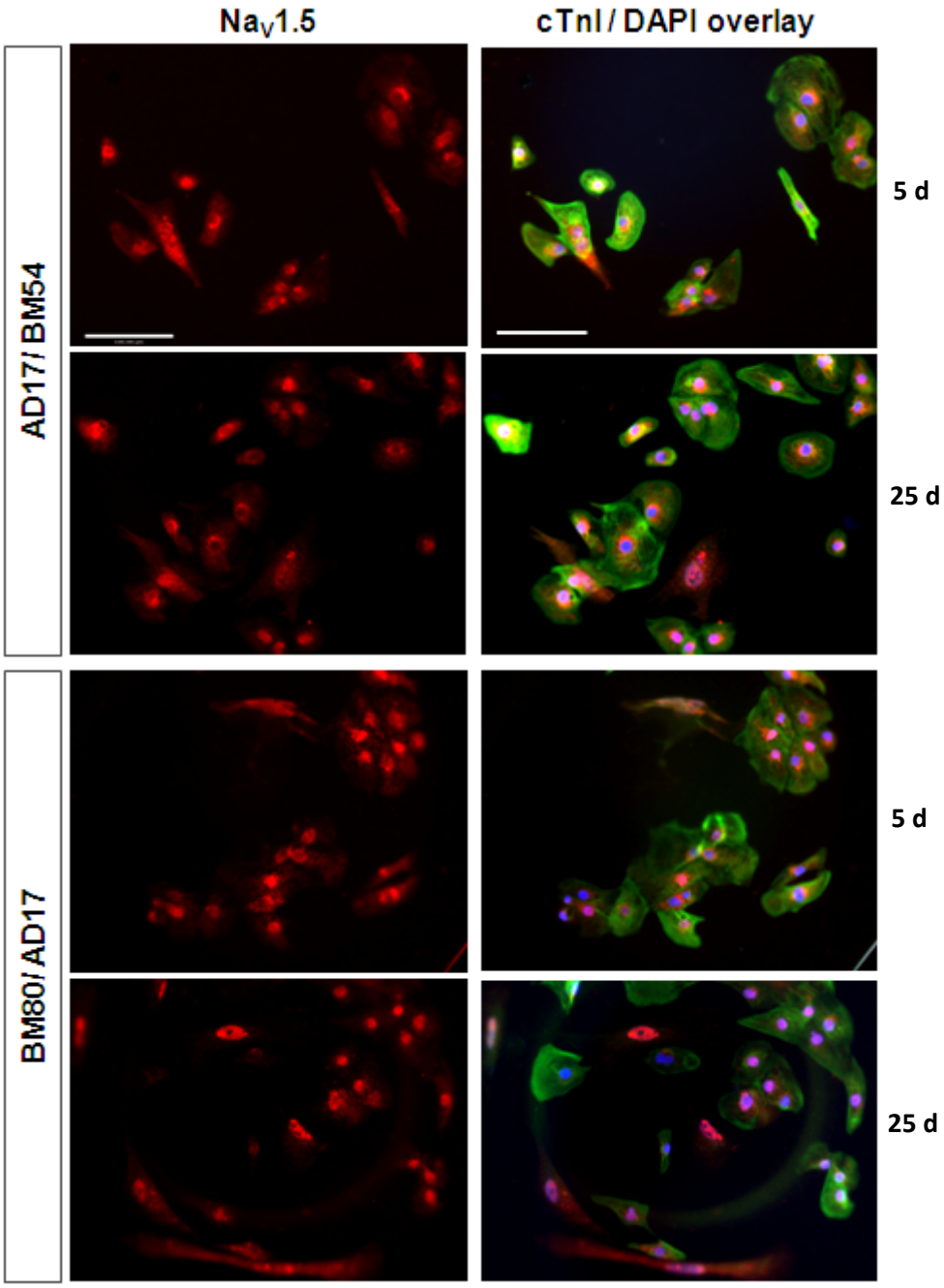


Figure 4.12 Sodium ($Na_V1.5$) channel and Cardiac Troponin I staining of Cardiomyocytes Cultured on Co-polymers.
Staining of ion channel was most intense in nuclear/ peri-nuclear region and little could be seen at the cell membrane.

4.3. DISCUSSION

In this chapter polymers identified from the microarray screen were selected based on cardiomyocyte attachment and spread. These selection criteria alone are not robust enough to claim benefit against currently used biological substrates such as gelatin. Functional maturity is one the most important criteria to achieve in order for cardiomyocytes to reach their full potential for *in vitro* use (Harris 2013). Therefore, electrophysiology, ion channel distribution and myofibril organisation was measured in cardiomyocytes cultured on the synthetic acrylate surfaces and control 0.1% gelatin substrate in serum free conditions. It was found that cardiomyocytes cultured on AD17/BM54 and BM80/AD17 had the most organised myofibril structure and fastest upstroke velocity compared to other co-polymers and control gelatin substrate.

4.3.1.1. Myofibril Organisation

Myofibril organisation forms the physical basis of contractility (Blazeski et al., 2012). The Z-lines of cardiomyocytes were measured for their uniformity (Z-line length:Cell width ratio) which enables efficient propagation of contraction throughout the cardiomyocyte and sarcomere length which influences contractile force. The sarcomere length did not differ significantly between the acrylate surfaces and gelatin control at 5 or 25 days culture. Similarly, at 5 days culture, Z-line uniformity did not differ significantly. However, at 25 days, cardiomyocytes cultured on polymers AD17/BM54 and BM80/AD17 maintained uniformity to a better degree than control. The influence of surface chemistry on myofibril uniformity has not been described in the literature. There is a greater breadth of research on the influence of surface topography and stiffness which can both alter myofibril organisation significantly (Rodriguez et al., 2011, Feinberg et al., 2012). These surface properties were neither measured nor controlled in these experiments and so their contribution to the polymer's ability to maintain myofibril organisation must be considered during future research of these substrates.

4.3.1.2. Electrophysiology

The 3 polymers with the most uniform myofibril organisation at 25 days were chosen to take forward for patch clamp electrophysiology, a limited number of polymers were chosen due to the labour intensive nature of this technique, these were AD17/BM54, BM80/AD17 and BM34/BM18. At 5 days culture, cardiomyocytes on all 3 polymers had a significantly less mature action potential phenotype in terms of resting potential and amplitude compared to gelatin control. Upstroke velocity of beating cardiomyocytes was fastest on AD17/BM54 and BM80/AD17 but still slow in relation to literature values for adult cardiomyocytes and within the range of that reported for human fetal cardiomyocytes.

Action potential duration (APD90) was significantly shorter at 5 days on all acrylate co-polymers. This, however, is not an indicator of immaturity. The average APD90 of cardiomyocytes cultured on gelatin was increased by two values at 455 ms and 478 ms which is notably longer than that seen in human adult cardiomyocytes (330 ms, see table 4.1). A prolonged action potential may indicate electrical abnormalities (Peng et al., 2010, Itzhaki et al., 2011a). At 25 days culture, the average APD90 of cardiomyocytes on 0.1% gelatin shortened to 155 ms and there was no significant difference compared to average APD90 of cardiomyocytes on any of the 3 polymers.

Mature atrial and ventricular cardiomyocytes do not beat spontaneously due to their stable resting membrane potential which normally does not exceed the threshold level required to trigger an AP without propagation of pacemaker excitation via gap junctions (Schram et al., 2002). A more positive resting potential due to lack of I_{K1} is a contributor to the spontaneous activity of cardiomyocytes (Satin et al., 2004). Therefore, patching spontaneously beating cells, as was done in this study, will inherently exclude a potentially mature population of cardiomyocytes and record a biased average from immature cells. A better method may be to externally pace electrically quiescent cells to elicit an action potential in potentially mature cardiomyocytes.

4.3.1.3. Ion Channel Distribution

Electrophysiological properties are founded on ion channel expression. The I_{K1}, the inward rectifier potassium current, is responsible for the more negative resting potential of the mature cardiac AP (Doss et al., 2012). I_{K1} current density has been shown to increase with extended *in vitro* culture of hESC-cardiomyocytes, however, corresponding Kir2.1 mRNA expression did not significantly increase (Sartiani et al., 2007). Similarly, the expression of the SCN5A gene encoding the $Na_V1.5$ sodium channel in hESC-cardiomyocytes was found to be significantly lower than fetal and adult heart tissue at 21 days. However, at 49 days of *in vitro* culture this increased to levels comparable to adult heart tissue. (Synnergren et al., 2012). Yet hESC-cardiomyocytes beyond 49 days *in vitro* culture still display upstroke velocities significantly lower than adult cardiomyocytes despite the increase in SCN5A (see table 4.1). This indicates that gene expression does not correlate to functional expression and a suite of experimental techniques would be required to determine functional expression; mRNA expression, translation, protein modification and localization can all be subject to regulation which will augment functionality (Sucher et al., 2000).

The Kir2.1 and $Na_V1.5$ ion channel proteins both require localization at the membrane and T-tubules in order to function (Petitprez et al., 2011). Therefore, ion channel immunostaining was performed to determine their distribution. The T tubule system is most prominent in adult ventricular cardiomyocytes (Brette and Orchard, 2007). Approximately, 59 % of the HUES7-cardiomyocyte population was of the ventricular sub-type yet only 8 % of cardiomyocytes on gelatin displayed Kir2.1 localisation at the Z-lines indicating that the T-tubule system may not be present in the majority of cardiomyocytes. This would require confirmation using for example, a ryanodine receptor marker but is in agreement with literature which has reported the lack of a T-tubule system in hESC-cardiomyocytes. Similarly, no localisation of $Na_V1.5$ at the membrane was observed in either control cardiomyocytes or those cultured on gelatin. However, there was a greater intensity of $Na_V1.5$ channel staining in the nuclear/ perinuclear region of cardiomyocytes cultured on synthetic acrylates. The increased upstroke velocity of cardiomyocytes on co-polymers, although not

statistically faster than control, may indicate a greater density of sodium channel current.

In summary, the limited number of synthetic acrylate surfaces studied in this chapter show promise for defined *in vitro* hESC-cardiomyocyte culture as assessed by myofibril organisation and electrophysiology. There remains a large number of co-polymers identified in chaper 3 that would be worthy of further investigation. Practical consideration must also be taken into account during the study of the synthetic substrates as exemplified by de-lamination of BM34/AD24 and high background fluorescence of BM34/BM18. This is an advantage of having a large library of substrates to choose from as it is unlikely that designing a few substrates based on limited knowledge of cell-surface interaction will yield surfaces that are suitable for both providing optimal cell support and also being a practical substrate in common culture conditions. Many criteria must be met apart from cell adhesion and maturity, including physical parameters of opacity and stability in culture.

4.4. LIMITATIONS AND FUTURE WORK

As mentioned, spontaneously beating cardiomyocytes were patched for electrophysiological study. In future study, electrically quiescent cardiomyocytes, which occurs upon maturation, should also be patched to limit bias towards patching immature, electrically spontaneous cells. Contractility measurements may aid understanding of cardiomyocyte functionality on the synthetic substrates

Surface topography has been shown to improve cardiomyocyte alignment. Traditionally, patterned surfaces coated with proteins such as fibronectin have been investigated. Future study looking at either coating patterned surfaces with the synthetic acrylates or patterning the acrylates themselves could provide greater control over cardiomyocyte morphology. This would require further study into the mechanical properties of the acrylates, such as elasticity.

CHAPTER 5

Influence of Surface Chemistry on Cardiomyocyte Behaviour

5.1. INTRODUCTION

Surface chemical characterisation is necessary to enable investigation of how this may influence material interaction with its environment. Two analytical techniques, X-Ray Photoelectron Spectroscopy (XPS) and Time of Flight Secondary Ion Mass Spectrometry (ToF-SIMS), were employed for surface characterisation. The physical surface property of wettability was also explored using pico-litre water contact angle measurements. The application of these techniques for high throughput surface characterisation of microarrays has been described by Urquhart *et al* (Urquhart et al., 2008).

5.1.1. Time of Flight Secondary Ion Mass Spectrometry

ToF-SIMS is used to characterise a surface of interest by bombarding it with high energy primary ions, provided by, for example, a bismuth or gallium liquid metal ion source. This results in the sputtering from the surface of secondary atomic or molecular species which may be ionised or neutral. It is the ionic species that will be detected during positive and negative detection mode which make up around 1 % of total sputtered ions, the remainder being neutral. Ions of differing masses are separated by acceleration through a flight tube such that all ions achieve the same kinetic energy. Ions are recorded by the detector at a time related to their mass; those with heavier mass/charge (m/z) will travel more slowly and be detected later. Flight times can therefore be translated into a mass spectrum (Vickerman and Briggs, 2001). The emission process is such that in static mode (primary ion dose < 10^{13} ions/cm^2) secondary ions are detected from only the top 1-2 nm of the surface, making ToF-SIMS a very surface specific and molecular structure rich technique. Data is normalised to total counts so that the relative intensity of each ion can be found.

The utility of ToF-SIMS for imaging has been demonstrated in chapter 3 where the technique was used to confirm the chemical layout of the array. This image is incredibly data rich and each pixel consists of corresponding spectra

containing all of the relative secondary ion intensities detected from the top 2 nm of the surface (fig.5.1).

ToF-SIMS identifies molecular fragments, some of which will be unique to the polymer from which it originated. There are a variety of primary ion sources including atomic (Ga^+), polyatomic (Ar_{3000}), and molecules such as buckminster fullerine (C_{60}^+). The choice of source depends on the type of analysis that is required.

For microarray analysis the bismuth cluster (Bi_3^+) was used because it achieves a good mass resolution and a spatial resolution of approximately 1µm. It also generates higher yields of larger mass species compared to atomic primary ions

A C_{60}^+ primary ion source will generate secondary ions with larger masses, these bigger fragments are better for identification of the parent compound but has poor mass resolution, so is typically used to etch away the top region prior to bombardment with a focussed metal ion source for depth profiling (Kovac, 2011, Brison et al., 2010).

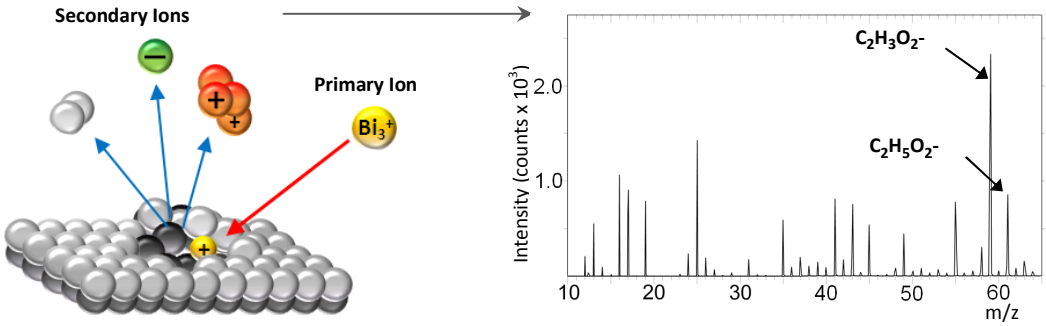


Figure 5.1 (A) Schematic of secondary ion generation in ToF-SIMS. (B) Negative ion mass spectrum of pHEMA.
The primary ion source is bismuth polyatomic clusters which bombard the surface and generate secondary ions upon impact. These secondary ions are from the top 2 nm of the surface, they are detected by the instrument and their mass recorded according to the time it takes to travel to the detector. The ions with mass 59 and 61 are identified as characteristic pHEMA ions $C_2H_3O_2^-$ and $C_2H_5O_2^-$ respectively when compared to reference spectra from (Briggs et al., 1990).

5.1.2. X ray Photoelectron Spectroscopy

XPS exploits the phenomenon of the photoelectric effect which describes the ejection of an electron from a surface through stimulated by photons of high enough energy to overcome the binding energy of the electron. The emitted electrons are termed photoelectrons. The X-rays penetrate up to 10 microns into the material being analysed. Atoms within the material absorb the x-rays which will displace an electron from different core levels of the atom, which have different binding energies (Briggs and Grant, 2003). The XPS spectra will display binding energy of the electron against intensity (counts per second), against a background of inelastically scattered electrons, as shown in figure 5.2. The binding energy of each core level peak is characteristic of its element. Elements with a higher atomic number have a higher binding energy and require greater energy to remove an electron from its orbital due to the attractive forces from a nucleus with an increasing number of protons (Van der Heide, 2011). The binding energy is deduced by subtraction of the kinetic energy of the emitted photoelectron from the photon energy, described by Einstein's equation in figure 5.2. Due to this relationship, the X axis of the spectra is plotted with decreasing binding energy (i.e increasing kinetic energy) from left to right (Hofmann, 2012).

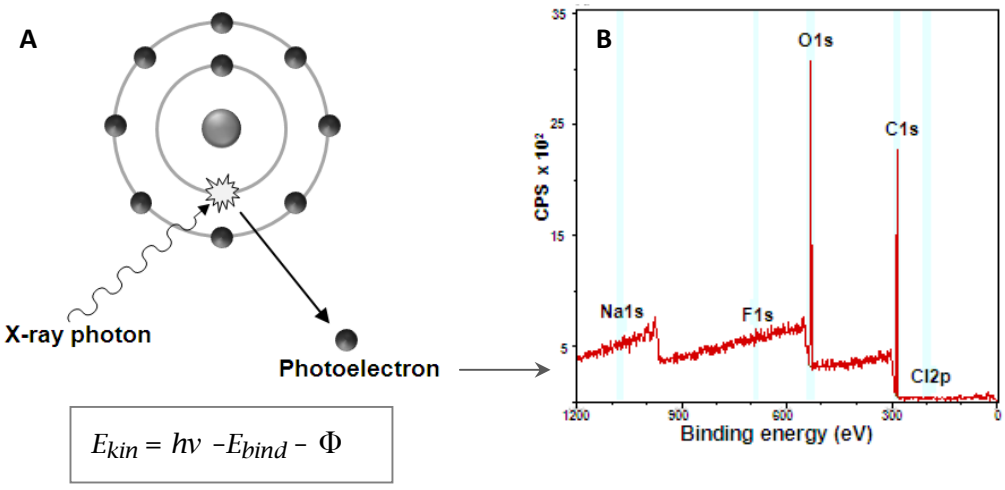


Figure 5.2 (A) Schematic of the photoelectric effect. (B) XPS survey of pHEMA.
The photoelectric effect occurs when photons of high enough energy are able to overcome the binding energy of electrons with the core of the atom. The displaced photoelectron is detected within the XPS instrument and its kinetic energy recorded to produce a survey displaying binding energy against intensity. The survey shown is that for pHEMA where only carbon and oxygen can be observed, quantification is achieved by calculating the area of the peak. Einstein's equation describes the relationship between binding energy and kinetic energy of core elecctrons; *Ekin* and *Ebind* is kinetic energy and binding energy of the core electron, respectively. *hv* is the energy of the x-ray, Φ is the work function of the spectrometer.

5.1.3. Wettability

The wettability of a solid describes the tendancy of a liquid, in this case water, to spread on a surface. This is measured by dosing a picolitre of water onto the surface and measuring the contact angle of the droplet. A drop that spreads to a greater degree on the surface will have a lower angle and that which repels water will have a higher angle giving an indication of the wettability of a surface (fig. 5.3). Surfaces that have a WCA larger than 90º are considered hydrophobic (Yuan and Lee, 2013).

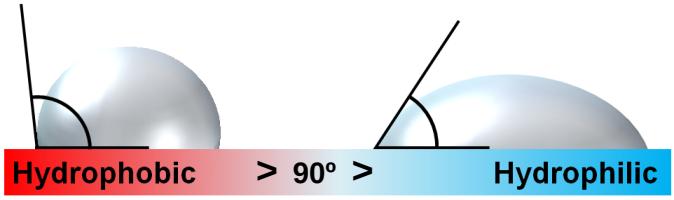


Figure 5.3 Schematic of water contact angles of relatively hydrophobic and hydrophilic surfaces.
A pico-litre of water is dispensed through a peizo unit and contact is captured by video. The first frame of contact is analysed by software to measure the angle of contact. On a hydrophobic surface the water contact angle is larger due to the reluctance of the drop to spread. Conversely, on a hydrophilic surface the drop is able to spread and the water contact angle is smaller.

Wettability is a property influenced by the chemistry and roughness of the top nanometer of a surface (Bain and Whitesides, 1988). Wettability has been shown to be an important factor for cell adhesion. A study by Tamada *et al*, varied the WCA of polyethylene, polytetrafluoroethylene, poly(ethylene terephthalate), polystyrene, and polypropylene by plasma treatment and found that on all surfaces, a WCA of 70º was optimal for adhesion of mouse fibroblasts (Tamada and Ikada, 1993). A decrease in WCA improves attachment as demonstrated by oxygen plasma treated polystyrene which is commonly used for tissue culture. The plasma treatment of polystyrene greatly improves attachment of a variety of cells including human endothelial cells, compared to non-treated polystyrene (Steele et al., 1993). The improvement may be attributed to the addition of hydrophilic groups through oxygen plasma treatment which decreases WCA from 80º to 75º, pre and post plasma treatment respectively(van Kooten et al., 2004).

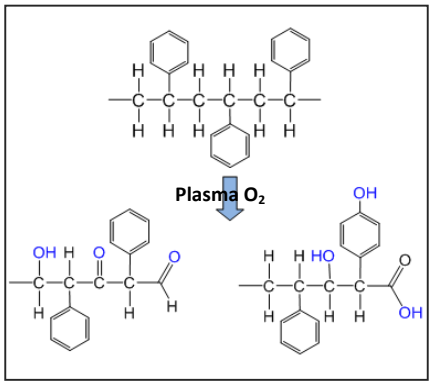


Figure 5.4 Oxygen plasma treatment of polystyrene.
Plasma treatment of polystyrene introduces a variety of hydrophilic groups including hydroxyl, carbonyl and carboxyl functionalities to improve wettability and cell adhesion.
Adapted from (Ryan, 2008).

Water contact angle is important to consider during surface optimisation, however its influence on cell adhesion is limited. Although optimal WCAs have been reported for specific cells, different cell types do not behave in the same manner. Other surface factors, such as surface chemistry, may be more important. To assess the influence of surface chemistry on cell adhesion, statistical modelling was used.

5.1.4. Partial Least Squares for the Prediction of Cell Response using Surface Chemistry.

ToF-SIMS spectra consist of hundreds of ion fragments detected during analysis. The influence of these ions (variables) on cell behaviour cannot be deduced simply. The data is multivariate in nature and requires an appropriate method of data analysis designed to handle the large and complex array of chemical species that may be presented at the surface. Such multivariate techniques include principal components analysis (PCA), partial least squares (PLS) and multiple linear regression (MLR) amongst others.

PCA reduces the number of variables in the dataset by creating combinations of the original variables that account for the greatest variation thereby reducing the dimensionality of the data to aid interpretation (Tyler et al., 2007). PCA will highlight differences between samples but cannot correlate these differences with a dependent variable such as cell attachment. MLR is able to

correlate variation in the independent ion intensity surface data (X) with variation in the dependent cell response (Y). However, data cannot be collinear which commonly occurs in spectrometric data. In contrast, PLS uses this property to combine collinear variables into components termed 'latent variables' to reduce dimensionality of the data (Wold et al., 2001) and so is a suitable technique for this application. PLS can correlate between X and Y and will produce a regression coefficient for each X value (fig.5.5), this coefficient describes the influence of each ion found through surface analysis on cell response (Lee and Gilmore, 2009, Geladi and Kowalski, 1986).

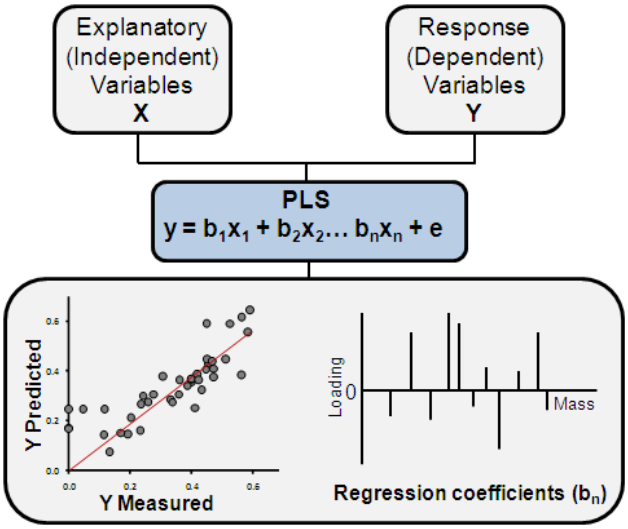


Figure 5.5 Partial Least Squares modelling.
This multivariate regression technique will find correlations in explanatory and response variables to model the relationship using regression coefficients, **b**, the loading of which describes how influential the X value is for predicting Y. The robustness of the model is tested by comparison of predicted and measured values.
e = error or residual.

The techniques described above are examples of supervised methods. This means they require measured input values to create and train a model which is then validated using values outside of the training data (Winkler and Burden, 2004). These models provide a means of study for systems where there is limited *a priori* knowledge and also removes subjective manual analysis of variables to create statistically valid models (Wagner et al., 2004).

5.2. RESULTS

5.2.1. Modelling Surface Chemistry and Cell Response

In order to characterise the top 2 nm of the surface ToF-SIMS was performed on first and second generation, homopolymer and co-polymer, microarrays. To investigate if there was any correlation between surface chemistry and cardiomyocyte response, which includes cell attachment (density) and spread (surface area), a model was constructed with the aid of PLS to identify the most influential chemical groups at the surface.

5.2.1.1. First Generation Homopolymer Microarray

The positive and negative secondary ions generated during ToF-SIMS analysis of the first generation homopolymer array is concatenated into one list termed the 'peak list' which consists of 1397 total ions that may be present in any part of the array.

The intensity of each of these ions in a polymer spot on the microarray can easily be extracted by drawing a region of interest around the polymer in the ToF-SIMS image. A mass spectrum was 'rebuilt' from the hyper-spectral data file for each of the 115 polymers in this manner. The different intensities of each of the 1397 ions for each polymer are the independent variables and have a corresponding cell response value (dependent variable). For the first generation array, only data from serum pre-conditioned arrays were used for analysis due to the limited number of 12 polymers that allowed attachment in serum free conditions, which would not allow for a robust model using training and test set data.

To improve reliability of the model, data that had a high coefficient of variation, over 60%, was excluded. The remaining data (54 sets) was then split into a 'training set' for building the model and a 'test set' to validate the predictability of the model. This was done using 80 % of data for training, and 20 % for the test set as described by Winkler *et al*, 2004.

To build the PLS model 43 data sets consisting of the mass spectra and cell response was processed by the software (training set). A 'leave one out' cross validation was applied to find the optimal number of latent variables for building the model. This will omit one data set per cycle and then try to predict that omitted response value. The error between predicted and measured values is recorded. This is repeated for each data set and the errors are recorded for the number of latent variables used per model. The number of latent variables that had the lowest root mean square error of cross validation (RMSECV) is chosen to build the final model. It was found that the number of latent variables to build an adequate model with the lowest RMSECV was 6 for cardiomyocyte density and 5 for cardiomyocyte area (fig.5.6.A and B inset). To further validate the model, 11 mass spectra that were not included in the training set were loaded into the model and it's predicted cell response was plotted against the measured data (test set in blue) alongside the training set for comparison (grey) (fig. 5.6.A and C).

It was found that the PLS model was able to establish a relationship between surface chemistry and cell response as shown by the correlation R^2 values of 0.53 and 0.72 for predicted and measured response values for cardiomyocyte attachment and area, respectively (figure 5.6). The model is built by assigning regression coefficients to each ion that was in the peak list. Positive coefficients were assigned to ions that promote cell attachment and/or spread and negative coefficients for those ions that are detrimental for these responses. The most influential coefficients for predicting cell attachment to a polymer is displayed in figure 5.6(B) which displays large positive coefficients for peaks at mass (m/z) 41.04 and 81.03, assigned as $C_3H_5^+$ and $C_5H_5O^+$ functionalities. The positive coefficients indicate that these ions will increase cell attachment. Negative coefficients such as the ion identified at mass 71.01 ($C_3H_3O_2$-), have been modelled to have a detrimental effect on cell attachment. The larger the number, the greater the influence of that ion in the model. Table 5.1, lists some of the most prominent ions identified by PLS analysis and its parent functionality.

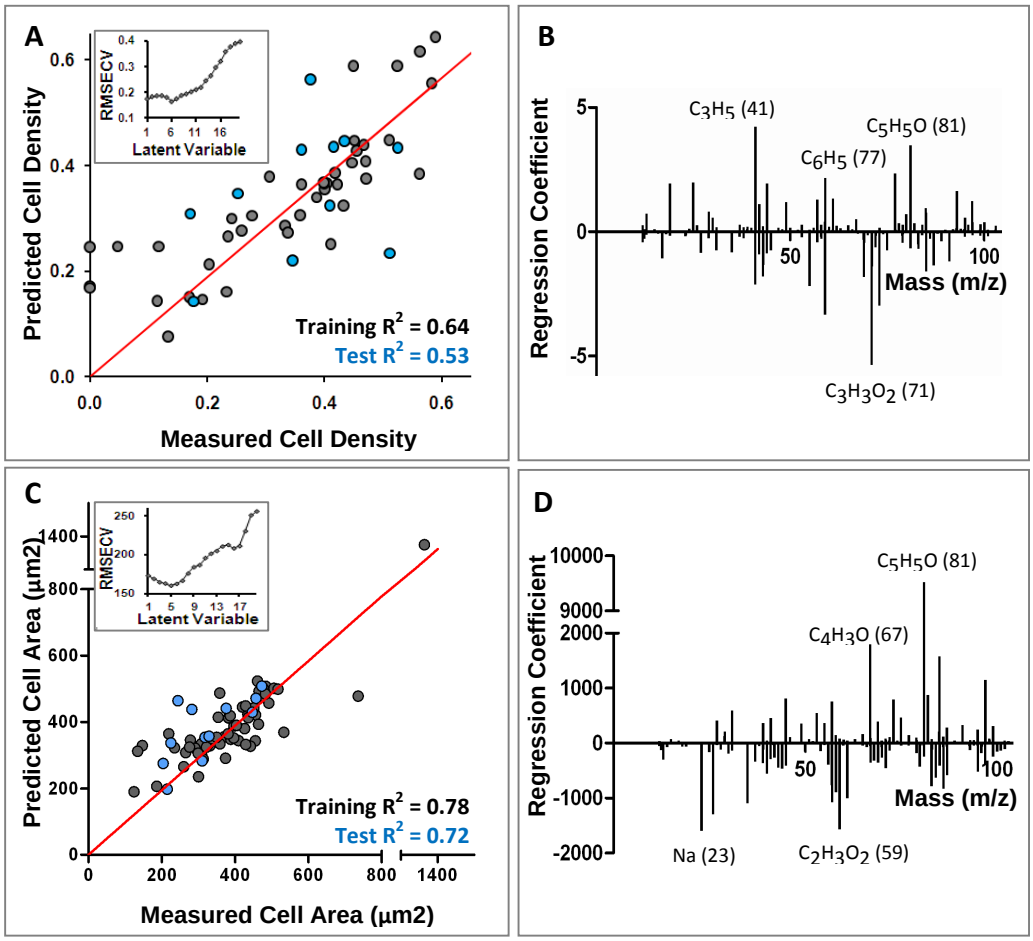


Figure 5.6 PLS model of cardiomyocyte attachment and area on polymers in first generation serum pre-conditioned arrays.
Tentative ion assignments are made based on mass (4d.p) and the intensity of that ion in each polymer. Model for density built with 6 LV and cell area with 5LV (n=4).

Table 5.1 Ions identified by PLS as influential for Cardiomyocyte Attachment and Area on first generation serum preconditioned homopolymer array.

Effect on Cell Response	Regression Coefficient		Ion (m/z)	Functionality	Greatest Intensity
	Density	Area			
Positive	4.2	458	$C_3H_5^+$ (41.04)	Acrylate backbone	Multi-acrylates
	3.5	9524	$C_5H_5O^+$ (81.03)	Aromatic	BM34
	2.3	92	$C_6H_5^+$ (77.04)	Aromatic	AM75
Negative	-3.4	-1569	$C_2H_3O_2$- (59.01)		pHEMA
	-0.2	-1596	Na+ (22.99)	Contaminant	-
	-5.4	22	$C_3H_3O_2$- (71.01)	Oxygen/Glycol monomers	AM54
Opposing	2.2	-420	$C_3H_7O^+$ (59.05)	Propylene Glycol	AD24
	1.9	-466	C_2H_6N+ (44.05)	Amine	BM49
	-1.2	327	$C_6H_5CH_2^+$ (91.06)	Aromatic	BM39

It is possible to subjectively identify ions which promote cell attachment and spread by looking at ion intensities in polymers which performed well. For example, the C_5H_5O+ (m/z 81.03) ion is most intense in BM34 (furfuryl methacrylate) where cell area and attachment are both high on this polymer (see fig 5.8). However, subtle relationships are more difficult to discern in large multivariate data sets. Figure 5.7, plots cell response against the intensity of the ions that were identified by PLS as having a detrimental (m/z 59.05) and positive (m/z 41.04) effects on attachment and cell area which were identified as ions from the acrylate backbone. There is indeed a respective negative and positive correlation for the ions. It is a weak correlation but its additive influence on cardiomyocyte response in the multivariate model has been identified to be of significance by PLS analysis.

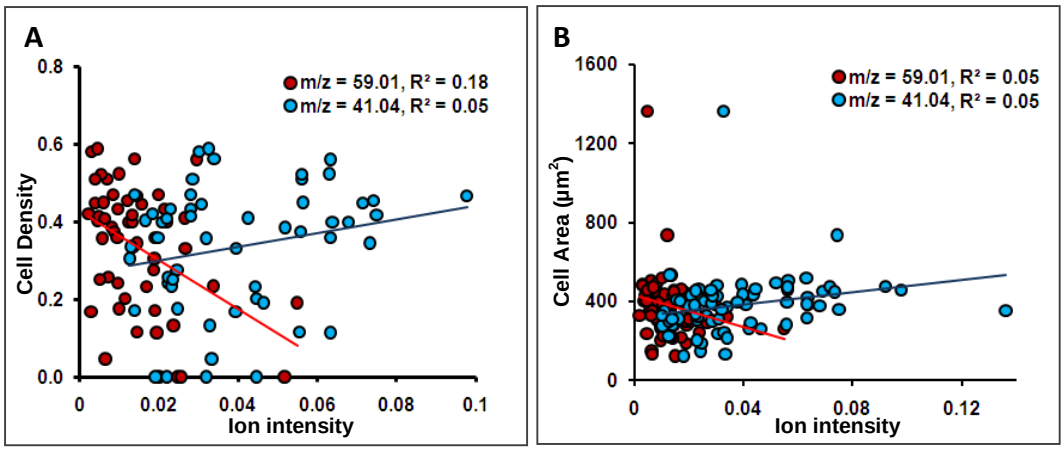
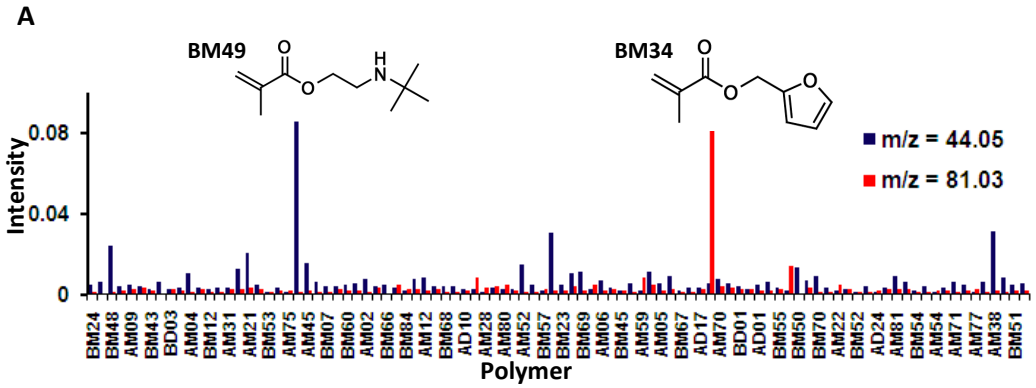
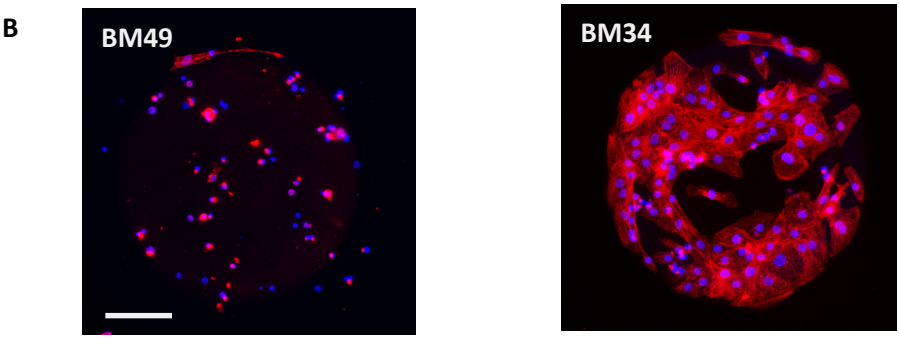


Figure 5.7 A) Cardiomyocyte attachment and B) area plotted against ion intensity of m/z 59 and 41 identified by PLS as being positive and negative for cell attachment and spread.

Negative and positive correlations of the two ions can be seen as predicted by PLS. This could not be determined by manually going through the ToF-SIMS data. Although the relationship seems weak alone, its additive effect has been determined to be of importance by PLS.

To check the function of the PLS process and explore what it reveals about interaction between surface and cell response it is useful to explore some specific examples. The ion at m/z 44.05 (C_2H_6N+) was identified to be positive for cardiomyocyte attachment (regression coefficient of +1.9) but negative for allowing the cardiomyocyte to spread (-466). This ion is most intense in BM49 (Tert-butylamino-ethyl methacrylate) where it can be seen in figure 5.8, that this relationship has been modelled correctly. BM49 has a relatively high cell attachment (0.56) comparable to BM34 (0.59) but the surface area of the attached cardiomyocytes on BM49 is significantly smaller 215µm^2 compared to 1364µm^2 (BM34).





C

Polymer (ion)	Average (+/s.d) n=4	
	Density	Area(μm^2)
BM49 (C_2H_6N+, m/z 44) Tert-butylamino-ethyl methacrylate	**0.56** (0.11)	**215** (30)
BM34 (C_5H_5O+, m/z 81) Furfuryl methacrylate	**0.59** (0.28)	**1364** (937)

Figure 5.8 (A) Intensity of ions m/z 44 and 81 in all homopolymers (B) Fluorescent images of cardiomyocyte attachment on BM49 and BM34.

(A) Ions are m/z 44 and 81 are most intense in BM49 and BM34 respectively. PLS identified the ion at m/z 44 as being positive for cell attachment but negative for area and m/z 81 as being positive for both (see table 5.1). (B) The fluorescent images show typical cardiomyocyte density and surface area of the cells on the two polymers. The table above shows measured cell attachment and area values and supports that this relationship has been correctly modelled by PLS.

5.2.1.2. Second Generation Co-Polymer Microarray

The PLS process described above was applied to data from the second generation co-polymer array. Application of PLS to cardiomyocytes seeded under serum free conditions was possible due to the greater attachment and therefore larger data set available. The inclusion criteria of reproducibility between replicate polymers were those with a coefficient of variation lower than 60 % which totalled 225 polymer identities from serum pre-conditioned arrays and 218 in serum free conditions of which 80% was used to build the model and 20% to test it.

In both conditions, a relatively good model was found for cardiomyocyte attachment, R^2 = 0.39 and 0.54 for serum preconditioned and serum free surfaces respectively. However, the predictability of cardiomyocyte area was weak for serum preconditioned arrays (R^2 = 0.072) and no relationship between surface chemistry and cell area could be modelled under serum free conditions (R^2 = –3.9) (fig. 5.9). The overall reduction in predictability for the second generation co-polymers compared to the first generation homopolymers may be due to the reduction in chemical diversity from 115 monomers to 24. Although, monomers with a range of cell responses were intentionally chosen to fabricate the second generation arrays, it may be that this diversity was insufficient to build a robust model.

Nevertheless, ions identified to have a positive influence on cell attachment in the first generation array, m/z 41.04 ($C_3H_5^+$) and 81.03 ($C_5H_5O^+$) were also found to have this effect in serum pre-conditioned second generation arrays. The most influential ions, found to have a positive effect on both cell attachment and spread in the second generation co-polymer array was identified at m/z 91.06 ($C_6H_5CH_2$+) and 55.05 (C_4H_7+) which had the highest intensities in co-polymers containing BM39 (benzyl methacrylate) and BM18 (lauryl methacrylate) respectively (Table 5.2).

Ions with m/z 59.05 ($C_3H_7O^+$), 71.01 ($C_3H_3O_2$-), 57.06 ($C_3H_7N^+$) were assigned negative regression coefficients for both cardiomyocyte attachment and spread. These ions were also identified in the first generation PLS but had

opposing effects in the two parameters (Table 5.1). Acrylamides, overall, performed poorly for cell attachment and spread (see figure 3.17) and the CNO- (m/z 42.00) ion from the acrylamide backbone was identified as the most negative scoring coefficient for cardiomyocyte spread for serum preconditioned second generation arrays. The ion 44.05 (C_2H_6N+) which was identified to have a positive effect on cell attachment but negative on cell area in homopolymer arrays was this time assigned negative coefficients for both responses on co-polymers.

Ions that were influential for cardiomyocyte attachment on co-polymer arrays that were seeded in serum free conditions included the recurring ions at m/z 41.01 ($C_3H_5^+$) and 81.03 ($C_5H_5O^+$). A different ion with m/z 43.05 (C_3H_7+) was also identified to be important for attachment and was found to be most intense in co-polymers containing the previously identified monomer, BM18. Similarly, the ions found to be negative for attachment were in agreement with those found previously at m/z 71.01 ($C_3H_3O_2-$) and 42.00 (CNO-). The Cl^- (m/z 34.97) ion was identified to be highly influential for resisting cell attachment under serum free conditions compared to serum pre-conditioned arrays.

Improved cell adhesion was seen on co-polymer AM38/BM39, which supported adhesion of cardiomyocytes that displayed a greater surface area compared to AM38 alone (fig.3.26). This synergy has been captured by the PLS model which identifies ion with m/z 91.06, $C_7H_7^+$, which is the aromatic moiety present in BM39 (benzyl methacrylate) as being highly influential for larger cardiomyocyte area of adhered cells (table 5.3).

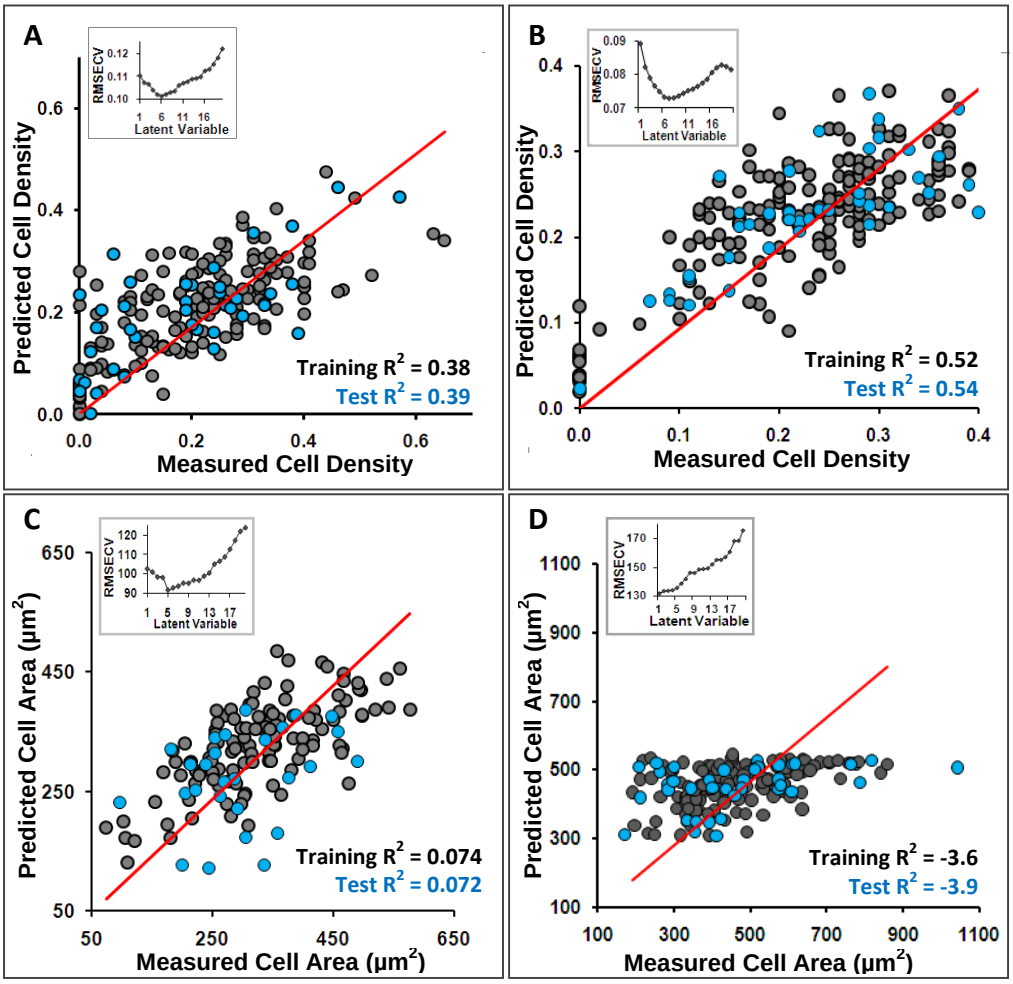


Figure 5.9 PLS measured verses predicted values for cardiomyocyte attachment and area on co-polymers in (A,C) Serum preconditioned (B,D) Serum free conditions.

Relatively good models were constructed for predicting cardiomyocyte density on co-polymers in both serum/free conditions. However, reliable models could not be built for predicting cardiomyocyte area.

Table 5.2 Chemical Moieties identified by PLS to be influential for cardiomyocyte adhesion and cell area on serum pre-conditioned co-polymer arrays.

Effect on Cell Response	Regression Coefficient		Ion (m/z)	Functionality	Greatest Intensity
	Density	Area			
Positive	1.69	1711	$C_6H_5CH_2^+$ (91.06)	Aromatic	BM39
	1.13	1125	$C_4H_7^+$ (55.05)	Hydrocarbon	BM18
	1.02	846	$C_5H_5O^+$ (81.03)	Aromatic	BM34
	0.61	849	$C_3H_5^+$ (41.04)	Acrylate backbone	Multi-acrylates
Negative	-0.78	-52	$C_3H_7O^+$ (59.05)	Propylene Glycol	AD24
	-0.67	-318	$C_3H_3O_2$- (71.01)	Oxygen/Glycol monomers	AM54
	-0.42	-498	C_3H_7N+ (57.06)	Amine	BM49
	-0.13	-1095	CNO- (42.00)	Acrylamide backbone	-

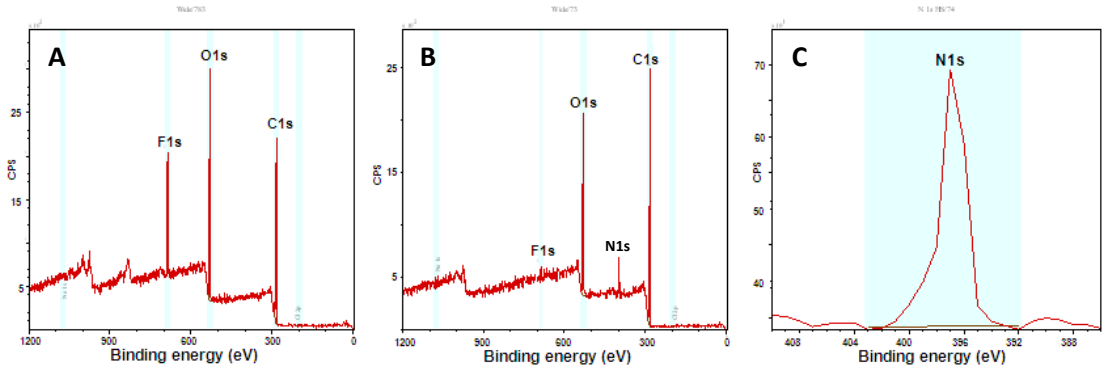
Table 5.3 Chemical Moieties identified by PLS to be influential for cardiomyocyte adhesion on co-polymer arrays in serum free conditions.

Effect on Cell Density	Regression Coefficient	Ion (m/z)	Functionality	Greatest Intensity
Positive	0.61	$C_3H_7^+$ (43.05)	Hydrocarbon	BM18
	0.42	$C_6H_5CH_2^+$ (91.06)	Aromatic	BM39
	0.40	$C_5H_5O^+$ (81.03)	Aromatic	BM34
	0.37	$C_3H_5^+$ (41.04)	Acrylate backbone	Multi-acrylates
Negative	-2.58	Cl- (34.97)	Chlorine	CM13
	-1.18	$C_3H_3O_2$- (71.01)	Oxygen/Glycol monomers	AM54
	-0.25	CNO- (42.00)	Acrylamide backbone	Acrylamides

5.2.2. X-ray Photoelectron Spectroscopy

XPS was conducted to firstly gain the absolute elemental concentration of the surface to complement the qualitative ToF-SIMS molecular structural data. Secondly, the data was used to establish whether elemental descriptors of carbon, nitrogen, oxygen and fluorine concentration could be adequate to predict cardiomyocyte response.

XPS spectra were quantified as shown in figure 5.10 and the fluorine and nitrogen concentrations across the array can be seen in figure 5.11. Electrons with a binding energy in the region of 285eV are from the carbon 1s core level; those with binding energies of approximately 531eV and 688eV are from the oxygen and fluorine 1s core level.



composition.

Figure 5.10 XPS wide survey scan of a fluorinated polymer, AM58 (A), a nitrogen containing polymer, AM36 (B) and a high sensitivity scan for the nitrogen peak of AM36 (C).
(A) The wide survey XPS scan for tridecafluorooctyl acrylate (AM58) shows the counts per second (CPS) of electrons with a certain binding energy. (B) The wide survey scan for diethylamino ethyl acrylate (AM36) shows an additional nitrogen peak, around 398eV. (C) The area of the peak above background (brown line) is proportional to the quantity of that element in the sample.

The amount of fluorine and nitrogen is highest in regions where they are to be expected (fig 5.11). However, there are some regions where these elements are unexpectedly present which may be due to contamination of the source monomer and others where it is missing. This may cause an issue for scale up of

'hit' polymers but for the purposes correlation to cell response, it is the surface analytical data that is being utilised and so these discrepancies are taken into account. This emphasises the need for full surface analytical data to be considered rather than using the structure of what is assumed to have been printed.

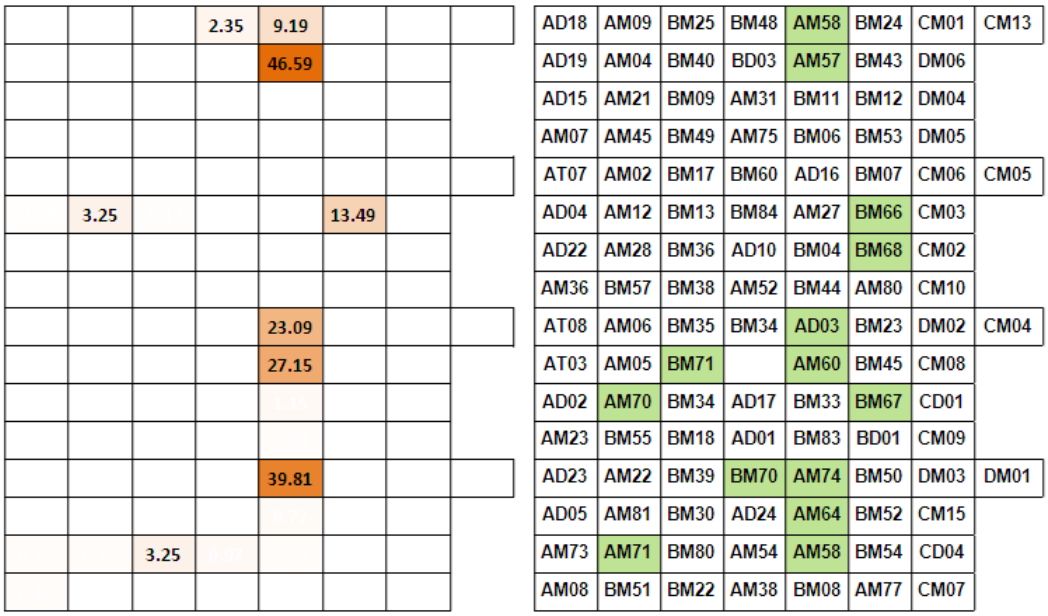


Figure 5.11 Fluorine XPS analysis of array
The orange regions are where asignificant amount of fluorine was detected (% elemental composition). These overlap with polymers that contain fluorine (green regions). However, 3.25% of fluorine was detected in AM12 and BM48. The source could be contaminated or occurred during printing. Fluorine was not detected in expected regions; BM68, 67, 71 and AM64,58,70.

Cardiomyocyte area and density was plotted against corresponding surface elemental composition to identify if there is any correlation (fig 5.12). There was no relationship observed between the amount of nitrogen, oxygen or fluorine present in the top 10 nm of the surface and cardiomyocyte density or area.

PLS was also carried out to validate that the analysis does not forge correlations when there are none. The model attempted to correlate the amount of each element in a polymer region with its corresponding cardiomyocyte response and no correlation was found for density (R^2=-9) or area (R^2=-10) (fig.5.13).

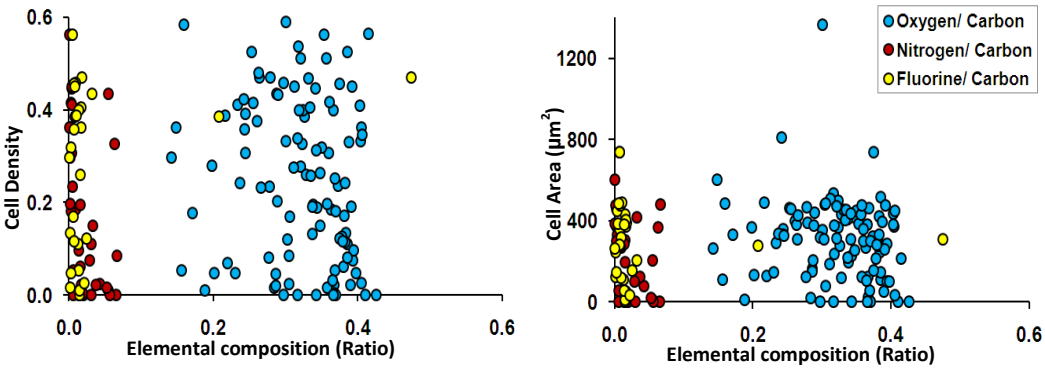


Figure 5.12 Elemental composition as determined by XPS and influence on cardiomyocyte adhesion and area on serum pre-conditioned first generation homopolymer arrays.
No correlation was observed between elemental compositions and cell response.

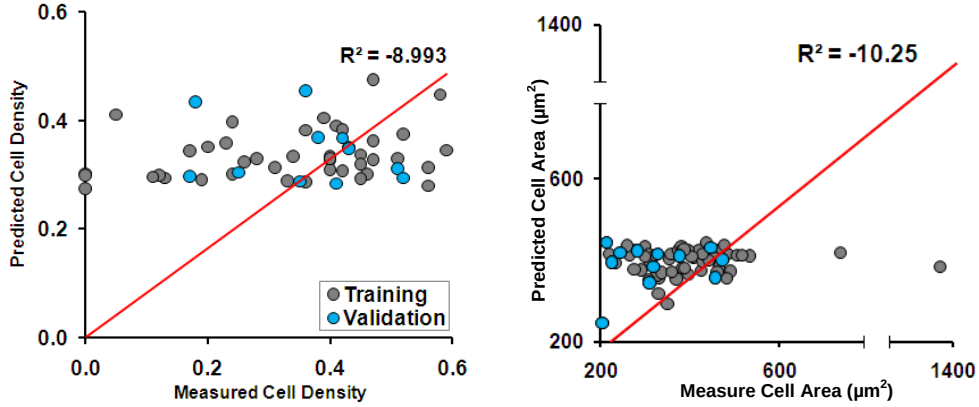


Figure 5.13 PLS model using elemental composition to predict cardiomyocyte attachment and area on serum preconditioned homopolymers.
No predictive model could be built using combined XPS elemental data which is in agreement with simple linear modelling of the individual elements.

5.2.3. Water Contact Angle

The water contact angle (WCA) on the polyacrylate and polyacrylamide surfaces was measured using pico-litre sessile water drop experiments to allow its relationship cardiomyocyte behaviour to be probed. Figure 5.14.A shows WCA measurements on BM66 (Heptadecafluorodecyl methacrylate), AM07 (Isobutyl acrylate) and AT03 (Trimethylolpropane triacrylate) which were found to have an average WCA (+/-s.d, n=3) of 108º (21), 71º (13) and 40º (3). A full list of measurements can be found in appendix 3. The measurements follow the general trend of fluorine containing monomers being more hydrophobic and those with a higher amount of polar oxygen being more hydrophilic. Figure 5.14.B displays this trend by plotting elemental composition as determined by XPS against WCA.

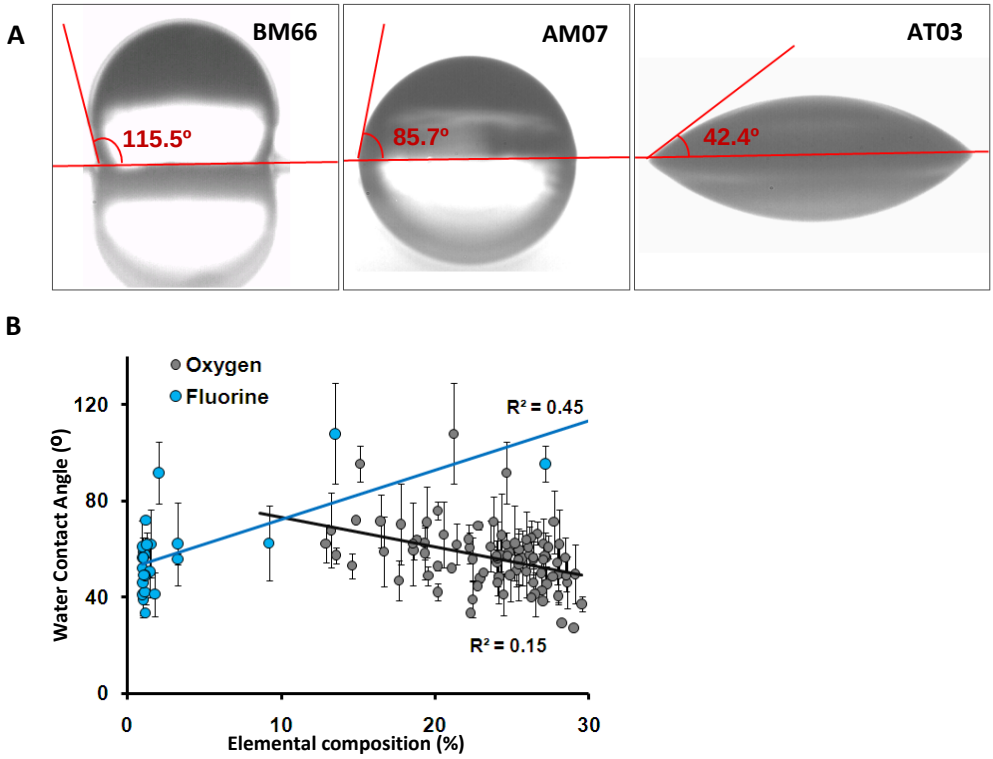


Figure 5.14 WCA measurements on homopolymers (A) and general trend of WCA with fluorine and oxygen elemental composition (B).
(A) BM66, a fluorinated polymer is relatively hydrophobic. AM07 and AT03 have very similar elemental composition but AT03 is significantly more hydrophilic. (B) An increase in fluorine concentration of the polymer decreased its hydrophilicity as indicated by a larger WCA and an increase in oxygen increases hydrophilicity. (WCA ± s.d, n=3)

To identify if there is any correlation between WCA and cardiomyocyte behaviour, WCAs were plotted against cell density and area. Polymers which contained nitrogen or fluorine are highlighted (fig.5.15). There is no obvious correlation but it is clear that polymers with the highest cell density and area are within a WCA range of 60º - 80º with both density and area dropping either side of that range. This may indicate an optimal range between hydrophilicity and cardiomyocyte interaction. The low cell densities and areas also observed within the 60º - 80º range indicates that cardiomyocyte attachment and area in response to WCA and is confounded with other factors such as surface chemistry as described by PLS.

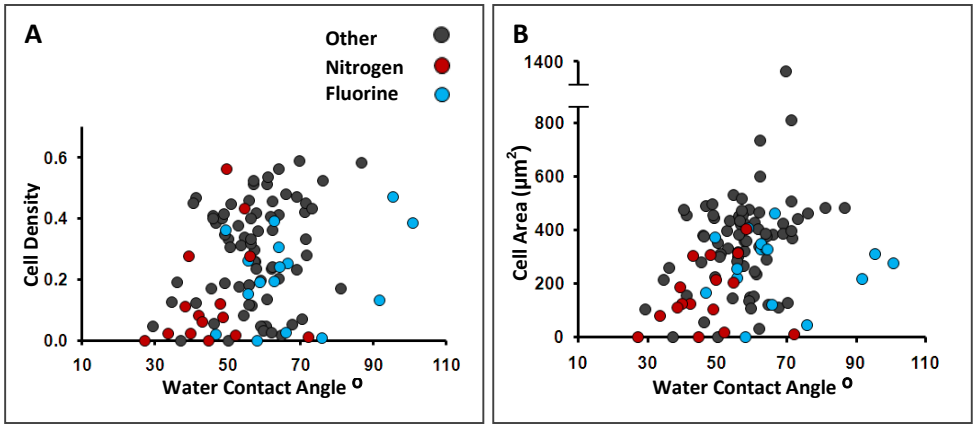


Figure 5.15 (A) Cardiomyocyte density and (B) area plotted against WCA of homopolymers in first generation array pre-conditioned with serum.
No correlation could be seen between cardiomyocyte response and water contact angle. The highest cell densities and areas were observed within a range of 60º – 80º. However, this range also had some of the lowest densities and cell areas.

This general trend was also observed in second generation co-polymer microarrays where there was no high cell densities observed on surfaces with a WCA lower than 50º or above 90º. Within this range diverse cell densities and area was observed indicating no clear relationship.

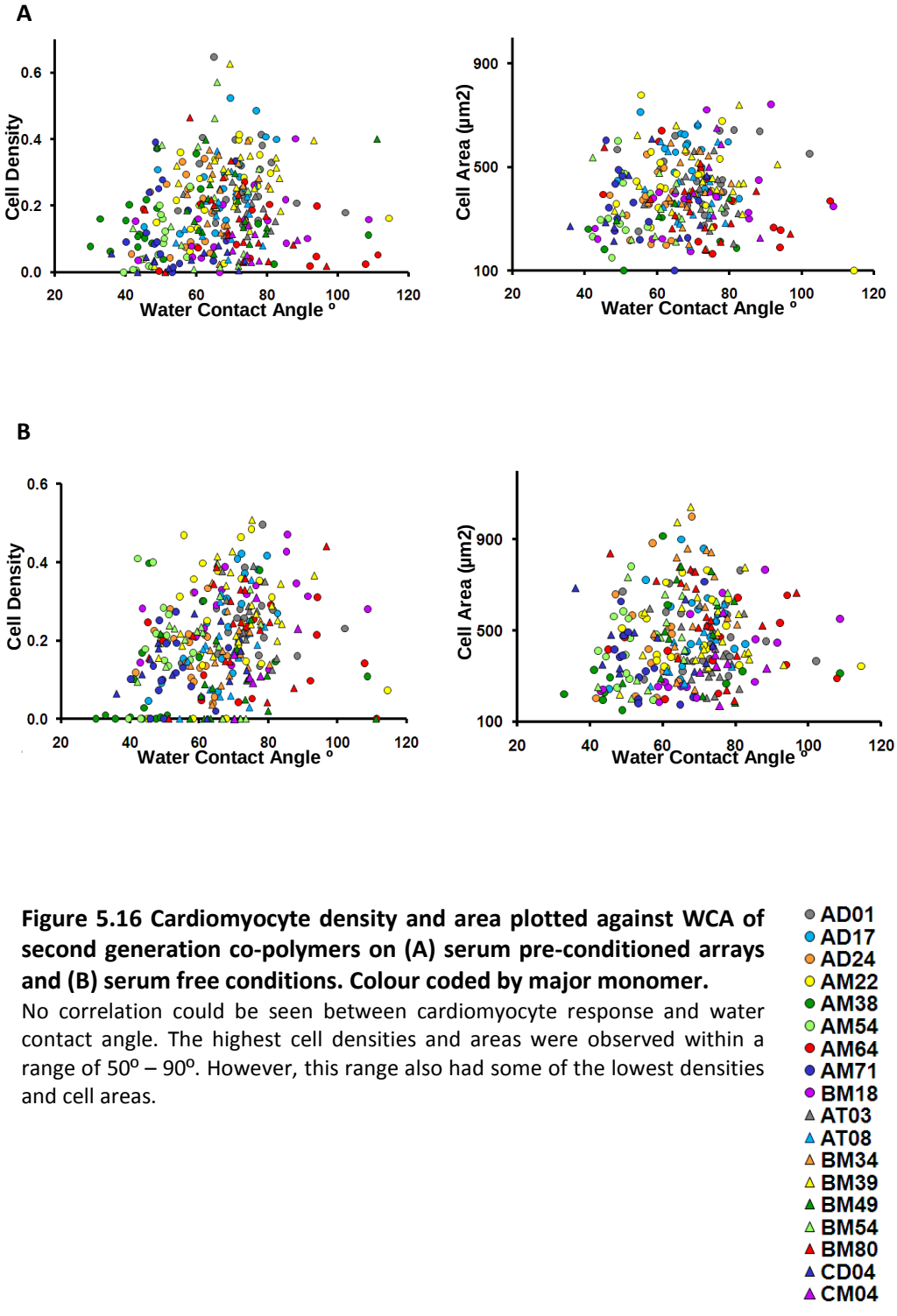


Figure 5.16 Cardiomyocyte density and area plotted against WCA of second generation co-polymers on (A) serum pre-conditioned arrays and (B) serum free conditions. Colour coded by major monomer.
No correlation could be seen between cardiomyocyte response and water contact angle. The highest cell densities and areas were observed within a range of 50º – 90º. However, this range also had some of the lowest densities and cell areas.

5.3. DISCUSSION

This chapter characterised the surface of polymers printed on microarrays using ToF-SIMS, XPS and WCA measurements. The use of PLS linear regression for the analysis of the multivariate data generated by ToF-SIMS was demonstrated to model a relationship between surface chemistry and cardiomyocyte behaviour on serum preconditioned first and second generation arrays. The model for surface chemistry and cardiomyocyte density in serum free conditions was weak and no correlation could be modelled for cardiomyocyte area in serum free conditions for second generation arrays. Correlation of univariate XPS and WCA data with cardiomyocyte response was attempted but no correlation was identified for either generation arrays.

5.3.1. Multivariate Linear Regression of ToF-SIMS data using PLS

It was found that surface chemical data acquired from ToF-SIMS analysis was able to moderately predict cardiomyocyte attachment and surface area using a PLS linear regression model. Models were generated for each experimental set up, homopolymer and co-polymer arrays that were pre-conditioned with 20% FBS and a co-polymer array that was seeded with cardiomyocytes in serum free conditions. Recurring ions were those at m/z 41.04 ($C_3H_5^+$) and 81.03 ($C_5H_5O^+$) which were assigned positive regression coefficients indicating that these functionalities are highly influential for increasing cardiomyocyte attachment and spread. Ion $C_3H_5^+$ is ubiquitous belonging to the acrylate backbone and occurred in varying intensities in many of the polymers. Ion $C_5H_5O^+$ is monomer specific, most intense in furfuryl containing polymers, BM34 (fufuryl methacrylate) and AM22 (Tetrahydrofurfuryl acrylate) (see fig.3.12.C).

Recurring ions that were assigned negative regression coefficients were those with m/z 71.01 ($C_3H_3O_2^+$) and 59.05 ($C_3H_7O^+$), both have relatively high intensities in AM54 (poly(propylene glycol) acrylate) and AD24 (poly(propylene glycol) diacrylate). Poly(propylene glycol) has been utilised for prevention of protein adsorption (Glidle et al., 2003) so the identification of these ions as being negative for cell adhesion is in agreement with this. In serum free conditions,

the PLS model identified chlorine (m/z 34.97) as a major negative influence on cardiomyocyte attachment which is present in DM07 (N-(3-Aminopropyl) methacrylamide Hydrochloride).

The investigation of surface chemistry and its influence on cardiomyocyte culture is limited and none have investigated a large range of chemistries. Natarajan *et al*, reported an increased attachment of rat cardiomyocytes on hydroxy group presenting surfaces compared to carboxyl presenting surfaces (Natarajan et al., 2008). A study by Lee *et al*, also reported superior adhesion of Chinese Hamster Overy cells to hydroxy functionalised surfaces compared to carboxyl functionalised surfaces. They attributed the difference to the hydroxy group being able to form polar bonds with cell surfaces. They also included an amine functionalised surface which displayed the highest cell attachment explained to occur due to the positive charge on the amine which has been reported to adsorb more protein compared to negatively charged surfaces (Lee et al., 1994). However, amines included in this study (AM38, BM49, BM48) displayed cardiomyocyte attachment in serum free conditions but the morphology of the attached cells is poor with low surface area and no myofibril banding (fig.5.17).

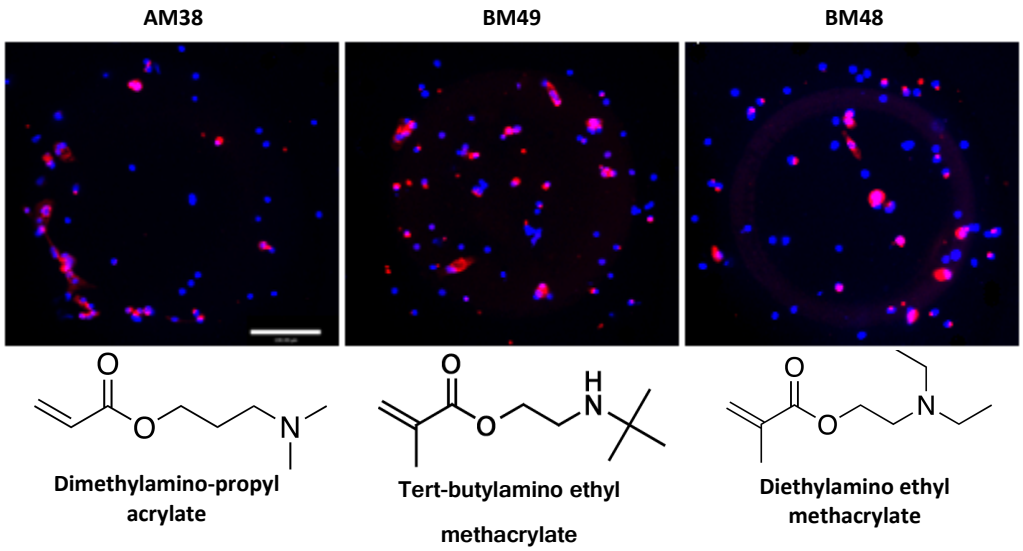


Figure 5.17 hESC-cardiomyocyte adhesion on amino acrylates in serum free conditions.
These polymers displayed some of the highest attachment in serum free conditions in first generation arrays. However, cell area is small and cells do not appear functional with lack of myofibril Z-line banding.

Chilkoti *et al*, was one of the first to investigate the effect of surface chemistry on bovine endothelial cell attachment to plasma treated polymers using PLS. Ions reported to be positive for cell attachment C_3H_5+(41) and negative for attachment $C_3H_3O_2$-(71) correspond to the ions identified in our cardiomyocyte model despite the different material library that was surveyed. Nitrogen containing ions such as CNO+ and C_2NH_2+ were found to be positive for endothelial cell attachment but for cardiomyocyte adhesion, this study found that the CNO- ion, with highest intensity in the acrylamides, was a negative for attachment and spread (Chilkoti et al., 1995). This could be due to multiple differences in the culture systems; cell type, media and substrate.

Aromatic ions at m/z 77.04 ($C_6H_5^+$), 91.06 ($C_6H_5CH_2^+$) and 81.03 ($C_5H_5O^+$) were assigned large positive co-efficients for cardiomyocyte spread in serum pre-conditioned homopolymer and co-polymer arrays and for attachment in co-polymer arrays that were cultured in serum free conditions. Interestingly, Kalaskar *et al*, reported that mouse fibroblasts cultured on cellulose modified with aromatic amino acids enabled a significantly greater degree of cell spreading compared to hydrophilic or aliphatic amino acid surfaces. The increased surface area of the seeded cells was shown to be linked to an increased adsorption of fibronectin from medium containing 10% FBS on the aromatic surfaces (Kalaskar et al., 2008).

PLS models identify relationships between independent variables (X) and response values (Y) based on co-variance. i.e a change in X causes a change in Y (Le et al., 2012). It does not help explain why this change is occurring and underlying mechanisms of cell-surface interaction. Further investigation would be required to identify whether the ions identified by PLS are having a direct effect on cardiomyocytes or on the protein adsorption from the FBS used to pre-condition the arrays or the extracellular matrix excreted by the cells.

The success of PLS modelling is based on the premise that the relationship between surface chemistry and cell response is linear in nature. This can restrict the reliability of the model if some variables do not follow this. Non-linear techniques may be employed such as polynomial regressions or techniques that can analyse both linear and non-linear relationships such as

neural networks. A benefit of PLS is that it can reduce the dimensionality of large datasets using latent variables. Neural networks can achieve this by first using an unsupervised method (Kohonen network) to reduce the dimensionality of the independent variables (Gasteiger et al., 2003). A supervised network can then be applied to correlate this to the dependent variable (cell response), again training data is used to construct a model which is then validated using test data. The success of the model will depend on the relevance of the variables or 'molecular descriptors' chosen to construct the model (Epa et al., 2012).

5.3.2. Water Contact Angle and XPS Elemental Composition

Polyacrylamide and polyacrylate substrates investigated in this study displayed WCAs ranging from 27º to 115º. The WCA altered with elemental composition, those higher in oxygen content having a lower WCA and those with a higher percentage of fluorine displaying higher WCAs. The XPS determined elemental composition did not correlate with cell attach adhesion supporting the need for more informative identification of chemical functional groups that are displayed on the surface.

Cardiomyocytes displayed the highest attachment and spread on polymers that had a WCA in the range of 60º – 80º. Attachment and spread decreased on surfaces with a WCA either side of this range. However, not all polymers that displayed a WCA between 60 – 80 had good cardiomyocyte attachment indicating that there are other factors that can dominate the degree of cell adhesion. This could be surface chemistry as described above, substrate stiffness and roughness which were not measured in this study.

The relationship between cell adhesion and the hydrophilicity of a surface has been reported to a greater extent compared to surface chemistry. WCA in relation to its effect on the adsorption of proteins on surfaces has been studied in detail for its importance during development of biomaterials where low adsorption is desired to prevent thrombotic events and infection due to

biofilm formation *in vivo* (Chen et al., 2010). Increased protein adsorption for cell culture purposes is desired as it has been shown to mediate cell attachment.

To study the effects of hydrophilicity on the attachment and spread of human mesenchymal stem cells (hMSC), Ayala *et al* systematically altered surface hydrophilicity by altering the length of the alkyl chain in co-polymers of amino acids and acrylamide. They probed 10 surfaces with WCA ranging from 27º to 85º and found that the surface with a WCA of 58º had highest hMSC attach and spread which fell either side of this value. The medium used for hMSC culture contained 10% FBS and they found that fibronectin and laminin was selectively adsorbed from serum to a greater extent on the surface that displayed the highest attachment with a WCA of 58º.

As well as screening for suitable culture surfaces, high throughput screening and surface analysis has generated further hypothesis that can be investigated further.

5.3.3. Limitations and Future Work

To further elucidate the influence of surface chemistry on cardiomyocyte response, other surface parameters such as roughness, surface patterning and stiffness should be considered. No study exists where all these parameters have been controlled and studied in parallel. Development of models that are able to handle such diverse data would aid the understanding of inter-relationships

For better insight into the mechanism underlying improved adhesion and area of cardiomyocytes on certain polymers used in this study, protein adsorption and conformation assays would be necessary. Quartz crystal microbalance analysis could detect the amount of protein being adsorbed onto different polymers, integrin binding studies could give binding sites that are being displayed on adsorbed proteins. The amount of protein adsorption can be misleading because it is the conformation of adsorbed proteins that can determine cell behaviour. Very hydrophilic surfaces can lead to a hydrated layer on the polymer, a film of water that can prevent strong adsorption of proteins.

Conversely, a highly hydrophobic material can adsorb proteins in altered conformations that do not display the requisite sites for integrin binding with cells (Bacakova et al., 2011).

Use of defined protein rather than FBS would also begin to unravel which proteins are most important for attachment. In serum free culture a robust PLS model could not be achieved. This could indicate that surface chemistry is more influential in the presence of serum proteins.

CHAPTER 6

General Discussion

The overall aims of this study were to, **1**. gain an understanding of the relationship between surface chemistry and cardiomyocyte behaviour and **2.** assess the suitability of synthetic non-biological substrates for the *in vitro* propagation of human stem cell derived cardiomyocytes**.**. The substrates chosen for this study were polymers of acrylate and acrylamide monomers. The chemical diversity of these polymers enables investigation of the first aim and their demonstrated use as biomaterials indicates promise as potential materials capable of being scaled up for use.

Initial screening was performed on microarrays consisting of homopolymers. There was limited attachment on the homopolymers in serum free conditions, with only 12 of the 115 polymers supported cardiomyocyte adhesion. The highest adhesion was on AM38 (dimethylamino-propyl acrylate) followed by BM49 (tert-butylamino-ethyl methacrylate). However, the cell area was relatively small on both of these substrates and myofibril banding could not be observed. All 12 polymers which supported cardiomyocyte adhesion were included in the 24 that were co-polymerised to generate 576 novel surfaces for investigation.

Primary screening could have been more robust if cell analysis software was optimised to be able to quantify myofibril alignment. This is a marker for maturity and if included at an early stage in the screening process could have eliminated materials that were detrimental to myofibril organisation. It would have also enabled substrate-cell interaction modelling of this parameter. With development of image analysis software and high quality image acquisition this should be possible.

Nevertheless, generation of a combinatorial library of materials based on the 24 monomers chosen from the first screen lead to the identification of co-polymers that supported attachment of cardiomyocytes with greater cell area than was observed on the homopolymers indicating synergy between mixtures of monomers. This was exemplified by AM38, which supported cardiomyocyte adhesion but cell area was relatively small, with no myofibrillar organisation. When the monomer was mixed with BM39, which displayed relatively large cardiomyocyte area, the co-polymer was able to support higher cell density and

area, with myofibril banding, than either polymer alone. Further research is required into how the co-polymers are interacting with the cardiomyocytes. Although, the medium is serum free there are other components such as the lipid additive that may be modulating cell adhesion.

Many other synergistic combinations which enabled better cardiomyocyte attachment may be in the library but were not investigated due to limited resources. This is one issue with high throughput platforms, in that the large data set generated is often difficult to analyse if the requisite automated analysis systems are either not adequate or not possible to achieve. Automated analysis requires manual validation and in this study manual correction of counts was needed in 7 % of images that had been assessed incorrectly due to background/auto fluorescence of polymers.

Once co-polymers that supported cardiomyocyte attachment in serum free conditions had been identified, five were chosen to perform more detailed cardiomyocyte characterisation. The number of polymers analysed could have been increased if 1. Automated electrophysiology was employed 2. Myofibril assessment by image analysis software was optimised.

Of the five co-polymers analysed, two showed promise as substrates that could potentially be non-biological substitutes for gelatin, as determined by comparable electrophysiology and myofibril organisation. However, scale up of polymers will eventually be required and this can change the physical properties of the polymers, such as stiffness, opacity and brittleness and would require further optimisation to maintain the cardiomyocyte-surface interactions that were observed during micro-scale analysis.

The relationship between surface chemistry and cardiomyocyte attachment and area was investigated using partial least squares multivariate regression analysis. Chemical species identified to be important for cardiomyocyte attachment in both serum replete and serum free conditions were $C_5H_5O^+$ and $C_3H_5^+$. In serum free conditions, $C_6H_5CH_2^+$ was identified to important for cell adhesion. The model assumes that relationships are linear in nature, so an increase in these ions would increase adhesion and a decrease

would lower adhesion. Polynomial relationships cannot be modelled using PLS and it may beneficial to use alternative models such as neural networks to avoid any assumptions about the cell-surface relationship. Libraries of material that combine all the positive chemistries identified during PLS may aid rational design of materials and may help to form hypotheses to unravel the basis of cell-surface interactions.

Bibliography

ABRAHAM, S., EROSHENKO, N. & RAO, R. R. 2009. Role of bioinspired polymers in determination of pluripotent stem cell fate. *Regenerative medicine,* 4**,** 561-578.

ANDERSON, D. G., LEVENBERG, S. & LANGER, R. 2004. Nanoliter-scale synthesis of arrayed biomaterials and application to human embryonic stem cells. *Nature biotechnology,* 22**,** 863-866.

ANDERSON, D. G., PUTNAM, D., LAVIK, E. B., MAHMOOD, T. A. & LANGER, R. 2005. Biomaterial microarrays: rapid, microscale screening of polymer–cell interaction. *Biomaterials,* 26**,** 4892-4897.

ANNABI, N., SELIMOVIC, S., ACEVEDO COX, J. P., RIBAS, J., AFSHAR BAKOOSHLI, M., HEINTZE, D., WEISS, A. S., CROPEK, D. & KHADEMHOSSEINI, A. 2013a. Hydrogel-coated microfluidic channels for cardiomyocyte culture. *Lab on a Chip,* 13**,** 3569-3577.

ANNABI, N., TSANG, K., MITHIEUX, S. M., NIKKHAH, M., AMERI, A., KHADEMHOSSEINI, A. & WEISS, A. S. 2013b. Highly Elastic Micropatterned Hydrogel for Engineering Functional Cardiac Tissue. *Advanced Functional Materials*.

ANSON, B. D., KOLAJA, K. L. & KAMP, T. J. 2011. Opportunities for Use of Human iPS Cells in Predictive Toxicology. *Clinical Pharmacology and Therapeutics,* 89**,** 754.

ARNOLD, S. J. & ROBERTSON, E. J. 2009. Making a commitment: cell lineage allocation and axis patterning in the early mouse embryo. *Nat Rev Mol Cell Biol,* 10**,** 91-103.

BACAKOVA, L., FILOVA, E., PARIZEK, M., RUML, T. & SVORCIK, V. 2011. Modulation of cell adhesion, proliferation and differentiation on materials designed for body implants. *Biotechnology advances,* 29**,** 739-767.

BAHARVAND, H., AZARNIA, M., PARIVAR, K. & ASHTIANI, S. K. 2005. The effect of extracellular matrix on embryonic stem cell-derived cardiomyocytes. *Journal of Molecular and Cellular Cardiology,* 38**,** 495-503.

BAIN, C. D. & WHITESIDES, G. M. 1988. Depth sensitivity of wetting: monolayers of. omega.-mercapto ethers on gold. *Journal of the American Chemical Society,* 110**,** 5897-5898.

BANERJEE, I., YEKKALA, K., BORG, T. K. & BAUDINO, T. A. 2006. Dynamic Interactions between Myocytes, Fibroblasts, and Extracellular Matrix. *Annals of the New York Academy of Sciences,* 1080**,** 76-84.

BARNETT, V. A. 2005. Cardiac myocytes. *Handbook of Cardiac Anatomy, Physiology, and Devices***,** 113-121.

BAX, N. A. M., VAN MARION, M. H., SHAH, B., GOUMANS, M.-J., BOUTEN, C. V. C. & VAN DER SCHAFT, D. W. J. 2012. Matrix production and remodeling capacity of cardiomyocyte progenitor cells during in vitro differentiation. *Journal of Molecular and Cellular Cardiology*.

BERECKI, G., WILDERS, R., DE JONGE, B., VAN GINNEKEN, A. C. G. & VERKERK, A. O. 2010. Re-Evaluation of the Action Potential Upstroke Velocity as a Measure of the Na+ Current in Cardiac Myocytes at Physiological Conditions. *PloS one,* 5**,** e15772.

BERGMANN, O., BHARDWAJ, R. D., BERNARD, S., ZDUNEK, S., BARNABÉ-HEIDER, F., WALSH, S., ZUPICICH, J., ALKASS, K., BUCHHOLZ, B. A., DRUID, H., JOVINGE, S. & FRISÉN, J. 2009. Evidence for Cardiomyocyte Renewal in Humans. *Science,* 324**,** 98-102.

BIRD, S. D., DOEVENDANS, P. A., VAN ROOIJEN, M. A., BRUTEL DE LA RIVIERE, A., HASSINK, R. J., PASSIER, R. & MUMMERY, C. L. 2003. The human adult cardiomyocyte phenotype. *Cardiovascular research,* 58**,** 423.

BLAZESKI, A., ZHU, R., HUNTER, D. W., WEINBERG, S. H., ZAMBIDIS, E. T. & TUNG, L. 2012. Cardiomyocytes derived from human induced pluripotent stem cells as models for normal and diseased cardiac electrophysiology and contractility. *Progress in Biophysics and Molecular Biology*.

BOUDOU, T., LEGANT, W. R., MU, A., BOROCHIN, M. A., THAVANDIRAN, N., RADISIC, M., ZANDSTRA, P. W., EPSTEIN, J. A., MARGULIES, K. B. & CHEN, C. S. 2011. A microfabricated platform to measure and manipulate the mechanics of engineered cardiac microtissues. *Tissue Engineering Part A,* 18**,** 910-919.

BRAAM, S. R., PASSIER, R. & MUMMERY, C. L. 2009. Cardiomyocytes from human pluripotent stem cells in regenerative medicine and drug discovery. *Trends in pharmacological sciences,* 30**,** 536-545.

BRAAM, S. R., TERTOOLEN, L., VAN DE STOLPE, A., MEYER, T., PASSIER, R. & MUMMERY, C. L. 2010. Prediction of drug-induced cardiotoxicity using human embryonic stem cell-derived cardiomyocytes. *Stem Cell Research,* 4**,** 107-116.

BRETTE, F. & ORCHARD, C. 2007. Resurgence of Cardiac T-Tubule Research. *Physiology,* 22**,** 167-173.

BRIGGS, D., BROWN, A., VICKERMAN, J. C. & ADAMS, F. 1990. Handbook of static secondary ion mass spectrometry (SIMS): Wiley, Chichester, 1989 (ISBN 0-471-91627-7). 156 pp. Price£ 125.00. *Analytica Chimica Acta,* 236**,** 509-510.

BRIGGS, D. & GRANT, J. T. 2003. *Surface analysis by Auger and X-ray photoelectron spectroscopy*, IM Publications Chichester, UK.

BRISON, J., MURAMOTO, S. & CASTNER, D. G. 2010. ToF-SIMS Depth Profiling of Organic Films: A Comparison between Single-Beam and Dual-Beam Analysis†. *The Journal of Physical Chemistry C,* 114**,** 5565-5573.

BRITO-MARTINS, M., HARDING, S. E. & ALI, N. N. 2008. B1- and B2-adrenoceptor responses in cardiomyocytes derived from human embryonic stem cells: comparison with failing and non-failing adult human heart. *British journal of pharmacology,* 153**,** 751-759.

BROCCHINI, S., JAMES, K., TANGPASUTHADOL, V. & KOHN, J. 1998. Structure-property correlations in a combinatorial library of degradable biomaterials. *Journal of Biomedical Materials Research,* 42**,** 66-75.

BUCKINGHAM, M., MEILHAC, S. & ZAFFRAN, S. 2005. Building the mammalian heart from two sources of myocardial cells. *Nat Rev Genet,* 6**,** 826-837.

BURRIDGE, P. W., ANDERSON, D., PRIDDLE, H., BARBADILLO MUÑOZ, M. D., CHAMBERLAIN, S., ALLEGRUCCI, C., YOUNG, L. E. & DENNING, C. 2007. Improved Human Embryonic Stem Cell Embryoid Body Homogeneity and Cardiomyocyte Differentiation from a Novel V-96 Plate Aggregation System Highlights Interline Variability. *Stem Cells,* 25**,** 929-938.

BURRIDGE, P. W., KELLER, G., GOLD, J. D. & WU, J. C. Production of De Novo Cardiomyocytes: Human Pluripotent Stem Cell Differentiation and Direct Reprogramming. *Cell stem cell,* 10**,** 16-28.

BURRIDGE, P. W., THOMPSON, S., MILLROD, M. A., WEINBERG, S., YUAN, X., PETERS, A., MAHAIRAKI, V., KOLIATSOS, V. E., TUNG, L. & ZAMBIDIS, E. T. 2011. A Universal System for Highly Efficient Cardiac Differentiation of Human Induced Pluripotent Stem Cells That Eliminates Interline Variability. *PloS one,* 6**,** e18293.

BUSSEK, A., WETTWER, E., CHRIST, T., LOHMANN, H., CAMELLITI, P. & RAVENS, U. 2009. Tissue slices from adult mammalian hearts as a model for pharmacological drug testing. *Cellular Physiology and Biochemistry,* 24**,** 527-536.

CARVAJAL-VERGARA, X., SEVILLA, A., D/'SOUZA, S. L., ANG, Y.-S., SCHANIEL, C., LEE, D.-F., YANG, L., KAPLAN, A. D., ADLER, E. D., ROZOV, R., GE, Y., COHEN, N., EDELMANN, L. J., CHANG, B., WAGHRAY, A., SU, J., PARDO, S., LICHTENBELT, K. D., TARTAGLIA, M., GELB, B. D. & LEMISCHKA, I. R. 2010. Patient-specific induced pluripotent stem-cell-derived models of LEOPARD syndrome. *Nature,* 465**,** 808-812.

CELIZ, A., SMITH, J., PATEL, A., LANGER, R., ANDERSON, D., BARRET, D., YOUNG, L., DAVIES, M., DENNING, C. & ALEXANDER, D. 2013. New Materials for Human Pluripotent Stem Cell Culture: High Throughput Discover and Prediction of Polymers that Promote Cell Attachment. *In Submission.*

CHEN, S., LI, L., ZHAO, C. & ZHENG, J. 2010. Surface hydration: Principles and applications toward low-fouling/nonfouling biomaterials. *Polymer,* 51**,** 5283-5293.

CHIEFARI, J., CHONG, Y. K., ERCOLE, F., KRSTINA, J., JEFFERY, J., LE, T. P. T., MAYADUNNE, R. T. A., MEIJS, G. F., MOAD, C. L. & MOAD, G. 1998. Living free-radical polymerization by reversible addition-fragmentation chain transfer: the RAFT process. *Macromolecules,* 31**,** 5559-5562.

CHILKOTI, A., SCHMIERER, A. E., PEREZ-LUNA, V. H. & RATNER, B. D. 1995. Investigating the relationship between surface chemistry and endothelial cell growth: partial least-squares regression of the static secondary ion mass spectra of oxygen-containing plasma-deposited films. *Analytical Chemistry,* 67**,** 2883-2891.

CLARK, R. B., TREMBLAY, A., MELNYK, P., ALLEN, B. G., GILES, W. R. & FISET, C. 2001. T-tubule localization of the inward-rectifier K+ channel in mouse ventricular myocytes: a role in K+ accumulation. *The Journal of physiology,* 537**,** 979-992.

COWAN, C. A., KLIMANSKAYA, I., MCMAHON, J., ATIENZA, J., WITMYER, J., ZUCKER, J. P., WANG, S., MORTON, C. C., MCMAHON, A. P., POWERS, D. & MELTON, D. A. 2004. Derivation of Embryonic Stem-Cell Lines from Human Blastocysts. *New England Journal of Medicine,* 350**,** 1353-1356.

CURRAN, J. M., CHEN, R. & HUNT, J. A. 2006. The guidance of human mesenchymal stem cell differentiation in vitro by controlled modifications to the cell substrate. *Biomaterials,* 27**,** 4783-4793.

DANG, S. M., GERECHT-NIR, S., CHEN, J., ITSKOVITZ-ELDOR, J. & ZANDSTRA, P. W. 2004. Controlled, Scalable Embryonic Stem Cell Differentiation Culture. *STEM CELLS,* 22**,** 275-282.

DAS, M., MOLNAR, P., GREGORY, C., RIEDEL, L., JAMSHIDI, A. & HICKMAN, J. J. 2004. Long-term culture of embryonic rat cardiomyocytes on an organosilane surface in a serum-free medium. *Biomaterials,* 25**,** 5643-5647.

DAVIES, M. C., ALEXANDER, M. R., HOOK, A. L., YANG, J., MEI, Y., TAYLOR, M., URQUHART, A. J., LANGER, R. & ANDERSON, D. G. 2010. High throughput surface characterization: A review of a new tool for screening prospective biomedical material arrays. *Journal of drug targeting,* 18**,** 741-51.

DAVIS, R. P., CASINI, S., VAN DEN BERG, C. W., HOEKSTRA, M., REMME, C. A., DAMBROT, C., SALVATORI, D., OOSTWAARD, D. W.-V., WILDE, A. A. M., BEZZINA, C. R., VERKERK, A. O., FREUND, C. & MUMMERY, C. L. 2012. Cardiomyocytes Derived From Pluripotent Stem Cells Recapitulate Electrophysiological Characteristics of an Overlap Syndrome of Cardiac Sodium Channel Disease. *Circulation,* 125**,** 3079-3091.

DAVIS, R. P., VAN DEN BERG, C. W., CASINI, S., BRAAM, S. R. & MUMMERY, C. L. 2011. Pluripotent stem cell models of cardiac disease and their implication for drug discovery and development. *Trends in Molecular Medicine,* 17**,** 475-484.

DAWSON, E., MAPILI, G., ERICKSON, K., TAQVI, S. & ROY, K. 2008. Biomaterials for stem cell differentiation. *Emerging Trends in Cell-Based Therapies,* 60**,** 215-228.

DE JONG, S. 1993. SIMPLS: an alternative approach to partial least squares regression. *Chemometrics and Intelligent Laboratory Systems,* 18**,** 251-263.

DE TOMBE, P. P., MATEJA, R. D., TACHAMPA, K., MOU, Y. A., FARMAN, G. P. & IRVING, T. C. 2010. Myofilament length dependent activation. *Journal of Molecular and Cellular Cardiology,* 48**,** 851-858.

DE GANS, B. J., DUINEVELD, P. C. & SCHUBERT, U. S. 2004. Inkjet Printing of Polymers: State of the Art and Future Developments. *Advanced Materials,* 16**,** 203-213.

DEL MONTE, F., O'GARA, P., POOLE-WILSON, P. A., YACOUB, M. & HARDING, S. E. 1995. Cell geometry and contractile abnormalities of myocytes from failing human left ventricle. *Cardiovascular Research,* 30**,** 281-290.

DENNING, C., ALLEGRUCCI, C., PRIDDLE, H., BARBADILLO-MUNOZ, M. D., ANDERSON, D., SELF, T., SMITH, N. M., PARKIN, C. T. & YOUNG, L. E. 2006. Common culture conditions for maintenance and cardiomyocyte

differentiation of the human embryonic stem cell lines, BG01 and HUES-7. *INTERNATIONAL JOURNAL OF DEVELOPMENTAL BIOLOGY,* 50**,** 27.

DERDA, R., LI, L., ORNER, B. P., LEWIS, R. L., THOMSON, J. A. & KIESSLING, L. L. 2007. Defined Substrates for Human Embryonic Stem Cell Growth Identified from Surface Arrays. *ACS Chemical Biology,* 2**,** 347-355.

DICK, E., RAJAMOHAN, D., RONKSLEY, J. & DENNING, C. 2010. Evaluating the utility of cardiomyocytes from human pluripotent stem cells for drug screening. *Biochemical Society transactions,* 38**,** 1037.

DIERICKX, P., DOEVENDANS, P., GEIJSEN, N. & LAAKE, L. 2012. Embryonic Template-Based Generation and Purification of Pluripotent Stem Cell-Derived Cardiomyocytes for Heart Repair. *Journal of Cardiovascular Translational Research,* 5**,** 566-580.

DIMARAKIS, I., LEVICAR, N., NIHOYANNOPOULOS, P., GORDON, M. Y. & HABIB, N. A. 2006. In vitro stem cell differentiation into cardiomyocytes: Part 2: Chemicals, extracellular matrix, physical stimuli and coculture assays. *Journal of Cardiothoracic-Renal Research,* 1**,** 115-121.

DOSS, M. X., DI DIEGO, J., GOODROW, R. J., WU, Y., CORDEIRO, J. M., NESTERENKO, V. V., BARAJAS-MARTINEZ, H., HU, D., URRUTIA, J. & DESAI, M. 2012. Maximum Diastolic Potential of Human Induced Pluripotent Stem Cell-Derived Cardiomyocytes Depends Critically on IKr. *PloS one,* 7**,** e40288.

DRIESEN, R., VERHEYEN, F., DIJKSTRA, P., THONÃ©, F., CLEUTJENS, J., LENDERS, M.-H. L. N., RAMAEKERS, F. S. & BORGERS, M. 2007. Structural remodelling of cardiomyocytes in the border zone of infarcted rabbit heart. *Molecular and cellular biochemistry,* 302**,** 225-232.

DROLET, B., YANG, T., DALEAU, P., RODEN, D. M. & TURGEON, J. 2003. Risperidone Prolongs Cardiac Repolarization by Blocking the Rapid Component of the Delayed Rectifier Potassium Current. *Journal of Cardiovascular Pharmacology,* 41.

DROUIN, E., CHARPENTIER, F., GAUTHIER, C., LAURENT, K. & LE MAREC, H. 1995. Electrophysiologic characteristics of cells spanning the left ventricular wall of human heart: Evidence for presence of M cells. *Journal of the American College of Cardiology,* 26**,** 185-192.

DYER, M. A., FARRINGTON, S. M., MOHN, D., MUNDAY, J. R. & BARON, M. H. 2001. Indian hedgehog activates hematopoiesis and vasculogenesis and can respecify prospective neurectodermal cell fate in the mouse embryo. *Development,* 128**,** 1717-1730.

EHRLICH, J. R. 2008. Inward rectifier potassium currents as a target for atrial fibrillation therapy. *Journal of cardiovascular pharmacology,* 52**,** 129.

ENGELMANN, G. L., BOEHM, K. D., HASKELL, J. F., KHAIRALLAH, P. A. & ILAN, J. 1989. Insulin-like growth factors and neonatal cardiomyocyte development: ventricular gene expression and membrane receptor variations in normotensive and hypertensive rats. *Molecular and cellular endocrinology,* 63**,** 1-14.

ENGLER, A. J., CARAG-KRIEGER, C., JOHNSON, C. P., RAAB, M., TANG, H. Y., SPEICHER, D. W., SANGER, J. W., SANGER, J. M. & DISCHER, D. E. 2008. Embryonic cardiomyocytes beat best on a matrix with heart-like elasticity: scar-like rigidity inhibits beating. *Journal of cell science,* 121**,** 3794.

EPA, V. C., YANG, J., MEI, Y., HOOK, A. L., LANGER, R., ANDERSON, D. G., DAVIES, M. C., ALEXANDER, M. R. & WINKLER, D. A. 2012. Modelling human embryoid body cell adhesion to a combinatorial library of polymer surfaces. *Journal of Materials Chemistry,* 22**,** 20902-20906.

ERTRACHT, O., LIANI, E., BACHNER-HINENZON, N., BAR-AM, O., FROLOV, L., OVCHARENKO, E., AWAD, H., BLUM, S., BARAC, Y., AMIT, T., ADAM, D., YOUDIM, M. & BINAH, O. 2011. The cardioprotective efficacy of TVP1022 in a rat model of ischaemia/reperfusion. *British Journal of Pharmacology,* 163**,** 755-769.

ESCOBAR, M., CARDENAS, C., COLAVITA, K., PETRENKO, N. B. & FRANZINI-ARMSTRONG, C. 2011. Structural evidence for perinuclear calcium microdomains in cardiac myocytes. *Journal of Molecular and Cellular Cardiology,* 50**,** 451-459.

EVANS, M. J. & KAUFMAN, M. H. 1981. Establishment in culture of pluripotential cells from mouse embryos. *Nature,* 292**,** 154-156.

EVSEENKO, D., ZHU, Y., SCHENKE-LAYLAND, K., KUO, J., LATOUR, B., GE, S., SCHOLES, J., DRAVID, G., LI, X., MACLELLAN, W. R. & CROOKS, G. M. 2010. Mapping the first stages of mesoderm commitment during differentiation of human embryonic stem cells. *Proceedings of the National Academy of Sciences,* 107**,** 13742-13747.

FEINBERG, A. W., ALFORD, P. W., JIN, H., RIPPLINGER, C. M., WERDICH, A. A., SHEEHY, S. P., GROSBERG, A. & PARKER, K. K. 2012. Controlling the contractile strength of engineered cardiac muscle by hierarchal tissue architecture. *Biomaterials,* 33**,** 5732-5741.

FOUASSIER, J.-P. & RABEK, J. F. 1993. *Radiation curing in polymer science and technology: Practical aspects and applications*, Springer.

FRISCH, S. M. & RUOSLAHTI, E. 1997. Integrins and anoikis. *Current opinion in cell biology,* 9**,** 701-706.

GALIE, P. A., KHALID, N., CARNAHAN, K. E., WESTFALL, M. V. & STEGEMANN, J. P. 2013. Substrate stiffness affects sarcomere and costamere structure and electrophysiological function of isolated adult cardiomyocytes. *Cardiovascular Pathology,* 22**,** 219-227.

GARCIA-MARTINEZ, V. & SCHOENWOLF, G. C. 1993. Primitive-streak origin of the cardiovascular system in avian embryos. *Developmental biology,* 159**,** 706-719.

GASTEIGER, J., TECKENTRUP, A., TERFLOTH, L. & SPYCHER, S. 2003. Neural networks as data mining tools in drug design. *Journal of physical organic chemistry,* 16**,** 232-245.

GELADI, P. & KOWALSKI, B. R. 1986. Partial least-squares regression: a tutorial. *Analytica Chimica Acta,* 185**,** 1-17.

GEORGES, M. K., VEREGIN, R. P. N., KAZMAIER, P. M. & HAMER, G. K. 1993. Narrow molecular weight resins by a free-radical polymerization process. *Macromolecules,* 26**,** 2987-2988.

GHERGHICEANU, M., BARAD, L., NOVAK, A., REITER, I., ITSKOVITZ-ELDOR, J., BINAH, O. & POPESCU, L. M. 2011. Cardiomyocytes derived from human embryonic and induced pluripotent stem cells: comparative ultrastructure. *Journal of Cellular and Molecular Medicine,* 15**,** 2539-2551.

GLIDLE, A., YASUKAWA, T., HADYOON, C. S., ANICET, N., MATSUE, T., NOMURA, M. & COOPER, J. M. 2003. Analysis of protein adsorption and binding at biosensor polymer interfaces using X-ray photon spectroscopy and scanning electrochemical microscopy. *Analytical chemistry,* 75**,** 2559-2570.

GRAICHEN, R., XU, X., BRAAM, S. R., BALAKRISHNAN, T., NORFIZA, S., SIEH, S., SOO, S. Y., THAM, S. C., MUMMERY, C., COLMAN, A., ZWEIGERDT, R. & DAVIDSON, B. P. 2008. Enhanced cardiomyogenesis of human embryonic stem cells by a small molecular inhibitor of p38 MAPK. *Differentiation,* 76**,** 357-370.

GUO, A., ZHANG, C., WEI, S., CHEN, B. & SONG, L.-S. 2013. Emerging mechanisms of T-tubule remodelling in heart failure. *Cardiovascular research*.

GWATHMEY, J. K., TSAIOUN, K. & HAJJAR, R. J. 2009. Cardionomics: a new integrative approach for screening cardiotoxicity of drug candidates. *Expert Opinion on Drug Metabolism & Toxicology,* 5**,** 647-660.

HARRIS, K., AYLOTT, M., CUI, Y., LOUTTIT, J. B., MCMAHON, N. C. & SRIDHAR, A. 2013. Comparison of electrophysiological data from human induced pluripotent stem cell derived cardiomyocytes (hiPSC-CMs) to functional pre-clinical safety assays. *Toxicological Sciences*.

HE, J. Q., MA, Y., LEE, Y., THOMSON, J. A. & KAMP, T. J. 2003. Human embryonic stem cells develop into multiple types of cardiac myocytes: action potential characterization. *Circulation research,* 93**,** 32.

HOFMANN, S. 2012. *Auger-and X-ray Photoelectron Spectroscopy in Materials Science: A User-oriented Guide*, Springer.

HOLLY, F. J. & REFOJO, M. F. 1975. Wettability of hydrogels I. Poly(2-hydroxyethyl methacrylate). *Journal of Biomedical Materials Research,* 9**,** 315-326.

HOOK, A. L., ANDERSON, D. G., LANGER, R., WILLIAMS, P., DAVIES, M. C. & ALEXANDER, M. R. 2010. High throughput methods applied in biomaterial development and discovery. *Biomaterials,* 31**,** 187-198.

HOOK, A. L., THISSEN, H. & VOELCKER, N. H. 2009. Advanced substrate fabrication for cell microarrays. *Biomacromolecules,* 10**,** 573-579.

IAIZZO, P. A. 2009. *Handbook of Cardiac Anatomy, Physiology, and Devices*, Springer.

IKONEN, L., KERKELÄ, E., METSELAAR, G., STUART, M. C. A., DE JONG, M. R. & AALTO-SETÄLÄ, K. 2012. 2D and 3D Self-Assembling Nanofiber Hydrogels for Cardiomyocyte Culture. *BioMed research international,* 2013.

IRWIN, E. F., GUPTA, R., DASHTI, D. C. & HEALY, K. E. 2011. Engineered polymer-media interfaces for the long-term self-renewal of human embryonic stem cells. *Biomaterials,* 32**,** 6912-6919.

ITZHAKI, I., MAIZELS, L., HUBER, I., ZWI-DANTSIS, L., CASPI, O., WINTERSTERN, A., FELDMAN, O., GEPSTEIN, A., ARBEL, G. & HAMMERMAN, H. 2011a. Modelling the long QT syndrome with induced pluripotent stem cells. *Nature,* 471**,** 225-229.

ITZHAKI, I., RAPOPORT, S., HUBER, I., MIZRAHI, I., ZWI-DANTSIS, L., ARBEL, G., SCHILLER, J. & GEPSTEIN, L. 2011b. Calcium Handling in Human Induced Pluripotent Stem Cell Derived Cardiomyocytes. *PLoS ONE,* 6**,** e18037.

JACOT, J. G., MCCULLOCH, A. D. & OMENS, J. H. 2008. Substrate stiffness affects the functional maturation of neonatal rat ventricular myocytes. *Biophysical journal,* 95**,** 3479-3487.

JAMES, W. P., CATERSON, I. D., COUTINHO, W., FINER, N., VAN GAAL, L. F., MAGGIONI, A. P., TORP-PEDERSEN, C., SHARMA, A. M., SHEPHERD, G. M., RODE, R. A. & RENZ, C. L. 2010. Effect of Sibutramine on Cardiovascular Outcomes in Overweight and Obese Subjects. *New England Journal of Medicine,* 363**,** 905-917.

JONSSON, M. K. B., VOS, M. A., MIRAMS, G. R., DUKER, G., SARTIPY, P., DE BOER, T. P. & VAN VEEN, T. A. B. 2012. Application of human stem cell-derived cardiomyocytes in safety pharmacology requires caution beyond hERG. *Journal of Molecular and Cellular Cardiology,* 52**,** 998-1008.

KALASKAR, D. M., GOUGH, J. E., ULIJN, R. V., SAMPSON, W. W., SCURR, D. J., RUTTEN, F. J., ALEXANDER, M. R., MERRY, C. L. R. & EICHHORN, S. J. 2008. Controlling cell morphology on amino acid-modified cellulose. *Soft Matter,* 4**,** 1059-1065.

KATTMAN, S. J., WITTY, A. D., GAGLIARDI, M., DUBOIS, N. C., NIAPOUR, M., HOTTA, A., ELLIS, J. & KELLER, G. 2011. Stage-Specific Optimization of Activin/Nodal and BMP Signaling Promotes Cardiac Differentiation of Mouse and Human Pluripotent Stem Cell Lines. *Cell Stem Cell,* 8**,** 228-240.

KATZ, A. M. 2002. Ernest Henry Starling, His Predecessors, and the "Law of the Heart". *Circulation,* 106**,** 2986-2992.

KEHAT, I., KENYAGIN-KARSENTI, D., SNIR, M., SEGEV, H., AMIT, M., GEPSTEIN, A., LIVNE, E., BINAH, O., ITSKOVITZ-ELDOR, J. & GEPSTEIN, L. 2001. Human embryonic stem cells can differentiate into myocytes with structural and functional properties of cardiomyocytes. *Journal of Clinical Investigation,* 108**,** 407-414.

KEIL, U. 1999. Survival after acute myocardial infarction. *European Heart Journal,* 20**,** 787-788.

KELL, D. B. & OLIVER, S. G. 2004. Here is the evidence, now what is the hypothesis? The complementary roles of inductive and hypothesis-driven science in the post-genomic era. *Bioessays,* 26**,** 99-105.

KESELOWSKY, B. G., COLLARD, D. M. & GARCÍA, A. J. 2003. Surface chemistry modulates fibronectin conformation and directs integrin binding and

specificity to control cell adhesion. *Journal of Biomedical Materials Research Part A,* 66A**,** 247-259.

KHANNA, I. 2012. Drug discovery in pharmaceutical industry: productivity challenges and trends. *Drug Discovery Today,* 17**,** 1088-1102.

KIM, K. S., KIM, E. J., LEE, H. A. & PARK, S. J. 2009. Effect of sibutramine HCl on cardiac hERG K channel. *Molecular and cellular biochemistry,* 320**,** 125-131.

KLEINMAN, H. K., MCGARVEY, M. L., LIOTTA, L. A., ROBEY, P. G., TRYGGVASON, K. & MARTIN, G. R. 1982. Isolation and characterization of type IV procollagen, laminin, and heparan sulfate proteoglycan from the EHS sarcoma. *Biochemistry,* 21**,** 6188-6193.

KOLA, I. & LANDIS, J. 2004. Can the pharmaceutical industry reduce attrition rates? *Nat Rev Drug Discov,* 3**,** 711-716.

KOLAHI, K. S., DONJACOUR, A., LIU, X., LIN, W., SIMBULAN, R. K., BLOISE, E., MALTEPE, E. & RINAUDO, P. 2012. Effect of Substrate Stiffness on Early Mouse Embryo Development. *PLoS ONE,* 7**,** e41717.

KOSTIN, S., SCHOLZ, D., SHIMADA, T., MAENO, Y., MOLLNAU, H., HEIN, S. & SCHAPER, J. 1998. The internal and external protein scaffold of the T-tubular system in cardiomyocytes. *Cell and tissue research,* 294**,** 449-460.

KOU, P. M., PALLASSANA, N., BOWDEN, R., CUNNINGHAM, B., JOY, A., KOHN, J. & BABENSEE, J. E. 2012. Predicting biomaterial property-dendritic cell phenotype relationships from the multivariate analysis of responses to polymethacrylates. *Biomaterials,* 33**,** 1699-1713.

KOVAC, J. 2011. Surface Characterization of Polymers by XPS and SIMS Techniques. *Materiali in tehnologije,* 45**,** 191-197.

KUO, P.-L., LEE, H., BRAY, M.-A., GEISSE, N. A., HUANG, Y.-T., ADAMS, W. J., SHEEHY, S. P. & PARKER, K. K. 2012. Myocyte Shape Regulates Lateral Registry of Sarcomeres and Contractility. *The American journal of pathology,* 181**,** 2030-2037.

LAFLAMME, M., CHEN, K., NAUMOVA, A., MUSKHELI, V., FUGATE, J., DUPRAS, S., REINECKE, H., XU, C., HASSANIPOUR, M. & POLICE, S. 2007. Cardiomyocytes derived from human embryonic stem cells in pro-survival factors enhance function of infarcted rat hearts. *Nature biotechnology,* 25**,** 1015-1024.

LAWRENCE, C. L., BRIDGLAND-TAYLOR, M. H., POLLARD, C. E., HAMMOND, T. G. & VALENTIN, J. P. 2006. A rabbit Langendorff heart proarrhythmia model: predictive value for clinical identification of torsades de pointes. *British journal of pharmacology,* 149**,** 845-860.

LE, T., EPA, V. C., BURDEN, F. R. & WINKLER, D. A. 2012. Quantitative structure–property relationship modeling of diverse materials properties. *Chemical Reviews,* 112**,** 2889-2919.

LEE, J. H., JUNG, H. W., KANG, I.-K. & LEE, H. B. 1994. Cell behaviour on polymer surfaces with different functional groups. *Biomaterials,* 15**,** 705-711.

LEE, J. L. S. & GILMORE, I. S. 2009. The application of multivariate data analysis techniques in surface analysis. *Surface Analysis-The Principal Techniques, 2nd Edition*, 563-612.

LEE, Y.-K., NG, K.-M., CHAN, Y.-C., LAI, W.-H., AU, K.-W., HO, C.-Y. J., WONG, L.-Y., LAU, C.-P., TSE, H.-F. & SIU, C.-W. 2010. Triiodothyronine promotes cardiac differentiation and maturation of embryonic stem cells via the classical genomic pathway. *Molecular Endocrinology,* 24**,** 1728-1736.

LEE, Y.-K., NG, K.-M., LAI, W.-H., CHAN, Y.-C., LAU, Y.-M., LIAN, Q., TSE, H.-F. & SIU, C.-W. 2011. Calcium Homeostasis in Human Induced Pluripotent Stem Cell-Derived Cardiomyocytes. *Stem Cell Reviews and Reports,* 7**,** 976-986.

LIANG, P., LAN, F., LEE, A. S., GONG, T., SANCHEZ-FREIRE, V., WANG, Y., DIECKE, S., SALLAM, K., KNOWLES, J. W., WANG, P. J., NGUYEN, P. K., BERS, D. M., ROBBINS, R. C. & WU, J. C. 2013. Drug Screening Using a Library of Human Induced Pluripotent Stem Cell–Derived Cardiomyocytes Reveals Disease-Specific Patterns of Cardiotoxicity. *Circulation,* 127**,** 1677-1691.

LIAO, S.-Y., TSE, H.-F., CHAN, Y.-C., MEI-CHU YIP, P., ZHANG, Y., LIU, Y. & LI, R. A. 2013. Overexpression of Kir2.1 channel in embryonic stem cell-derived cardiomyocytes attenuates posttransplantation proarrhythmic risk in myocardial infarction. *Heart Rhythm,* 10**,** 273-282.

LIEU, D. K., FU, J.-D., CHIAMVIMONVAT, N., TUNG, K. C., MCNERNEY, G. P., HUSER, T., KELLER, G., KONG, C.-W. & LI, R. A. 2013. Mechanism-Based Facilitated Maturation of Human Pluripotent Stem Cell-Derived Cardiomyocytes. *Circulation: Arrhythmia and Electrophysiology,* 6**,** 191-201.

LOHR, J. L. & YOST, H. J. 2000. Vertebrate model systems in the study of early heart development: Xenopus and zebrafish. *American journal of medical genetics,* 97**,** 248-257.

LOUGH, J. & SUGI, Y. 2000. Endoderm and heart development. *Dev Dyn,* 217**,** 327-342.

LOWE, G. 1995. Combinatorial chemistry. *Chem. Soc. Rev.,* 24**,** 309-317.

LUNDY, S. D., ZHU, W.-Z., REGNIER, M. & LAFLAMME, M. A. 2013. Structural and Functional Maturation of Cardiomyocytes Derived From Human Pluripotent Stem Cells. *Stem Cells and Development*.

MA, D., TANEJA, T., HAGEN, B., KIM, B.-Y., ORTEGA, B., LEDERER, J. & WELLING, P. 2011a. Golgi Export of the Kir2.1 Channel Is Driven by a Trafficking Signal Located within Its Tertiary Structure. *Cell,* 145**,** 1102-1115.

MA, J., GUO, L., FIENE, S. J., ANSON, B. D., THOMSON, J. A., KAMP, T. J., KOLAJA, K. L., SWANSON, B. J. & JANUARY, C. T. 2011b. High purity human-induced pluripotent stem cell-derived cardiomyocytes: electrophysiological properties of action potentials and ionic currents. *American Journal of Physiology - Heart and Circulatory Physiology,* 301**,** H2006-H2017.

MAKKAR, R. R., SMITH, R. R., CHENG, K. E., MALLIARAS, K., THOMSON, L. E. J., BERMAN, D., CZER, L. S. C., MARBÁN, L., MENDIZABAL, A. & JOHNSTON, P. V. 2012. Intracoronary cardiosphere-derived cells for heart regeneration

after myocardial infarction (CADUCEUS): a prospective, randomised phase 1 trial. *The Lancet,* 379**,** 895-904.

MANDEL, Y., WEISSMAN, A., SCHICK, R., BARAD, L., NOVAK, A., MEIRY, G., GOLDBERG, S., LORBER, A., ROSEN, M. R., ITSKOVITZ-ELDOR, J. & BINAH, O. 2012. Human Embryonic and Induced Pluripotent Stem Cells-Derived Cardiomyocytes Exhibit Beat Rate Variability and Power-Law Behavior. *Circulation*.

MARVIN, M. J., DI ROCCO, G., GARDINER, A., BUSH, S. M. & LASSAR, A. B. 2001. Inhibition of Wnt activity induces heart formation from posterior mesoderm. *Genes & development,* 15**,** 316-327.

MATSA, E., RAJAMOHAN, D., DICK, E., YOUNG, L., MELLOR, I., STANIFORTH, A. & DENNING, C. 2011. Drug evaluation in cardiomyocytes derived from human induced pluripotent stem cells carrying a long QT syndrome type 2 mutation. *European heart journal,* 32**,** 952-62.

MEHTA, A., CHUNG, Y. Y., NG, A., ISKANDAR, F., ATAN, S., WEI, H., DUSTING, G., SUN, W., WONG, P. & SHIM, W. 2011. Pharmacological response of human cardiomyocytes derived from virus-free induced pluripotent stem cells. *Cardiovascular Research,* 91**,** 577-586.

MELKOUMIAN, Z., WEBER, J. L., WEBER, D. M., FADEEV, A. G., ZHOU, Y., DOLLEY-SONNEVILLE, P., YANG, J., QIU, L., PRIEST, C. A., SHOGBON, C., MARTIN, A. W., NELSON, J., WEST, P., BELTZER, J. P., PAL, S. & BRANDENBERGER, R. 2010. Synthetic peptide-acrylate surfaces for long-term self-renewal and cardiomyocyte differentiation of human embryonic stem cells. *Nat Biotech,* 28**,** 606-610.

MEYER, T., BOVEN, K.-H., GÃ¼NTHER, E. & FEJTL, M. 2004. Micro-electrode arrays in cardiac safety pharmacology. *Drug Safety,* 27**,** 763-772.

MOHLER, P. J., SCHOTT, J.-J., GRAMOLINI, A. O., DILLY, K. W., GUATIMOSIM, S., DUBELL, W. H., SONG, L.-S., HAUROGNE, K., KYNDT, F., ALI, M. E., ROGERS, T. B., LEDERER, W. J., ESCANDE, D., MAREC, H. L. & BENNETT, V. 2003. Ankyrin-B mutation causes type 4 long-QT cardiac arrhythmia and sudden cardiac death. *Nature,* 421**,** 634-639.

MOHR, J. C., ZHANG, J., AZARIN, S. M., SOERENS, A. G., DE PABLO, J. J., THOMSON, J. A., LYONS, G. E., PALECEK, S. P. & KAMP, T. J. 2010. The microwell control of embryoid body size in order to regulate cardiac differentiation of human embryonic stem cells. *Biomaterials,* 31**,** 1885-1893.

MUMMERY, C., WARD-VAN OOSTWAARD, D., DOEVENDANS, P., SPIJKER, R., VAN DEN BRINK, S., HASSINK, R., VAN DER HEYDEN, M., OPTHOF, T., PERA, M., DE LA RIVIERE, A. B., PASSIER, R. & TERTOOLEN, L. 2003. Differentiation of Human Embryonic Stem Cells to Cardiomyocytes: Role of Coculture With Visceral Endoderm-Like Cells. *Circulation,* 107**,** 2733-2740.

MUMMERY, C. L., ZHANG, J., NG, E. S., ELLIOTT, D. A., ELEFANTY, A. G. & KAMP, T. J. 2012. Differentiation of Human Embryonic Stem Cells and Induced Pluripotent Stem Cells to Cardiomyocytes: A Methods Overview. *Circulation research,* 111**,** 344-358.

NAGAOKA, M., SI-TAYEB, K., AKAIKE, T. & DUNCAN, S. 2010. Culture of human pluripotent stem cells using completely defined conditions on a recombinant E-cadherin substratum. *BMC Developmental Biology,* 10**,** 60.

NASS, R. D., AIBA, T., TOMASELLI, G. F. & AKAR, F. G. 2008. Mechanisms of Disease: ion channel remodeling in the failing ventricle. *Nat Clin Pract Cardiovasc Med,* 5**,** 196-207.

NATARAJAN, A., CHUN, C., HICKMAN, J. J. & MOLNAR, P. 2008. Growth and electrophysiological properties of rat embryonic cardiomyocytes on hydroxyl-and carboxyl-modified surfaces. *Journal of Biomaterials Science, Polymer Edition,* 19**,** 1319-1331.

NATARAJAN, A., STANCESCU, M., DHIR, V., ARMSTRONG, C., SOMMERHAGE, F., HICKMAN, J. J. & MOLNAR, P. 2011. Patterned cardiomyocytes on microelectrode arrays as a functional, high information content drug screening platform. *Biomaterials,* 32**,** 4267-4274.

NEHER, E. & SAKMANN, B. 1976. Single-channel currents recorded from membrane of denervated frog muscle fibres. *Nature,* 260**,** 799-802.

NELSON, D. A. & BENSON, E. S. 1963. ON THE STRUCTURAL CONTINUITIES OF THE TRANSVERSE TUBULAR SYSTEM OF RABBIT AND HUMAN MYOCARDIAL CELLS. *The Journal of cell biology,* 16**,** 297-313.

NERBONNE, J. M. 2004. Studying Cardiac Arrhythmias in the Mouse—A Reasonable Model for Probing Mechanisms? *Trends in Cardiovascular Medicine,* 14**,** 83-93.

NIBBELINK, K. A., TISHKOFF, D. X., HERSHEY, S. D., RAHMAN, A. & SIMPSON, R. U. 2007. 1,25(OH)2-vitamin D3 actions on cell proliferation, size, gene expression, and receptor localization, in the HL-1 cardiac myocyte. *13th Workshop on Vitamin D (Victoria, British Columbia, Canada, April 2006),* 103**,** 533-537.

NICHOLS, J., ZEVNIK, B., ANASTASSIADIS, K., NIWA, H., KLEWE-NEBENIUS, D., CHAMBERS, I., SCHÖLER, H. & SMITH, A. 1998. Formation of Pluripotent Stem Cells in the Mammalian Embryo Depends on the POU Transcription Factor Oct4. *Cell,* 95**,** 379-391.

NUNES, S. S., MIKLAS, J. W., LIU, J., ASCHAR-SOBBI, R., XIAO, Y., ZHANG, B., JIANG, J., MASSE, S., GAGLIARDI, M., HSIEH, A., THAVANDIRAN, N., LAFLAMME, M. A., NANTHAKUMAR, K., GROSS, G. J., BACKX, P. H., KELLER, G. & RADISIC, M. 2013. Biowire: a platform for maturation of human pluripotent stem cell-derived cardiomyocytes. *Nat Meth,* 10**,** 781-787.

ODIAN, G. 2004. Radical Chain Polymerization. *Principles of Polymerization.* John Wiley & Sons, Inc.

ODORICO, J. S., KAUFMAN, D. S. & THOMSON, J. A. 2001. Multilineage differentiation from human embryonic stem cell lines. *Stem Cells,* 19**,** 193-204.

OJALA, M., RAJALA, K., PEKKANEN-MATTILA, M., MIETTINEN, M., HUHTALA, H. & AALTO-SETÄLÄ, K. 2012. Culture Conditions Affect Cardiac Differentiation Potential of Human Pluripotent Stem Cells. *PLoS ONE,* 7**,** e48659.

OLSON, E. N. & SCHNEIDER, M. D. 2003. Sizing up the heart: development redux in disease. *Genes & Development,* 17**,** 1937-1956.

OPIE, L. H. 2004. *Heart physiology: from cell to circulation, 4th Ed.*, Philadelphia: Lippincott-Raven.

PAIGE, S. L., OSUGI, T., AFANASIEV, O. K., PABON, L., REINECKE, H. & MURRY, C. E. 2010. Endogenous Wnt/β-Catenin Signaling Is Required for Cardiac Differentiation in Human Embryonic Stem Cells. *PLoS ONE,* 5**,** e11134.

PAL, R., TOTEY, S., MAMIDI, M. K., BHAT, V. S. & TOTEY, S. 2009. Propensity of Human Embryonic Stem Cell Lines During Early Stage of Lineage Specification Controls Their Terminal Differentiation into Mature Cell Types. *Experimental Biology and Medicine,* 234**,** 1230-1243.

PANTOS, C., MALLIOPOULOU, V., VARONOS, D. D. & COKKINOS, D. V. 2004. Thyroid hormone and phenotypes of cardioprotection. *Basic research in cardiology,* 99**,** 101-120.

PASSIER, R., OOSTWAARD, D. W.-V., SNAPPER, J., KLOOTS, J., HASSINK, R. J., KUIJK, E., ROELEN, B., DE LA RIVIERE, A. B. & MUMMERY, C. 2005. Increased Cardiomyocyte Differentiation from Human Embryonic Stem Cells in Serum-Free Cultures. *Stem Cells,* 23**,** 772-780.

PEKKANEN-MATTILA, M., CHAPMAN, H., KERKELA, E., SUURONEN, R., SKOTTMAN, H., KOIVISTO, A.-P. & AALTO-SETALA, K. 2010. Human embryonic stem cell-derived cardiomyocytes: demonstration of a portion of cardiac cells with fairly mature electrical phenotype. *Experimental Biology and Medicine,* 235**,** 522-530.

PENG, S., LACERDA, A. E., KIRSCH, G. E., BROWN, A. M. & BRUENING-WRIGHT, A. 2010. The action potential and comparative pharmacology of stem cell-derived human cardiomyocytes. *Journal of Pharmacological and Toxicological Methods,* 61**,** 277-286.

PENNER, R. 1995. A practical guide to patch clamping. *Single-channel recording.* Springer.

PETITPREZ, S. V., ZMOOS, A.-F., OGRODNIK, J., BALSE, E., RAAD, N., EL-HAOU, S., ALBESA, M., BITTIHN, P., LUTHER, S., LEHNART, S. E., HATEM, S. P. N., COULOMBE, A. & ABRIEL, H. 2011. SAP97 and Dystrophin Macromolecular Complexes Determine Two Pools of Cardiac Sodium Channels Nav1.5 in Cardiomyocytes. *Circulation research,* 108**,** 294-304.

RAHMANY, M. B. & VAN DYKE, M. 2012. Biomimetic approaches to modulate cellular adhesion in biomaterials: A review. *Acta biomaterialia.*

RANGEL, M. C., KARASAWA, H., CASTRO, N. P., NAGAOKA, T., SALOMON, D. S. & BIANCO, C. 2012. Role of Cripto-1 during Epithelial-to-Mesenchymal Transition in Development and Cancer. *The American Journal of Pathology,* 180**,** 2188-2200.

RAO, C., PRODROMAKIS, T., KOLKER, L., CHAUDHRY, U. A. R., TRANTIDOU, T., SRIDHAR, A., WEEKES, C., CAMELLITI, P., HARDING, S. E. & DARZI, A. 2012. The effect of microgrooved culture substrates on calcium cycling of cardiac myocytes derived from human induced pluripotent stem cells. *Biomaterials.*

REN, Y., LEE, M. Y., SCHLIFFKE, S., PAAVOLA, J., AMOS, P. J., GE, X., YE, M., ZHU, S., SENYEI, G., LUM, L., EHRLICH, B. E. & QYANG, Y. 2011. Small molecule Wnt inhibitors enhance the efficiency of BMP-4-directed cardiac differentiation of human pluripotent stem cells. *Journal of Molecular and Cellular Cardiology,* 51**,** 280-287.

RHEE, D., SANGER, J. M. & SANGER, J. W. 1994. The premyofibril: evidence for its role in myofibrillogenesis. *Cell motility and the cytoskeleton,* 28**,** 1-24.

RODAWAY, A. & PATIENT, R. 2001. Mesendoderm: An Ancient Germ Layer? *Cell,* 105**,** 169-172.

RODIN, S., DOMOGATSKAYA, A., STRÃM, S., HANSSON, E. M., CHIEN, K. R., INZUNZA, J., HOVATTA, O. & TRYGGVASON, K. 2010. Long-term self-renewal of human pluripotent stem cells on human recombinant laminin-511. *Nature biotechnology,* 28**,** 611-615.

RODRIGUEZ, A. G., HAN, S. J., REGNIER, M. & SNIADECKI, N. J. 2011. Substrate Stiffness Increases Twitch Power of Neonatal Cardiomyocytes in Correlation with Changes in Myofibril Structure and Intracellular Calcium. *Biophysical journal,* 101**,** 2455-2464.

ROSS, A. M., JIANG, Z., BASTMEYER, M. & LAHANN, J. Physical Aspects of Cell Culture Substrates: Topography, Roughness, and Elasticity.

RYAN, J. 2008. Evolution of Cell Culture Surfaces. *BioFiles,* 3**,** 21.

SANGUINETTI, M. & KEATING, M. 1997. Role of Delayed Rectifier Potassium Channels in Cardiac Repolarization and Arrhythmias. *Physiology,* 12**,** 152-157.

SANGUINETTI, M. C. & TRISTANI-FIROUZI, M. 2006. hERG potassium channels and cardiac arrhythmia. *Nature,* 440**,** 463-469.

SARTIANI, L., BETTIOL, E., STILLITANO, F., MUGELLI, A., CERBAI, E. & JACONI, M. E. 2007. Developmental Changes in Cardiomyocytes Differentiated from Human Embryonic Stem Cells: A Molecular and Electrophysiological Approach. *Stem Cells,* 25**,** 1136-1144.

SATHANANTHAN, H., SELVARAJ, K. & CLARK, J. 2011. The fine structure of human germ layers in vivo: clues to the early differentiation of embryonic stem cells in vitro. *Reproductive biomedicine online,* 23**,** 227-233.

SATIN, J., KEHAT, I., CASPI, O., HUBER, I., ARBEL, G., ITZHAKI, I., MAGYAR, J., SCHRODER, E. A., PERLMAN, I. & GEPSTEIN, L. 2004. Mechanism of spontaneous excitability in human embryonic stem cell derived cardiomyocytes. *The Journal of physiology,* 559**,** 479.

SCHRAM, G., POURRIER, M., MELNYK, P. & NATTEL, S. 2002. Differential Distribution of Cardiac Ion Channel Expression as a Basis for Regional Specialization in Electrical Function. *Circulation research,* 90**,** 939-950.

SEO, J.-H., KAKINOKI, S., INOUE, Y., NAM, K., YAMAOKA, T., ISHIHARA, K., KISHIDA, A. & YUI, N. 2013. The significance of hydrated surface molecular mobility in the control of the morphology of adhering fibroblasts. *Biomaterials.*

SHEN, M. & HORBETT, T. A. 2001. The effects of surface chemistry and adsorbed proteins on monocyte/macrophage adhesion to chemically modified polystyrene surfaces. *Journal of Biomedical Materials Research,* 57**,** 336-345.

SHENG, X., REPPEL, M., NGUEMO, F., MOHAMMAD, F. I., KUZMENKIN, A., HESCHELER, J. & PFANNKUCHE, K. 2012. Human Pluripotent Stem Cell-Derived Cardiomyocytes: Response to TTX and Lidocain Reveals Strong Cell to Cell Variability. *PloS one,* 7**,** e45963.

SINCLAIR, K. D. & SINGH, R. 2007. Modelling the developmental origins of health and disease in the early embryo. *Theriogenology,* 67**,** 43-53.

SMITH, R. R., MARBÁN, E. & MARBÁN, L. 2013. Enhancing retention and efficacy of cardiosphere-derived cells administered after myocardial infarction using a hyaluronan-gelatin hydrogel. *Biomatter,* 3**,** e24490.

SNIR, M., KEHAT, I., GEPSTEIN, A., COLEMAN, R., ITSKOVITZ-ELDOR, J., LIVNE, E. & GEPSTEIN, L. 2003. Assessment of the ultrastructural and proliferative properties of human embryonic stem cell-derived cardiomyocytes. *American Journal of Physiology - Heart and Circulatory Physiology,* 285**,** H2355-H2363.

STEELE, J. G., DALTON, B. A., JOHNSON, G. & UNDERWOOD, P. A. 1993. Polystyrene chemistry affects vitronectin activity: An explanation for cell attachment to tissue culture polystyrene but not to unmodified polystyrene. *Journal of Biomedical Materials Research,* 27**,** 927-940.

SUCHER, N. J., DEITCHER, D. L., BARO, D. J., WARRICK, R. M. H. & GUENTHER, E. 2000. Genes and channels: patch/voltage-clamp analysis and single-cell RT-PCR. *Cell and tissue research,* 302**,** 295-307.

SYLVA, M., VAN DEN HOFF, M. J. B. & MOORMAN, A. F. M. 2013. Development of the Human Heart. *American Journal of Medical Genetics Part A***,** 000-000.

SYNNERGREN, J., AMEEN, C., JANSSON, A. & SARTIPY, P. 2012. Global transcriptional profiling reveals similarities and differences between human stem cell-derived cardiomyocyte clusters and heart tissue. *Physiological Genomics,* 44**,** 245-258.

TAKAHASHI, K., TANABE, K., OHNUKI, M., NARITA, M., ICHISAKA, T., TOMODA, K. & YAMANAKA, S. 2007. Induction of Pluripotent Stem Cells from Adult Human Fibroblasts by Defined Factors. *Cell,* 131**,** 861-872.

TAMADA, Y. & IKADA, Y. 1993. Cell adhesion to plasma-treated polymer surfaces. *Polymer,* 34**,** 2208-2212.

TAYLOR, J. M., ROVIN, J. D. & PARSONS, J. T. 2000. A Role for Focal Adhesion Kinase in Phenylephrine-induced Hypertrophy of Rat Ventricular Cardiomyocytes. *Journal of Biological Chemistry,* 275**,** 19250-19257.

THOMSON, J. A., ITSKOVITZ-ELDOR, J., SHAPIRO, S. S., WAKNITZ, M. A., SWIERGIEL, J. J., MARSHALL, V. S. & JONES, J. M. 1998. Embryonic stem cell lines derived from human blastocysts. *Science,* 282**,** 1145.

TOURNIAIRE, G., COLLINS, J., CAMPBELL, S., MIZOMOTO, H., OGAWA, S., THABURET, J.-F. & BRADLEY, M. 2006. Polymer microarrays for cellular adhesion. *Chemical Communications*, 2118-2120.

TULLOCH, N. L., MUSKHELI, V., RAZUMOVA, M. V., KORTE, F. S., REGNIER, M., HAUCH, K. D., PABON, L., REINECKE, H. & MURRY, C. E. 2011. Growth of Engineered Human Myocardium With Mechanical Loading and Vascular Coculture*Novelty and Significance. *Circulation research,* 109, 47-59.

TYLER, B. J., RAYAL, G. & CASTNER, D. G. 2007. Multivariate analysis strategies for processing ToF-SIMS images of biomaterials. *Imaging Techniques for Biomaterials Characterization,* 28, 2412-2423.

URQUHART, A. J., TAYLOR, M., ANDERSON, D. G., LANGER, R., DAVIES, M. C. & ALEXANDER, M. R. 2008. TOF-SIMS analysis of a 576 micropatterned copolymer array to reveal surface moieties that control wettability. *Anal.Chem,* 80, 135-142.

VAN DER HEIDE, P. 2011. *X-ray Photoelectron Spectroscopy: An Introduction to Principles and Practices*, John Wiley & Sons.

VAN DER HEYDEN, M. A. G. & DEFIZE, L. H. K. 2003. Twenty one years of P19 cells: what an embryonal carcinoma cell line taught us about cardiomyocyte differentiation. *Cardiovascular research,* 58, 292-302.

VAN DER VELDEN, J., DE JONG, J. W., OWEN, V. J., BURTON, P. B. J. & STIENEN, G. J. M. 2000. Effect of protein kinase A on calcium sensitivity of force and its sarcomere length dependence in human cardiomyocytes. *Cardiovascular research,* 46, 487-495.

VAN KOOTEN, T. G., SPIJKER, H. T. & BUSSCHER, H. J. 2004. Plasma-treated polystyrene surfaces: model surfaces for studying cell–biomaterial interactions. *Biomaterials,* 25, 1735-1747.

VANWINKLE, W. B., SNUGGS, M. B. & BUJA, L. M. 1996. Cardiogel: a biosynthetic extracellular matrix for cardiomyocyte culture. *In Vitro Cellular & Developmental Biology-Animal,* 32, 478-485.

VENUGOPAL, J. R., PRABHAKARAN, M. P., MUKHERJEE, S., RAVICHANDRAN, R., DAN, K. & RAMAKRISHNA, S. 2012. Biomaterial strategies for alleviation of myocardial infarction. *Journal of The Royal Society Interface,* 9, 1-19.

VERKERK, A. O., WILDERS, R., VAN BORREN, M. M. G. J., PETERS, R. J. G., BROEKHUIS, E., LAM, K., CORONEL, R., DE BAKKER, J. M. T. & TAN, H. L. 2007. Pacemaker current (If) in the human sinoatrial node. *European Heart Journal,* 28, 2472-2478.

VERMA, V., PURNAMAWATI, K., MANASI & SHIM, W. 2013. Steering signal transduction pathway towards cardiac lineage from human pluripotent stem cells: A review. *Cellular Signalling,* 25, 1096-1107.

VICKERMAN, J. C. & BRIGGS, D. 2001. *ToF-SIMS: surface analysis by mass spectrometry*, IM publications Chichester.

VIDARSSON, H., HYLLNER, J. & SARTIPY, P. 2010. Differentiation of Human Embryonic Stem Cells to Cardiomyocytes for In Vitro and In Vivo Applications. *Stem Cell Reviews and Reports,* 6, 108-120.

WAGNER, M. S., GRAHAM, D. J., RATNER, B. D. & CASTNER, D. G. 2004. Maximizing information obtained from secondary ion mass spectra of organic thin films using multivariate analysis. *Surface Science,* 570**,** 78-97.

WANG, J.-S. & MATYJASZEWSKI, K. 1995. Controlled/" living" radical polymerization. Atom transfer radical polymerization in the presence of transition-metal complexes. *Journal of the American Chemical Society,* 117**,** 5614-5615.

WANG, L., LIU, L., LI, X., MAGOME, N., AGLADZE, K. & CHEN, Y. 2013. Multi-electrode monitoring of guided excitation in patterned cardiomyocytes. *Microelectronic Engineering,* 111**,** 267-271.

WANG, P.-Y., YU, J., LIN, J.-H. & TSAI, W.-B. 2011. Modulation of alignment, elongation and contraction of cardiomyocytes through a combination of nanotopography and rigidity of substrates. *Acta Biomaterialia,* 7**,** 3285-3293.

WEI, H., TAN, G., MANASI, QIU, S., KONG, G., YONG, P., KOH, C., OOI, T. H., LIM, S. Y., WONG, P., GAN, S. U. & SHIM, W. 2012a. One-step derivation of cardiomyocytes and mesenchymal stem cells from human pluripotent stem cells. *Stem Cell Research,* 9**,** 87-100.

WEI, H., ZHANG, G., QIU, S., LU, J., SHENG, J., MANASI, TAN, G., WONG, P., GAN, S. U. & SHIM, W. 2012b. Hydrogen Sulfide Suppresses Outward Rectifier Potassium Currents in Human Pluripotent Stem Cell-Derived Cardiomyocytes. *PloS one,* 7**,** e50641.

WEITZER, G. 2006. Embryonic Stem Cell-Derived Embryoid Bodies: An In Vitro Model of Eutherian Pregastrulation Development and Early Gastrulation. *In:* WOBUS, A. & BOHELER, K. (eds.) *Stem Cells.* Springer Berlin Heidelberg.

WILLEMS, E. & MERCOLA, M. 2011. What Your Heart Doth Know. *Cell stem cell,* 8**,** 124-126.

WILLEMS, E., SPIERING, S., DAVIDOVICS, H., LANIER, M., XIA, Z., DAWSON, M., CASHMAN, J. & MERCOLA, M. 2011. Small-Molecule Inhibitors of the Wnt Pathway Potently Promote Cardiomyocytes From Human Embryonic Stem Cell–Derived Mesoderm. *Circulation Research,* 109**,** 360-364.

WINKLER, D. A. & BURDEN, F. R. 2004. Bayesian neural nets for modeling in drug discovery. *Drug Discovery Today: BIOSILICO,* 2**,** 104-111.

WOLD, S., SJÖSTRÖM, M. & ERIKSSON, L. 2001. PLS-regression: a basic tool of chemometrics. *Chemometrics and intelligent laboratory systems,* 58**,** 109-130.

WOODCOCK, E. A. & MATKOVICH, S. J. 2005. Cardiomyocytes structure, function and associated pathologies. *The international journal of biochemistry & cell biology,* 37**,** 1746-1751.

WYSOWSKI, D. K. & SWARTZ, L. 2005. Adverse drug event surveillance and drug withdrawals in the United States, 1969-2002: the importance of reporting suspected reactions. *Archives of internal medicine,* 165**,** 1363.

XU, C., INOKUMA, M. S., DENHAM, J., GOLDS, K., KUNDU, P., GOLD, J. D. & CARPENTER, M. K. 2001. Feeder-free growth of undifferentiated human embryonic stem cells. *Nature biotechnology,* 19**,** 971-974.

XU, C., POLICE, S., RAO, N. & CARPENTER, M. K. 2002. Characterization and enrichment of cardiomyocytes derived from human embryonic stem cells. *Circulation research,* 91**,** 501.

YANG, Y.-P., LI, H.-R., CAO, X.-M., WANG, Q.-X., QIAO, C.-J. & YA, J. 2013. Second heart field and the development of the outflow tract in human embryonic heart. *Development, Growth & Differentiation,* 55**,** 359-367.

YILDIRIM, Y., NAITO, H., DIDIÉ, M., KARIKKINETH, B. C., BIERMANN, D., ESCHENHAGEN, T. & ZIMMERMANN, W.-H. 2007. Development of a Biological Ventricular Assist Device Preliminary Data From a Small Animal Model. *Circulation,* 116**,** I-16.

YOUNG, J. L. & ENGLER, A. J. 2011. Hydrogels with time-dependent material properties enhance cardiomyocyte differentiation in vitro. *Biomaterials,* 32**,** 1002-1009.

YUAN, Y. & LEE, T. R. 2013. Contact Angle and Wetting Properties. *In:* BRACCO, G. & HOLST, B. (eds.) *Surface Science Techniques.* Springer Berlin Heidelberg.

YUASA, S., ITABASHI, Y., KOSHIMIZU, U., TANAKA, T., SUGIMURA, K., KINOSHITA, M., HATTORI, F., FUKAMI, S.-I., SHIMAZAKI, T., OKANO, H., OGAWA, S. & FUKUDA, K. 2005. Transient inhibition of BMP signaling by Noggin induces cardiomyocyte differentiation of mouse embryonic stem cells. *Nat Biotech,* 23**,** 607-611.

ZHANG, J., WILSON, G. F., SOERENS, A. G., KOONCE, C. H., YU, J., PALECEK, S. P., THOMSON, J. A. & KAMP, T. J. 2009. Functional cardiomyocytes derived from human induced pluripotent stem cells. *Circulation research,* 104**,** e30-e41.

ZHANG, Q., JIANG, J., HAN, P., YUAN, Q., ZHANG, J., ZHANG, X., XU, Y., CAO, H., MENG, Q., CHEN, L., TIAN, T., WANG, X., LI, P., HESCHELER, J., JI, G. & MA, Y. 2011. Direct differentiation of atrial and ventricular myocytes from human embryonic stem cells by alternating retinoid signals. *Cell Res,* 21**,** 579-587.

APPENDICES

Asha K. Patel
School of Medicine, University of Nottingham

APPENDIX 1 : MONOMER IDENTITY.

Polymer ID	Name	Emperical	Type	CAS no.
AM08	Isooctyl acrylate	H2C=CHCO2(CH2)5CH(CH3)2	Monoacrylates	29590-42-9
BM51	Nitrophenoxyethyl methacrylate	C12H13NO5	Methacrylates - Nitrogen	88613-26-7
BM22	Stearyl methacrylate	H2C=C(CH3)CO2(CH2)17CH3	Methacrylates	32360-05-7
AM38	Dimethylamino-propyl acrylate	H2C=CHCO2(CH2)3N(CH3)2	Monoacrylates - Nitrogen	18526-07-3
BM08	Butyl methacrylate	CH2=C(CH3)COO(CH2)3CH3	Methacrylates	97-88-1
AM77	Poly(ethylene glycol) methyl ether acrylate	H2C=CHCO2(CH2CH2O)nCH3	Monoacrylates - Glycol	32171-39-4
CM07	N-(3-Methoxypropyl)acrylamide	C7H13NO2	Acrylamides	107374-86-7
AM73	Isodecyl acrylate	H2C=CHCO2C10H21	Monoacrylates	1330-61-6
AM71	Heptafluorobutyl acrylate	C7H5F7O2	Monoacrylates	424-64-6
BM80	Methacryloyloxy)ethyl acetoacetate	CH3COCH2CO2CH2CH2O2CC(CH3)=CH2	Methacrylates	21282-97-3
AM54	Poly(propylene glycol) acrylate	H2C=CHCO[OCH2CH(CH3)]nOH	Monoacrylates - Oxygen/Glycol	50858-51-0
AM58	Tridecafluorooctyl acrylate	H2C=CHCO2CH2CH2(CF2)5CF3	Monoacrylates - Halogen	17527-29-6
BM54	Ethoxyethyl methacrylate	H2C=C(CH3)CO2CH2CH2OC2H5	Methacrylates - Oxygen/Glycol	2370-63-0
CD04	N,N'-Methylenebisacrylamide	$(H_2C=CHCONH)_2CH_2$	Acrylamides	110-26-9
AD05	Neopentyl glycol diacrylate	(H2C=CHCO2CH2)2C(CH3)2	Di/Triacrylates	2223-82-7
AM81	Cyanoethyl acrylate	C6H7NO2	Monoacrylates	106-71-8
BM30	Cyclohexyl methacrylate	CH2=C(CH3)COOC6H11	Methacrylates - Aromatics	101-43-9
AD24	Poly(propylene glycol) diacrylate	H2C=CHCO(OC3H6)nO2CCH=CH2	Multiacrylates - Glycol	52496-08-9
AM64	Hexadecafluoro-9-(trifluoromethyl)decyl acrylate	H2C=CHCO2CH2CH2(CF2)6CF(CF3)2	Monoacrylates - Halogen	15577-26-1
BM52	Butoxyethyl methacrylate	H2C=C(CH3)CO2CH2CH2O(CH2)3CH3	Methacrylates - Oxygen/Glycol	13532-94-0
CM15	N-(Hydroxymethyl)acrylamide	CH_2=CHCONHCH$_2$OH	Acrylamides	924-42-5
AD23	Neopentyl glycol propoxylate diacrylate	[H2C=CHCO2(C3H6O)nCH2]2C(CH3)2	Di/Triacrylates - Glycol	84170-74-1
AM22	Tetrahydrofurfuryl acrylate	C8H12O3	Monoacrylates - Aromatic	2399-48-6
BM39	Benzyl methacrylate	H2C=C(CH3)CO2CH2C6H5	Methacrylates - Aromatics	2495-37-6
BM70	Heptafluorobutyl methacrylate	H2C=C(CH3)CO2CH2CF2CF2CF3	Methacrylates - Halogen	13695-31-3
AM74	Octafluoropentyl acrylate	H2C=CHCO2CH2(CF2)3CHF2	Monoacrylates - Halogen	376-84-1
BM50	Dimethylamino-ethyl methacrylate	CH2=C(CH3)COOCH2CH2N(CH3)2	Methacrylates	2867-47-2
DM03	N-(4-Hydroxyphenyl)methacrylamide		Methacrylamides Aromatic	19243-95-9
DM01	N-[3-		Methacrylamides	5205-93-6

Asha K. Patel
School of Medicine, University of Nottingham

	(Dimethylamino)propyl]methacrylamide			
AM23	Isobornyl acrylate	C13H20O2	Monoacrylates - Aromatic	5888-33-5
BM55	Ethylene glycol methyl ether methacrylate	H2C=C(CH3)CO2CH2CH2OCH3	Methacrylates - Glycol	6976-93-8
BM18	Lauryl methacrylate	CH2=C(CH3)COO(CH2)11CH3	Methacrylates	142-90-5
AD01	Butanediol diacrylate	(H2C=CHCO2CH2CH2-)2	Multiacrylates	1070-70-8
BM83	2-Isocyanatoethyl methacrylate	CH2=C(CH3)COO(CH2)2NCO	0	30674-80-7
BD01	Acryloyloxy-2-hydroxypropyl methacrylate	H2C=C(CH3)CO2CH2CH(OH)CH2O2CCH=CH2	Methacrylates - Oxygen/Glycol	1709-71-3
CM09	N-(Isobutoxymethyl)acrylamide		Acrylamides	16669-59-3
AD02	Butanediol-1,3 diacrylate	H2C=CHCO2CH2CH2CH(CH3)O2CCH=CH2	Di/Triacrylates	19485-03-1
AM70	Hexafluoroisopropyl acrylate	C6H4F6O2	Monoacrylates	2160-89-6
BM34	Furfuryl methacrylate	C9H10O3	Methacrylates - Aromatics	3454-28-2
AD17	Hexanediol ethoxylate diacrylate	[H2C=CHCO2(CH2CH2O)nCH2CH2CH2-]2	Multiacrylates - Glycol	0
BM33	Glycidyl methacrylate	C7H10O3	Methacrylates	106-91-2
BM67	Pentafluoropropyl methacrylate	H2C=C(CH3)CO2CH2CF2CF3	Methacrylates - Halogen	45115-53-5
CD01	N,N'-Ethylenebisacrylamide		Acrylamides	2956-58-3
AT03	Trimethylolpropane triacrylate	(H2C=CHCO2CH2)3CC2H5	Di/Triacrylates	15625-89-5
AM05	Ethylhexyl acrylate	CH2=CHCOOCH2CH(C2H5)(CH2)3CH3	Monoacrylates	103-11-7
BM71	Octafluoropentyl methacrylate	H2C=C(CH3)CO2CH2(CF2)4H	Methacrylates - Halogen	355-93-1
AM59	Tridecafluoro-2-hydroxynonyl acrylate	H2C=CHCO2CH2CH(OH)CH2(CF2)5CF3	Monoacrylates - Halogen	127377-12-2
AM60	Dodecafluoro-7-(trifluoromethyl)-octyl acrylate	H2C=CHCO2CH2CH2(CF2)4CF(CF3)2	Monoacrylates - Halogen	50836-65-2
BM45	Hydroxypropyl methacrylate	CH2=C(CH3)COO(C3H6OH)	Methacrylates - Oxygen/Glycol	27813-02-1
CM08	Acrylamide		Acrylamides	79-06-1
AT08	Glycerol propoxylate triacrylate	[H2C=CHCO2CH(CH3)CH2O]3[-CH(CH2-)2]	Di/Triacrylates - Glycol	52408-84-1
AM06	Hexyl acrylate	H2C=CHCO2(CH2)5CH3	Monoacrylates	2499-95-8
BM35	Tetrahydrofurfuryl methacrylate	C9H14O3	Methacrylates - Aromatics	2455-24-5
BM69	Hexafluoroisopropyl methacrylate	H2C=C(CH3)CO2CH(CF3)2	Methacrylates - Halogen	3063-94-3
AD03	Hexafluoropent-1,5-diyl diacrylate	C11H10O4F6	Multiacrylates	918-36-5
BM23	Ter-butyl methacrylate	H2C=C(CH3)CO2C(CH3)3	Methacrylates	585-07-9
DM02	N-tert-Butylmethacrylamide		Methacrylamides	6554-73-0
CM04	N-(Butoxymethyl)acrylamide		Acrylamides	1852-16-0
AM36	Diethylamino ethyl acrylate	CH2=CHCOOCH2CH2N(C2H5)2	Monoacrylates	2426-54-2
BM57	Ethylene glycol phenyl ether methacrylate	H2C=C(CH3)CO2CH2CH2OC6H5	Methacrylates - Glycol	10595-06-9
BM38	Norbornyl methacrylate	C11H16O2	Methacrylates -	29753-02-4

Asha K. Patel
School of Medicine, University of Nottingham

			Aromatics	
AM52	Carboxyethyl acrylate	CH2=CHCO2(CH2)2CO2H	Monoacrylates - Oxygen/Glycol	24615-84-7
BM44	Hydroxyethyl methacrylate	CH2=C(CH3)COOCH2CH2OH	Methacrylates - Oxygen/Glycol	868-77-9
AM80	Acryloyloxy-β,β-dimethyl-γ-butyrolactone	C9H12O4	Monoacrylates - Aromatic	102096-60-6
CM10	N-Hydroxyethyl acrylamide		Acrylamides	7646-67-5
AD22	Methyl-1,2-ethanediyl bis[oxy(methyl-2,1-ethanediyl)]diacrylate	H2C=CHCO(OC3H6)3O2CCH=CH2	Di/Triacrylates - Glycol	42978-66-5
AM28	Hydroxypropyl acrylate	C6H10O3	Monoacrylates - Oxygen	999-61-1
BM36	Isobornyl methacrylate	C14H22O2	Methacrylates - Aromatics	7534-94-3
AD10	Tricyclodecane-dimethanol diacrylate	C18H24O4	Multiacrylates - Aromatic	42594-17-2
BM04	Ethyl 2-ethylacrylate	C2H5C(CH2)CO2C2H5	Methacrylates	3070-65-3
BM68	Hexafluorobutyl methacrylate	CH2=C(CH3)COOCH2CF2CFHCF3	Methacrylates - Halogen	36405-47-7
CM02	N-[Tris(hydroxymethyl)methyl]acrylamide		Acrylamides	13880-05-2
AD04	Hexamethylene diacrylate	[H2C=CHCO2(CH2)3-]2	Di/Triacrylates	13048-33-4
AM12	Propargyl acrylate	CH2=CHCO2CH2C≡CH	Monoacrylates	10477-47-1
BM13	Ethylhexyl methacrylate	CH2=C(CH3)COOCH2CH(C2H5)(CH2)3CH3	Methacrylates	688-84-6
BM84	t-butyl cyclohexyl methacrylate	CH2=C(CH3)COOC6H10C(CH3)3	Methacrylates - Glycol	46729-07-1
AM27	Hydroxybutyl acrylate	H2C=CHCO2(CH2)4OH	Monoacrylates - Oxygen/Glycol	2478-10-6
BM66	Heptadecafluorodecyl methacrylate	H2C=C(CH3)CO2CH2CH2(CF2)7CF3	Methacrylates - Halogen	1996-88-9
CM03	N-tert-Butylacrylamide		Acrylamides	107-58-4
AT07	Trimethylolpropane ethoxylate triacrylate	[H2C=CHCO2(CH2CH2O)nCH2]3CC2H5	Di/Triacrylates - Glycol	28961-43-5
AM02	Butyl acrylate	CH2=CHCOO(CH2)3CH3	Monoacrylates	141-32-2
BM17	Isodecyl methacrylate	H2C=C(CH3)CO2C10H21	Methacrylates	29964-84-9
BM60	Chloro-2-hydroxy-propyl methacrylate	H2C=C(CH3)CO2CH2CH(OH)CH2Cl	Methacrylates - Halogen	13159-52-9
AD16	Ethylene glycol diacrylate	(H2C=CHCO2CH2-)2	Multiacrylates - Glycol	2274-11-5
BM07	Allyl methacrylate	CH2=C(CH3)COOCH2CH=CH2	Methacrylates	96-05-9
CM06	N-Isopropylacrylamide	#N/A	Acrylamides	2210-25-5
CM05	N,N'-Dimethylacrylamide	#N/A	Acrylamides	2680-03-7
AM07	Isobutyl acrylate	CH2=CHCOOCH2CH(CH3)2	Monoacrylates	106-63-8
AM45	Di(ethylene glycol) ethyl ether acrylate	H2C=CHCO2(CH2CH2O)2C2H5	Monoacrylates - Glycol	7328-17-8
BM49	Tert-butylamino-ethyl methacrylate	C10H19NO2	Methacrylates - Nitrogen	3775-90-4
AM75	Poly(ethylene glycol) phenyl ether acrylate	CH2CHCO2(CH2CH2O)nC6H5	Monoacrylates - Glycol	56641-05-5
BM06	Methyl 3-hydroxy-2-	CH3CH(OH)C(=CH2)	Methacrylates -	18020-65-0

Asha K. Patel
School of Medicine, University of Nottingham

	methylenebutyrate	CO2CH3	Oxygen/Glycol	
BM53	Di(ethylene glycol) methyl ether methacrylate	H2C=C(CH3)CO2(CH2CH2O)2CH3	Methacrylates - Oxygen/Glycol	45103-58-0
DM05	N-Methylmethacrylamide		Methacrylamides	3887-02-3
AD15	Di(ethylene glycol) diacrylate	(H2C=CHCO2CH2CH2)2O	Di/Triacrylates - Glycol	4074-88-8
AM21	Glycidyl acrylate	C6H8O3	Monoacrylates - Aromatic	106-90-1
BM09	Caprolactone 2-(methacryloyloxy)ethyl ester	HO(CH2)5CO2CH2CH2O2CC(CH3)=CH2	Methacrylates	85099-10-1
AM31	Hydroxy-3-phenoxypropyl acrylate	H2C=CHCO2CH2CH(OH)CH2OC6H5	Monoacrylates - Oxygen/Glycol	16969-10-1
BM11	Decyl methacrylate	CH2=C(CH3)COO(CH2)9CH3	Methacrylates	3179-47-3
BM12	Ethyl methacrylate	CH2=C(CH3)COOC2H5	Methacrylates	97-63-2
DM04	Methacrylamide		Methacrylamides	79-39-0
AD19	Trimethylolpropane ethoxylate methyl ether diacrylate	(H2C=CHCO2CH2CH2OCH2)2C(C2H5)CH2OCH2CH2OCH3	Di/Triacrylates - Glycol	302911-84-8
AM04	Ethyl acrylate	CH2=CHCOOC2H5	Monoacrylates	140-88-5
BM40	Phenyl methacrylate	H2C=C(CH3)CO2C6H5	Methacrylates - Aromatics	2177-70-0
BD03	Ethylene glycol dimethacrylate	H2C=C(CH3)CO2CH2CH2OCOC(CH3)=CH	Methacrylates - Glycol	97-90-5
AM57	Dodecafluoroheptyl acrylate	H2C=CHCO2CH2(CF2)5CHF2	Monoacrylates - Halogen	2993-85-3
BM43	Hydroxybutyl methacrylate	CH3CH2CH[OR(H)]CH2OH(R), R = -COC(CH3)=CH2	Methacrylates - Oxygen/Glycol	29008-35-3
DM06	N-Phenylmethacrylamide		Methacrylamides	1611-83-2
AD18	Tetra(ethylene glycol) diacrylate	(H2C=CHCO2CH2CH2OCH2CH2)2O	Di/Triacrylates - Glycol	17831-71-9
AM09	Lauryl acrylate	CH2=CHCOOC12H25	Monoacrylates	2156-97-0
BM25	Methylthioethyl methacrylate	H2C=C(CH3)CO2CH2CH2SCH3	Methacrylates	14216-23-0
BM48	Diethylaminoethyl methacrylate	H2C=C(CH3)CO2CH2CH2N(C2H5)2	Methacrylates - Nitrogen	105-16-8
AM58	Tridecafluorooctyl acrylate	H2C=CHCO2CH2CH2(CF2)5CF3	Monoacrylates - Halogen	17527-29-6
BM24	Vinyl methacrylate	H2C=C(CH3)CO2CH=CH2	Methacrylates	4245-37-8
CM01	Diacetone acrylamide		Acrylamides	2873-97-4
DM07	N-(3-Aminopropyl) methacrylamide HCl		Acrylamides	72607-53-5

Asha K. Patel
School of Medicine, University of Nottingham

APPENDIX 2: CARDIOMYOCYTE ATTACHMENT AND AREA

First Generation Homopolymer Serum conditioned Arrays

		7 days				24 hours			
Polymer ID	**Grid Ref**	**Ave Cell Density**	**SD**	**Ave Cell Area (μm^2)**	**SD**	**Ave Cell Density**	**SD**	**Ave Cell Area (μm^2)**	**SD**
AM08	1.1	0.18	0.05	331	77	0.32	0.06	477	199
BM51	1.2	0.20	0.13	404	133	0.46	0.09	347	48
BM22	1.3	0.05	0.03	147	86	0.51	0.03	269	45
AM38	1.4	0.28	0.16	186	24	0.04	0.01	132	60
BM08	1.5	0.17	0.07	278	74	0.44	0.55	514	277
AM77	1.6	0.05	0.07	103	116	0.00	0.00	0	0
CM07	1.7	0.10	0.02	286	51	0.00	0.00	0	0
AM73	2.1	0.30	0.21	265	155	0.31	0.06	328	29
AM71	2.2	0.39	0.35	327	118	0.72	0.25	386	42
BM80	2.3	0.18	0.16	300	50	0.22	0.16	223	8
AM54	2.4	0.47	0.24	456	70	0.55	0.63	291	40
AM58-b	2.5	0.15	0.15	219	90	0.25	0.21	266	10
BM54	2.6	0.34	0.15	533	245	0.15	0.14	359	32
CD04	2.7	0.15	0.20	416	270	0.10	0.01	217	45
AD05	3.1	0.36	0.18	602	459	0.22	0.21	436	95
AM81	3.2	0.12	0.10	308	103	0.13	0.03	268	33
BM30	3.3	0.38	0.14	397	71	0.54	0.01	277	16
AD24	3.4	0.33	0.20	354	65	0.11	0.08	1911	2345
AM64	3.5	0.02	0.02	162	125	0.59	0.24	367	84
BM52	3.6	0.45	0.25	309	67	0.11	0.16	179	-
CM15	3.7	0.00	0.01	26	46	0.00	0.00	0	0
AD23	4.1	0.20	0.13	475	88	0.44	0.27	385	45
AM22	4.2	0.31	0.29	435	183	0.47	0.15	261	10
BM39	4.3	0.42	0.17	810	669	0.55	0.04	343	32
BM70	4.4	0.19	0.14	409	87	0.64	0.06	290	15
AM74	4.5	0.31	0.26	330	106	0.28	0.18	295	27
BM50	4.6	0.28	0.20	313	95	0.26	0.21	454	290
DM03	4.7	0.19	0.16	196	116	0.00	0.00	0	0
DM01	4.8	0.00	0.00	0	0	0.00	0.00	0	0
AM23	5.1	0.17	0.05	484	64	0.36	0.01	352	80
BM55	5.2	0.23	0.14	426	146	0.25	0.28	287	40
BM18	5.3	0.41	0.23	291	48	0.29	0.34	236	112
AD01	5.4	0.45	0.10	506	196	0.51	0.12	314	39
BM83	5.5	0.00	0.00	0	0	0.05	0.00	275	11
BD01	5.6	0.11	0.06	420	138	0.19	0.10	238	32

CM09	5.7	0.33	0.26	368	106	0.00	0.00	0	0
AD02	6.1	0.39	0.14	492	193	0.34	0.04	297	53
AM70	6.2	0.25	0.08	464	106	0.72	0.40	399	51
BM34	6.3	0.59	0.28	1364	937	0.49	0.47	279	5
AD17	6.4	0.32	0.21	451	65	0.41	0.36	289	29
BM33	6.5	0.26	0.16	429	172	0.06	0.00	194	16
BM67	6.6	0.26	0.25	256	159	0.16	0.07	371	115
CD01	6.7	0.18	0.07	267	43	0.00	0.00	0	0
AT03	7.1	0.45	0.13	477	103	0.34	0.20	258	76
AM05	7.2	0.05	0.06	151	155	0.30	0.13	303	88
BM71	7.3	0.13	0.08	217	137	0.31	0.06	277	29
Blank	7.4	-	-	-	-	-	-	-	-
AM60	7.5	0.47	0.26	310	36	0.10	0.07	210	48
BM45	7.6	0.00	0.00	0	0	0.01	0.01	218	-
CM08	7.7	0.02	0.04	53	59	0.00	0.00	0	0
AT08	8.1	0.46	0.15	736	356	0.22	0.06	310	44
AM06	8.2	0.26	0.09	455	92	0.28	0.17	314	37
BM35	8.3	0.23	0.14	465	96	0.36	0.06	262	50
BM69	8.4	0.00	0.00	0	0	0.09	0.13	243	-
AD03	8.5	0.02	0.03	164	174	0.30	0.24	254	11
BM23	8.6	0.24	0.09	322	82	0.10	0.08	225	29
DM02	8.7	0.00	0.00	0	0	0.00	0.00	0	0
CM04	8.8	0.08	0.03	479	220	0.12	0.01	210	34
AM36	9.1	0.08	0.07	124	47	0.01	0.01	538	-
BM57	9.2	0.48	0.31	382	8	0.30	0.02	342	39
BM38	9.3	0.28	0.18	370	127	0.22	0.04	238	9
AM52	9.4	0.00	0.00	0	0	0.27	0.03	253	66
BM44	9.5	0.05	0.09	57	98	0.04	0.02	288	205
AM80	9.6	0.02	0.02	122	142	0.01	0.01	225	-
CM10	9.7	0.06	0.03	305	65	0.00	0.00	0	0
AD22	10.1	0.42	0.12	358	64	0.33	0.37	341	13
AM28	10.2	0.19	0.03	260	73	0.03	0.04	267	-
BM36	10.3	0.58	0.24	483	130	0.44	0.08	279	18
AD10	10.4	0.52	0.21	461	133	0.36	0.03	313	82
BM04	10.5	0.47	0.20	388	85	0.18	0.01	288	58
BM68	10.6	0.36	0.16	374	113	0.20	0.16	352	167
CM02	10.7	0.07	0.07	103	111	0.00	0.00	0	0
AD04	11.1	0.51	0.10	473	102	0.49	0.59	305	29
AM12	11.2	0.24	0.06	337	105	0.32	0.16	297	46
BM13	11.3	0.43	0.14	442	96	0.09	0.01	446	184
BM84	11.4	0.05	0.05	112	112	0.14	0.02	288	25
AM27	11.5	0.12	0.11	155	93	0.07	0.03	275	10
BM66	11.6	0.39	0.33	276	15	0.17	0.11	458	115
CM03	11.7	0.02	0.03	18	31	0.00	0.00	0	0

Asha K. Patel
School of Medicine, University of Nottingham

AT07	12.1	0.52	0.24	517	212	0.38	0.48	374	34
AM02	12.2	0.51	0.12	429	112	0.18	0.06	352	19
BM17	12.3	0.05	0.03	134	28	0.15	0.01	304	32
BM60	12.4	0.03	0.03	107	114	0.11	0.02	236	32
AD16	12.5	0.33	0.19	436	182	0.10	0.05	348	31
BM07	12.6	0.31	0.18	299	33	0.24	0.15	305	83
CM06	12.7	0.00	0.00	0	0	0.00	0.00	0	0
CM05	12.8	0.00	0.00	0	0	0.00	0.00	0	0
AM07	13.1	0.33	0.26	396	137	0.30	0.20	285	10
AM45	13.2	0.41	0.20	381	65	0.48	0.61	400	65
BM49	13.3	0.56	0.11	215	30	0.14	0.00	170	17
AM75	13.4	0.40	0.02	497	144	0.13	0.08	396	156
BM06	13.5	0.08	0.06	146	95	0.00	0.00	0	0
BM53	13.6	0.13	0.15	215	92	0.03	0.04	288	-
DM05	13.7	0.02	0.03	124	125	0.00	0.00	0	0
AD15	14.1	0.12	0.05	282	74	0.17	0.16	308	136
AM21	14.2	0.03	0.05	32	56	0.27	0.11	427	135
BM09	14.3	0.40	0.19	376	33	0.10	0.04	324	48
AM31	14.4	0.20	0.07	376	76	0.05	0.02	288	64
BM11	14.5	0.36	0.15	359	66	0.17	0.20	249	23
BM12	14.6	0.54	0.32	235	29	0.09	0.09	290	109
DM04	14.7	0.11	0.15	109	67	0.05	0.00	221	24
AD19	15.1	0.40	0.07	382	72	0.23	0.30	431	102
AM04	15.2	0.40	0.09	404	112	0.31	0.36	367	169
BM40	15.3	0.07	0.08	126	157	0.20	0.08	338	35
BD03	15.4	0.56	0.20	387	95	0.08	0.03	188	82
AM57	15.5	0.19	0.15	350	87	0.21	0.28	336	306
BM43	15.6	0.13	0.07	244	48	0.02	0.02	307	-
DM06	15.7	0.01	0.02	12	20	0.00	0.00	0	0
AD18	16.1	0.35	0.16	447	59	0.19	0.18	448	36
AM09	16.2	0.46	0.32	318	42	0.13	0.17	353	21
BM25	16.3	0.42	0.19	457	121	0.11	0.11	352	78
BM48	16.4	0.43	0.14	204	28	0.05	0.06	193	88
AM58	16.5	0.24	0.28	329	87	0.15	0.14	287	45
BM24	16.6	0.19	0.17	225	66	0.33	0.29	389	28
CM01	16.7	0.02	0.03	79	81	0.00	0.00	0	0
CM13	16.8	0.00	0.00	0	0	0.00	0.00	0	0

Asha K. Patel
School of Medicine, University of Nottingham

Cardiomyocyte Attachment and Area on Second Generation Co-polymers in Serum Free conditions

Polymer ID	GridRef	Ave Cell Density	SD	Ave Cell Area (µm2)	SD
AM54/ BM34	1,1	0.15	0.14	311	188
BM18/ AM64	1,2	0.26	0.07	551	126
AM54/ BM39	1,3	0.19	0.14	584	11
BM18/ AT03	1,4	0.31	0.16	446	110
AM54	1,5	0.17	0.10	385	34
BM18/ AD17	1,6	0.32	0.24	665	366
AM54/ BM54	1,7	0.23	0.17	276	142
BM18/ AM38	1,8	0.31	0.30	253	187
AM54/ BM49	1,9	0.00	0.00	0	0
BM18/ AM71	1,10	0.28	0.40	241	0
AM54/ BM71	1,11	0.39	0.17	409	191
BM18/ CM09	1,12	0.21	0.26	184	11
AM54/ CD04	1,13	0.22	0.15	545	186
BM18/ BD03	1,14	0.31	0.21	537	72
AM54/ AD04	1,15	0.08	0.12	548	0
BM18/ CM04	1,16	0.31	0.32	483	105
BM71/ DM07	1,17	0.41	0.18	418	245
BM71/ BM36	1,18	0.29	0.15	330	74
BM71/ BM18	1,19	0.19	0.09	336	44
BM71/ AD01	1,20	0.34	0.10	576	265
BM71/ AT08	1,21	0.51	0.35	546	105
BM71/ AD24	1,22	0.28	0.08	488	97
BM71/ BM80	1,23	0.20	0.10	535	40
BM71/ AM22	1,24	0.36	0.16	491	54
BM80/ BM34	2,1	0.33	0.25	517	9
AM38/ AM64	2,2	0.09	0.13	311	0
BM80/ BM39	2,3	0.28	0.05	684	148
AM38/ AT03	2,4	0.00	0.01	149	0
BM80/ AM54	2,5	0.15	0.11	839	262
AM38/ AD17	2,6	0.00	0.00	0	0
BM80/ BM54	2,7	0.32	0.19	377	168
AM38	2,8	0.00	0.01	36	51
BM80/ BM49	2,9	0.04	0.05	191	270
AM38/ AM71	2,10	0.03	0.04	228	0
BM80/ BM71	2,11	0.22	0.18	237	128
AM38/ CM09	2,12	0.01	0.01	61	0
BM80/ CD04	2,13	0.17	0.23	376	70
AM38/ BD03	2,14	0.37	0.29	397	45
BM80/ AD04	2,15	0.24	0.24	437	53
AM38/ CM04	2,16	0.00	0.00	0	0

BD03/ DM07	2,17	0.17	0.16	458	106
BD03/ BM36	2,18	0.36	0.20	323	74
BD03/ BM18	2,19	0.27	0.03	477	160
BD03/ AD01	2,20	0.23	0.13	459	206
BD03/ AT08	2,21	0.53	0.24	537	78
BD03/ AD24	2,22	0.29	0.11	431	80
BD03/ BM80	2,23	0.31	0.13	512	67
BD03/ AM22	2,24	0.25	0.04	482	40
BM18/ AM22	3,1	0.05	0.00	273	77
AM54/ AM64	3,2	0.26	0.04	782	465
BM18/ BM80	3,3	0.36	0.15	572	104
AM54/ AT03	3,4	0.20	0.15	552	339
BM18/ AD24	3,5	0.28	0.20	255	102
AM54/ AD17	3,6	0.28	0.25	391	120
BM18/ AT08	3,7	0.41	0.18	274	80
AM54/ AM38	3,8	0.00	0.00	0	0
BM18/ AD01	3,9	0.44	0.31	462	40
AM54/ AM71	3,10	0.39	0.37	561	146
BM18	3,11	0.12	0.17	203	0
AM54/ CM09	3,12	0.25	0.20	538	285
BM18/ BM36	3,13	0.15	0.10	270	14
AM54/ BD03	3,14	0.19	0.15	578	164
BM18/ DM07	3,15	0.16	0.23	366	0
AM54/ CM04	3,16	0.17	0.12	367	147
BM71/ AD04	3,17	0.21	0.14	460	124
BM71/ CD04	3,18	0.16	0.04	357	42
BM71	3,19	0.27	0.06	444	74
BM71/ BM49	3,20	0.27	0.13	431	63
BM71/ BM54	3,21	0.50	0.16	518	245
BM71/ AM54	3,22	0.30	0.14	587	82
BM71/ BM39	3,23	0.30	0.11	548	87
BM71/ BM34	3,24	0.19	0.17	465	6
AM38/ AM22	4,1	0.01	0.01	220	0
BM80/ AM64	4,2	0.14	0.12	1089	260
AM38/ BM80	4,3	0.10	0.07	326	25
BM80/ AT03	4,4	0.23	0.12	523	198
AM38/ AD24	4,5	0.00	0.00	0	0
BM80/ AD17	4,6	0.37	0.09	709	80
AM38/ AT08	4,7	0.00	0.00	0	0
BM80/ AM38	4,8	0.00	0.00	0	0
AM38/ AD01	4,9	0.00	0.00	0	0
BM80/ AM71	4,10	0.43	0.42	666	262
AM38/ BM18	4,11	0.39	0.33	294	86
BM80/ CM09	4,12	0.31	0.18	545	143

Asha K. Patel
School of Medicine, University of Nottingham

AM38/ BM36	4,13	0.15	0.05	265	81
BM80/ BD03	4,14	0.12	0.07	453	186
AM38/ DM07	4,15	0.00	0.00	0	0
BM80/ CM04	4,16	0.13	0.11	408	213
BD03/ AD04	4,17	0.17	0.05	355	124
BD03/ CD04	4,18	0.20	0.07	531	92
BD03/ BM71/CD04	4,19	0.23	0.05	397	105
BD03/ BM49	4,20	0.35	0.09	572	117
BD03/ BM54	4,21	0.22	0.06	580	137
BD03/ AM54	4,22	0.26	0.10	667	260
BD03/ BM39	4,23	0.25	0.09	785	280
BD03/ BM34	4,24	0.28	0.13	520	63
AM54/ AM22	5,1	0.06	0.06	579	78
BM18/ BM34	5,2	0.32	0.10	766	235
AM54/ BM80	5,3	0.16	0.09	483	154
BM18/ BM39	5,4	0.31	0.16	425	73
AM54/ AD24	5,5	0.19	0.11	287	106
BM18/ AM54	5,6	0.14	0.06	235	79
AM54/ AT08	5,7	0.13	0.03	468	254
BM18/ BM54	5,8	0.31	0.12	251	74
AM54/ AD01	5,9	0.14	0.05	194	77
BM18/ BM49	5,10	0.11	0.16	1219	0
AM54/ BM18	5,11	0.21	0.21	249	77
BM18/ BM71	5,12	0.22	0.13	250	6
AM54/ BM36	5,13	0.21	0.18	406	12
BM18/ CD04	5,14	0.11	0.09	348	58
AM54/ DM07	5,15	0.03	0.05	536	0
BM18/ AD04	5,16	0.16	0.09	358	27
BM71/ CM04	5,17	0.19	0.10	467	57
BM71/ BD03	5,18	0.33	0.14	397	75
BM71/ CM09	5,19	0.24	0.09	405	83
BM71/ AM71	5,20	0.33	0.11	466	77
BM71/ AM38	5,21	0.30	0.10	476	207
BM71/ AD17	5,22	0.25	0.05	443	66
BM71/ AT03	5,23	0.25	0.02	532	87
BM71/ AM64	5,24	0.02	0.01	468	276
BM80/ AM22	6,1	0.23	0.12	512	213
AM38/ BM34	6,2	0.13	0.10	321	2
BM80	6,3	0.14	0.03	769	222
AM38/ BM39	6,4	0.29	0.03	612	170
BM80/ AD24	6,5	0.20	0.09	718	178
AM38/ AM54	6,6	0.00	0.00	0	0
BM80/ AT08	6,7	0.32	0.26	559	111

Asha K. Patel
School of Medicine, University of Nottingham

AM38/ BM54	6,8	0.17	0.13	194	17
BM80/ AD01	6,9	0.23	0.16	389	172
AM38/ BM49	6,10	0.14	0.19	914	0
BM80/ BM18	6,11	0.07	0.05	521	280
AM38/ BM71	6,12	0.35	0.25	268	5
BM80/ BM36	6,13	0.22	0.08	546	153
AM38/ CD04	6,14	0.22	0.31	692	0
BM80/ DM07	6,15	0.20	0.13	412	4
AM38/ AD04	6,16	0.21	0.22	278	36
BD03/ CM04	6,17	0.24	0.10	503	150
BD03	6,18	0.37	0.23	641	180
BD03/ CM09	6,19	0.22	0.13	439	68
BD03/ AM71	6,20	0.25	0.11	588	126
BD03/ AM38	6,21	0.30	0.06	590	236
BD03/ AD17	6,22	0.28	0.10	656	276
BD03/ AT03	6,23	0.23	0.09	729	84
BD03/ AM64	6,24	0.12	0.12	405	116
AD24/ BM34	7,1	0.05	0.04	275	72
AM71/ AM64	7,2	0.00	0.00	0	0
AD24/ BM39	7,3	0.15	0.05	999	578
AM71/ AT03	7,4	0.10	0.02	477	135
AD24/ AM54	7,5	0.21	0.01	658	17
AM71/ AD17	7,6	0.08	0.06	334	14
AD24/ BM54	7,7	0.26	0.10	566	180
AM71/ AM38	7,8	0.00	0.00	0	0
AD24/ BM49	7,9	0.01	0.01	136	0
AM71	7,10	0.02	0.02	173	0
AD24/ BM71	7,11	0.31	0.23	486	271
AM71/ CM09	7,12	0.18	0.10	295	200
AD24/ CD04	7,13	0.40	0.31	570	31
AM71/ BD03	7,14	0.39	0.28	662	118
AD24/ AD04	7,15	0.26	0.27	712	89
AM71/ CM04	7,16	0.08	0.08	373	32
CM09/ DM07	7,17	0.00	0.00	0	0
CM09/ BM36	7,18	0.30	0.06	492	167
CM09/ BM18	7,19	0.26	0.09	345	74
CM09/ AD01	7,20	0.28	0.33	451	60
CM09/ AT08	7,21	0.14	0.06	338	127
CM09/ AD24	7,22	0.06	0.05	415	30
CM09/ BM80	7,23	0.05	0.07	376	0
CM09/ AM22	7,24	0.22	0.11	488	159
AM64/ BM34	8,1	0.10	0.08	411	65
BM54/ AM64	8,2	0.05	0.03	220	82
AM64/ BM39	8,3	0.05	0.05	199	17

Asha K. Patel
School of Medicine, University of Nottingham

BM54/ AT03	8,4	0.37	0.18	653	125
AM64/ AM54	8,5	0.21	0.15	349	47
BM54/ AD17	8,6	0.21	0.08	536	186
AM64/ BM54	8,7	0.10	0.01	238	58
BM54/ AM38	8,8	0.37	0.27	471	104
AM64/ BM49	8,9	0.00	0.00	0	0
BM54/ AM71	8,10	0.23	0.18	201	43
AM64/ BM71	8,11	0.25	0.15	307	60
BM54/ CM09	8,12	0.23	0.22	281	53
AM64/ CD04	8,13	0.16	0.06	191	80
BM54/ BD03	8,14	0.43	0.17	548	87
AM64/ AD04	8,15	0.39	0.18	430	18
BM54/ CM04	8,16	0.28	0.26	308	73
DM07	8,17	0.00	0.00	0	0
DM07/ BM36	8,18	0.00	0.00	0	0
DM07/ BM18	8,19	0.02	0.03	161	0
DM07/ AD01	8,20	0.10	0.11	298	168
DM07/ AT08	8,21	0.03	0.04	122	0
DM07/ AD24	8,22	0.02	0.02	346	0
DM07/ BM80	8,23	0.03	0.05	192	0
DM07/ AM22	8,24	0.00	0.00	0	0
AM71/ AM22	9,1	0.09	0.04	1035	813
AD24/ AM64	9,2	0.20	0.16	357	136
AM71/ BM80	9,3	0.19	0.07	492	30
AD24/ AT03	9,4	0.13	0.10	516	38
AM71/ AD24	9,5	0.14	0.11	417	129
AD24/ AD17	9,6	0.11	0.08	472	62
AM71/ AT08	9,7	0.07	0.07	383	22
AD24/ AM38	9,8	0.12	0.17	202	0
AM71/ AD01	9,9	0.18	0.15	206	10
AD24/ AM71	9,10	0.20	0.03	212	33
AM71/ BM18	9,11	0.12	0.09	321	163
AD24/ CM09	9,12	0.09	0.06	203	55
AM71/ BM36	9,13	0.21	0.09	415	275
AD24/ BD03	9,14	0.24	0.12	419	108
AM71/ DM07	9,15	0.15	0.12	697	433
AD24/ CM04	9,16	0.13	0.16	271	108
CM09/ AD04	9,17	0.11	0.09	672	243
CM09/ CD04	9,18	0.11	0.05	232	82
CM09/ BM71	9,19	0.15	0.11	355	50
CM09/ BM49	9,20	0.00	0.00	0	0
CM09/ BM54	9,21	0.02	0.01	471	28
CM09/ AM54	9,22	0.05	0.07	221	0
CM09/ BM39	9,23	0.10	0.04	381	239

Asha K. Patel
School of Medicine, University of Nottingham

CM09/ BM34	9,24	0.01	0.02	147	0
BM54/ AM22	10,1	0.21	0.03	469	51
AM64	10,2	0.19	0.03	470	169
BM54/ BM80	10,3	0.22	0.02	658	132
AM64/ AT03	10,4	0.28	0.11	643	81
BM54/ AD24	10,5	0.13	0.10	734	3
AM64/ AD17	10,6	0.29	0.12	654	20
BM54/ AT08	10,7	0.30	0.04	415	165
AM64/ AM38	10,8	0.00	0.00	0	0
BM54/ AD01	10,9	0.18	0.04	372	165
AM64/ AM71	10,10	0.05	0.07	224	0
BM54/ BM18	10,11	0.19	0.15	237	43
AM64/ CM09	10,12	0.09	0.09	533	8
BM54/ BM36	10,13	0.19	0.08	501	317
AM64/ BD03	10,14	0.24	0.12	376	161
BM54/ DM07	10,15	0.04	0.06	593	0
AM64/ CM04	10,16	0.24	0.11	376	148
DM07/ AD04	10,17	0.00	0.00	0	0
DM07/ CD04	10,18	0.00	0.00	0	0
DM07/ BM71	10,19	0.00	0.00	0	0
DM07/ BM49	10,20	0.00	0.00	0	0
DM07/ BM54	10,21	0.00	0.00	0	0
DM07/ AM54	10,22	0.00	0.00	0	0
DM07/ BM39	10,23	0.00	0.00	0	0
DM07/ BM34	10,24	0.00	0.00	0	0
AD24/ AM22	11,1	0.19	0.04	883	551
AM71/ BM34	11,2	0.23	0.16	627	158
AD24/ BM80	11,3	0.20	0.06	517	84
AM71/ BM39	11,4	0.19	0.04	714	263
AD24	11,5	0.14	0.05	418	102
AM71/ AM54	11,6	0.03	0.03	845	261
AD24/ AT08	11,7	0.13	0.15	321	31
AM71/ BM54	11,8	0.12	0.08	180	42
AD24/ AD01	11,9	0.03	0.05	383	0
AM71/ BM49	11,10	0.26	0.04	198	63
AD24/ BM18	11,11	0.03	0.04	809	0
AM71/ BM71	11,12	0.09	0.12	390	0
AD24/ BM36	11,13	0.21	0.25	293	244
AM71/ CD04	11,14	0.32	0.09	240	89
AD24/ DM07	11,15	0.00	0.00	0	0
AM71/ AD04	11,16	0.20	0.15	353	185
CM09/ CM04	11,17	0.25	0.16	259	48
CM09/ BD03	11,18	0.22	0.08	388	56
CM09	11,19	0.12	0.05	249	25

Asha K. Patel
School of Medicine, University of Nottingham

CM09/ AM71	11,20	0.10	0.04	196	48
CM09/ AM38	11,21	0.00	0.00	0	0
CM09/ AD17	11,22	0.09	0.05	534	305
CM09/ AT03	11,23	0.10	0.06	873	1028
CM09/ AM64	11,24	0.12	0.09	248	162
AM64/ AM22	12,1	0.07	0.03	392	147
BM54/ BM34	12,2	0.30	0.31	627	9
AM64/ BM80	12,3	0.21	0.14	369	86
BM54/ BM39	12,4	0.23	0.06	665	224
AM64/ AD24	12,5	0.24	0.07	416	65
BM54/ AM54	12,6	0.09	0.13	252	252
AM64/ AT08	12,7	0.24	0.07	471	288
BM54	12,8	0.00	0.00	0	0
AM64/ AD01	12,9	0.14	0.12	289	43
BM54/ BM49	12,10	0.00	0.00	0	0
AM64/ BM18	12,11	0.04	0.06	83	83
BM54/ BM71	12,12	0.00	0.00	0	0
AM64/ BM36	12,13	0.00	0.00	0	0
BM54/ CD04	12,14	0.09	0.12	265	0
AM64/ DM07	12,15	0.00	0.00	0	0
BM54/ AD04	12,16	0.11	0.16	288	288
DM07/ CM04	12,17	0.00	0.00	0	0
DM07/ BD03	12,18	0.00	0.00	0	0
DM07/ CM09	12,19	0.00	0.00	0	0
DM07/ AM71	12,20	0.00	0.00	0	0
DM07/ AM38	12,21	0.06	0.06	162	53
DM07/ AD17	12,22	0.00	0.00	0	0
DM07/ AT03	12,23	0.00	0.00	0	0
DM07/ AM64	12,24	0.00	0.00	0	0
AT03/ BM34	13,1	0.36	0.26	368	373
BM49/ AM64	13,2	0.00	0.00	0	0
AT03/ BM39	13,3	0.27	0.14	389	153
BM49/ AT03	13,4	0.17	0.12	213	188
AT03/ AM54	13,5	0.14	0.03	597	452
BM49/ AD17	13,6	0.20	0.15	270	231
AT03/ BM54	13,7	0.28	0.12	209	50
BM49/ AM38	13,8	0.00	0.00	0	0
AT03/ BM49	13,9	0.16	0.13	203	46
BM49/ AM71	13,10	0.00	0.00	0	0
AT03/ BM71	13,11	0.13	0.18	243	0
BM49/ CM09	13,12	0.00	0.00	0	0
AT03/ CD04	13,13	0.09	0.13	176	0
BM49/ BD03	13,14	0.11	0.15	244	0
AT03/ AD04	13,15	0.11	0.15	115	0

Asha K. Patel
School of Medicine, University of Nottingham

BM49/ CM04	13,16	0.03	0.05	301	0
BM36/ DM07	13,17	0.22	0.19	392	274
BM36	13,18	0.14	0.20	172	0
BM36/ BM18	13,19	0.20	0.14	306	94
BM36/ AD01	13,20	0.38	0.33	289	69
BM36/ AT08	13,21	0.32	0.21	362	136
BM36/ AD24	13,22	0.22	0.04	482	172
BM36/ BM80	13,23	0.38	0.06	608	49
BM36/ AM22	13,24	0.32	0.30	465	159
BM34	14,1	0.22	0.08	602	169
AT08/ AM64	14,2	0.35	0.19	576	419
BM34/ BM39	14,3	0.13	0.04	525	253
AT08/ AT03	14,4	0.22	0.12	461	229
BM34/ AM54	14,5	0.04	0.05	270	0
AT08/ AD17	14,6	0.15	0.03	493	253
BM34/ BM54	14,7	0.13	0.04	736	335
AT08/ AM38	14,8	0.00	0.00	0	0
BM34/ BM49	14,9	0.00	0.00	0	0
AT08/ AM71	14,10	0.05	0.07	52	74
BM34/ BM71	14,11	0.00	0.00	0	0
AT08/ CM09	14,12	0.00	0.00	0	0
BM34/ CD04	14,13	0.00	0.00	0	0
AT08/ BD03	14,14	0.18	0.26	156	221
BM34/ AD04	14,15	0.17	0.24	200	282
AT08/ CM04	14,16	0.00	0.00	0	0
AD04/ DM07	14,17	0.08	0.11	109	109
AD04/ BM36	14,18	0.28	0.21	249	43
AD04/ BM18	14,19	0.34	0.12	213	34
AD04/ AD01	14,20	0.26	0.12	289	97
AD04/ AT08	14,21	0.18	0.06	297	123
AD04/ AD24	14,22	0.16	0.11	442	258
AD04/ BM80	14,23	0.24	0.14	410	27
AD04/ AM22	14,24	0.26	0.03	406	77
BM49/ AM22	15,1	0.09	0.12	483	0
AT03/ AM64	15,2	0.33	0.05	352	174
BM49/ BM80	15,3	0.10	0.08	630	433
AT03	15,4	0.13	0.08	514	302
BM49/ AD24	15,5	0.07	0.10	725	0
AT03/ AD17	15,6	0.15	0.07	574	207
BM49/ AT08	15,7	0.05	0.07	497	0
AT03/ AM38	15,8	0.29	0.08	284	92
BM49/ AD01	15,9	0.19	0.13	783	524
AT03/ AM71	15,10	0.19	0.04	316	195
BM49/ BM18	15,11	0.25	0.23	612	351

Asha K. Patel
School of Medicine, University of Nottingham

AT03/ CM09	15,12	0.26	0.13	419	333
BM49/ BM36	15,13	0.21	0.23	450	435
AT03/ BD03	15,14	0.25	0.15	272	115
BM49/ DM07	15,15	0.04	0.04	150	37
AT03/ CM04	15,16	0.19	0.13	652	73
BM36/ AD04	15,17	0.22	0.17	258	142
BM36/ CD04	15,18	0.22	0.15	272	93
BM36/ BM71/CM09	15,19	0.29	0.04	253	18
BM36/ BM49	15,20	0.29	0.07	306	120
BM36/ BM54	15,21	0.34	0.13	366	96
BM36/ AM54	15,22	0.11	0.09	286	74
BM36/ BM39	15,23	0.35	0.19	605	163
BM36/ BM34	15,24	0.26	0.11	560	157
AT08/ AM22	16,1	0.07	0.05	449	50
BM34/ AM64	16,2	0.24	0.12	554	78
AT08/ BM80	16,3	0.03	0.04	546	0
BM34/ AT03	16,4	0.17	0.14	858	591
AT08/ AD24	16,5	0.17	0.05	323	126
BM34/ AD17	16,6	0.13	0.09	485	51
AT08	16,7	0.18	0.04	318	17
BM34/ AM38	16,8	0.13	0.09	778	314
AT08/ AD01	16,9	0.20	0.01	262	39
BM34/ AM71	16,10	0.18	0.25	429	0
AT08/ BM18	16,11	0.22	0.16	341	22
BM34/ CM09	16,12	0.11	0.16	239	0
AT08/ BM36	16,13	0.22	0.04	417	228
BM34/ BD03	16,14	0.19	0.19	810	276
AT08/ DM07	16,15	0.10	0.15	533	0
BM34/ CM04	16,16	0.28	0.03	425	123
AD04	16,17	0.33	0.11	293	65
AD04/ CD04	16,18	0.22	0.18	325	146
AD04/ BM71/DM07	16,19	0.11	0.16	550	0
AD04/ BM49	16,20	0.30	0.17	320	83
AD04/ BM54	16,21	0.28	0.21	291	112
AD04/ AM54	16,22	0.17	0.02	638	357
AD04/ BM39	16,23	0.36	0.18	682	192
AD04/ BM34	16,24	0.34	0.18	454	117
AT03/ AM22	17,1	0.18	0.06	517	163
BM49/ BM34	17,2	0.04	0.06	761	0
AT03/ BM80	17,3	0.17	0.05	612	276
BM49/ BM39	17,4	0.02	0.03	184	0
AT03/ AD24	17,5	0.20	0.12	329	107

Asha K. Patel
School of Medicine, University of Nottingham

BM49/ AM54	17,6	0.08	0.11	465	0
AT03/ AT08	17,7	0.21	0.03	296	49
BM49/ BM54	17,8	0.00	0.00	0	0
AT03/ AD01	17,9	0.37	0.09	296	139
BM49	17,10	0.00	0.00	0	0
AT03/ BM18	17,11	0.18	0.05	390	131
BM49/ BM71	17,12	0.22	0.19	291	61
AT03/ BM36	17,13	0.17	0.17	405	87
BM49/ CD04	17,14	0.00	0.00	0	0
AT03/ DM07	17,15	0.12	0.09	340	146
BM49/ AD04	17,16	0.20	0.01	363	155
BM36/ CM04	17,17	0.41	0.20	437	102
BM36/ BD03	17,18	0.26	0.09	212	59
BM36/ CM09	17,19	0.20	0.08	330	109
BM36/ AM71	17,20	0.12	0.02	218	55
BM36/ AM38	17,21	0.21	0.11	311	132
BM36/ AD17	17,22	0.37	0.10	401	148
BM36/ AT03	17,23	0.20	0.08	786	454
BM36/ AM64	17,24	0.10	0.03	416	270
BM34/ AM22	18,1	0.15	0.11	852	335
AT08/ BM34	18,2	0.16	0.07	454	130
BM34/ BM80	18,3	0.20	0.19	478	276
AT08/ BM39	18,4	0.18	0.12	615	245
BM34/ AD24	18,5	0.30	0.12	819	88
AT08/ AM54	18,6	0.14	0.05	254	129
BM34/ AT08	18,7	0.08	0.06	692	332
AT08/ BM54	18,8	0.30	0.22	267	194
BM34/ AD01	18,9	0.26	0.02	517	46
AT08/ BM49	18,10	0.06	0.08	410	0
BM34/ BM18	18,11	0.34	0.02	842	253
AT08/ BM71	18,12	0.31	0.09	414	162
BM34/ BM36	18,13	0.20	0.06	437	213
AT08/ CD04	18,14	0.24	0.09	299	74
BM34/ DM07	18,15	0.13	0.13	745	454
AT08/ AD04	18,16	0.23	0.12	289	134
AD04/ CM04	18,17	0.23	0.15	264	77
AD04/ BD03	18,18	0.15	0.11	575	373
AD04/ CM09	18,19	0.32	0.32	265	182
AD04/ AM71	18,20	0.31	0.25	361	150
AD04/ AM38	18,21	0.24	0.11	363	101
AD04/ AD17	18,22	0.14	0.13	571	172
AD04/ AT03	18,23	0.29	0.14	705	190
AD04/ AM64	18,24	0.14	0.07	530	147
BM39/ BM34	19,1	0.19	0.02	417	147

Asha K. Patel
School of Medicine, University of Nottingham

AD01/ AM64	19,2	0.22	0.12	366	162
BM39	19,3	0.19	0.10	398	60
AD01/ AT03	19,4	0.20	0.09	489	108
BM39/ AM54	19,5	0.18	0.10	579	293
AD01/ AD17	19,6	0.21	0.04	520	96
BM39/ BM54	19,7	0.21	0.07	392	74
AD01/ AM38	19,8	0.14	0.05	285	45
BM39/ BM49	19,9	0.23	0.07	373	179
AD01/ AM71	19,10	0.28	0.14	418	157
BM39/ BM71	19,11	0.24	0.08	337	22
AD01/ CM09	19,12	0.24	0.06	374	60
BM39/ CD04	19,13	0.03	0.04	558	0
AD01/ BD03	19,14	0.25	0.08	292	23
BM39/ AD04	19,15	0.19	0.10	399	171
AD01/ CM04	19,16	0.20	0.08	465	27
CD04/ DM07	19,17	0.00	0.00	0	0
CD04/ BM36	19,18	0.10	0.10	533	232
CD04/ BM18	19,19	0.13	0.10	315	20
CD04/ AD01	19,20	0.21	0.18	442	85
CD04/ AT08	19,21	0.10	0.08	448	168
CD04/ AD24	19,22	0.07	0.06	688	286
CD04/ BM80	19,23	0.23	0.17	616	232
CD04/ AM22	19,24	0.15	0.10	425	6
AM22/ BM34	20,1	0.18	0.08	434	290
AD17/ AM64	20,2	0.23	0.14	604	56
AM22/ BM39	20,3	0.33	0.11	522	94
AD17/ AT03	20,4	0.24	0.17	538	437
AM22/ AM54	20,5	0.29	0.11	570	84
AD17	20,6	0.15	0.15	408	48
AM22/ BM54	20,7	0.24	0.17	384	62
AD17/ AM38	20,8	0.05	0.07	243	0
AM22/ BM49	20,9	0.00	0.00	0	0
AD17/ AM71	20,10	0.36	0.20	470	89
AM22/ BM71	20,11	0.34	0.08	368	76
AD17/ CM09	20,12	0.40	0.24	424	71
AM22/ CD04	20,13	0.16	0.02	512	231
AD17/ BD03	20,14	0.28	0.08	374	78
AM22/ AD04	20,15	0.28	0.04	559	155
AD17/ CM04	20,16	0.10	0.06	360	156
CM04/ DM07	20,17	0.00	0.00	0	0
CM04/ BM36	20,18	0.18	0.08	411	33
CM04/ BM18	20,19	0.33	0.21	341	80
CM04/ AD01	20,20	0.08	0.10	240	97
CM04/ AT08	20,21	0.11	0.07	422	85

Asha K. Patel
School of Medicine, University of Nottingham

CM04/ AD24	20,22	0.05	0.07	412	0
CM04/ BM80	20,23	0.12	0.11	643	27
CM04/ AM22	20,24	0.08	0.03	391	127
AD01/ AM22	21,1	0.13	0.05	396	36
BM39/ AM64	21,2	0.12	0.11	254	27
AD01/ BM80	21,3	0.15	0.06	452	159
BM39/ AT03	21,4	0.25	0.13	777	194
AD01/ AD24	21,5	0.21	0.08	707	288
BM39/ AD17	21,6	0.49	0.22	585	51
AD01/ AT08	21,7	0.24	0.09	367	112
BM39/ AM38	21,8	0.15	0.11	218	101
AD01	21,9	0.22	0.17	364	96
BM39/ AM71	21,10	0.20	0.13	394	248
AD01/ BM18	21,11	0.28	0.08	299	34
BM39/ CM09	21,12	0.36	0.17	370	68
AD01/ BM36	21,13	0.19	0.09	470	157
BM39/ BD03	21,14	0.26	0.07	451	60
AD01/ DM07	21,15	0.17	0.15	320	48
BM39/ CM04	21,16	0.23	0.04	339	22
CD04/ AD04	21,17	0.25	0.13	468	321
CD04	21,18	0.24	0.11	636	300
CD04/ BM71	21,19	0.17	0.05	356	209
CD04/ BM49	21,20	0.00	0.00	0	0
CD04/ BM54	21,21	0.17	0.07	332	142
CD04/ AM54	21,22	0.11	0.02	490	318
CD04/ BM39	21,23	0.14	0.07	480	90
CD04/ BM34	21,24	0.06	0.05	685	60
AD17/ AM22	22,1	0.14	0.08	721	253
AM22/ AM64	22,2	0.07	0.04	343	198
AD17/ BM80	22,3	0.15	0.08	860	488
AM22/ AT03	22,4	0.13	0.05	638	77
AD17/ AD24	22,5	0.06	0.09	1039	0
AM22/ AD17	22,6	0.36	0.10	754	291
AD17/ AT08	22,7	0.11	0.03	593	247
AM22/ AM38	22,8	0.00	0.00	0	0
AD17/ AD01	22,9	0.41	0.19	517	221
AM22/ AM71	22,10	0.32	0.41	393	41
AD17/ BM18	22,11	0.40	0.18	419	36
AM22/ CM09	22,12	0.15	0.09	635	158
AD17/ BM36	22,13	0.26	0.04	441	43
AM22/ BD03	22,14	0.47	0.18	571	144
AD17/ DM07	22,15	0.06	0.05	343	140
AM22/ CM04	22,16	0.16	0.13	341	4
CM04/ AD04	22,17	0.10	0.08	344	93

Asha K. Patel
School of Medicine, University of Nottingham

CM04/ CD04	22,18	0.09	0.05	170	22
CM04/ BM71	22,19	0.22	0.01	334	38
CM04/ BM49	22,20	0.00	0.00	0	0
CM04/ BM54	22,21	0.03	0.04	381	0
CM04/ AM54	22,22	0.17	0.06	397	21
CM04/ BM39	22,23	0.15	0.05	334	137
CM04/ BM34	22,24	0.04	0.04	499	63
BM39/ AM22	23,1	0.15	0.11	975	124
AD01/ BM34	23,2	0.16	0.02	617	248
BM39/ BM80	23,3	0.28	0.09	572	127
AD01/ BM39	23,4	0.27	0.11	764	287
BM39/ AD24	23,5	0.39	0.13	599	146
AD01/ AM54	23,6	0.21	0.18	670	80
BM39/ AT08	23,7	0.33	0.16	1043	446
AD01/ BM54	23,8	0.27	0.08	574	108
BM39/ AD01	23,9	0.42	0.41	646	22
AD01/ BM49	23,10	0.29	0.14	580	91
BM39/ BM18	23,11	0.36	0.20	348	66
AD01/ BM71	23,12	0.48	0.09	384	80
BM39/ BM36	23,13	0.34	0.13	405	69
AD01/ CD04	23,14	0.37	0.09	438	162
BM39/ DM07	23,15	0.27	0.10	492	126
AD01/ AD04	23,16	0.33	0.14	569	46
CD04/ CM04	23,17	0.09	0.06	318	88
CD04/ BD03	23,18	0.19	0.21	311	20
CD04/ CM09	23,19	0.12	0.02	433	225
CD04/ AM71	23,20	0.10	0.11	349	24
CD04/ AM38	23,21	0.04	0.03	154	23
CD04/ AD17	23,22	0.09	0.06	289	43
CD04/ AT03	23,23	0.11	0.07	238	84
CD04/ AM64	23,24	0.05	0.03	333	75
AM22	24,1	0.19	0.04	509	169
AD17/ BM34	24,2	0.22	0.03	756	69
AM22/ BM80	24,3	0.13	0.11	711	212
AD17/ BM39	24,4	0.29	0.10	642	100
AM22/ AD24	24,5	0.45	0.14	552	153
AD17/ AM54	24,6	0.09	0.06	476	119
AM22/ AT08	24,7	0.35	0.20	765	71
AD17/ BM54	24,8	0.44	0.38	899	173
AM22/ AD01	24,9	0.46	0.31	419	90
AD17/ BM49	24,10	0.31	0.43	287	0
AM22/ BM18	24,11	0.39	0.39	335	46
AD17/ BM71	24,12	0.37	0.17	574	86
AM22/ BM36	24,13	0.30	0.11	347	74

Asha K. Patel
School of Medicine, University of Nottingham

AD17/ CD04	24,14	0.29	0.03	622	181
AM22/ DM07	24,15	0.00	0.00	0	0
AD17/ AD04	24,16	0.26	0.07	439	31
CM04	24,17	0.10	0.04	393	49
CM04/ BD03	24,18	0.15	0.10	317	63
CM04/ CM09	24,19	0.11	0.03	355	7
CM04/ AM71	24,20	0.29	0.07	580	238
CM04/ AM38	24,21	0.00	0.00	0	0
CM04/ AD17	24,22	0.06	0.04	294	155
CM04/ AT03	24,23	0.11	0.04	357	26
CM04/ AM64	24,24	0.18	0.07	358	108

Asha K. Patel
School of Medicine, University of Nottingham

WATER CONTACT AND XPS (1ST GENERATION)

			WCA ° (n=3)		XPS % (n=1)			
ID	Array Location (Row.Column) and Name		Ave.	S.D	C 1s	N 1s	O 1s	F 1s
BD01	5.6	Acryloyloxy-2-hydroxypropyl methacrylate	57	1	71.2	0.2	27.2	0.3
CM09	5.7	N-(Isobutoxymethyl)acrylamide			71.6	4.5	23.1	0.2
AD02	6.1	Butanediol-1,3 diacrylate	47	8	81.5	0.2	17.6	0.9
AM70	6.2	Hexafluoroisopropyl acrylate	67	5	72.4	0.2	26.7	0.3
BM34	6.3	Furfuryl methacrylate	70	2	75.7	0.7	22.8	0.7
AD17	6.4	Hexanediol ethoxylate diacrylate	56	11	73.4	0.5	25.7	0.3
BM33	6.5	Glycidyl methacrylate	58	7	73.9	0.6	24.2	1.1
BM67	6.6	Pentafluoropropyl methacrylate	56	11	73.1	0.4	25.4	0.0
CD01	6.7	N,N'-Ethylenebisacrylamide			73.2	0.7	26.6	0.0
AT03	7.1	Trimethylolpropane triacrylate	40	3	71.5	0.3	28.0	0.6
AM05	7.2	Ethylhexyl acrylate	61	7	77.7	0.1	22.3	0.0
BM71	7.3	Octafluoropentyl methacrylate	92	13	73.1	0.2	24.6	2.0
AM60	7.5	Dodecafluoro-7-(trifluoromethyl)-octyl acrylate	95	7	57.2	0.1	15.1	27.1
BM45	7.6	Hydroxypropyl methacrylate	50	8	72.7	0.3	26.9	0.0
CM08	7.7	Acrylamide			70.6	1.2	27.5	0.0
AT08	8.1	Glycerol propoxylate triacrylate	62	10	72.1	0.5	27.0	0.5
AM06	8.2	Hexyl acrylate	57	2	73.8	0.4	24.7	0.5
BM35	8.3	Tetrahydrofurfuryl methacrylate	62	9	76.9	0.4	21.4	0.6
BM69	8.4	Hexafluoroisopropyl methacrylate	58	7				
AD03	8.5	Hexafluoropent-1,5-diyl diacrylate	47	31	59.2	0.1	16.9	23.1
BM23	8.6	Ter-butyl methacrylate	58	20	71.1	0.4	26.5	0.6
DM02	8.7	N-tert-Butylmethacrylamide			72.6	1.5	24.9	1.0
CM04	8.8	N-(Butoxymethyl)acrylamide			72.0	4.8	21.9	0.6
AM36	9.1	Diethylamino ethyl acrylate	42	3	72.8	4.7	20.1	1.1
BM57	9.2	Ethylene glycol phenyl ether methacrylate	66	14	78.3	0.4	20.6	0.8
BM38	9.3	Norbornyl methacrylate	72	11	82.8	0.6	16.4	0.7
AM52	9.4	Carboxyethyl acrylate	37	3	69.4	0.4	29.5	0.6
BM44	9.5	Hydroxyethyl methacrylate	46	6	71.5	0.5	26.4	1.0
AM80	9.6	Acryloyloxy-β,β-dimethyl-γ-butyrolactone	65	7	73.3	0.1	26.2	0.2
CM10	9.7	N-Hydroxyethyl acrylamide	43	0	70.9	1.1	26.9	0.9
AD22	10.1	Methyl-1,2-ethanediyl bis[oxy(methyl-2,1-ethanediyl)] diacrylate	58	12	72.5	0.3	26.1	0.2
AM28	10.2	Hydroxypropyl acrylate	36	3	71.6	0.2	28.0	0.0
BM36	10.3	Isobornyl methacrylate	57	51	86.7	0.1	13.8	0.3
AD10	10.4	Tricyclodecane-dimethanol diacrylate	76	4	79.6	0.6	20.1	0.0
BM04	10.5	Ethyl 2-ethylacrylate	69	21	76.6	0.5	21.4	1.4
BM68	10.6	Hexafluorobutyl methacrylate	49	13	69.1	0.2	28.0	1.2
CM02	10.7	N-[Tris(hydroxymethyl)methyl] acrylamide	49	0	70.2	2.0	27.6	0.0
AD04	11.1	Hexamethylene diacrylate	57	7	74.8	0.3	24.0	0.0
AM12	11.2	Propargyl acrylate	62	17	78.1	0.4	18.5	3.3
BM13	11.3	Ethylhexyl methacrylate	73	30	77.6	0.4	22.5	0.0

Asha K. Patel
School of Medicine, University of Nottingham

			WCA ° (n=3)		XPS % (n=1)			
ID	**Array Location (Row.Column) and Name**		**Ave.**	**S.D**	**C 1s**	**N 1s**	**O 1s**	**F 1s**
BM84	11.4	t-Butyl cyclohexyl methacrylate	68	16	84.7	0.3	13.2	0.8
AM27	11.5	Hydroxybutyl acrylate	41	9	70.5	0.0	26.5	1.8
BM66	11.6	Heptadecafluorodecyl methacrylate	108	21	64.9	0.5	21.2	13.5
CM03	11.7	N-tert-Butylacrylamide	52	0	74.2	3.9	21.1	1.0
AT07	12.1	Trimethylolpropane ethoxylate triacrylate	57	10	70.4	0.4	27.1	0.5
AM02	12.2	Butyl acrylate	61	3	73.0	0.4	26.0	0.4
BM17	12.3	Isodecyl methacrylate	59	14	82.8	0.2	16.7	0.0
BM60	12.4	Chloro-2-hydroxy-propyl methacrylate	60	3	69.7	0.4	25.4	0.4
AD16	12.5	Ethylene glycol diacrylate	56	8	70.4	0.1	28.4	1.0
BM07	12.6	Allyl methacrylate	51	11	72.1	0.6	25.9	1.4
CM06	12.7	N-Isopropylacrylamide	45	0	71.9	4.1	22.8	0.7
CM05	12.8	N,N'-Dimethylacrylamide	27	0	70.7	1.0	29.0	0.5
AM07	13.1	Isobutyl acrylate	71	13	71.5	0.4	27.7	0.0
AM45	13.2	Di(ethylene glycol) ethyl ether acrylate	46	11	70.8	0.3	28.6	-0.4
BM49	13.3	Tert-butylamino-ethyl methacrylate	50	12	70.2	0.2	29.1	0.5
AM75	13.4	Poly(ethylene glycol) phenyl ether acrylate	48	11	74.5	0.2	24.1	0.4
BM06	13.5	Methyl 3-hydroxy-2-methylenebutyrate	54	9	72.4	0.5	27.9	0.0
BM53	13.6	Di(ethylene glycol) methyl ether methacrylate	35	14	72.1	0.2	27.3	0.1
DM05	13.7	N-Methylmethacrylamide	40	0	71.5	2.7	26.2	0.1
AD15	14.1	Di(ethylene glycol) diacrylate	56	7	71.4	0.3	27.0	0.5
AM21	14.2	Glycidyl acrylate	62	14	69.2	0.4	28.1	1.5
BM09	14.3	Caprolactone 2-(methacryloyloxy) ethyl ester	46	2	75.5	0.2	24.0	0.3
AM31	14.4	Hydroxy-3-phenoxypropyl acrylate	64	6	76.9	0.2	22.2	0.1
BM11	14.5	Decyl methacrylate	58	11	79.2	0.4	19.3	0.6
BM12	14.6	Ethyl methacrylate	61	11	74.2	0.5	23.6	1.0
DM04	14.7	Methacrylamide	38	0	70.0	2.2	27.0	0.9
AD19	15.1	Trimethylolpropane ethoxylate methyl ether diacrylate	56	7	72.1	0.2	26.4	1.0
AM04	15.2	Ethyl acrylate	62	5	73.6	0.3	24.6	1.2
BM40	15.3	Phenyl methacrylate	70	17	80.8	0.4	17.8	0.8
BD03	15.4	Ethylene glycol dimethacrylate	64	12	73.4	0.1	25.9	0.4
AM57	15.5	Dodecafluoroheptyl acrylate	63	20	44.1	0.2	8.6	46.6
BM43	15.6	Hydroxybutyl methacrylate	61	5	71.4	0.4	27.4	0.2
DM06	15.7	N-Phenylmethacrylamide	72	0	79.1	4.3	14.9	1.2
AD18	16.1	Tetra(ethylene glycol) diacrylate	49	7	70.2	0.5	28.5	1.1
AM09	16.2	Lauryl acrylate	56	9	75.3	0.4	22.4	0.7
BM25	16.3	Methylthioethyl methacrylate	49	4	76.5	0.2	19.5	0.2
BM48	16.4	Diethylaminoethyl methacrylate	55	24	72.0	3.9	20.7	2.4
AM58	16.5	Tridecafluorooctyl acrylate	62	16	65.8	0.3	25.2	9.2
BM24	16.6	Vinyl methacrylate	49	11	72.4	0.6	24.9	1.0
CM01	16.7	Diacetone acrylamide	34	0	73.1	3.1	22.3	1.2
CM13	16.8	N-[3-(Dimethylamino)propyl] acrylamide			73.3	1.0	25.6	0.5

Asha K. Patel
School of Medicine, University of Nottingham

			WCA ° (n=3)		XPS % (n=1)			
ID	Array Location (Row.Column) and Name		Ave.	S.D	C 1s	N 1s	O 1s	F 1s
AM08	1.1	Isooctyl acrylate	53	5	85.1	0.1	14.6	0.1
BM51	1.2	Nitrophenoxyethyl methacrylate	58	2				
BM22	1.3	Stearyl methacrylate	60	4	80.7	0.2	18.6	0.2
AM38	1.4	Dimethylamino-propyl acrylate	39	7	72.1	4.3	22.4	1.0
BM08	1.5	Butyl methacrylate	46	7	71.4	0.3	27.2	0.5
AM77	1.6	Poly(ethylene glycol) methyl ether acrylate	29	1	71.0	0.0	28.2	0.5
CM07	1.7	N-(3-Methoxypropyl)acrylamide			70.2	1.0	27.7	0.8
AM73	2.1	Isodecyl acrylate	57	3	95.3	0.2	13.6	0.1
AM71	2.2	Heptafluorobutyl acrylate	63	7	78.8	0.4	19.3	0.2
BM80	2.3	Methacryloyloxy)ethyl acetoacetate	56	2	71.3	0.2	26.4	3.2
AM54	2.4	Poly(propylene glycol) acrylate	41	9	73.7	0.4	24.5	1.0
BM54	2.6	Ethoxyethyl methacrylate	55	5	75.8	0.3	24.0	0.1
CD04	2.7	N,N'-Methylenebisacrylamide			72.1	2.4	25.1	0.3
AD05	3.1	Neopentyl glycol diacrylate	62	8	86.7	0.1	12.9	0.4
AM81	3.2	Cyanoethyl acrylate	48	2	75.6	1.7	22.9	0.0
BM30	3.3	Cyclohexyl methacrylate	53	2	77.1	0.5	20.1	0.8
AD24	3.4	Poly(propylene glycol) diacrylate	50	1	76.9	0.4	23.1	0.0
AM64	3.5	Hexadecafluoro-9-(trifluoromethyl)decyl acrylate	66	17	74.2	0.7	24.3	0.7
BM52	3.6	Butoxyethyl methacrylate	51	7	73.8	0.3	25.3	0.4
CM15	3.7	N-(Hydroxymethyl)acrylamide			72.2	1.4	26.5	0.0
AD23	4.1	Neopentyl glycol propoxylate diacrylate	59	18	73.7	0.1	26.3	0.0
AM22	4.2	Tetrahydrofurfuryl acrylate	54	15	74.3	0.4	25.4	0.0
BM39	4.3	Benzyl methacrylate	71	15	80.5	0.3	19.5	0.0
BM70	4.4	Heptafluorobutyl methacrylate	59	0	73.5	0.4	24.8	1.1
AM74	4.5	Octafluoropentyl acrylate	64	19	48.1	0.2	11.8	39.8
BM50	4.6	Dimethylamino-ethyl methacrylate	56	15	74.9	0.7	24.1	0.3
DM03	4.7	N-(4-Hydroxyphenyl) methacrylamide			73.3	1.2	24.8	0.0
DM01	4.8	N-[3-(Dimethylamino) propyl]methacrylamide			72.6	4.7	21.6	1.1
AM23	5.1	Isobornyl acrylate	81	20	76.4	0.0	23.4	0.5
BM55	5.2	Ethylene glycol methyl ether methacrylate	69	23	77.1	0.3	20.5	0.6
BM18	5.3	Lauryl methacrylate	64	2	80.5	0.3	18.8	0.5
AD01	5.4	Butanediol diacrylate	71	10	76.3	0.2	23.8	0.0
BM83	5.5	2-Isocyanatoethyl methacrylate	0	0	71.5	2.2	26.2	0.0

Asha K. Patel
School of Medicine, University of Nottingham

WCA of 2nd Generation Co-polymer Array

PolymerID	GridRef	WCA
AM54/ BM34	1,1	50
BM18/ AM64	1,2	108.8
AM54/ BM39	1,3	49.2
BM18/ AT03	1,4	91.5
AM54	1,5	44.4
BM18/ AD17	1,6	76.4
AM54/ BM54	1,7	
BM18/ AM38	1,8	58.7
AM54/ BM49	1,9	43.1
BM18/ AM71	1,10	43.6
AM54/ BM71	1,11	42.2
BM18/ CM09	1,12	59
BM80/ BM34	2,1	73.3
AM38/ AM64	2,2	108.7
BM80/ BM39	2,3	69.1
AM38/ AT03	2,4	48.9
BM80/ AM54	2,5	45.5
AM38/ AD17	2,6	35.7
BM80/ BM54	2,7	64.2
AM38	2,8	40.1
BM80/ BM49	2,9	79.7
AM38/ AM71	2,10	44
BM80/ BM71	2,11	77.6
AM38/ CM09	2,12	50.8
BM18/ AM22	3,1	60.6
AM54/ AM64	3,2	51.3
BM18/ BM80	3,3	67.5
AM54/ AT03	3,4	50.6
BM18/ AD24	3,5	65
AM54/ AD17	3,6	49.7
BM18/ AT08	3,7	85.3
AM54/ AM38	3,8	39.5
BM18/ AD01	3,9	85.5
AM54/ AM71	3,10	46.6
BM18	3,11	69.3
AM54/ CM09	3,12	
AM38/ AM22	4,1	32.9
BM80/ AM64	4,2	68.9
AM38/ BM80	4,3	41.1
BM80/ AT03	4,4	72.1
AM38/ AD24	4,5	43.5
BM80/ AD17	4,6	65
AM38/ AT08	4,7	45.9
BM80/ AM38	4,8	51.2
AM38/ AD01	4,9	47.5
BM80/ AM71	4,10	96.8
AM38/ BM18	4,11	45.5
BM80/ CM09	4,12	73.2

Asha K. Patel
School of Medicine, University of Nottingham

AM54/ AM22	5,1	
BM18/ BM34	5,2	88.1
AM54/ BM80	5,3	58.2
BM18/ BM39	5,4	73.8
AM54/ AD24	5,5	50.8
BM18/ AM54	5,6	42.9
AM54/ AT08	5,7	51
BM18/ BM54	5,8	66.6
AM54/ AD01	5,9	57.4
BM18/ BM49	5,10	80.2
AM54/ BM18	5,11	47.5
BM18/ BM71	5,12	61.5
BM80/ AM22	6,1	69.8
AM38/ BM34	6,2	82
BM80	6,3	67.6
AM38/ BM39	6,4	61.3
BM80/ AD24	6,5	58.2
AM38/ AM54	6,6	30.1
BM80/ AT08	6,7	72
AM38/ BM54	6,8	43.5
BM80/ AD01	6,9	80.4
AM38/ BM49	6,10	60
BM80/ BM18	6,11	87.4
AM38/ BM71	6,12	77.5
AD24/ BM34	7,1	64.4
AM71/ AM64	7,2	45.9
AD24/ BM39	7,3	68
AM71/ AT03	7,4	49.4
AD24/ AM54	7,5	47
AM71/ AD17	7,6	57.7
AD24/ BM54	7,7	51.6
AM71/ AM38	7,8	49.8
AD24/ BM49	7,9	
AM71	7,10	64.8
AD24/ BM71	7,11	62.5
AM71/ CM09	7,12	53.5
AM64/ BM34	8,1	61.3
BM54/ AM64	8,2	
AM64/ BM39	8,3	60.6
BM54/ AT03	8,4	65.3
AM64/ AM54	8,5	94
BM54/ AD17	8,6	61
AM64/ BM54	8,7	
BM54/ AM38	8,8	65.2
AM64/ BM49	8,9	
BM54/ AM71	8,10	51.4
AM64/ BM71	8,11	
BM54/ CM09	8,12	52.9
AM71/ AM22	9,1	40.2
AD24/ AM64	9,2	56.9
AM71/ BM80	9,3	50.5

Asha K. Patel
School of Medicine, University of Nottingham

AD24/ AT03	9,4	61.9
AM71/ AD24	9,5	46.7
AD24/ AD17	9,6	57.7
AM71/ AT08	9,7	48.3
AD24/ AM38	9,8	41.7
AM71/ AD01	9,9	68.5
AD24/ AM71	9,10	52.6
AM71/ BM18	9,11	55.3
AD24/ CM09	9,12	58.4
BM54/ AM22	10,1	59.4
AM64	10,2	49.5
BM54/ BM80	10,3	60.6
AM64/ AT03	10,4	80.7
BM54/ AD24	10,5	50.4
AM64/ AD17	10,6	94.2
BM54/ AT08	10,7	66
AM64/ AM38	10,8	111.4
BM54/ AD01	10,9	65.7
AM64/ AM71	10,10	75.3
BM54/ BM18	10,11	55.9
AM64/ CM09	10,12	92.2
AD24/ AM22	11,1	57.2
AM71/ BM34	11,2	48.5
AD24/ BM80	11,3	62.4
AM71/ BM39	11,4	71.5
AD24	11,5	56.1
AM71/ AM54	11,6	
AD24/ AT08	11,7	60.2
AM71/ BM54	11,8	53.3
AD24/ AD01	11,9	64
AM71/ BM49	11,10	53.3
AD24/ BM18	11,11	
AM71/ BM71	11,12	49
AM64/ AM22	12,1	
BM54/ BM34	12,2	74.7
AM64/ BM80	12,3	73.7
BM54/ BM39	12,4	77.8
AM64/ AD24	12,5	45.1
BM54/ AM54	12,6	42.2
AM64/ AT08	12,7	75.8
BM54	12,8	72
AM64/ AD01	12,9	107.9
BM54/ BM49	12,10	66.8
AM64/ BM18	12,11	71.4
BM54/ BM71	12,12	73.5
AT03/ BM34	13,1	66.7
BM49/ AM64	13,2	111.2
AT03/ BM39	13,3	76.7
BM49/ AT03	13,4	71
AT03/ AM54	13,5	56.4
BM49/ AD17	13,6	48.9

Asha K. Patel
School of Medicine, University of Nottingham

AT03/ BM54	13,7	74.3
BM49/ AM38	13,8	62.7
AT03/ BM49	13,9	72.1
BM49/ AM71	13,10	57.4
AT03/ BM71	13,11	81.1
BM49/ CM09	13,12	71.8
BM34	14,1	71.6
AT08/ AM64	14,2	75.1
BM34/ BM39	14,3	80.5
AT08/ AT03	14,4	74.6
BM34/ AM54	14,5	63.8
AT08/ AD17	14,6	71.3
BM34/ BM54	14,7	74.2
AT08/ AM38	14,8	54.3
BM34/ BM49	14,9	66.6
AT08/ AM71	14,10	69.1
BM34/ BM71	14,11	67
AT08/ CM09	14,12	70
BM49/ AM22	15,1	73.8
AT03/ AM64	15,2	79
BM49/ BM80	15,3	79.7
AT03	15,4	
BM49/ AD24	15,5	63.9
AT03/ AD17	15,6	82.4
BM49/ AT08	15,7	60.6
AT03/ AM38	15,8	67.9
BM49/ AD01	15,9	65
AT03/ AM71	15,10	73.5
BM49/ BM18	15,11	75.1
AT03/ CM09	15,12	74.5
AT08/ AM22	16,1	63.1
BM34/ AM64	16,2	77.8
AT08/ BM80	16,3	74.5
BM34/ AT03	16,4	66.8
AT08/ AD24	16,5	61.1
BM34/ AD17	16,6	57.5
AT08	16,7	61.8
BM34/ AM38	16,8	64.6
AT08/ AD01	16,9	65.7
BM34/ AM71	16,10	63.2
AT08/ BM18	16,11	78.9
BM34/ CM09	16,12	68.8
AT03/ AM22	17,1	65.1
BM49/ BM34	17,2	73.4
AT03/ BM80	17,3	70.2
BM49/ BM39	17,4	80
AT03/ AD24	17,5	71.7
BM49/ AM54	17,6	61.7
AT03/ AT08	17,7	72.7
BM49/ BM54	17,8	61.5
AT03/ AD01	17,9	75.7

Asha K. Patel
School of Medicine, University of Nottingham

BM49	17,10	63.4
AT03/ BM18	17,11	
BM49/ BM71	17,12	59.5
BM34/ AM22	18,1	72
AT08/ BM34	18,2	70
BM34/ BM80	18,3	74.7
AT08/ BM39	18,4	76.8
BM34/ AD24	18,5	63.8
AT08/ AM54	18,6	56.7
BM34/ AT08	18,7	66.4
AT08/ BM54	18,8	66
BM34/ AD01	18,9	68.2
AT08/ BM49	18,10	66
BM34/ BM18	18,11	73.3
AT08/ BM71	18,12	66.3
BM39/ BM34	19,1	71.4
AD01/ AM64	19,2	102.2
BM39	19,3	82.6
AD01/ AT03	19,4	73.8
BM39/ AM54	19,5	55.1
AD01/ AD17	19,6	72.7
BM39/ BM54	19,7	54.6
AD01/ AM38	19,8	54.9
BM39/ BM49	19,9	83.9
AD01/ AM71	19,10	71.8
BM39/ BM71	19,11	72.6
AD01/ CM09	19,12	73
AM22/ BM34	20,1	71.4
AD17/ AM64	20,2	62.2
AM22/ BM39	20,3	77.4
AD17/ AT03	20,4	74.7
AM22/ AM54	20,5	54.4
AD17	20,6	66.6
AM22/ BM54	20,7	62.3
AD17/ AM38	20,8	45.3
AM22/ BM49	20,9	67.9
AD17/ AM71	20,10	73.2
AM22/ BM71	20,11	58.4
AD17/ CM09	20,12	71.1
AD01/ AM22	21,1	77.5
BM39/ AM64	21,2	
AD01/ BM80	21,3	88.4
BM39/ AT03	21,4	82.7
AD01/ AD24	21,5	61.8
BM39/ AD17	21,6	75.3
AD01/ AT08	21,7	71
BM39/ AM38	21,8	48.3
AD01	21,9	68.4
BM39/ AM71	21,10	70.7
AD01/ BM18	21,11	78.1
BM39/ CM09	21,12	69.1

Asha K. Patel
School of Medicine, University of Nottingham

AD17/ AM22	22,1	55.4
AM22/ AM64	22,2	114.5
AD17/ BM80	22,3	71.3
AM22/ AT03	22,4	78
AD17/ AD24	22,5	64.8
AM22/ AD17	22,6	65.4
AD17/ AT08	22,7	69.7
AM22/ AM38	22,8	45.2
AD17/ AD01	22,9	72.3
AM22/ AM71	22,10	58.4
AD17/ BM18	22,11	79.7
AM22/ CM09	22,12	73.5
BM39/ AM22	23,1	64.1
AD01/ BM34	23,2	77.3
BM39/ BM80	23,3	81
AD01/ BM39	23,4	81.3
BM39/ AD24	23,5	65.3
AD01/ AM54	23,6	49
BM39/ AT08	23,7	67.8
AD01/ BM54	23,8	65
BM39/ AD01	23,9	69.6
AD01/ BM49	23,10	60.9
BM39/ BM18	23,11	93.3
AD01/ BM71	23,12	78.4
AM22	24,1	48.8
AD17/ BM34	24,2	68.4
AM22/ BM80	24,3	60.9
AD17/ BM39	24,4	72.3
AM22/ AD24	24,5	55.6
AD17/ AM54	24,6	49.1
AM22/ AT08	24,7	72.2
AD17/ BM54	24,8	65.1
AM22/ AD01	24,9	72.1
AD17/ BM49	24,10	64.8
AM22/ BM18	24,11	61
AD17/ BM71	24,12	77
AD01/ BM36	21,13	78.7
BM39/ BD03	21,14	76.5
AD01/ DM07	21,15	65.5
BM39/ CM04	21,16	75
CD04/ AD04	21,17	58.6
CD04	21,18	66.3
CD04/ BM71	21,19	72
CD04/ BM49	21,20	62.2
CD04/ BM54	21,21	48.2
CD04/ AM54	21,22	52.2
CD04/ BM39	21,23	45.8
CD04/ BM34	21,24	36
AD17/ BM36	22,13	82.7
AM22/ BD03	22,14	75.1
AD17/ DM07	22,15	65.4

AM22/ CM04	22,16	60.4
CM04/ AD04	22,17	74.7
CM04/ CD04	22,18	75.6
CM04/ BM71	22,19	88.6
CM04/ BM49	22,20	70.3
BM39/ BM36	23,13	83.6
AD01/ CD04	23,14	73.2
BM39/ DM07	23,15	75.2
AD01/ AD04	23,16	77.6
CD04/ CM04	23,17	68.8
CD04/ BD03	23,18	48.1
CD04/ CM09	23,19	73.8
CD04/ AM71	23,20	43.4
AM22/ BM36	24,13	81
AD17/ CD04	24,14	68
AM22/ DM07	24,15	58.2
AD17/ AD04	24,16	67.7
CM04	24,17	74.4
CM04/ BD03	24,18	70.2
CM04/ CM09	24,19	77.8
CM04/ AM71	24,20	76.6